Sila- and Germacyclopentadienes:

Radicals, Anions, and a New Type of Tetrylene

An der Fakultät für Mathematik und Naturwissenschaften

der Carl von Ossietzky Universität Oldenburg

zur Erlangung des Grades und Titels eines

Doktors der Naturwissenschaften (Dr. rer. nat.)

angenommene Dissertation

von

Herrn M.Sc. Crispin R. W. Reinhold

geboren am 30. Juni 1985 in Ratzeburg

The research for this work was performed at the Institute for Chemistry at the Carl von Ossietzky University Oldenburg under supervision of Prof. Thomas Müller from December 2012 until December 2016.

Referee: Prof. Thomas Müller

Second referee: Prof. Rüdiger Beckhaus

Day of thesis defence: 3 March 2017

Acknowledgements

First and foremost, I would like to thank my advisor, Prof. Thomas Müller, not only for the opportunity to prepare this thesis under his guidance but also for the interesting topic as well as for the dedicated support and constant discussion during this time. I would further like to thank Prof. Rüdiger Beckhaus for agreeing to be the second referee of this thesis. The Heinz Neumüller Foundation is thanked for providing financial support through a scholarship.

I would like to thank Dr. Annemarie Schäfer for her scientific expertise and her professional support. Additionally, I thank Maria for keeping the labs running as well as Petra for taking care of bureaucratic obstacles.

Furthermore, I would like to thank the analytical department. Andrea and Dieter for recording numerous NMR spectra, Marc and Wolfgang for X-ray analyses, Rainer for measuring GC/MS spectra and countless bad jokes, Francesco for measuring mass spectra, and Burghard for performing elemental analyses. Dr. Bernhard Schnetger is thanked for measuring X-ray fluorescence spectra and Dr. Stefan Harfst for solving any computational issues in an instant.

A very important factor for this work was the good atmosphere in our group and the whole department. Therefore, I would like to thank Sandra, Jelte, Anastasia, Saskia, Xiao, and all other former members especially Patrick and Matti as well as the Beckhaus and Wickleder groups. Specifically, I have to thank Dennis for our marriage-like situation in our small writing office, Lena for the good times in our lab and for all the inspiring and/or funny discussions, Zhaowen for his skills in the lab as well as in the kitchen, his endless ambition to push our topic to the limit and for teaching me cursing in Chinese, and Henning for sharing the same passion about climbing. You made the last years very special. I thank Sandra, Iris, Jelte, Henning S., Julian K., Julian G., Mathis, and Thorben for their contributions to this work.

I would like to thank Prof. Kim Baines not only for her help in the writing process of this thesis but also for her support and all the interesting and entertaining discussions we had at every occasion since I joined her group during my masters. Also Prof. Yitzhak Apeloig is thanked for his support and supervision during an internship in his group. Especially the members Boris, Dimitry, and Arseni taught me a lot but also Yosi, Daniel, Alexander, Boris, Evgeni and Lieby made me feel very welcome. Thank you!

My special thanks go to my friends Maren and Birger for proofreading of this work and for sharing daily PhD problems. The inspiring coffee breaks with them and also with Aaron and Olli were essential. Many thanks to all my other friends, the Kicker n. e. V., and everyone related with the Oldenbloc for the regular after work fun and sports.

Most importantly, I would like to thank my family. My parents for their guidance and the endless support. My brothers Rico and Julian, you live so far away but are with me every minute. Finally, I would like to thank Julia for her never-ending patience and love and especially for laughing about my worst jokes during this time. Without you this would not have been possible.

I hereby declare that I wrote this thesis independently and that I used only the indicated sources. I did not submit this thesis as a whole or in parts to any other university for evaluation for a conferral of a doctorate.

I confirm that I followed the general principals of good scientific practice, as they are specified in the guidelines of the Carl von Ossietzky University of Oldenburg. In connection with this dissertation project, I did not claim any commercial mentoring services.

Oldenburg, March 2017

Publications

Two publications resulted from this work of which one was an international cooperation with the work group of Prof. Marschner at the Technische Universität Graz and Dr. Baumgartner at the Karl Franzens Universität, Graz, Austria. The publications can be found as follows:

A Germylene Stabilized by Homoconjugation

Z. Dong, C. R. W. Reinhold, M. Schmidtmann, T. Müller, *Angew. Chem. Int. Ed.* **2016**, *55*, 15899.

The synthesis of a bicyclic germylene from the reaction of a germole dianion with hafnocene dichloride is reported. This germylene is stabilized by a homoconjugative interaction of the dicoordinated germanium atom with a remote C=C double bond. First reactivity studies revealed its nucleophilic character and resulted in the synthesis of bimetallic hafnium/iron and hafnium/tungsten complexes with a germylene group linker.

Oligosilanylated Antimony Compounds

R. Zitz, K. Gatterer, C. R. W. Reinhold, T. Müller, J. Baumgartner, C. Marschner, *Organometallics* **2015**, *34*, 1419.

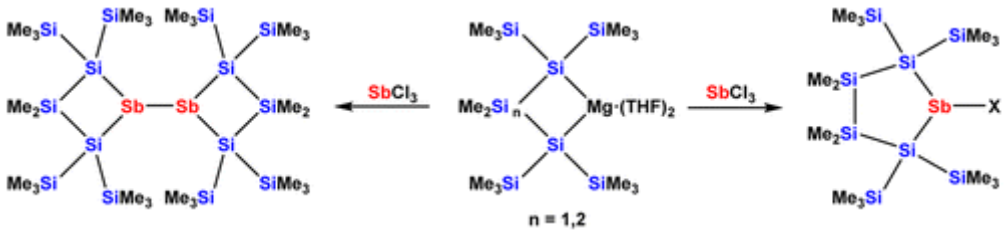

By reactions of magnesium oligosilanides with $SbCl_3$, a number of oligosilanylated antimony compounds were obtained. When oligosilanyl dianions were used either the expected cyclic disilylated halostibine was obtained or alternatively the formation of a distibine was observed. Deliberate formation of the distibine from the disilylated halostibine was achieved by reductive coupling with C_8K. Computational studies of Sb–Sb bond energies, barriers of pyramidal inversion at Sb, and the conformational behavior of distibines provided insight for the understanding of the spectroscopic properties.

Abstract

Siloles and germoles, the heavier group 14 homologues of cyclopentadiene, have developed a great interest in material design in the recent past. Because of their remarkable electronic and photo-physical properties highly functionalised compounds were synthesised. By the addition of localised spin centres in these macromolecules magnetic properties could be added. The first step of this approach is the synthesis of stable silolyl and germolyl radicals and the investigation of their stability which is the focus of this work.

To achieve this, several siloles and germoles with different substitution patterns were prepared and their behaviour under various reductive conditions investigated. In this context, persistent silolyl and germolyl radicals were successfully synthesised and identified by EPR spectroscopy and trapping reactions. These radicals showed remarkable stability, even in solution at room temperature. The experimental results were supported by extensive quantum mechanical calculations. By comparing several substituents in 1-position, the bulky $Si(SiMe)_3$ group was found to be most suitable to stabilise the radicals and to supress a dimerisation reaction. Furthermore, the calculations revealed that the pyramidalisation of the radical centre has significant influence on its hyperfine coupling constant (hfcc). The agreement of the experimentally obtained hfcc with the computed suggested accurate structures, which revealed pyramidalised radical centres with a mainly localised spin density distribution. This high thermodynamic stability and the distinct localisation of the spin density are fundamental for the use of sila- and germacyclopentadienyl radicals as localised spin centres.

During the investigations of the radicals, several potassium salts of anionic heterolyl compounds were also synthesised and structurally characterised. Even though various group 14 heterolyl mono- and dianions have been reported in the literature, unprecedented compounds with unexpected structural motifs in the solid state were observed and discussed in this work. It was found that the interplay between electron delocalisation (aromaticity) and coordination in these class of compounds is very subtle.

Apart from the described efforts to synthesise group 14 heterolyl radicals, an unexpected rearrangement reaction was discovered in which a germole is transformed into a silole. If the same reaction was carried out by using an analogue silole as starting material the formation of a new type of stable silylene was observed. Extensive DFT calculations revealed that the most important factor for the astonishing stability of the silylene is a homoconjugative interaction of the dicoordinated silicon atom with a remote alkenyl function. The decisive experimental evidence for this interaction is the unique high field shift of the ^{29}Si NMR resonance. This homoconjugative stabilisation of tetrylenes was found to be more efficient than conventional electron delocalisation

which is indicated by the fact that the tetrylenes are significantly favoured over the isomeric heavier homologues of benzene. The calculated HOMO/LUMO gap for the silylene is substantial and suggests a mostly nucleophilic reactivity pattern which was also investigated experimentally by the formation of a $Fe(CO)_4$ complex. The here presented type of tetrylene is unprecedented, and therefore, it might bear a great potential to be used in bond activation and in coordination chemistry.

Kurzzusammenfassung

Silole und Germole, die höheren Homologe des Cyclopentadiens, haben in den letzten Jahren großes Interesse gewonnen. Wegen ihrer besonderen elektronischen und photophysikalischen Eigenschaften konnten sie für die Synthese hochfunktionaler Werkstoffe eingesetzt werden. Durch das Einbringen von lokalen Spinzentren in diese Makromoleküle könnten magnetische Eigenschaften erzeugt werden. Der erste Schritt um derartige Materialien zu verwirklichen ist die Synthese von persistenten Heterolylradikalen, was im Rahmen dieser Arbeit untersucht wurde.

Hierfür wurden diverse Silole und Germole mit unterschiedlichen Substitutionsmustern synthetisiert und ihr Verhalten unter verschiedenen reduktiven Bedingungen untersucht. Auf diese Weise konnten persistente Silolyl- und Germolylradikale hergestellt werden, welche durch EPR Spektroskopie und Abfangreaktionen identifiziert wurden. Diese Radikale zeichnen sich durch ihre hohe Stabilität auch in Lösung bei Raumtemperatur aus. Die experimentellen Ergebnisse wurden durch quantenmechanische Rechnungen unterstützt und geleitet, wobei der Einfluss des Substituenten in 1-Position auf die Stabilität der Radikale und die Unterdrückung einer Dimerisierungsreaktion fokussiert wurde. Des Weiteren zeigten die Rechnungen, dass die Pyramidalisierung am Radikalzentrum großen Einfluss auf die Hyperfeinkopplungskonstante hat. Die Übereinstimmung von experimentellen und theoretischen Ergebnissen bestätigte die Qualität der Rechnungen, wodurch gezeigt werden konnte, dass die Zentren beider Radikale pyramidalisiert sind und ihre Spindichte jeweils überwiegend lokalisiert ist. Die unter Beweis gestellte thermodynamische Stabilität und die Lokalisierung der Spins bilden die Grundvoraussetzung für den Einsatz von Silolyl- und Germolylradikale als lokale Spinzentren.

Bei den Untersuchungen der Heterolylradikale wurden zusätzlich diverse Kaliumsalze von anionischen Heterolylverbindungen synthetisiert und strukturell charakterisiert. Obwohl bereits eine Vielzahl an Gruppe 14 Heterolylmonoanionen und -dianionen literaturbekannt sind, wurden im Zuge dieser Arbeit neuartige Verbindungen, welche ungewöhnliche Strukturmotive im Festkörper zeigten, synthetisiert und untersucht. Hierbei zeigte sich ein sehr bemerkenswerter Zusammenhang zwischen Elektronendelokalisation (Aromatizität) und Koordination der Gegenionen in diesen Verbindungsklassen.

Des Weiteren wurde im Rahmen dieser Arbeit eine Umlagerungsreaktion beobachtet, bei der ein Germol in ein Silol transformiert wird. Bei der Durchführung dieser Reaktion ausgehend von einem Silol wurde die Bildung eines neuartigen stabilen Silylens beobachtet. Durch quantenmechanische Untersuchungen konnte eine homokonjugative Wechselwirkung zwischen dem zweifach-koordinierten Siliciumatom und einer Alkenyleinheit als entscheidender Faktor für die erstaunliche Stabilität dieses Silylens identifiziert werden. Ein deutlicher experimenteller Beleg für diese

Wechselwirkung ist die ungewöhnliche Hochfeldverschiebung der ^{29}Si NMR Resonanz. Diese homokonjugative Stabilisierung der Tetrylene erweist sich als effizienter als konventionelle Elektronendelokalisierung, was sich in der Tatsache äußert, dass diese Tetrylene energetisch gegenüber den isomeren schweren Homologen des Benzols deutlich bevorzugt sind. Der berechnete Unterschied zwischen HOMO und LUMO des Silylens ist beträchtlich, wodurch ein nukleophiles Reaktionsverhalten erwartet wird. Dies wurde zusätzlich durch die Synthese eines entsprechenden $Fe(CO)_4$ Komplexes bestätigt. Tetrylene sind wichtige Verbindungsklassen für Bindungsaktivierungen und in der Koordinationschemie, wodurch die Synthese neuartiger Typen, wie dem hier gezeigten Silylen, von großem Interesse ist.

Table of Contents

1 Introduction 1

1.1 Heteroles 1

1.2 Group 14 Heteroles 1

1.2.1 Electronic Structure 1

1.2.2 Properties in Material Design 4

1.2.3 Synthesis 5

1.3 Radicals 7

1.3.1 Silolyl Radicals 7

1.3.2 Radicals in π-Conjugated Systems 8

1.3.3 Bisradical Systems 9

1.3.4 Potential of Heterolyl Radicals in Material Design 10

1.4 Group 14 Heterolyl Anions 10

1.5 Heterole Based Silylenes 12

1.6 Previous Attempts on the Synthesis of Heterolyl Radicals 13

2 Motivation 15

3 Results and Discussion 17

3.1 Synthesis and Functionalisation of Group 14 Heteroles 17

3.1.1 Synthesis and Functionalisation of Germoles 17

3.1.2 Synthesis and Functionalisation of Siloles 21

3.2 Sila- and Germacyclopentadienyl Radicals 24

3.2.1 Reduction Reactions of 1-Halo Group 14 Heteroles to their Radicals 25

3.2.2 Attempted Cleavage of the Ge-Ge Bond of Bisgermoles 29

3.2.3 Theoretical Determination of Suitable Substituents for Stable Radicals 30

3.2.4 Reduction of 1-Tris(trimethylsilyl)silylgermolyl chloride 33

3.2.5 Reduction of 1-Tris(trimethylsilyl)silylsilolyl chloride 46

3.2.6 Formation of 1-Tris(trimethylsilyl)silyl Sila- and Germacyclopentadienyl Radicals . 55

3.3 Sila- and Germacyclopentadienyl Anions 58

3.3.1 Germole Anions 58
3.3.2 Silole Anions 64
3.4 Rearrangement Reactions of Sila- and Germacyclopentadienes 74
3.4.1 Rearrangement Reactions of Germoles 74
3.4.2 Rearrangement Reactions of Siloles 79
4 Summary and Outlook 97
5 Experimental 103
5.1 General Preparative Procedures 103
5.2 Starting Materials 104
5.2.1 Synthesis of Germoles 105
5.2.2 Functionalisation of Germoles 109
5.2.3 Synthesis of Siloles 114
5.2.4 Functionalisation of Siloles 116
5.3 Reduction Reactions of Germoles and Siloles 118
5.4 Rearrangement Reactions 122
6 Literature 127
7 Appendix 132
7.1 Computational Details 132
7.1.1 Gaussian Example Input 133
7.1.2 ORCA Example Input 134
7.1.3 EasySpin Toolbox for MATLAB Inputs 135
7.2 Crystallographic Data 136
7.3 Abbreviations 155
8 Curriculum Vitae 157

1 Introduction

1.1 Heteroles

Heteroles are unsaturated five-membered rings which contain at least two different types of elements. In the context of this work the homologues of cyclopentadiene which bear one heteroatom were focused. This class of compounds containing elements of group 15 and 16 are, due to their natural abundance, extensively investigated and are of great importance for organic synthesis.

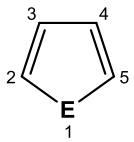

E = CH_2	Cyclopentadiene
E = SiH_2	**Silole**
E = GeH_2	**Germole**
E = NH	Azole (Pyrrole)
E = PH	Phosphole
E = O	Oxole (Furan)
E = S	Thiole (Thiophene)

In comparison, the field of application for heteroles of heavier group 14 elements is quite narrow, and therefore, they gained less attention in the past. However, in the last 30 years, various different compounds based on sila- and germacyclopentadienes (siloles and germoles)[1] with remarkable electronic and photo-physical properties were synthesised.[2-4] Among these are chromophores with fluorescing properties and copolymers which show, upon doping with iodine vapour, conductivity in the range of semiconductors. These features can be explained by the unique electronic structure[3,5] of heavier group 14 heteroles which makes them very promising precursors for the design of highly functionalised materials.

1.2 Group 14 Heteroles

1.2.1 Electronic Structure

Even though siloles and germoles are the next heavier homologues of cyclopentadiene, the difference in their electronic structure is significant.[3,5] Atwell et al.,[6] as well as Breeden and O'Brien,[7] claimed that siloles can be reduced by alkali metals to get the respective di- and tetraanions (Scheme 1).

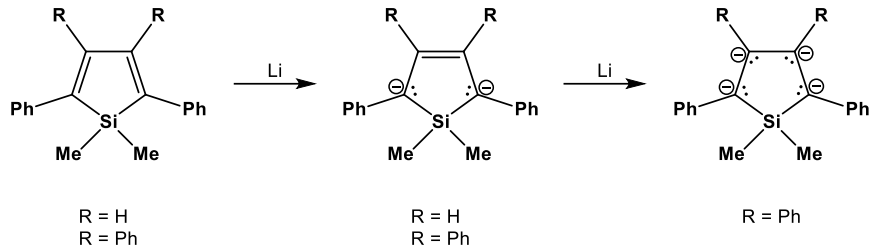

Scheme 1: Reduction of siloles to di- and tetraanions.[6,7]

This high electron affinity was further investigated by quantum mechanical calculations by Tamao et al., which revealed significant differences in the orbital energies (Figure 1, given values were recalculated at the more accurate M06-2X/Def2-TZVPD level of theory while the trend remained the same and the values for germole, stannole and plumbole were added).[3] While the energy level of the HOMO of silole is $\Delta E_{C/Si}$ = 0.47 eV lower compared to the HOMO of cyclopentadiene, the LUMO energy is even $\Delta E_{C/Si}$ = 1.03 eV lower, leading to a much smaller HOMO/LUMO gap $\Delta E_{H/L}$.

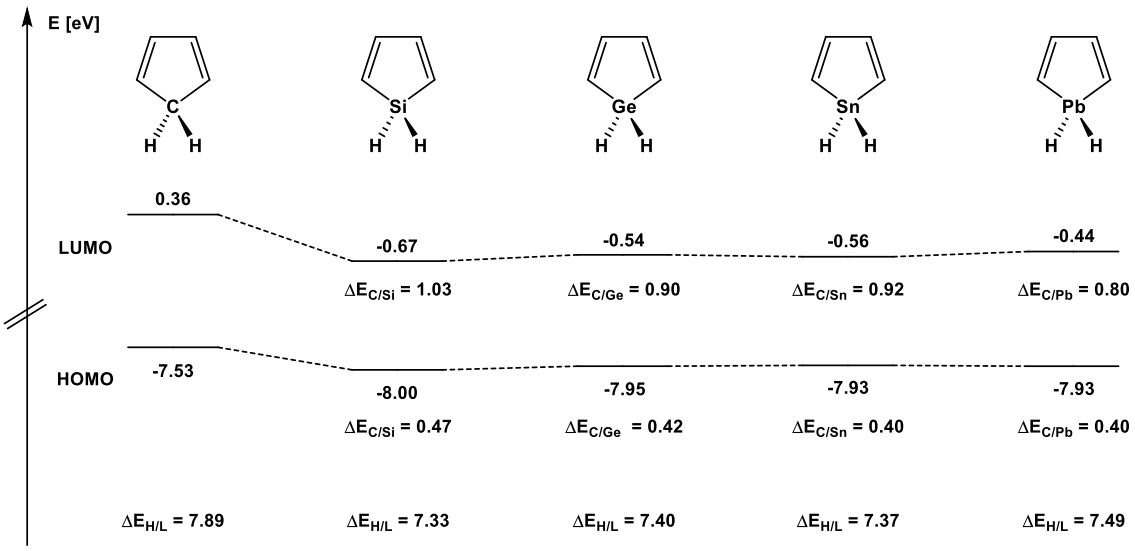

Figure 1: Caclulated orbital energies and HOMO/LUMO gaps $\Delta E_{H/L}$ of group 14 heteroles in comparison to cyclopentadiene. Given values by Tamao et al. were recalculated at the more accurate M06-2X/ Def2-TZVPD level of theory and the orbital energies of germole, stannole and plumbole were added.[3]

When comparing the HOMO and LUMO energies of the heavier group 14 homologues to those of cyclopentadiene, the trend remains the same, suggesting that a similar reactivity for germoles, stannoles, and plumboles can be expected.

The reason for such low LUMO energies of the heteroles can be found in a favourable orbital overlap of the σ*-orbitals of the exocyclic σ-bonded substituents at the heteroatom with the π*-orbital of the butadiene system. Such a σ*-π*-conjugation is barely developed in the cyclopentadiene due to the significant higher energy of the σ*-orbitals of the exocyclic substituents compared to the π*-orbital of the butadiene system (Figure 2).[3]

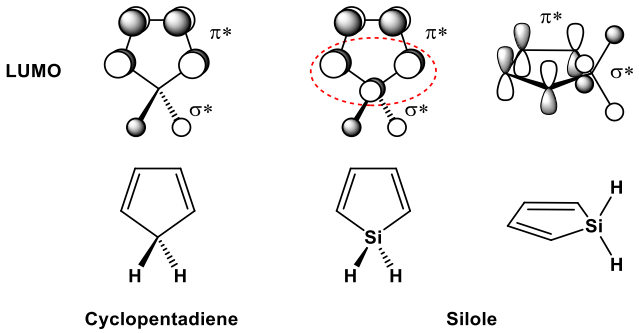

Figure 2: Favourable σ*-π*-orbital overlap of siloles.[3]

In addition to the comparison of group 14 heteroles, Tamao et al. also calculated the orbital energies of pyrrole, furan, thiophene and pyridine and compared them to those of silole. The obtained values, summarised in Figure 3, reveal that silole has the lowest LUMO energy which leads to the smallest HOMO/LUMO gap $\Delta E_{H/L}$ (given values were recalculated at the more accurate M06-2X/Def2-TZVPD level of theory while the trend remained the same).[3] These electronic properties of silole derivatives and their heavier homologues opened the field for their application in functionalised materials.

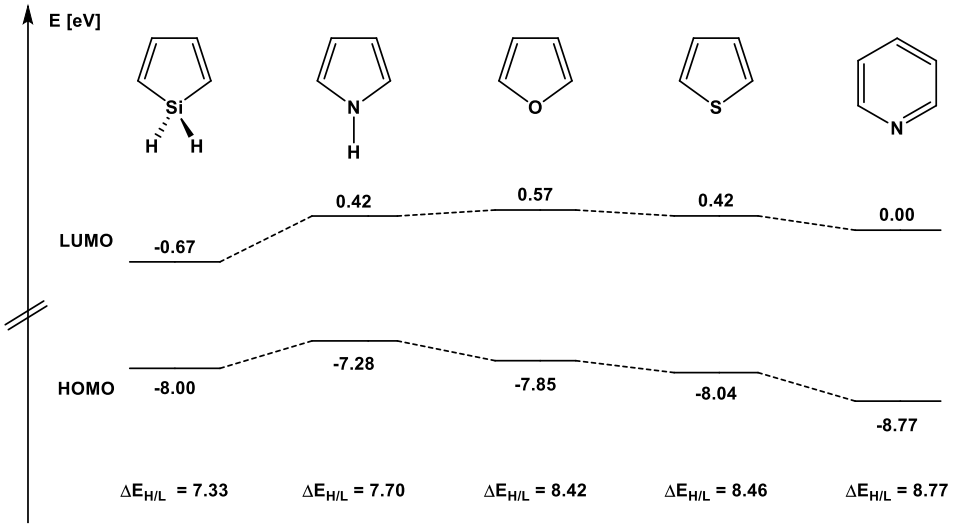

Figure 3: Caclulated orbital energies and HOMO/LUMO gaps $\Delta E_{H/L}$ of silole and several different heteroles and pyridine. Given values by Tamao et al. were recalculated at the more accurate M06-2X/Def2-TZVPD level of theory.[3]

1.2.2 Properties in Material Design

Based on the unique electronic structure of group 14 heteroles, they became important building blocks in material design. The low LUMO orbital energy allowed the use of siloles and germoles in the design of organic light emitting diodes (OLED) and functional polymeric materials.[8,9] Tamao et al.[2,4] succeeded to synthesise several luminescent siloles in which the wavelength of the photoluminescence was altered by changing the substituents in 2,5-position. The aryl or thiophenyl substituted compounds **1**-**3** are three examples.

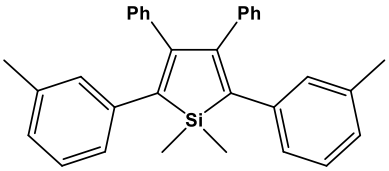

1
λ_{em} = 471 nm
green-blue

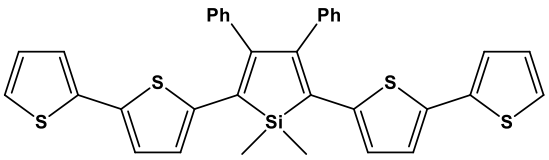

2
λ_{em} = 556 nm
red-orange

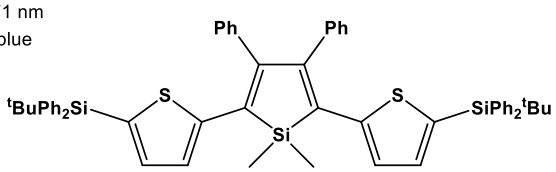

3
λ_{em} = 515 nm
yellow-green

Another area of application of group 14 heteroles is their use in π-conjugated copolymers. Copolymers of siloles or germoles in combination with arenes or other heteroles showed remarkable chromophoric and luminescent properties such as in **4** or **5**. Additionally, the small HOMO/LUMO gap of the group 14 heteroles in these copolymers led to narrow valence and conduction band gaps. Therefore, thiophene bridged silole copolymers, such as **5**, revealed, upon doping with iodine vapour, conductivity in the range of semiconductors.[10-12]

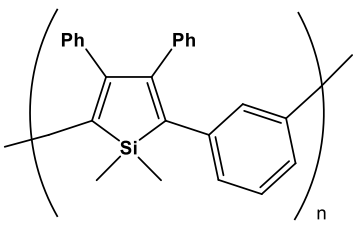

4
M_n = 2800
λ_{em} = 310 nm

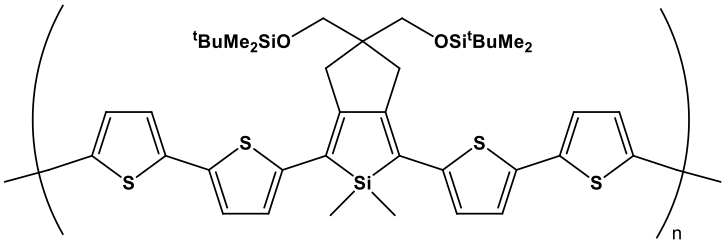

5
M_n = 31700
λ_{em} = 549 nm
σ = 2.4 S cm^{-1}

Furthermore, Tilley et al. investigated germole-arene copolymers, such as **6**, which were also chromophoric with photoluminescent properties. Interestingly, they were able to show the influence of the polymeric chain length on the respective wavelength of the luminescence.[13]

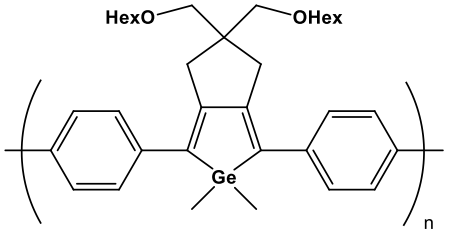

6

M_n = 1900 λ_{em} = 486 nm
M_n = 4700 λ_{em} = 498 nm
M_n = 20000 λ_{em} = 500 nm

1.2.3 Synthesis

1.2.3.1 Siloles

For the synthesis of siloles several different approaches are reported.[1] However, two pathways emerged to be the most applicable (Scheme 2). One is the cyclisation of 1,4-dilithio-1,3-butadienes with silicon tetrahalides or tetramethoxysilane (**I**, Scheme 2). The other is the reductive cyclisation of bisalkinyl substituted silanes with lithiumnaphthalide (**II**, Scheme 2).[14-17]

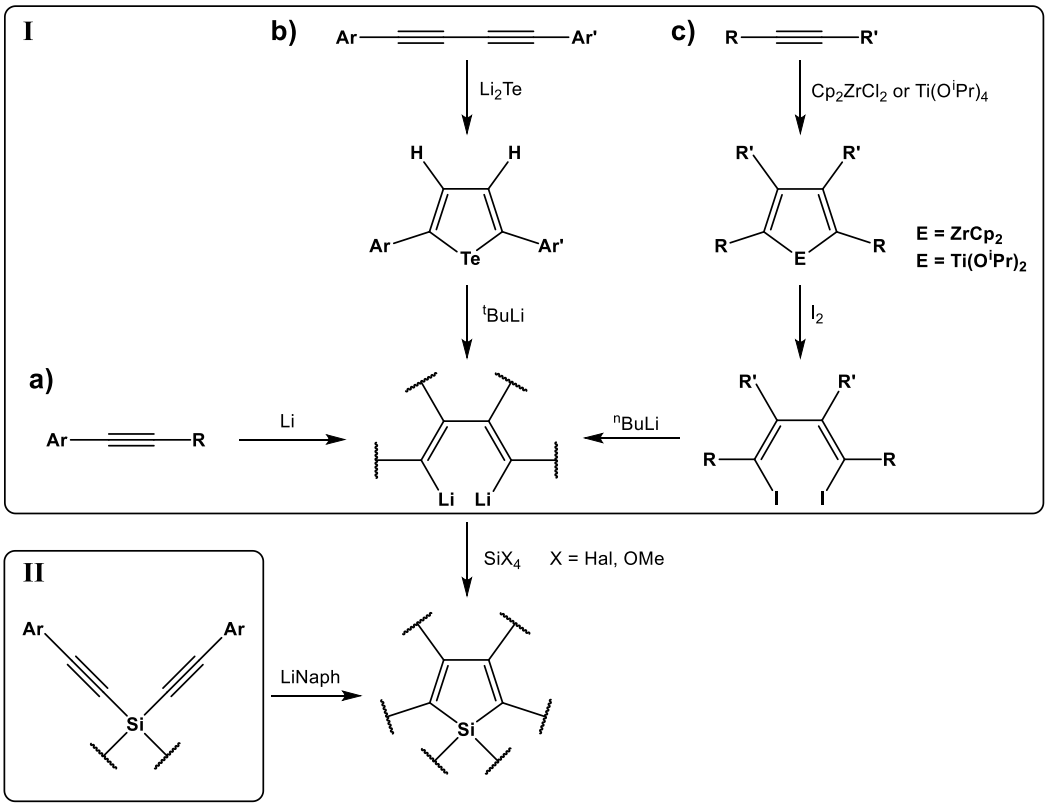

Scheme 2: Possible approaches for the synthesis of siloles.

To obtain the 1,4-dilithio-1,3-butadienes, which are needed in pathway **I**, different approaches are possible (**I a**, **b** and **c**, Scheme 2). Alkynes can be reduced by lithium to yield the 1,4-dilithio-1,3-butadienes (**a**). However, this reaction only performs well if at least monoaryl substituted alkynes are used.[18-20] Another path is the reaction of bisalkynes to telluracyclopentadienes which can be lithiated by tert-butyllithium leading to the corresponding dilithiobutadienes (**b**). This method is also described to work exclusively with bisalkynes which bear terminal aryl substitution.[21] The third approach is the coupling of alkynes to zircona-[22-27] or titanacyclopentadienes[28,29] which can be treated with iodine to obtain 1,4-diiodobutadienes. These can be reacted with n-butyllithium to form respective 1,4-dilithio-1,3-butadienes (**c**). The advantage of this type of reaction is the broad variety of alkynes which can be used. The synthesised dilithio compounds can be cyclised to silole derivatives in the reaction with functionalised silanes such as silicon tetrachloride. Tamao et al. reported that the cyclisation reaction does not proceed selectively if the substituents on the butadiene are sterically too demanding. The performance of this reaction was increased significantly by using tetramethoxysilane as cyclisation reagent.[24,30,31]

1.2.3.2 Germoles

For the synthesis of germoles **8**, analogue methods are described. Terminal aryl substituted alkynes can be reduced to 1,4-dilithio-1,3-butadienes **7** which can be cyclised with the respective germanium tetrahalide (Scheme 3).[32]

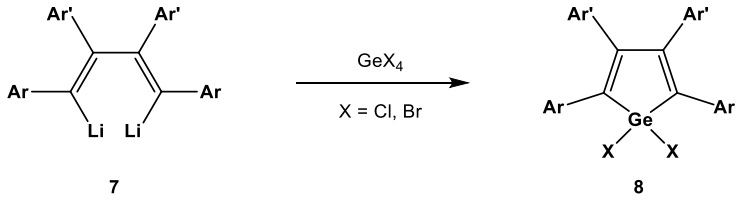

7 8

Scheme 3: Cyclisation reaction of 1,4-dilithio-1,3-butadienes **7** with germanium tetrahalide to yield germole derivatives **8**.[32]

The most convenient way synthesising germoles **11** is via zirconacyclopentadienes **10**. In contrast to the silole synthesis, the zirconacyclopentadienes **10** perform a metal exchange reaction in which the $ZrCp_2$-fragment is replaced by a dihalogermane and the starting material Cp_2ZrX_2 is formed (Scheme 4).[26,33,34] However, this method is not applicable for the synthesis of siloles **9** because silicon tetrachloride does not react at all in this reaction and the use of silicon tetrabromide only result in very low yields.[35]

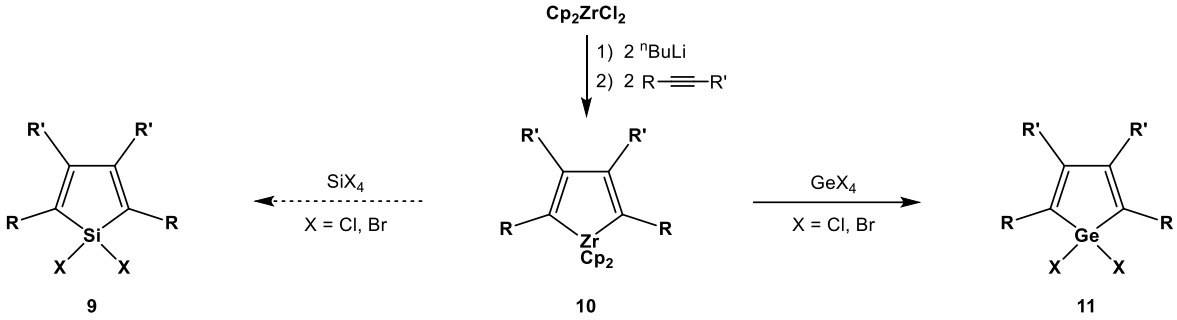

Scheme 4: Synthesis of zirconacyclopentadienes **10** and the following metal exchange reaction to germoles **11**.[26,33,34]

1.3 Radicals

1.3.1 Silolyl Radicals

Janzen, Pickett, and Atwell were able to reduce 1,1-dimethyl-2,3,4,5-tetraphenyl silole **12** not only to the respective dianion **14** but also to the radical anion **13** (Scheme 5). The formation of the radical species **13** was observed by EPR and UV-Vis spectroscopy.[6]

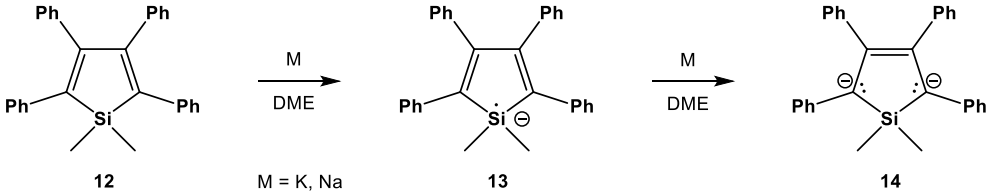

Scheme 5: Reduction of 1,1-dimethyl-2,3,4,5-tetraphenyl silole **12** to the respective radical anion **13** and the dianion **14** by alkali metals.[6]

Furthermore, West et al. described the synthesis of a bis(silafluorenyl radical) dianion **16** which was obtained by the reaction of silafluorenyl dianion **15** with potassium in the presence of 18-crown-6 and dimethoxyethane (DME) (Scheme 6).[36]

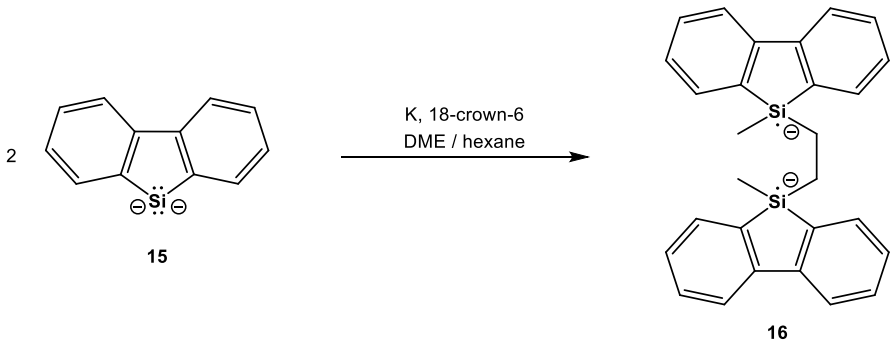

Scheme 6: Synthesis of the bis(silafluorenylradical) dianion **16**.[36]

The first neutral, tricoordinated silolyl radical compound was also synthesised by West et al. by reacting the silolyl dianion **18** with 1,1-dichloro-2,3-diphenylpropene **19**. The product of this reaction was the bisradical **20** and the derived rearrangement product **21** (Scheme 7).[37] The rearrangement reaction was accelerated by heating the sample or exposing it to air. Under inert atmosphere the bisradical **20** showed high stability. After 2.5 years only 2/3 of the bisradical **20** reacted to the rearrangement product **21**. Furthermore, the bisradical **20** was described to be inert in the presence of water, methanol or chloroform. Such high stability implies that heavier group 14 heteroles are promising precursors for the synthesis of persistent main group radicals in a highly functionalised π-conjugated system which can be exploited in material design.

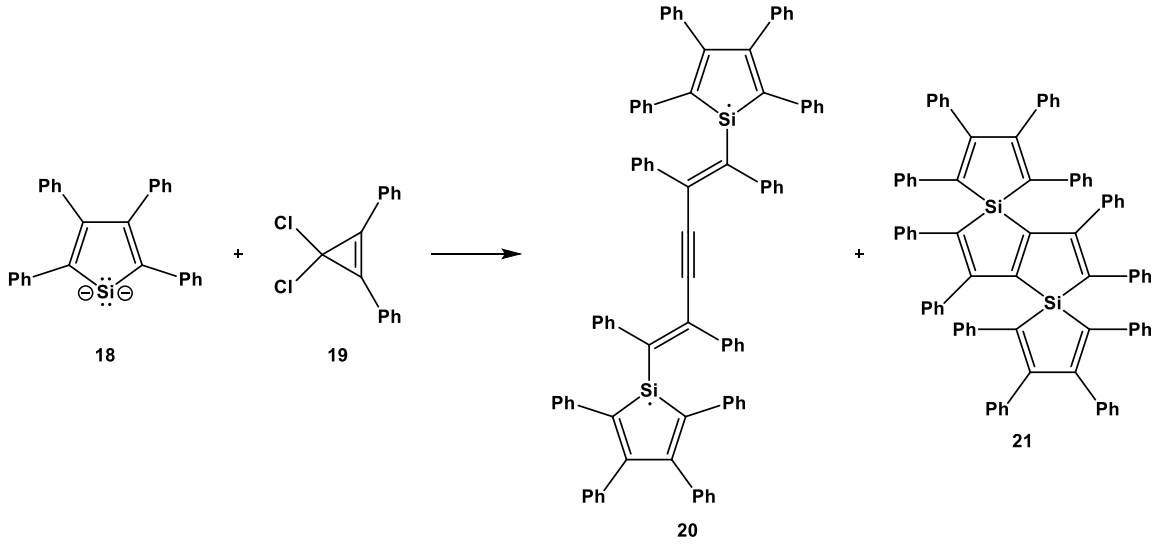

Scheme 7: Synthesis of the first neutral silolyl radical **20** and its rearrangement reaction.[37]

1.3.2 Radicals in π-Conjugated Systems

Radicals which are connected through π-conjugated systems can show singlet or triplet coupling. Essential for this phenomenon is the spin polarisation. Spin densities of neighbouring nuclei prefer opposite spins α = 1/2 and β = -1/2. Based on the equation of Ovchinnikov (eq. 1-3), in which n_α and n_β describe the number of the respective spins α or β, the resulting net spin can be determined.[38]

$$S = n_\alpha \alpha + n_\beta \beta \qquad \text{eq. 1}$$

$$S = n_\alpha \cdot \left(\frac{1}{2}\right) + n_\beta \cdot \left(-\frac{1}{2}\right) \qquad \text{eq. 2}$$

$$S = \frac{n_\alpha - n_\beta}{2} \qquad \text{eq. 3}$$

Based on eq. 3, no net spin will result ($S = 0$), if each of the spins are paired (e.g. $n_\alpha = 1$, $n_\beta = 1$). This represents antiferromagnetic coupling and a singlet ground state. If the number of spins are uneven (e.g. $n_\alpha = 2$, $n_\beta = 0$, for a bisradical), a net spin will result ($S = 1$) which represents ferromagnetic coupling and a triplet ground state. In conclusion, a net spin will only result if the number of atoms between two radical centres in a π-conjugated system is uneven.[39] Such a spin coupling is also known as the Goodenough Kanamori rule.[40-42]

1.3.3 Bisradical Systems

Bisradical systems have been studied extensively in the past to further investigate the coupling of radicals and the mechanism of bond breaking and formation processes.[43-45] Especially the homologues derived from cyclobutanediyl attracted great interest in the past two decades (Figure 4). While Niecke et al.,[46-52] followed by Bertrand et al.,[53,54] carried out pioneering work in this field, Power et al.[55] and Sekiguchi et al.[56] reported the first heavier group 14 homologues. Schulz et al.[57,58] contributed analogue group 15 derivatives in the recent past.

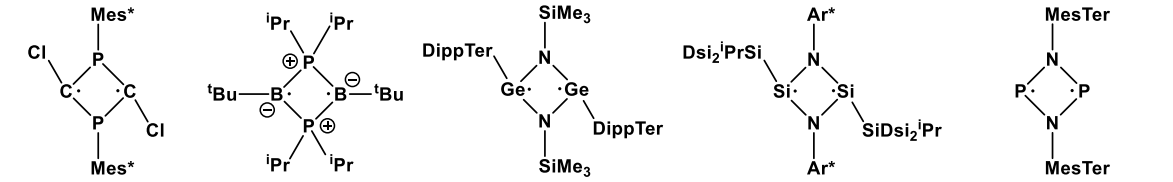

Niecke et al.[46] Bertrand et al.[53,54] Power et al.[55] Sekiguchi et al.[56] Schulz et al.[57,58]

Figure 4: Bisradical systems derived from cyclobutanediyl.

The sensitive equilibrium between open and closed shell systems in the cyclobutanediyl homologues was investigated extensively and most of these compounds revealed a singlet ground state with bisradical character. The terminology of "bisradicaloids" was found to be more suitable for these systems.

In contrast, different heavier group 14 bisradical systems were reported by Sekiguchi et al.[59] This group succeeded to synthesise the *p*- and *m*-phenylene bridged, halogen substituted bissilanes **22** and **24** which were reduced by two equivalents of potassium graphite. In case of the *p*-bridged compound **22** the reduction resulted in the formation of a bissilaquinodimethane structure **23**. In contrast, in the *m*-bridged bissilane **24** the conjugation does not allow the formation of a bissilaquinone structure. Therefore, the reduction led to the formation of the bisradical **25** which was found to have a triplet ground state (Scheme 8).

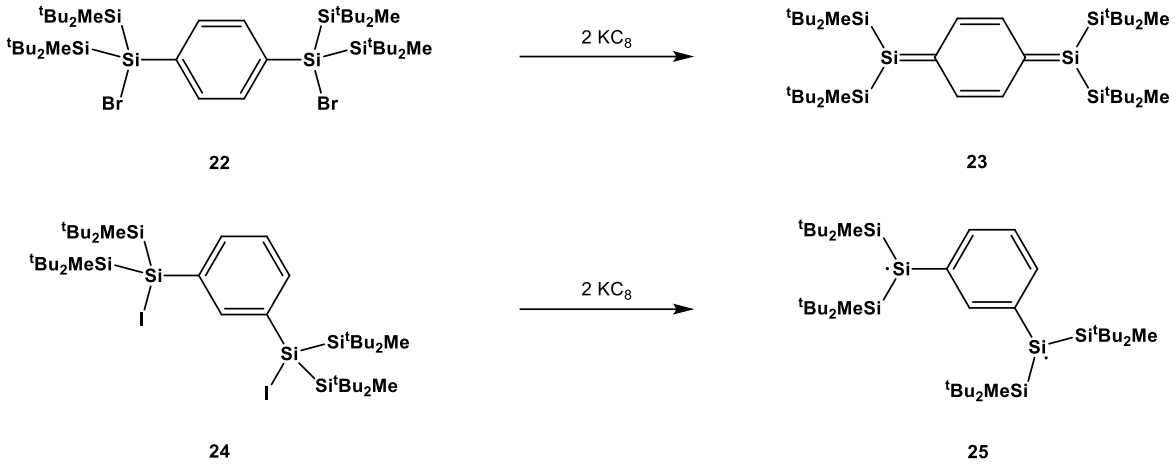

Scheme 8: Synthesis of a bissilaquinodimethane **23** and a triplet bissilabisradical **25**.[59]

1.3.4 Potential of Heterolyl Radicals in Material Design

As already discussed in Chapter 1.2.2, group 14 heteroles are, due to their unique photo-physical (**II** , Figure 5) and electronic properties (**III** , Figure 5), of great interest for the design of highly functionalised materials.[2-4] By creating localised spin centres in those heterocycles, interesting functionalities could be added (**I** , Figure 5). Especially the incorporation of these systems in macromolecules could lead to cooperative effects.[59] Therefore, persistent heterolyl radicals are promising precursors for the design of magnetic molecular building blocks for highly functionalised polymers.

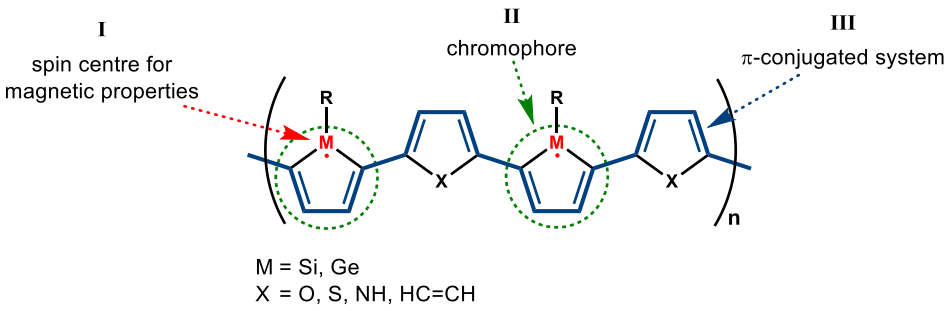

Figure 5: Potential of group 14 heterole copolymers for the design of highly functionalised materials.

1.4 Group 14 Heterolyl Anions

The cyclopentadienyl anion and its derivatives are, due to the six π-electron aromatic ring system, among the most important ligands in transition metal coordination chemistry. Therefore, the use of the heavier group 14 homologues was investigated extensively in the past and significant differences to the cyclopentadienyl anion are reported (Figure 6).[36,60-68] Solid state structures of

such anions obtained by X-ray diffraction analysis, supported by quantum mechanical calculations, revealed that in 1-positon monosubstituted silolyl or germolyl anions are, unlike to the carbon analogue, pyramidalised at the central element. The lone pair is localised at the silicon or germanium atom instead of being conjugated in the ring system. This lack of conjugation is also indicated by the alternating carbon-carbon bond lengths which are clearly defining two double bonds and one single bond. Therefore, group 14 heterolyl monoanions are non-aromatic.[63,68,69]

Interestingly though, these monoanions can be used in coordination chemistry of transition metals which is shown in the ruthenium, hafnium or zirconium complexes in Figure 6. In these complexes, the heterolyl anions are η^5-coordinated to the respective metal, similar to the analogue cyclo-pentadienyl anion complexes. The planar coordination at the element centre and the equalising carbon-carbon bond lengths clearly indicate conjugation of the lone pair in the ring system, which suggests an aromatic structure.[62,64,65]

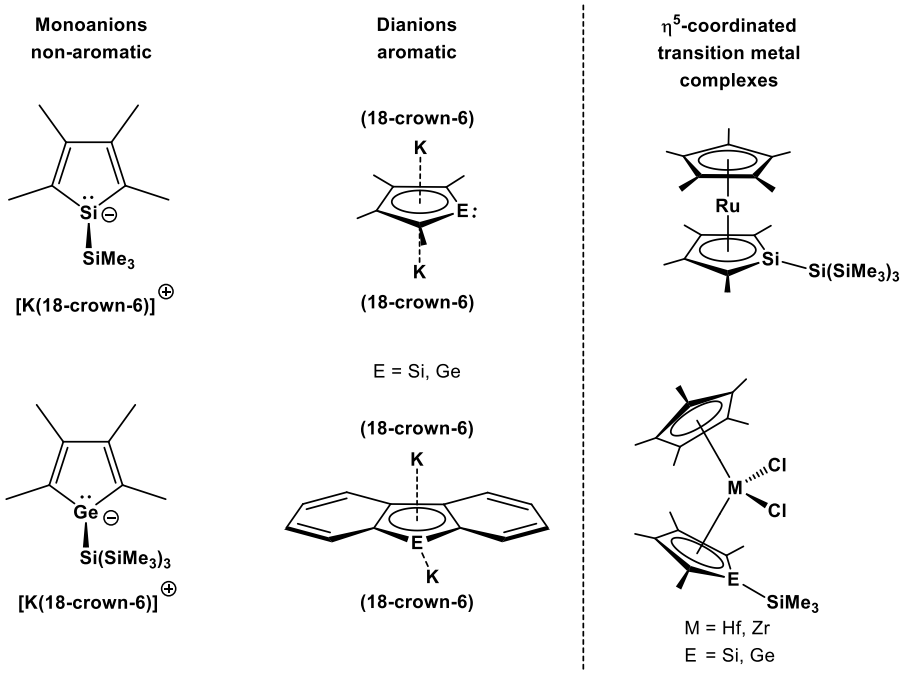

Figure 6: Examples of group 14 heterolyl mono- and dianions and η^5-coordinated transition metal complexes.[36,60-68]

In contrast to the monoanions, the dianions of group 14 heteroles revealed a different structure. Reported silolyl and germolyl dianions and the derived sila- or germafluorenyl dianions showed a high degree of conjugation with a planar structure and equalising carbon-carbon bond lengths. Supported by theoretical investigations, these dianions are suggested to have significant aromatic character. Their structure is best described to have one delocalised lone pair in the five-membered ring system while the other lone pair is localised at the central heteroelement.[60,63,66,70-72] Therefore, the description of these dianions as reduced silylenes should also be considered.

1.5 Heterole Based Silylenes

Another interesting type of structure is the silole based silylene **26** which was reported by Cui et al.[73] These so called silolylenes have four π-electrons and constitute a cyclic conjugated system involving the empty 3p orbital at the silicon. Therefore, they have to be considered as antiaromatic and highly reactive. Previous investigations only succeeded in frozen hydrocarbon matrices with subsequent trapping reactions.[74] However, the isolation of the silolylene **26** was accomplished by the stabilisation with a NHC (Figure 7).[73] The bonding situation in NHC stabilised silylenes is a very delicate topic and it has been reported that these types of structures can also be considered as neutral silyl anion equivalents (**26b**).[75] At a closer look, the structural metrics of the silolylene **26**, such as the sum of angles at the silicon centre as indicator for the pyramidalisation of ∑α(Si) = 303°, are comparable to those which are expected for in 1-position monosubstituted silolyl anions (e.g. ∑α(Si) = 281° for **27**) . Additionally, the presented ^{29}Si NMR shift of δ^{29}Si = -43.6 is in the same range as of the potassium salt of the 1-trimethylsilyl substituted silolyl anion **27** of δ^{29}Si = -41.5 reported by Tilley et al., which supports the suggested similarity.[63]

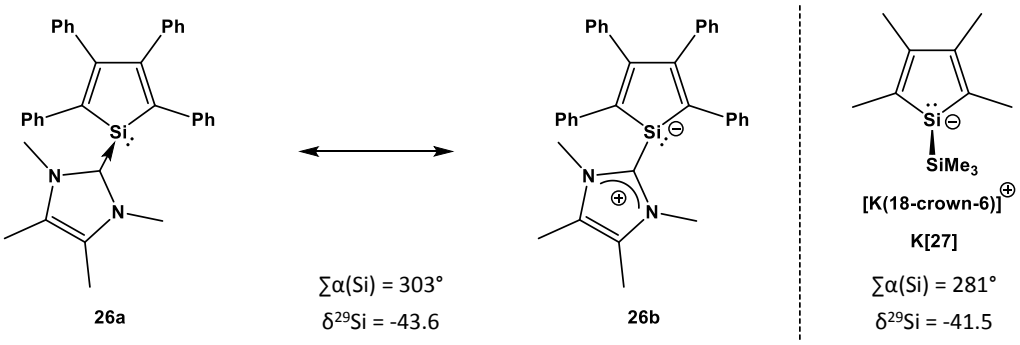

Figure 7: Possible resonance structures of NHC stabilised silolylene **26** by Cui et al. and comparison to the potassium salt of silolyl anion **27** by Tilley et al.[63,73]

1.6 Previous Attempts on the Synthesis of Heterolyl Radicals

In previous works, a broad variety of silolyl and germolyl compounds have been synthesised.[76-78] The basic idea was the synthesis of *p*- and *m*-arylene bridged 1-hydrogen substituted heteroles as precursors for the respective radical species. By using different synthetic approaches, compounds with several substitution patterns in the 2,3,4,5-position were synthesised and additional arylene bridging in 1-position and 3-position was achieved.

First attempts on the synthesis of silolyl radicals were performed in cooperation with the work group of Prof. Apeloig at the Technion in Haifa, Israel.[77] To investigate the reactivity, 1-hydrogen substituted siloles were treated with radicals known to be able to abstract hydrogen. In case of pentaphenylsilole **28**, which was reacted with the $Cp(CO)_3Mo$ radical, the allylic radical **30** was observed. This radical was most likely formed by the reaction of the expected silolyl radical **29** with residual starting silole **28** (Scheme 9).

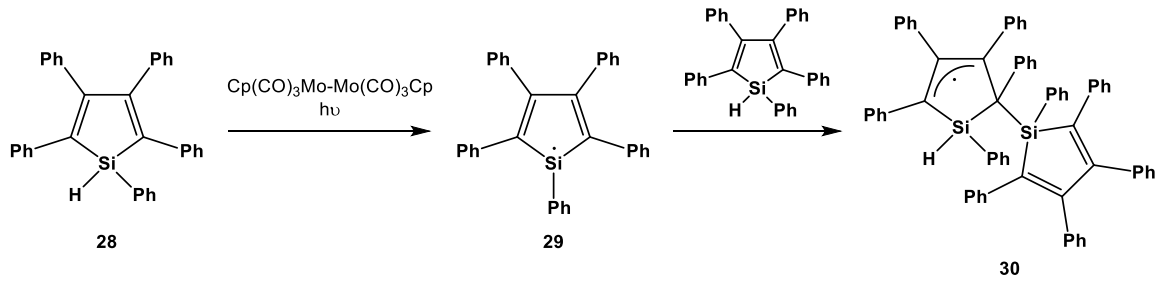

Scheme 9: Attempts on the synthesis of pentaphenylsilolyl radical **29**.[77]

Additionally, 1-phenyl-2,5-bistrimethylsilylsilole **31** was treated with $[(^iPrO)_2(O)P]_2Hg$ and irradiated. In this case, the formation of an allylic radical (**32**) was also observed. Unlike to the previous reaction, the detection of a coupling of the electron to a ^{31}P nuclei suggested the $(^iPrO)_2(O)P$ radical fragment was added in 2-position to the silole **31**, instead of generating a silicon centred radical (Scheme 10).

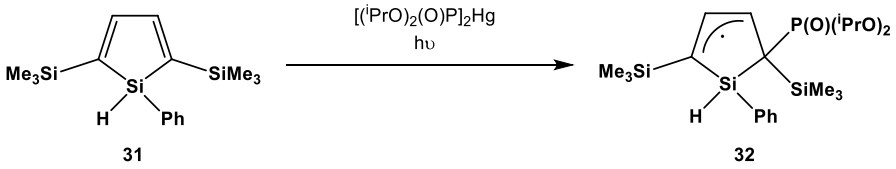

Scheme 10: Attempts on generating a silolyl radical with the $(^iPrO)_2(O)P$-radical fragment.[77]

Generating group 14 heterolyl radicals based on 1-hydrogen substituted precursor compounds did not seem to be a promising approach. Therefore, a different method was investigated. The 1-chloro-1-phenylgermole **33** was reduced with one equivalent of potassium graphite but instead

of the expected radical species **34** a dimeric structure **35** was observed (Scheme 11). However, the most reasonable explanation for the formation of the bisgermole **35** is the dimerisation of the germolyl radical **34**. These results classified the reduction of 1-halogene substituted group 14 heteroles with alkali metals to be a promising approach for the synthesis of heterolyl radicals.[76]

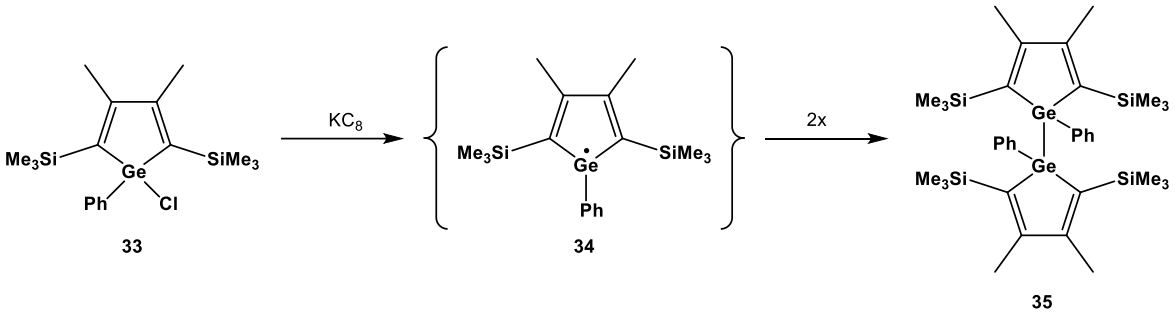

Scheme 11: Reduction of the chlorogermole **33** with potassium graphite yielding the bisgermole **35**.[76]

The reduction of the *p*-phenylene bridged bisgermole **36** with two equivalents of potassium graphite did not result in the formation of a radical species or an identifiable product such as **37** (Scheme 12).[76]

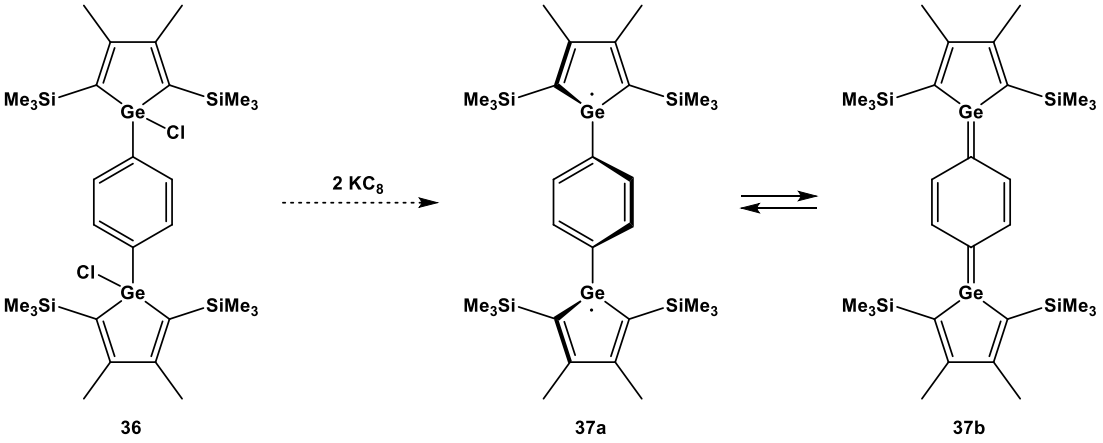

Scheme 12: Unsuccessful attempts on the reduction of the *p*-phenylene bridged bisgermole **36** with potassium graphite.[76]

2 Motivation

The focus of this thesis was the synthesis of halogen substituted sila- and germacyclopentadiene derivatives and the investigation of their behaviour under various reductive conditions. The aim was to obtain stable silolyl and germolyl radicals to further develop the potential of group 14 heteroles for the design of highly functionalised materials

To achieve this, the synthesis of several siloles and germoles with different substitution patterns (**38**) was focused on and the effect of these substituents on the stability of heterolyl radicals, especially in 1-position, was evaluated by the use of quantum mechanical calculations.

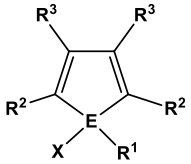

38

E = Si, Ge
X = Cl, Br
R^1 = ^{t}Bu, Pemp (C_6Me_5), $Si(SiMe_3)_3$, $Ge(SiMe_3)_3$
R^2 = $SiMe_3$, $SiEt_3$, Si^tBuMe_2
R^3 = Me, Ph

Subsequently, the potential of these halogen substituted siloles and germoles to form radical species by reduction reactions with different reagents, such as alkali metals or organometallic compounds, were investigated (Scheme 13).

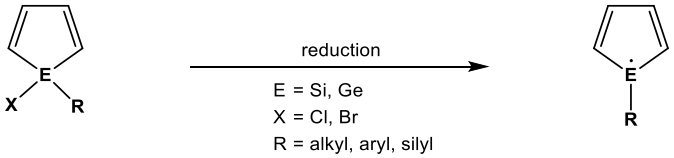

Scheme 13: Reduction reactions of 1-halogene substituted heteroles to the respective radicals.

The equilibrium of the radical species and their dimerisation products, as observed in previous work, was investigated (Scheme 14). In this context, the substituent in 1-position has the most significant influence to suppress a dimerisation reaction and was therefore concentrated on.

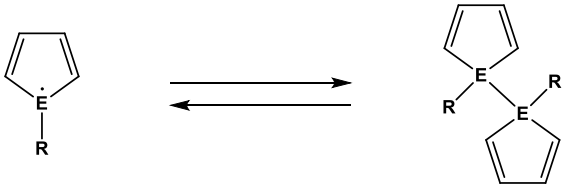

Scheme 14: Equilibrium of heterolyl radicals and their respective dimers.

The synthesis of persistent group 14 heterolyl radicals is of great interest because it represents the first step in the approach to exploit localised spin centres to add magnetic properties to macromolecules. Therefore, they are promising precursor compounds for the design of magnetic molecular building blocks for highly functionalised polymers.

3 Results and Discussion

3.1 Synthesis and Functionalisation of Group 14 Heteroles

For the synthesis of group 14 heteroles, two different approaches to construct the five-membered rings were considered. In the following the syntheses of 1-halogen substituted sila- and germacyclopentadienes are described. 1-Hydrogen substituted siloles which were used in some reactions have been synthesised in previous works and were available.[77]

3.1.1 Synthesis and Functionalisation of Germoles

All germacyclopentadienes were synthesised by a procedure developed by Fagan and Nugent,[22,23] in which alkynes are cyclised to zirconacyclopentadienes **10** in a Negishi coupling reaction.[27] Then, these heteroles can be used in an element exchange reaction with a broad variety of main group halides including germanium tetrachloride and tetrabromide (Scheme 15).

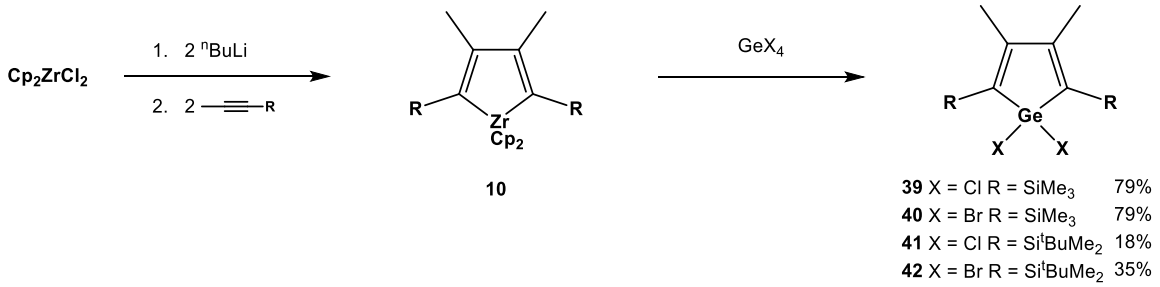

Scheme 15: Synthesis of germacyclopentadienes **39**-**42**.[22,23,27,63,76,79-81]

To prevent side reactions on the germole ring in the following steps, sterically demanding substituents in the 2,5-position are needed. Therefore, 1-(trimethylsilyl)propyne and 1-(tert-butyldimethylsilyl)propyne were used in the cyclisation reaction. In this way, 1,1-dichlorides and 1,1-dibromides of the 2,5-trimethylsilyl and 2,5-tert-butyldimethylsilyl substituted germoles **39**-**42** were synthesised. By performing this reaction as a one pot synthesis, in which the zirconacyclopentadiene is formed *in situ* before the element exchange, the procedure was simplified significantly. Additionally, using a solvent mixture of pentane and THF (4:1) the reaction time of the element exchange reaction was decreased by days compared to using only pentane. The workup was also simplified due to the precipitation of Cp_2ZrX_2 compared to performing the reaction in THF. A fast aqueous workup and additional washing with cold ethanol were feasible for chlorogermole **39** which sped up the process and increased the purity of the product drastically. Using 1-phenyl-

2-(trimethylsilyl)-acetylene in the cyclisation reaction to form 2,5-(trimethylsilyl)-3,4-phenyl substituted germoles did not succeed.

NMR spectroscopic data of the synthesised 1,1-dihalo germoles **39**-**42** are summarised in Table 1 and selected structural metrics obtained by X-ray diffraction analysis are given in Table 2. No distinct differences were noted in the collected data of the products, all values were within the standard ranges for 1,1-dihalogermoles.[79]

Table 1: NMR spectroscopic data of 1,1-dihalogermoles shown in Scheme 15 in C_6D_6.

Germole	^{1}H NMR	^{13}C NMR ring carbon atoms	^{29}Si NMR
39 X = Cl R = $SiMe_3$	0.35 $SiMe_3$ 1.68 CMe	132.8 $CSiMe_3$ 160.9 CMe	-7.7 $SiMe_3$
40 X = Br R = $SiMe_3$	0.39 $SiMe_3$ 1.70 CMe	134.6 $CSiMe_3$ 159.3 CMe	-7.4 $SiMe_3$
41 X = Cl R = Si^tBuMe_2	0.40 $SiMe_2$ 1.00 Si^tBu 1.85 CMe	132.0 CSi^tBuMe_2 161.7 CMe	0.4 Si^tBuMe_2
42 X = Br R = Si^tBuMe_2	0.46 $SiMe_2$ 1.01 Si^tBu 1.85 CMe	134.0 CSi^tBuMe_2 159.9 CMe	0.7 Si^tBuMe_2

Table 2: Structural metrics of 1,1-dihalogermoles **39**, **40** and **42** obtained by X-ray diffraction analysis.

Germole	C-C [pm]	C=C [pm]	C-Ge [pm]	X-Ge [pm]	C-Ge-C
39 X = Cl R = $SiMe_3$[79]	153	134	192	216	96°
40 X = Br R = $SiMe_3$	153	136	192	231	96°
42 X = Br R = Si^tBuMe_2	153	135	193	232	96°

Dihalogermoles are suitable precursor compounds for the synthesis of monosubstituted germoles in 1-position via salt metathesis reactions. In this way, a variety of substituents can be introduced. The 1,1-dibromogermole **40** was reacted with tert-butyllithium to form the tert-butyl substituted bromogermole **43**. Notably, tert-butyllithium was the only organometallic reagent which reacted with 1,1-dibromogermoles selectively. Several other reagents, including PempLi (Pemp = C_6Me_5),

PempMgBr, PempCu·MgBrCl, C_6F_5Li, C_6F_5MgBr, $C_6F_5MgBr{\cdot}CuCl_{cat.}$ or $KSi(SiMe_3)_3$, gave complex reaction mixtures which contained only traces of the desired 1-substituted germoles **44** (Scheme 16) or, in case of C_6F_5 organometallics, the double substituted product. Altering the reaction conditions such as solvent, temperature, concentration and sequencing did not improve the selectivity, which suggests that 1,1-dibromogermoles are not well suited as starting materials to achieve monosubstitution at the germanium.

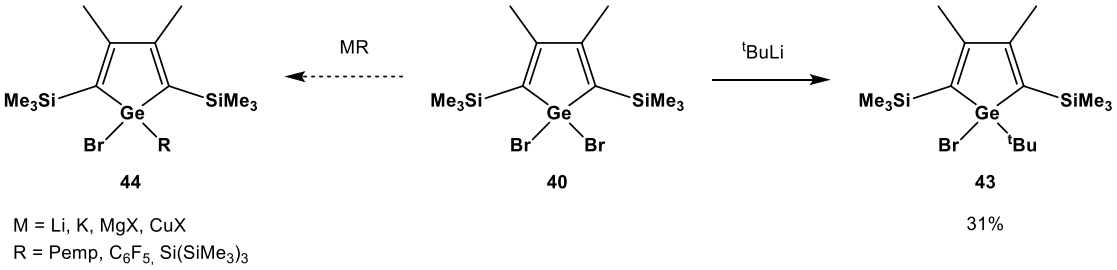

Scheme 16: Functionalisation reactions of 1,1-dibromogermole **40**.

1,1-Dichlorogermoles **39** and **41** on the other hand show a different behaviour. They readily undergo selective monosubstitution reactions at the 1-position under the same reaction conditions. In this way, Pemp, $Si(SiMe_3)_3$, $Ge(SiMe_3)_3$ substituents were successfully introduced and chlorogermoles **45**-**48** were obtained (Scheme 17). The crude product of these reactions already showed a very selective formation of the respective monosubstituted germole. The main reason for some mediocre isolated yields is the good solubility and the poor crystallisation behaviour of these kind of compounds even in various solvents.

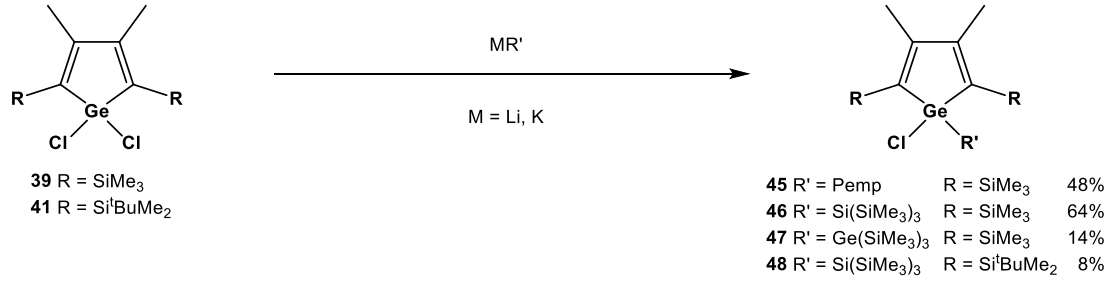

Scheme 17: Functionalisation reactions of 1,1-dichlorogermoles **39** and **41**.

NMR spectroscopic data of the synthesised monosubsituted germoles **45**-**48** are summarised in Table 3 and selected structural metrics obtained by X-ray diffraction analysis are given in Table 4. No distinct differences were noted in the collected data of these products and all values were within the standard ranges.[67]

Table 3: NMR spectroscopic data of monosubstituted germolyl halides shown in Scheme 16 and Scheme 17 in C_6D_6.

Germole	^{1}H NMR		^{13}C NMR ring carbon atoms		^{29}Si NMR	
1-bromo-1-tert-butyl germole **43**	0.37 1.24 1.91	$SiMe_3$ ^{t}Bu CMe	137.2 163.2	$CSiMe_3$ CMe	-8.8	$SiMe_3$
45 R' = Pemp R = $SiMe_3$	0.30 1.97 2.01, 2.59	$SiMe_3$ CMe Pemp	142.7 159.9	$CSiMe_3$ CMe	-8.6	$SiMe_3$
46 R' = $Si(SiMe_3)_3$ R = $SiMe_3$	0.40 0.45 2.01	$Si(SiMe_3)_3$ $SiMe_3$ CMe	150.5 160.6	$CSiMe_3$ CMe	-109.0 -9.0 -8.3	$Si(SiMe_3)_3$ $Si(SiMe_3)_3$ $SiMe_3$
47 R' = $Ge(SiMe_3)_3$ R = $SiMe_3$	0.43 0.45 2.02	$Ge(SiMe_3)_3$ $SiMe_3$ CMe	132.0 161.7	$CSiMe_3$ CMe	-9.1 -2.4	$SiMe_3$ $Ge(SiMe_3)_3$
48 R' = $Si(SiMe_3)_3$ R = Si^tBuMe_2	0.39 0.43, 062 1.04 2.07	$Si(SiMe_3)_3$ $SiMe_2$ Si^tBu CMe	154.3 158.9	CSi^tBuMe_2 CMe	-106.4 -8.1 -2.8	$Si(SiMe_3)_3$ $Si(SiMe_3)_3$ Si^tBuMe_2

Table 4: Structural metrics of monosubstituted germolyl chlorides **46**-**48** obtained by X-ray diffraction analysis.

Germole	C-C [pm]	C=C [pm]	C-Ge [pm]	R'-Ge [pm]	C-Ge-C
46 R' = $Si(SiMe_3)_3$ R = $SiMe_3$	151	136	196	242	92°
47 R' = $Ge(SiMe_3)_3$ R = $SiMe_3$	151	136	196	245	92°
48 R' = $Si(SiMe_3)_3$ R = Si^tBuMe_2	151	135	195	243	92°

3.1.2 Synthesis and Functionalisation of Siloles

The convenient element exchange reaction to synthesise germoles described in Chapter 3.1.1 cannot be extended to silicon. It is reported that silicon tetrabromide only gives very poor yields and that silicon tetrachloride does not react at all in this reaction.[23] Therefore, a different approach for the synthesis of 1,1-dihalosilacyclopentadienes was carried out.

All siloles were synthesised according to a procedure reported by Tamao et al.[82] where the bis(diethylamino) protected bisalkynylsilane **49** was cyclised by reduction with lithium naphthalenide to the silolyl-2,5-dianion **50** which was reacted *in situ* with trimethyl- or triethylchlorosilane to form the bis(diethylamino) protected siloles **51** or **52** (Scheme 18).

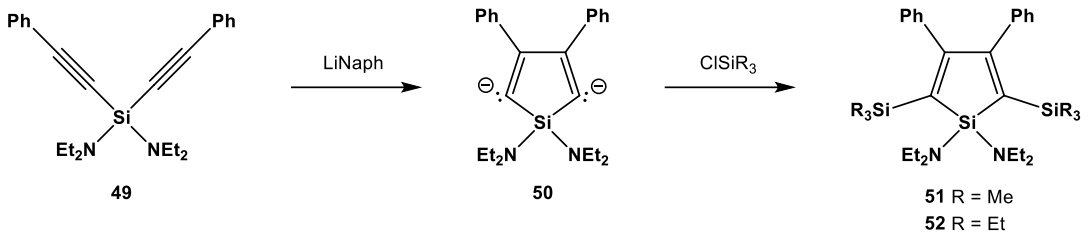

Scheme 18: Synthesis of silacyclopentadienes **51** and **52**.[82-86]

Introduction of sterically more demanding groups in 2,5-position (**53**) by using different silyl electrophiles such as ClSi^{t}BuMe$_2$[85], ClSiMe$_2$Ph[86] or TfOSi^{t}BuMe$_2$[84] did not succeed (Scheme 19).

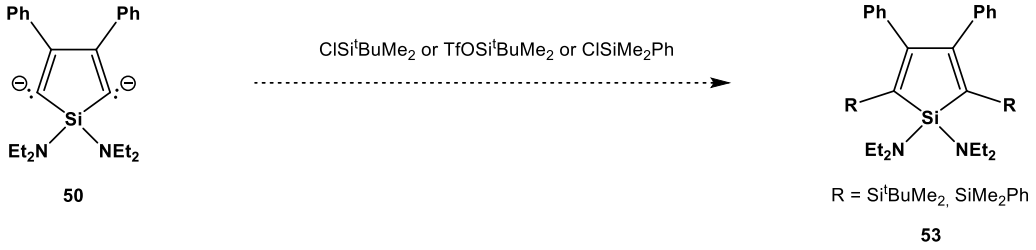

Scheme 19: Unsuccessful functionalisation attempts at the 2,5-position (**53**).[84-86]

The diethylamino siloles **51** and **52** were deprotected by treatment with anhydrous HCl. Previously this reaction was reported using gaseous HCl, which was introduced by a gas cylinder or by *in situ* reaction of NH_4Cl and H_2SO_4.[78,82] A more convenient method was developed by adding a commercially available solution of HCl in dioxane at low temperature to a solution of the respective silole in diethyl ether. After 30 min, the reaction mixture was warmed to room temperature and all solvents and residual HCl were removed by vacuum distillation. Dissolving the residue in hexane or pentane allowed the removal of precipitated ammonium chloride by filtration.[83] The resulting syntheses of 1,1-dichlorosiloles **54** and **55** were significantly simplified (Scheme 20).[83,85-87]

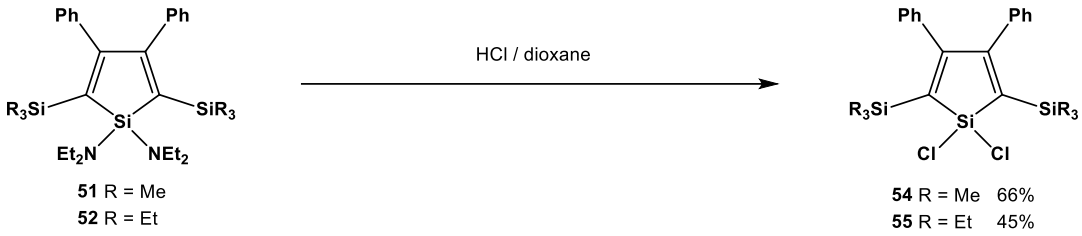

51 R = Me
52 R = Et

54 R = Me 66%
55 R = Et 45%

Scheme 20: Chlorination of bis(diethylamino)siloles **51** and **52** to 1,1-chlorosiloles **54** and **55**.[83,85-87]

Monosubstitution reactions of a chloride were performed under the same conditions as with the dichlorogermoles. The 1,1-dichlorosiloles **54** and **55** were treated with potassium tris(trimethylsilyl)silanide[88] to form the 2,5-$SiMe_3$ and 2,5-$SiEt_3$ substituted 1-tris(trimethylsilyl)silylsiloles **56** and **57**[86,87] (Scheme 21).

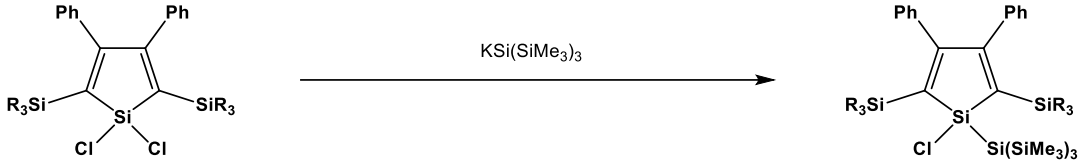

54 R = Me
55 R = Et

56 R = Me 68%
57 R = Et 51%

Scheme 21: Functionalisation reactions of 1,1-dichlorosiloles **54** and **55**[86,87] with potassium tris(trimethylsilyl)silanide.[88]

However, reacting dichlorosilole **54** with tert-butyllithium solution led to a mixture of mono- and disubstituted products **58** and **59** along with residual starting material (Scheme 22).

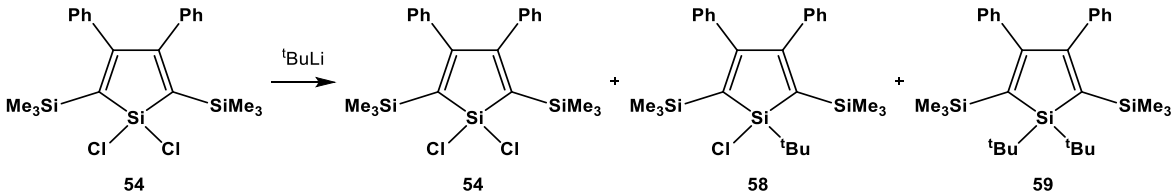

54 **54** **58** **59**

Scheme 22: Functionalisation attempt of 1,1-dichlorosilole **54** with tert-butyllithium.

The NMR spectroscopic data of the 2,5-$SiMe_3$ and 2,5-$SiEt_3$ subsituted 1,1-dichlorosiloles **54** and **55** and the 1-chloro-1-tris(trimethylsilyl)silylsiloles **56** and **57** are summarised in Table 5 and selected structural metrics obtained by X-ray diffraction analysis are given in Table 6. No distinct differences were noted in the collected data of the products and all values were within the standard ranges.[82]

Table 5: NMR spectroscopic data of siloles **54**-**57** shown in Scheme 20 and Scheme 21 in C_6D_6.

Silole	^{1}H NMR		^{13}C NMR ring carbon atoms		^{29}Si NMR	
54 1,1-dichlorosilole R = Me[82,83]	0.16 6.74-6.85	$SiMe_3$ Ph	136.5 170.2	$CSiMe_3$ CPh	-8.0 19.2	$SiMe_3$ $SiCl_2$
55 1,1-dichlorosilole R = Et[87]	0.68 1.02 6.79-6.88	$SiEt_3$ $SiEt_3$ Ph	134.9 170.7	$CSiMe_3$ CPh	0.3 19.0	$SiEt_3$ $SiCl_2$
56 1-chloro-1-Si($SiMe_3$)$_3$ silole R = Me	0.25 0.52 6.84-7.09	$SiMe_3$ $Si(SiMe_3)_3$ Ph	151.2 168.8	$CSiMe_3$ CPh	-124.0 -8.6 -8.4 29.7	$Si(SiMe_3)_3$ $SiMe_3$ $Si(SiMe_3)_3$ SiCl
57 1-chloro-1-Si($SiMe_3$)$_3$ silole R = Et[87]	0.52 0.67-0.74 0.96-1.06 6.84-7.10	$Si(SiMe_3)_3$ $SiEt_3$ $SiEt_3$ CPh	150.6 168.5	$CSiMe_3$ CPh	-122.7 -8.2 -2.0 28.9	$Si(SiMe_3)_3$ $Si(SiMe_3)_3$ $SiEt_3$ SiCl

Table 6: Structural metrics of siloles **54**-**57** obtained by X-ray diffraction analysis.

Silole	C-C [pm]	C=C [pm]	C-Si [pm]	Cl/R'-Si [pm]	C-Si-C
54 1,1-dichlorosilole R = Me[89]	153	136	185	205	98°
55 1,1-dichlorosilole R = Et[86]	152	136	185	205	98°
56 1-chloro-1-Si($SiMe_3$)$_3$ silole R = Me	151	136	187	207/238	95°
57 1-chloro-1-Si($SiMe_3$)$_3$ silole R = Et[86]	151	136	187	209/239	95°

3.2 Sila- and Germacyclopentadienyl Radicals

To create persistent radicals based on group 14 heteroles, different approaches were examined. Initially, the 1-hydrogen substituted pentaphenyl silole **28** was treated with lead(IV)oxide as an oxidant (Scheme 23) to form the silolyl radical **29**. Rieker et al.[90] oxidised several bisphenol derivatives to their corresponding quinones, however in this case, no reaction was observed even at higher temperature.

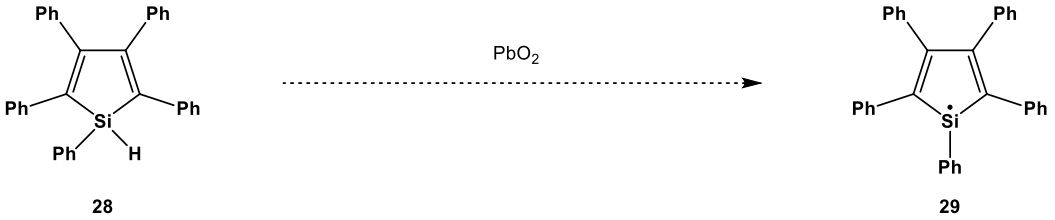

28 **29**

Scheme 23: Unsuccessful oxidation attempt of 1-hydridosilole **28** to the respective silolyl radical **29**.

A radical abstraction reaction of the 1-hydrogen substituted siloles **28** and **60** using the triphenylmethyl radical was also investigated (Scheme 24). In the case of the pentaphenylsilole **28**, the formation of triphenylmethane as byproduct was observed by GC/MS and NMR analysis, however, a radical species was not detected using EPR spectroscopy. Additionally, the only other signals in the NMR spectra of the reaction mixture, which could be assigned, were those of the silole starting material. Given that there was no evidence for the formation of addition or dimerisation products derived from the silole and the presence of the starting material suggested that this reaction is not very selective. Surprisingly, the 2,5-bis(triisopropylsilyl)silole **60** did not show a reaction with the trityl radical at all.

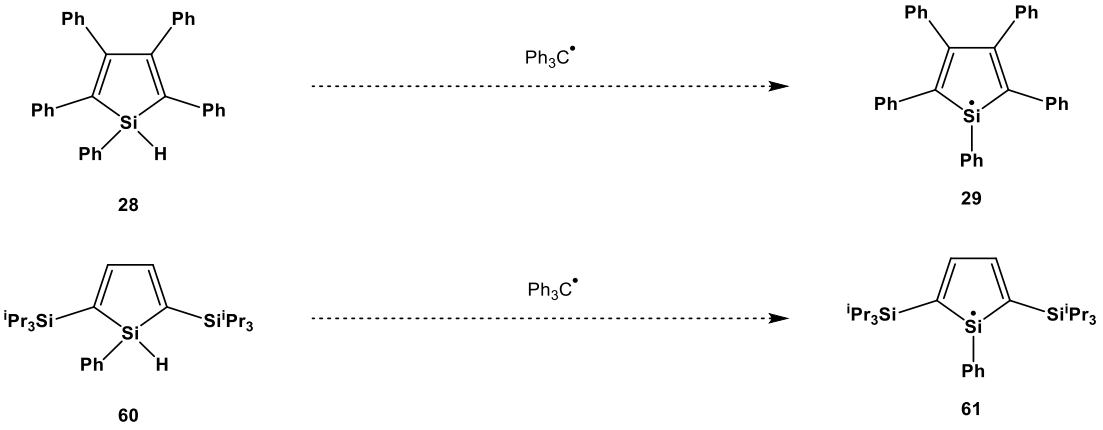

28 **29**

60 **61**

Scheme 24: Unsuccessful attempts of a hydrogen atom transfer from 1-hydrogen substituted siloles **28** and **60** to the triphenylmethyl radical to yield the respective silolyl radicals **29** and **61**.

These results are in agreement with previous works[76,77] which showed, after examining several approaches, that 1-hydrogen substituted group 14 heteroles are not suitable precursor compounds for the synthesis of persistent radicals. To achieve this, a different synthetic method was needed.

3.2.1 Reduction Reactions of 1-Halo Group 14 Heteroles to their Radicals

A more promising method for the formation of stable radicals is the reduction of 1-halo siloles and germoles. Power et al.[91] and Sekiguchi et al.[92] have demonstrated that halogen substituted germanes or silanes can be reduced using potassium graphite to give isolable radicals.

Furthermore, previous work[76] showed that reducing the 1-phenyl germole **33** leads to the bis-germole **35** (Scheme 25). Formation of this product originated most likely from a dimerisation reaction and it was therefore a clear sign for the intermediary presence of the radical species **34**.

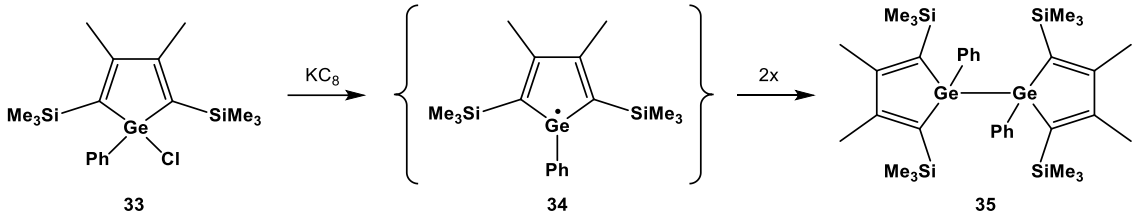

Scheme 25: Previous reduction of 1-chlorogermole **33** with potassium graphite to its Ge-Ge bonded dimer **35**.[76]

Based on these results, germoles with different bulky substituents in 1-position, such as tert-butyl or Pemp, were synthesised in an attempt to suppress the dimerisation reaction and their reduction with potassium graphite was investigated.

Despite using a tert-butyl group as a substituent, which is sterically more demanding[93,94] compared to a phenyl group, the results of the reduction reaction were similar. The isolated product of the reaction of **43** with KC_8 was the dimer **63** which again suggested the intermediate formation of the radical species **62** (Scheme 26).

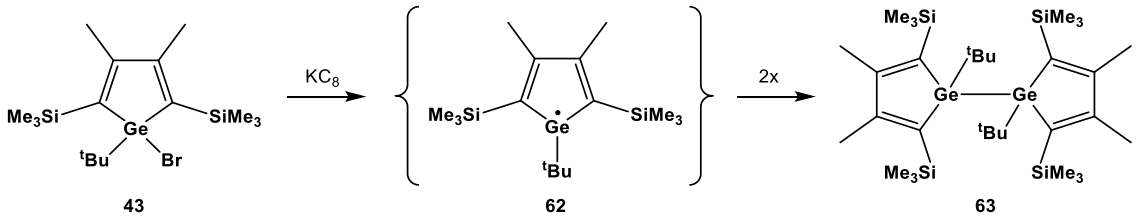

Scheme 26: Reduction of 1-tert-butyl-1-bromogermole **43** with potassium graphite.

One difference between the phenyl and the tert-butyl substituted dimers worth mentioning were the NMR analyses. While the phenyl bisgermole **35** showed high symmetry in the NMR data, and therefore, only one set of signals was observed for both rings, the bis(tert-butylgermole) **63** showed different signals for the two rings. The $SiMe_3$ groups, however, were detected as a very broad signal in the ^1H NMR spectra (Figure 8) and the carbon atoms of the ring were not detected at all in the $^{13}C\{^1H\}$ NMR spectra at room temperature (Figure 9).

When a dynamic process such as the rotation along a single bond, is hindered, broad signals are observed due to the fact that the process occurs with a rate constant that is of the same order of magnitude as the NMR time scale. Further reduction of the rate constant by lowering the temperature of the sample will allow the observation of the magnetically inequivalent states of the molecule. Therefore, the NMR spectra of **63** were also conducted at -40 °C. In the resulting ^1H NMR spectra, the broad signal of the trimethylsilyl groups resolves into two sharp singlets. The methyl groups in the 3,4-position are also detected as two distinct signals. However, the signal assigned to the tert-butyl groups are still present as one singlet (Figure 8).

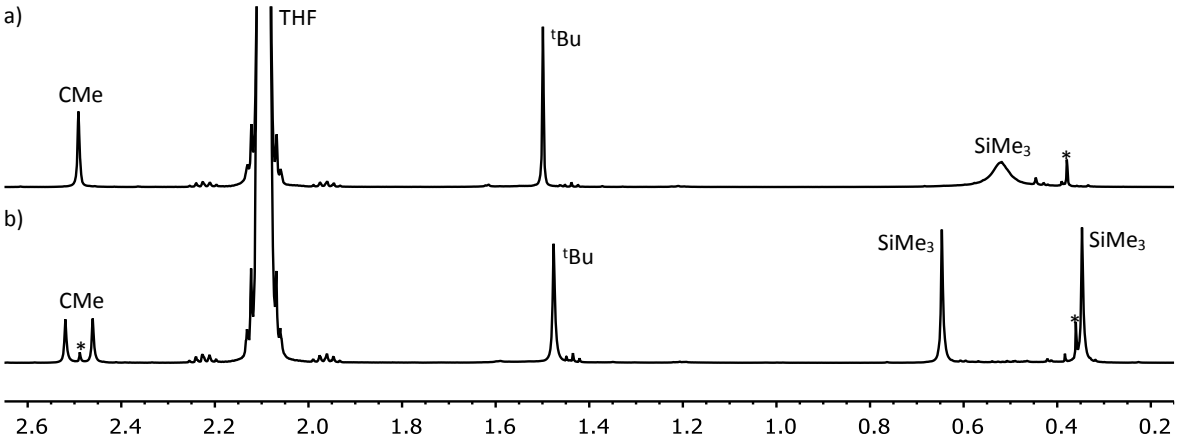

Figure 8: Excerpt of the ^1H NMR spectra of bisgermole **63** in THF; a) 499.9 MHz, 305 K, benzene-d_6 lock; b) 499.9 MHz, 233 K, acetone-d_6 lock; * impurities.

Similar results were observed in the $^{13}C\{^1H\}$ NMR spectra of **63** where the signals attributed to the methyl and trimethylsilyl substituents on the ring split into two separate singlets each. Additionally, the signals assigned to the sp^2 carbon atoms of the ring, which were not detected at room temperature, are now seen as four signals for each of the magnetically inequivalent carbon atoms. Again, the tert-butyl groups only exhibit one set of signals (Figure 9).

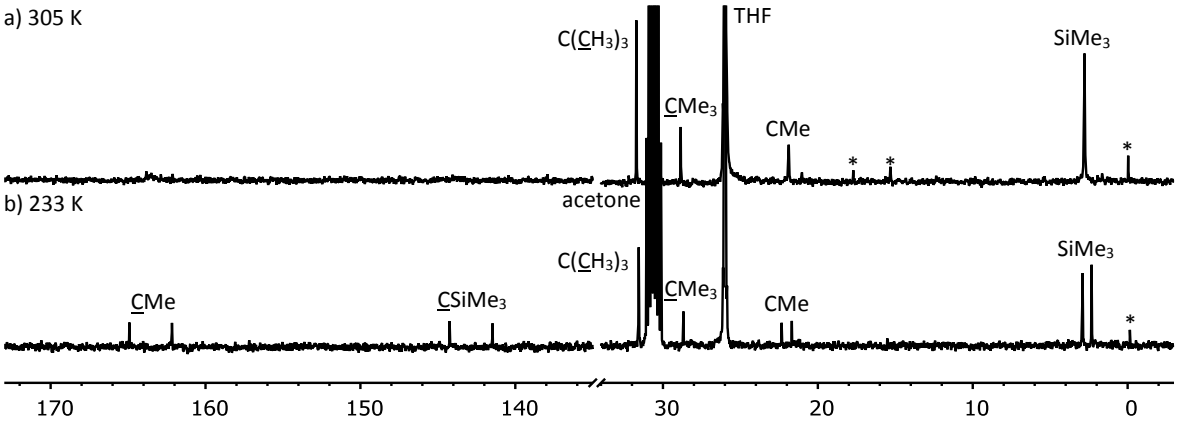

Figure 9: Excerpts of the $^{13}C\{^1H\}$ NMR spectra of bisgermole **63** in THF; a) 125.7 MHz, 305 K, benzene-d_6 lock; b) 125.7 MHz, 233 K, acetone-d_6 lock; * impurities.

In the $^{29}Si\{^1H\}$ NMR spectrum of **63** two signals are observed by measuring the spectrum at -40 °C. The fact that the tert-butyl groups are only detected as one set of signals even at low temperature but the germole ring and its substituents show two sets of signals suggests that the hindered rotation is along the Ge-Ge bond and that the rings are oriented in gauche conformation. In this way, the tert-butyl groups are spectroscopically equivalent but the atoms of the rings and their substituents are not. The same conformation can be seen in the molecular structures in the solid state (Figure 10). Compounds **35** and **63** are orientated similarly in the solid state but only the tert-butyl substituted one **63** exhibits hindered rotation in the NMR spectra.

However, a hindered rotation along the Ge-Ge bond is not necessarily an indicator for the tert-butyl group stretching and therefore weakening it. The strength of this bond, which correlates to its length, is an important factor for the substituent to be able to stabilise the radical while supressing the dimerisation reaction. Therefore, the molecular structures of bisgermoles **35** and **63** in the solid state were investigated.

Single crystals of the bis(tert-butylgermole) **63**, suitable for X-ray diffraction analysis, were obtained and the resulting structural metrics were compared to those of the previous analysed bis(phenyl-germole) **35**[76] (Figure 10, Table 7).

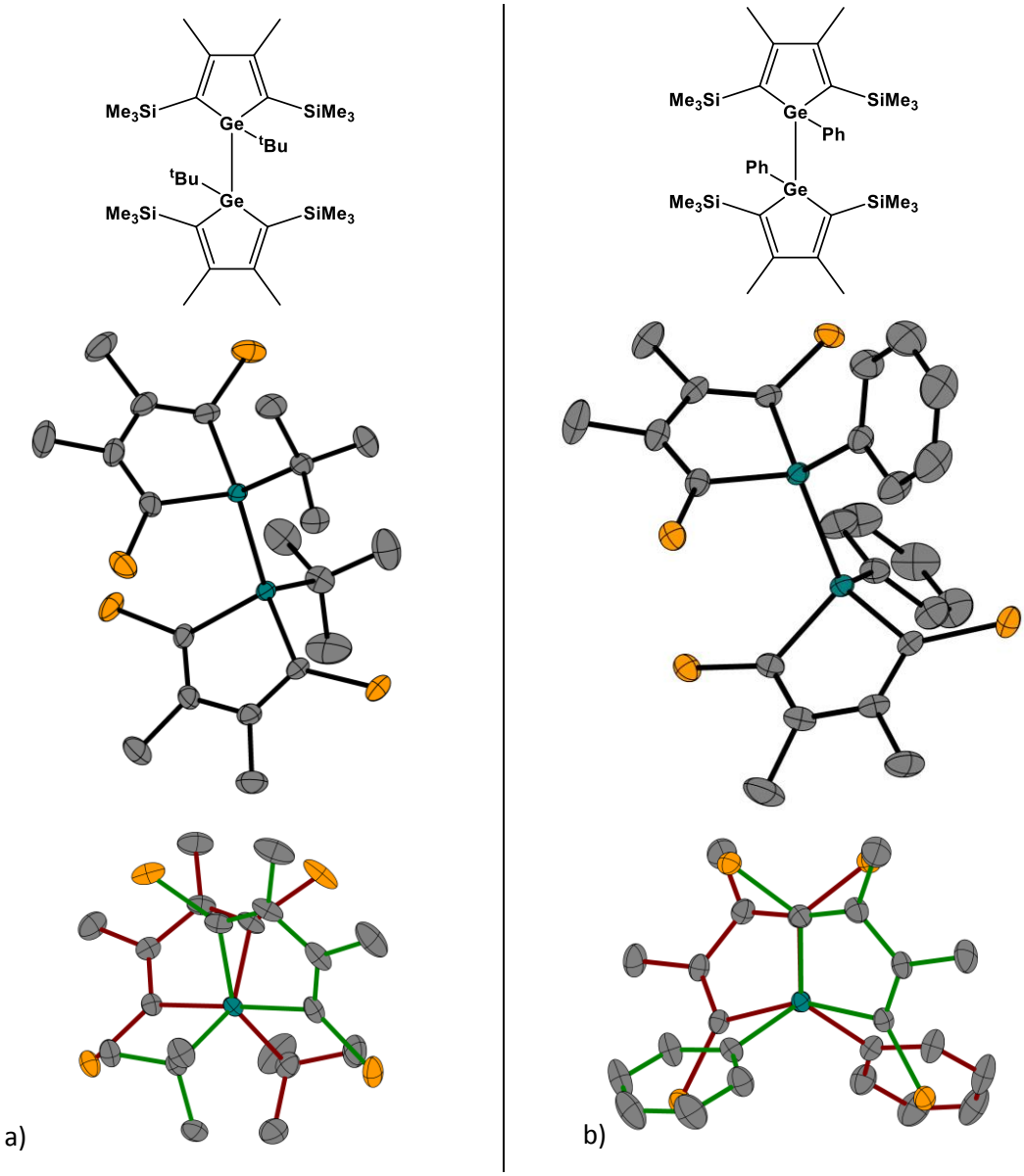

Figure 10: a) Bis(tert-butylgermole) **63**, b) bis(phenylgermole) **35**[76]; top: Lewis structure; middle: molecular structure; bottom: view along the Ge-Ge bond, front part: green bonds, back part: red bonds; carbon: grey; silicon: yellow; germanium: turquoise; hydrogen atoms and methyl groups of trimethylsilyl groups are omitted for clarity; thermal ellipsoids at 50% probability level.

The differences are found to be marginal. In both structures the germole rings are gauche-oriented towards each other which is indicated by the torsion angle of the tert-butyl or phenyl substituents along the Ge-Ge bond (Table 7). The difference between the two Ge-Ge bond lengths is only Δd(Ge-Ge) = 2 pm which means there is no significant increase in the length of the bond between the two species. Compared to the sum of the single bond radii,[95] the Ge-Ge bond in **35** or **63** is only slightly elongated. The calculated Ge-Ge bond length of Ge_2Me_6 at the M06-2x/6-311+G(d,p) level of theory is d(Ge-Ge) = 245 pm which is only slightly shorter than the bond lengths of the dimers **36** and **63**.

Table 7: Structural parameters of the bisgermoles **35** and **63**.

	Ge-Ge [pm]	C-C [pm]	C=C [pm]	C-Ge [pm]	Ge-R [pm]	Torsion angle R-Ge-Ge-R
Bisgermole **63** R = ^{t}Bu	**248**	150	136	197	201	88°
Bisgermole **35** R = Ph	**246**	150	135	196	196	112°
Ge_2Me_6 calculated at M06-2X/6-311+G(d,p)	**245**	-	-	-	-	-
Sum of single bond radii[95]	**242**	150	134	196	196	-

Attempts to reduce the 1-pentamethylphenyl-1-chlorogermole **45** with potassium graphite gave no evidence for the formation of a radical species in EPR spectroscopy. NMR analysis of the reaction showed a complex mixture without any indication of the formation of a dimer (Scheme 27).

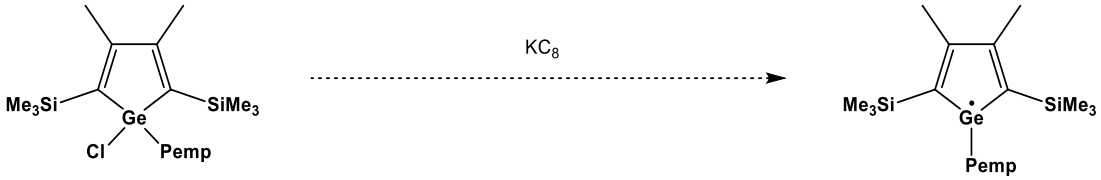

45 **64**

Scheme 27: Unsuccessful reduction attempt of 1-pentamethylphenyl-1-chlorogermole **45** with potassium graphite.

3.2.2 Attempted Cleavage of the Ge-Ge Bond of Bisgermoles

Another possible approach to create radicals is the homolytic cleavage of bonds by thermolysis or irradiation. Gudat et al. reported the dissociation of N-heterocyclic diphosphanes **65** into their respective radicals **66**.[96,97] This reversible dissociation is temperature dependant and the reaction barrier was found to be low that even at room temperature the radical species were present (Scheme 28).

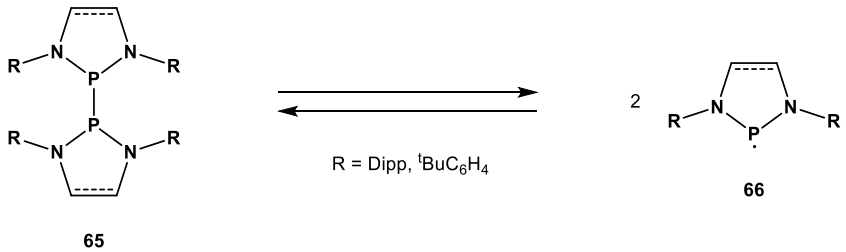

65 **66**

Scheme 28: Reversible dissociation of N-heterocyclic diphosphanes **65** and their respective radicals **66**.[96,97]

Group 14 element-element bonds can also be cleaved either by irradiation[98,99] or by thermolysis,[100] and thus, the photolysis of bisgermoles **63** and **35** was investigate (Scheme 29).

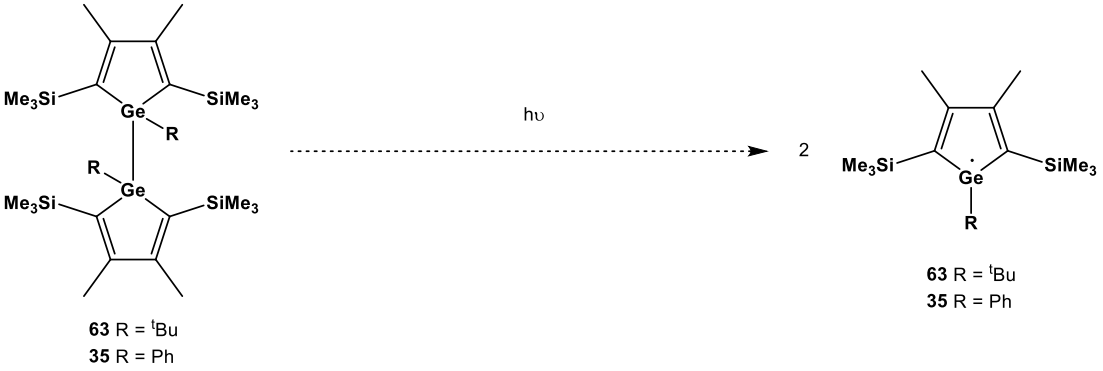

Scheme 29: Unsuccessful attempts of cleaving the Ge-Ge bond of bisgermoles **63** and **35** by irradiation.

A solution of the bis(phenylgermole) **35** in pentane and a solution of the bis(tert-butylgermole) **63** in THF were each placed in capillaries and irradiated in the probe of the EPR spectrometer at various temperatures. The temperature was varied stepwise from -150 °C to 25 °C. In case of the tert-butyl substituted compound, irradiation at 80 °C was also examined. A mercury-vapour lamp (240 nm to 400 nm, 250 nm band enhanced) was used as the irradiation source.

All experiments performed with the bis(phenylgermole) **35** did not result in the detection of any radical species. Using the bis(tert-butylgermole) **63**, only traces of radical species were detected. The fact that no characteristic hyperfine coupling was observed and due to the low intensities, the signals were most likely related to impurities.

Additionally, NMR spectroscopic analysis of the same samples after irradiation showed in both cases only the intact starting materials. The Ge-Ge bond of the 1-phenyl and 1-tert-butyl bisgermoles **63** and **35** cannot be cleaved homolytically under these reaction conditions.

3.2.3 Theoretical Determination of Suitable Substituents for Stable Radicals

Based on the experimental results of the inexpedient 1-phenyl- and 1-tert-butyl substituted germoles, quantum mechanical calculations at the DFT level of theory were performed to determine a suitable substituent to stabilise a radical species and to supress the dimerisation reaction. To quantify the thermodynamic stabilising effect of different substituents R on radicals, an isodesmic reaction was formulated (Scheme 30). In this method, only a Ge-H bond is exchanged, the number and nature of all other bonds remain the same. As a consequence, the stabilising effects of the substituent R can be estimated and compared (Figure 11).

Scheme 30: Isodesmic reaction used to determine substituent effects on the thermodynamic stability of germolyl radicals by DFT calculations (Figure 11).

Figure 11 shows the relative stabilising energies, ΔE_{iso}, computed at the M06-2X/6-311+G(d,p) level of theory of several substituents R relative to hydrogen. Even though the range of energies is quite narrow, a clear trend can be observed. Notably the experimentally tested phenyl- and tert-butyl substituents have positive values indicating that the isodesmic reactions are endothermic, and therefore, the thermodynamic stabilising effects of these substituents are inferior to that of hydrogen.

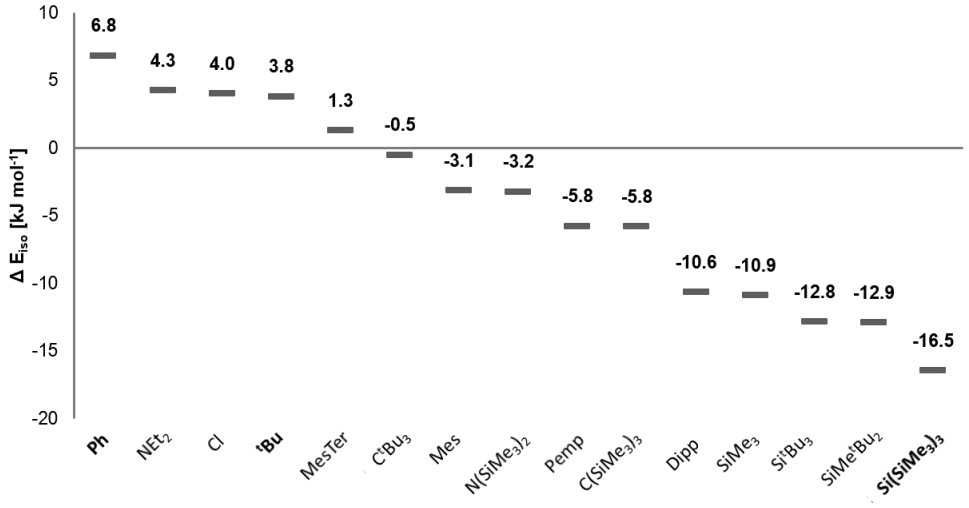

Figure 11: Relative stabilisation energies ΔE_{iso} calculated according to the isodesmic reaction in Scheme 30 at the M06-2X/6-311+G(d,p) level of theory.

Interestingly, the most favourable substituents are the groups which bear an alpha silicon atom such as $SiMe_3$, $SiMe^tBu_2$ and $Si(SiMe_3)_3$. These results are consistent with a previous theoretical study by Schiesser et al.[101] in which the 1-silyl substituted silole was suggested to be a better hydrogen donor towards a methyl radical compared to the methyl or hydrogen substituted siloles. This observation by Schiesser et al. is an indirect indication for a stabilising effect of silyl substitution on silole radicals. The diisopropylphenyl group (Dipp) appears to have a similar stabilising effect, however, the calculated structure shows a very short distance from the hydrogen at the tertiary carbon atom of the isopropyl substituent to the radical centre. To avoid a potential hydrogen shift from the isopropyl group to the germyl radical, the diisopropylphenyl substituted germole was not examined experimentally.

The most promising substituent to stabilise a germolyl radical appears to be the $Si(SiMe_3)_3$ group. Not only does it exhibit the highest calculated stabilising effect in the isodesmic reaction (Scheme 30, Figure 11), it is also quite bulky which is required for kinetic stabilisation of the radical and to supress dimerisation. Additionally, the use of the readily available tris(trimethylsilyl)silyl anion[88] in a salt metathesis reaction with 1,1-dichlorogermole, as shown in Chapter 3.1.1, was a convenient synthetic approach.

Another important quantitative assessment of the suitability of a substituent in the stabilisation of a germolyl radical is the dimerisation energy of the radical species which can be determined from the bond dissociation energy, ΔE_{diss}. If the magnitude of ΔE_{diss} is decreased compared to the standard Ge-Ge dissociation enthalpy, a radical species might be favoured over the respective dimer. Accordingly, the energies of the hydrogen, phenyl, tert-butyl and $Si(SiMe_3)_3$ substituted germolyl radicals **34**, **62**, **67**, **69** and their respective dimers **35**, **63**, **68**, **70** were calculated at the M06-2X/6-311+G(d,p) level of theory and the reaction energy determined (Scheme 31).

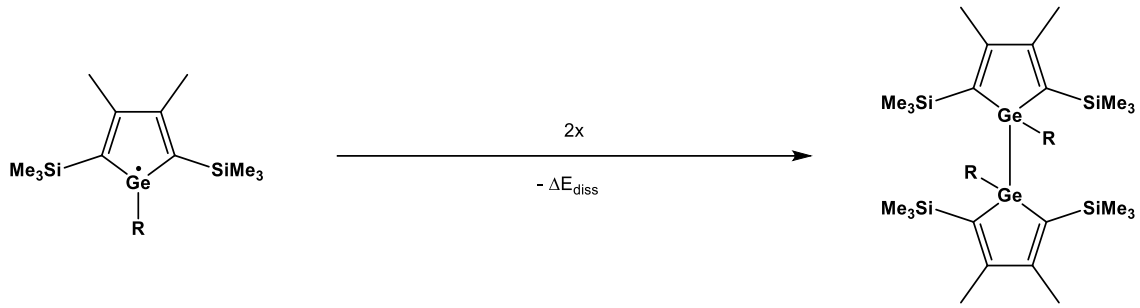

67 R = H
34 R = Ph
62 R = ^{t}Bu
69 R = $Si(SiMe_3)_3$

68 R = H
35 R = Ph
63 R = ^{t}Bu
70 R = $Si(SiMe_3)_3$

Scheme 31: Dimerisation reactions of 1-hydrogen, 1-phenyl, 1-tert-butyl and 1-$Si(SiMe_3)_3$ substituted germolyl radicals to determine the bond dissociation energies ΔE_{diss} (Table 8).

The obtained values for the dimerisation energies and the Ge-Ge bond lengths are quite interesting (Table 8). While the bond dissociation energy ΔE_{diss} for hydrogen, phenyl and tert-butyl substituted derivatives are in the range of ΔE_{diss} = 267-277 kJ mol^{-1}, which are not significantly decreased compared to the dissociation enthalpy of $Me_3Ge\text{-}GeMe_3$ (ΔE_{diss} = 273 kJ mol^{-1}), the value for the $Si(SiMe_3)_3$ substituted germole is ΔE_{diss} = 96 kJ mol^{-1}. Although the dissociation remains endothermic, the fact that the value is three times less than of the other substituents is a crucial difference. The contrast is also reflected in the Ge-Ge bond length which is d(Ge-Ge) = 265 pm for the $Si(SiMe_3)_3$ substituted germole, an increase of Δd(Ge-Ge) = 20 pm compared to hexamethyldigermane and Δd(Ge-Ge) = 14-18 pm compared to the other three substituents.

Table 8: Calculated bond dissociation energies ΔE_{diss} and Ge-Ge bond lengths d(Ge-Ge) of bisgermoles **35**, **63**, **68**, **70** (Scheme 31) and Me_3Ge-$GeMe_3$ at the M06-2X/6-311+G(d,p) level of theory.

R =	**68** H	**35** Ph	**63** ^tBu	**70** $Si(SiMe_3)_3$	Me_3Ge-$GeMe_3$
ΔE_{diss} [kJ mol^{-1}]	277	280	267	**96**	273
d(Ge-Ge) [pm]	247	249	251	**265**	245

In summary, the theoretical studies underline that the $Si(SiMe_3)_3$ group is a very promising substituent for the stabilisation of a germolyl radical and for the suppression of a dimerisation reaction. Therefore, all further experimental studies were performed using the tris(trimethylsilyl)-silyl substituent at germanium.

3.2.4 Reduction of 1-Tris(trimethylsilyl)silylgermolyl chloride

Since the results of the theoretical investigation suggested the 1-tris(trimethylsilyl)silyl group to be the most suitable substituent to stabilise a radical species, the respective chlorogermole **46** was synthesised and the reduction with potassium graphite investigated (Scheme 32).

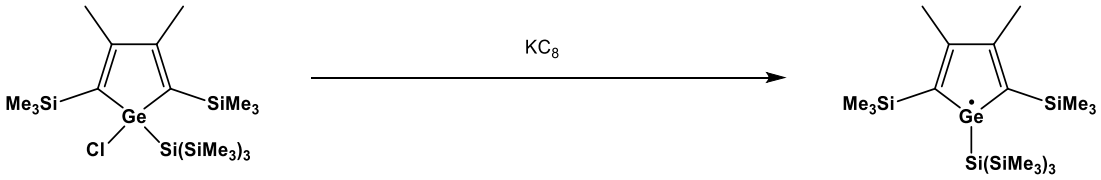

46 **69**

Scheme 32: Reduction of 1-chloro-1-tris(trimethylsilyl)silyl germole **46** to the respective germolyl radical **69**.

The chlorogermole **46** was dissolved in THF and the solution was cooled to -30 °C before potassium graphite was added. While warming to room temperature, the colour of the solution turned from colourless to dark red. Interestingly, when this reaction mixture was examined by EPR spectroscopy, no radical species was detected. However, after the THF has been removed and replaced by a nonpolar solvent such as pentane, hexane or benzene, an intense signal due to a radical species was detected by EPR spectroscopy (Figure 12). The radical is apparently only present in nonpolar solvents. This fact will be important for the formulation of a reaction mechanism (see Chapter 3.2.6).

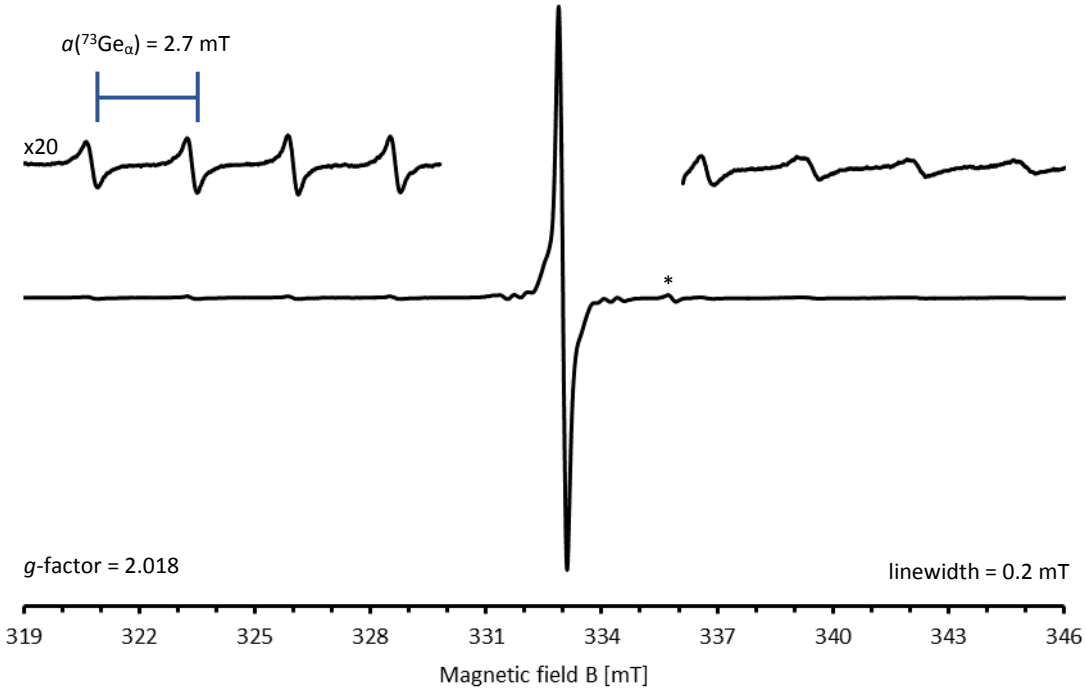

Figure 12: EPR spectrum of the 1-tris(trimethylsilyl)silyl germolyl radical **69** in hexane at room temperature; 9404.5 MHz; Mod.-Ampl. = 0.075 mT; MW-Att. = 3.0 dB; * impurity.

In the EPR spectrum of the solution, an intense singlet for an unpaired electron was detected. Upon closer examination the characteristic hyperfine coupling of the ^{73}Ge nucleus was observed. The spin of $I(^{73}\text{Ge}) = 9/2$ gives rise to a decet with the intensity of its natural abundance of 7.8%. This typical splitting pattern with a hyperfine coupling constant (hfcc) of $a(^{73}\text{Ge}_\alpha) = 2.7$ mT not only indicates the presence of germanium but also its magnitude, which falls in the typical range of germyl radicals[91,102,103], is highly suggesting the structural motif to be a germanium centred radical.

Closer to the centre of the signal, four additional hyperfine couplings were observed (Figure 13). The closest to the main signal can be assigned to a silicon coupling of $a(^{29}\text{Si}_\gamma) = 0.8$ mT ($I(^{29}\text{Si}) = 1/2$, natural abundance 4.7%). Due to its intensity the signal can be assigned to the three equivalent silicon atoms of the tris(trimethylsilyl)silyl group. The remaining three doublets could not be assigned unequivocally, however, considering the given structural motif, the coupling of the carbon atoms of the ring system ($I(^{13}\text{C}) = 1/2$, natural abundance 1.1%) and a coupling of the silicon atom directly connected to the germanium centre are possible. Therefore, a possible assignment of the couplings, according to their intensities, are $a(^{29}\text{Si}_\beta) = 1.7$ mT for the silicon atom and $a(^{13}\text{C}_{\beta/\gamma}) = 2.3$ mT and $a(^{13}\text{C}_{\beta/\gamma}) = 3.0$ mT for two sets of two spectroscopically equivalent carbon atoms of the ring. A small overlap of the signals due to germanium and one of the carbon signals can be seen.

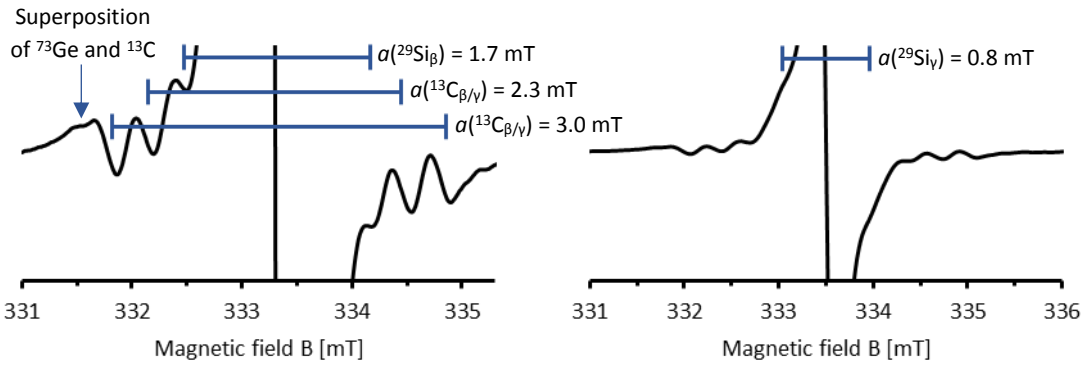

Figure 13: Excerpts of the EPR spectrum of the germolyl radical **69** and assumed assignment of hyperfine coupling constants; left: higher zoom; right: lower zoom.

If the centre of the spectrum is recorded using low modulation frequency another coupling is observed in the second order derivative of the main signal (Figure 14). The splitting of the signal was detected with different samples but surprisingly not in every sample. A possible explanation is that small hyperfine couplings, such as the observed one, are sometimes not resolved if the concentration of the solution is too high.

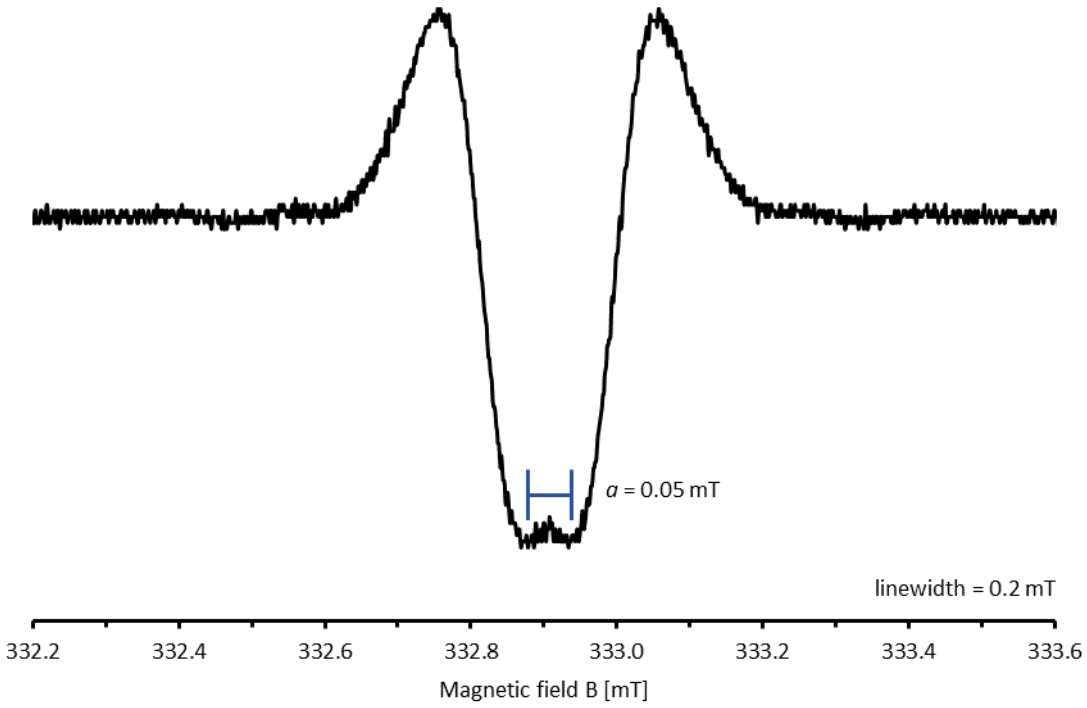

Figure 14: Second order derivative of the low modulation frequency EPR spectrum of the 1-tris(trimethylsilyl)silylgermolyl radical **69** in hexane at room temperature; 9412.0 MHz; Mod.-Ampl. = 0.005 mT; MW-Att. = 30.0 dB.

The detected doublet has a hfcc of a = 0.05 mT and is only resolved in the second order derivation of the spectrum. An obvious explanation for this observation cannot be given at this point. The fact that the main signal is split into a doublet indicates a coupling of a I = 1/2 nucleus with a natural abundance of 100%, such as hydrogen. However, the structural motif of **69** does not have a substitution pattern which would lead to such a coupling. A possible explanation might be the orientation of a methyl group of the tris(trimethylsilyl)silyl group to allow this interaction. However, coupling with a methyl group should lead to a quartet due to the free rotation of the group giving rise to three spectroscopically equal hydrogen atoms.

At 103 K, the EPR spectrum of the frozen solution was obtained, which is shown in Figure 15. The signal is split into each of its tensor eigenvalues (g_{11} = 2.031, g_{22} = 2.026, g_{33} = 1.997). The mean of these values gives the isotropic *g*-factor, which is the same as the one obtained in solution at room temperature (g_{iso} = 2.018). Due to the loss of intensity of the signal in frozen solution, the hyperfine couplings of the low abundant ^{73}Ge and ^{29}Si isotopes were not resolved.

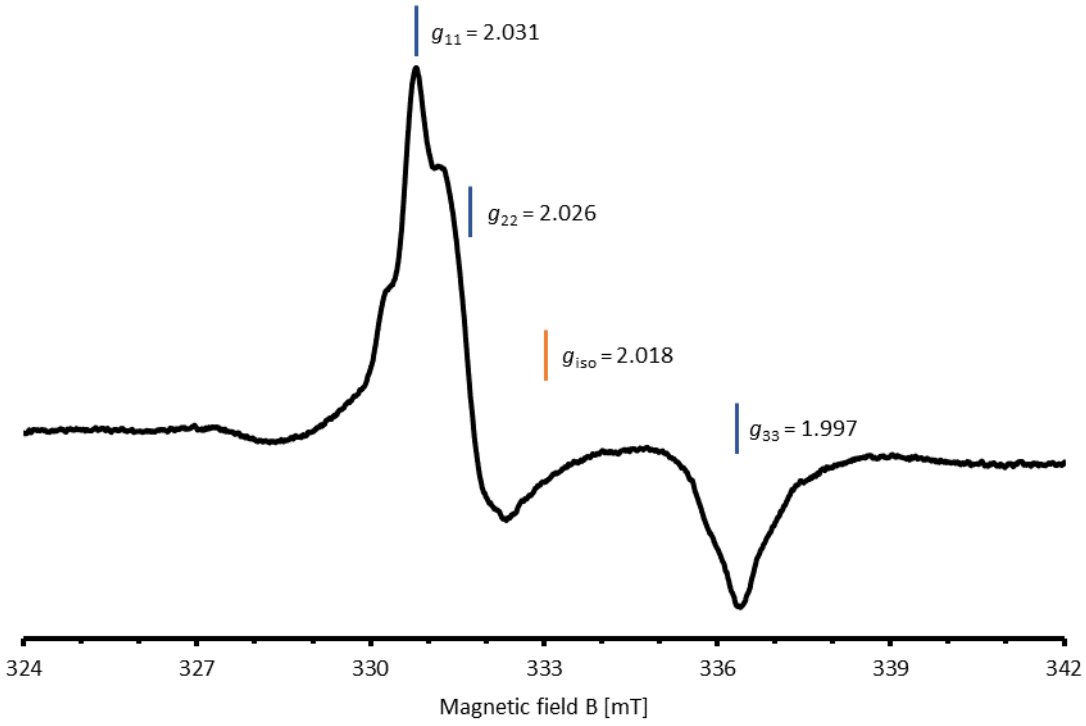

Figure 15: Low temperature (103 K) EPR spectrum of the 1-tris(trimethylsilyl)silylgermolyl radical **69** in hexane; 9404.5 MHz; Mod.-Ampl. = 0.075 mT; MW-Att. = 3.0 dB.

The hyperfine couplings of **69** are in good agreement with the expected structural motif, and are therefore, a good indication that the reduction to the 1-tris(trimethylsilyl)silylgermolyl radical **69** succeeded. The parameters and the hyperfine coupling constants of the experimental spectrum were also used to simulate the spectrum. In combination of the assigned nuclei, the simulated EPR

spectrum should show a similar shape. Figure 16 shows the simulated spectrum generated using the EasySpin[104] toolbox for MATLAB and it can be seen that it is in good agreement with the experimentally obtained spectrum (further details are presented in Chapter 7.1.2). This is another indication that the germolyl radical **69** has indeed been synthesised.

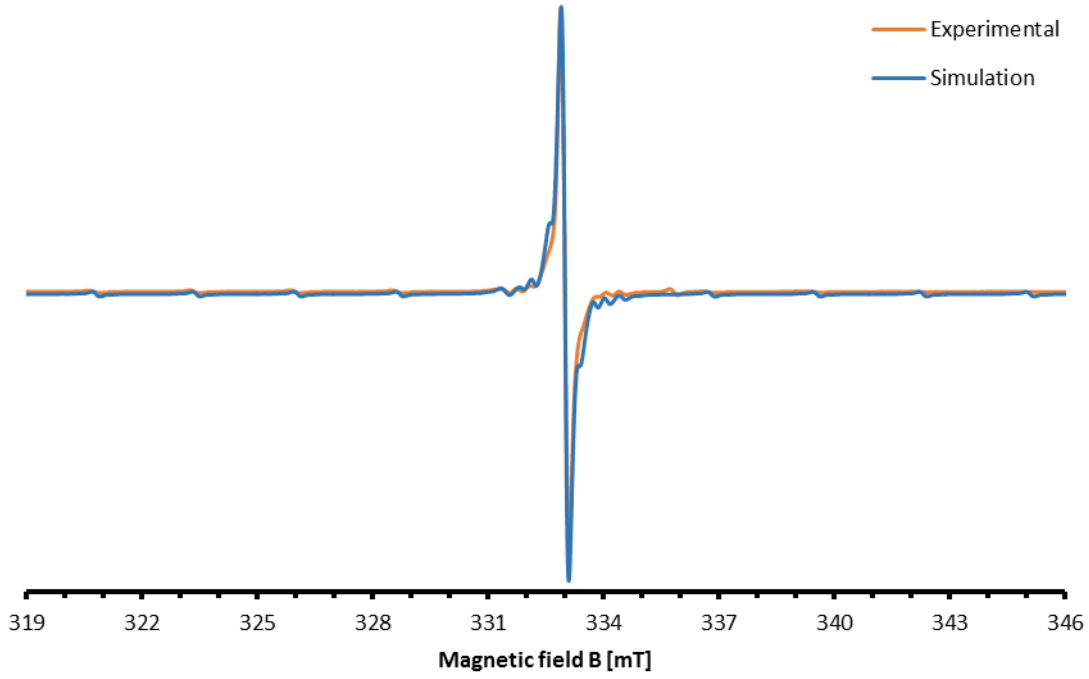

Figure 16: Simulated EPR spectrum of the tris(trimethylsilyl)silyl germolyl radical **69** with EasySpin.[104]

The synthesised germolyl radical **69** shows remarkable stability. Even in solution at room temperature the intensity of the EPR signal of the same sample did not significantly decrease over a time period of eight weeks.

A clear trend is observed upon comparison of the EPR parameters and hyperfine coupling constants of the germolyl radical **69** to those of known germanium centred radicals by Power et al.[91] and Sekiguchi et al.[102] (Figure 17). The cyclotrigermyl radical **71** by Power et al.[91] has a hfcc of $a(^{73}Ge_{\alpha})$ = 1.6 mT which is smaller in comparison to the $a(^{73}Ge_{\alpha})$ = 2.0 mT of the germyl radical **72** by Sekiguchi et al.[102] The difference between both molecules is that the structure of radical **71** has a conjugated, planar three-membered ring in which the electron is highly delocalised. The radical **72** of Sekiguchi et al. is lacking this kind of π-conjugated due to its silyl group substitution pattern. However, the structure still has a planar germyl radical centre.

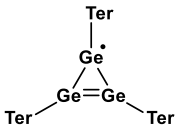

71 by Power et al.[91]

g-factor = 2.007

$a(^{73}Ge_{\alpha})$ = 1.6 mT

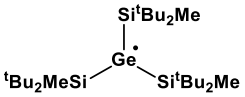

72 by Sekiguchi et al.[102]

g-factor = 2.023

$a(^{73}Ge_{\alpha})$ = 2.0 mT

$a(^{29}Si_{\beta})$ = 0.7 mT

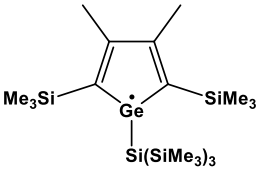

Germolyl radical **69**

g-factor = 2.018

$a(^{73}Ge_{\alpha})$ = 2.7 mT

Figure 17: Comparison of the germolyl radical **69** with other germanium centred radicals by Power et al. (**71**)[91] and Sekiguchi et al. (**72**)[102]

Hyperfine coupling constants are strongly dependent on the character of the orbital in which the unpaired electron is localised, and therefore, the coordination environment of the radical centre.[103] A smaller hfcc indicates there is less σ-contribution to the orbital which bears the unpaired electron. This leads to a decreased Fermi contact term. Furthermore, a small hfcc also signifies that the π-contribution to that orbital is increased which favours a planar structure that allows delocalisation of the electron. This is consistent with the structures of known germyl radicals. The cyclic germyl radical **71** has a planar structure and a delocalised electron, and therefore, a small hfcc. The germyl radical **72** which also has a planar structure but lacks the π-conjugation has an increased hfcc. An increased hyperfine coupling constant indicates an enlarged σ-contribution of the orbital in which the unpaired electron is located and therefore a larger Fermi contact term.

Based on this, the structure of the germolyl radical **69**, presented in this work, can be derived. The radical has the largest hyperfine coupling constant ($a(^{73}Ge_{\alpha})$ = 2.7 mT) compared to the other two. This strongly suggests that the electron is localised at the germanium centre even though it is connected to a conjugated π-system. Additionally, lacking the π-conjugation and having a larger hfcc than the germyl radical **72**, the structure of the germolyl radical **69** most likely has a pyramidalised germanium centre.

To support these structural assessments, quantum mechanical calculations of a model germolyl radical **73** at the M06-2X/6-311+G(d,p) level of theory were performed (Figure 18 and Figure 19). In a Z-matrix of the model compound, the angle between the Ge-Si vector and the orthogonal vector to the plane of the five-membered ring through the germanium atom, has been alternated in 5° steps to investigate the change in energy and the hfcc $a(^{73}Ge_{\alpha})$ going from a planar to a tetrahedral structure of these germole radicals (Scheme 33).

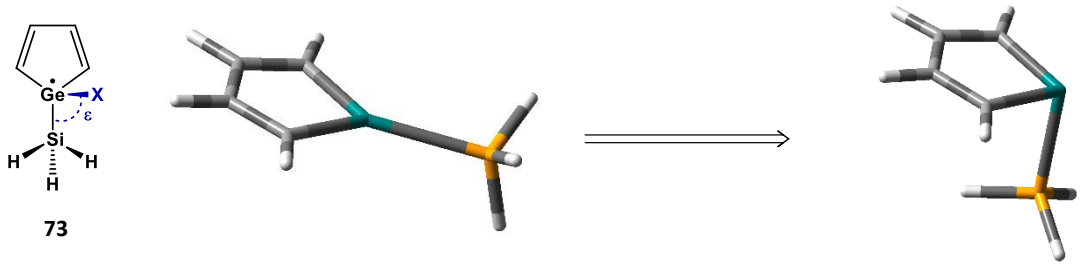

Scheme 33: Model germolyl radical **73**; left: Lewis structure; middle: calculated planar structure ε(X-Ge-Si) = 90°; right: calculated pyramidalised structure ε(X-Ge-Si) = 175°; carbon: grey, hydrogen: white, silicon: yellow, germanium: turquoise.

In Figure 18, the energy change as a function of the angle ε(X-Ge-Si), and hence the pyramidalisation of the germanium centre, is displayed. The planar structure with an angle of ε(X-Ge-Si) = 90° was set to zero and all other energy values are related to it. The angle was increased stepwise to ε(X-Ge-Si) = 175° which places the substituent at an almost orthogonal orientation to the plane of the germole ring. The energy decreases slightly as the angle is increased. The energy minimum at an angle of ε(X-Ge-Si) = 125° is quite shallow. Above ε(X-Ge-Si) = 145°, a significant increase of the energy is observed. These calculations support the structural assessment of the germolyl radical **69** to be pyramidalised at the germanium centre.

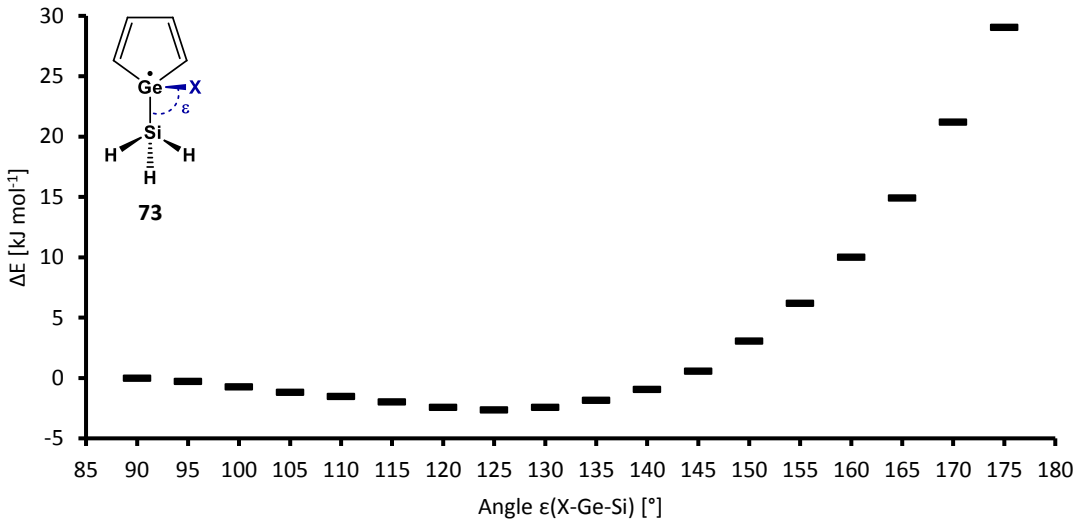

Figure 18: Bending potential of the SiH_3 group in the model germolyl radical **73** at the M06-2X/6-311+G(d,p) level of theory. The angle between the Ge-Si vector and the orthogonal vector to the plane of the five-membered ring through the germanium atom ε(X-Ge-Si), has been alternated in 5° steps to investigate the energy change ΔE between a planar and tetrahedral structure of these germolyl radicals.

As already mentioned the pyramidalisation of the radical centre also has a significant influence on the magnitude of the hyperfine coupling constant. To evaluate this effect for germolyl radicals, the same method was used. The calculations on the model germolyl radical **73** with different

substituent angles at the M06-2X/6-311+G(d,p) level of theory were performed to determine the hyperfine coupling constant at each step. In Figure 19, the dependence of the hfcc $a(^{73}Ge_{\alpha})$ on the change of the angle ε(X-Ge-Si) is shown. The planar structure has a value of $a(^{73}Ge_{\alpha})$ = 1.9 mT which correlates to previously mentioned germyl radicals **71** and **72** (Figure 17). By changing the angle of the SiH_3 substituent, the coupling increases up to $a(^{73}Ge_{\alpha})$ = 9.1 mT at an angle of ε(X-Ge-Si) = 170°. At the most stable structure, according to the energy change shown in Figure 18, the coupling has a value of $a(^{73}Ge_{\alpha})$ = 4.8 mT. Notably, the calculated hyperfine coupling constants are not accurate as they were determined for a model compound and the level of theory used is known to be of insufficient accuracy for germanium centred radicals. This will be described further in the next paragraph. The important information is that by changing the coordination environment of the germyl radical centre from a planar to a pyramidalised structure, a significant change in the hfcc is observed from $a(^{73}Ge_{\alpha})$ = 1.9 mT up to $a(^{73}Ge_{\alpha})$ = 9.1 mT.

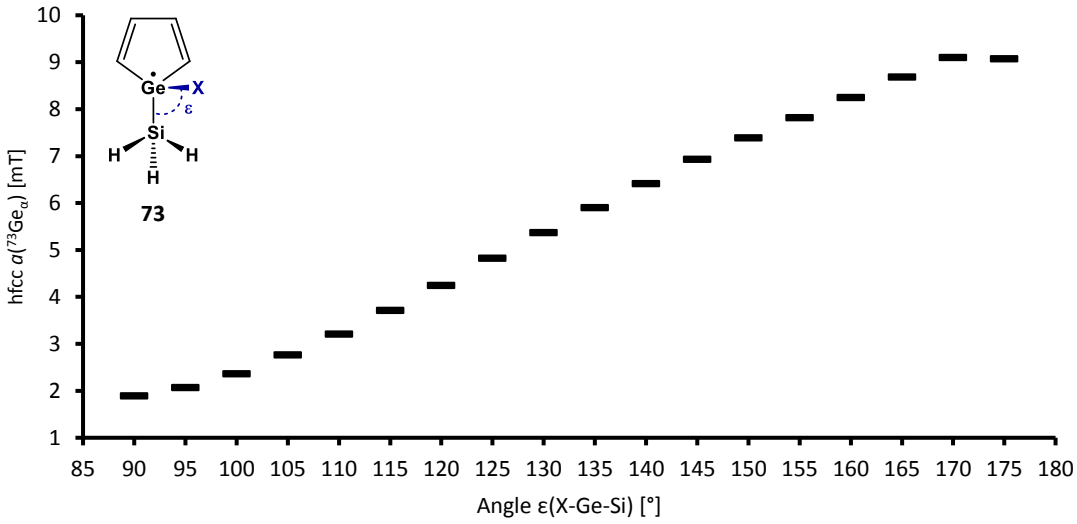

Figure 19: Dependence of the hfcc $a(^{73}Ge_{\alpha})$ on the bending angle ε of the SiH_3 group in the model germolyl radical **73** at the M06-2X/6-311+G(d,p) level of theory. The angle between the Ge-Si vector and the orthogonal vector to the plane of the five-membered ring through the germanium atom ε(X-Ge-Si), has been alternated in 5° steps to investigate the change in $a(^{73}Ge_{\alpha})$ between a planar and tetrahedral structure of these germolyl radicals.

It can also be seen that the value of the hfcc is approximately linear dependent on the angle ε(X-Ge-Si) whereas the energy, change shown in Figure 18, has a very soft bending potential in the range of ε(X-Ge-Si) = 90°-140°. These results indicate that an accurate geometry is critical for the determination of the hyperfine coupling $a(^{73}Ge_{\alpha})$ by quantum mechanical calculations. To achieve this for the germolyl radical **69**, several methods and basis sets were investigated for the optimisation of the geometry and the determination of the hfcc. The results given by Gaussian[105] and ORCA[106], which is known to be more suitable for open shell systems, were analysed.

To compare the calculated results, the sum of angles at the radical centre was used as indicator for the pyramidalisation. In Table 9, the hyperfine coupling constants $a(^{73}Ge_{\alpha})$ and the sum of angles at the germanium centre ∑(Ge), obtained at different levels of theory, are summarised. The calculations were performed using the B3LYP, M06-2X and PBE0 methods in combination with the 6-311+G(d,p), Def2-TZVP and Def2-TZVPD basis sets.[107,108] Def2-TZVPD could only be used in single point calculations due to limited computational resources.

Table 9: Calculated hfcc $a(^{73}Ge_{\alpha})$ and the sum of angles at the germanium centre ∑(Ge) as indicator for the pyramidalisation of **69** at different levels of theory with Gaussian[105] and ORCA.[106]

Software and basis set	**Method**		
	B3LYP	M06-2X	PBE0
	$a(^{73}Ge_{\alpha})$ ∑(Ge)	$a(^{73}Ge_{\alpha})$ ∑(Ge)	$a(^{73}Ge_{\alpha})$ ∑(Ge)
Gaussian 6-311+G(d,p)	3.98 mT 333.3°	4.07 mT 337.9°	-
Gaussian Def2-TZVP	-	3.12 mT 340.3°	3.25 mT 341.9°
ORCA Def2-TZVP	-	3.83 mT 336.5°	3.74 mT 338.5°
ORCA single point on Gaussian opt. Def2-TZVPD // Def2-TZVP	-	2.64 mT 340.3°	2.63 mT 341.9°
ORCA single point on ORCA opt. Def2-TZVPD // Def2-TZVP	-	2.84 mT 336.5°	2.84 mT 338.5°

In general, the calculated hfcc are larger than the experimentally observed ones ($a_{exp.}(^{73}Ge_{\alpha})$ = 2.6 mT), and thus, at all levels of theory, the optimised structure seem to be more pyramidalised than the experimental structure. Therefore, the sum of angles at the germanium centre appears to be a good indicator for comparison of the optimised structure with the synthesised one. Consequently, if the sum of angles at the germanium is smaller, the germanium shows a higher pyramidalisation and has a larger hfcc. If the sum of angles is higher, the germanium centre is less pyramidalised and the hfcc is smaller, and therefore, closer to the experimentally obtained one.

Using B3LYP/6-311+G(d,p), the most pyramidalised structure was obtained with a corresponding large value for the hfcc. Upon changing the level of theory to M06-2X/6-311+G(d,p), the optimised structure was less pyramidalised, however, the hfcc was still in the range of 4 mT. Increasing the basis set to Def2-TZVP using the same method gave a better agreement in the hfcc even though the structure was only altered marginally. Apparently, using a large basis set is of great importance for the determination of the hfcc. Surprisingly, performing the same calculation with ORCA gave optimised structures which were more pyramidalised at the Ge and had larger hfcc. Therefore, the

optimised structures obtained by using the Def2-TZVP basis set in Gaussian were assessed to agree best with the experiment even though the hfcc did not match the experimental value closely. By performing a single point calculation in ORCA on these optimised structures with the Def2-TZVPD basis set gave values for the hyperfine coupling constant $a(^{73}Ge_{\alpha})$ which agree closely with the ones obtained by the experiment. Performing the same single point calculation in Gaussian did not succeed. Additionally, all calculations were performed using the PBE0 method which is known to be suitable for open shell systems.[106] However, there were no significant differences observed compared to the results obtained using the M06-2X method. The optimised structure obtained in Gaussian at the M06-2X/Def2-TZVP level of theory is shown in Figure 20. The germanium atom is pyramidalised with a sum of angles at the germanium centre of ∑(Ge) = 340°. The single and double bond lengths of the ring system are similar to those of the starting chlorogermole **46** (Table 4) and they are therefore well defined and do not show any π-conjugation with the radical centre which supports a pyramidalised structure.

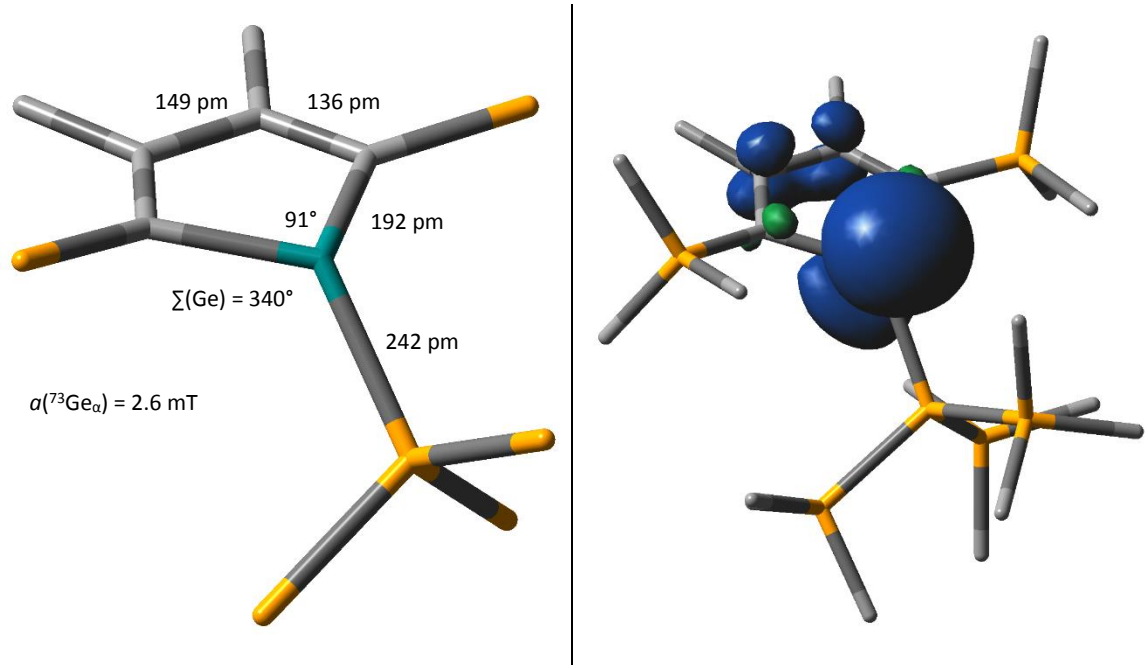

Figure 20: Calculated structure of germolyl radical **69**; ORCA single point calculation on optimised structure by Gaussian, M06-2X/Def2-TZVPD//M06-2X/Def2-TZVP; carbon: grey; silicon: yellow; germanium: turquoise; left: molecular structure, hydrogen atoms and methyl groups of trimethylsilyl groups are omitted for clarity; right: spin density at isovalue = 0.004, hydrogen atoms are omitted for clarity.

On the right side of Figure 20 the spin density distribution, obtained by a single point calculation using ORCA at the M06-2X/Def2-TZVPD level of theory, is shown. As expected by the hyperfine coupling constant and a pyramidalised structure, the spin density is mostly localised at the germanium centre with some delocalisation into the π-system. The hyperfine coupling constant

was determined to be $a(^{73}Ge_{\alpha}) = 2.6$ mT. Further details about the calculations performed with ORCA are given in Chapter 7.1.2.

To support the calculated structural parameters by comparison with a solid state structure did not succeed. Numerous attempts to obtain single crystals of the radical using different solvents at various temperatures did only result in the formation of sticky oily residues. The high sensitivity of main group radical species limited the choice of solvents and the high solubility of these compounds due to the numerous trimethylsilyl groups made crystallisation attempts difficult. Alkanes, benzene, toluene or THF were tested. However, the only single crystals obtained were those of the respective germolyl anion **74**. The anion was most likely synthesised by over reduction of the chlorogermole **46** and it has, due to its polarity, lower solubility in nonpolar solvents, and thus, easily crystallises. The formation of the anion is important for the formulation of a reaction mechanism which will be given in Chapter 3.2.6. The structure of the anion will be discussed in Chapter 3.3.1.

As additional evidence for the synthesis of germolyl radical **69**, trapping reactions were performed. The reaction mixture was treated with I_2, CBr_4, 2,2,6,6-tetramethylpiperidinyloxyl (TEMPO), 1,3-cyclohexadiene and MeOD but none of the reactions resulted in identifiable products. Only the reaction with 1,4-cyclohexadiene gave the 1-hydridogermole **75** in a selective reaction (Scheme 34).

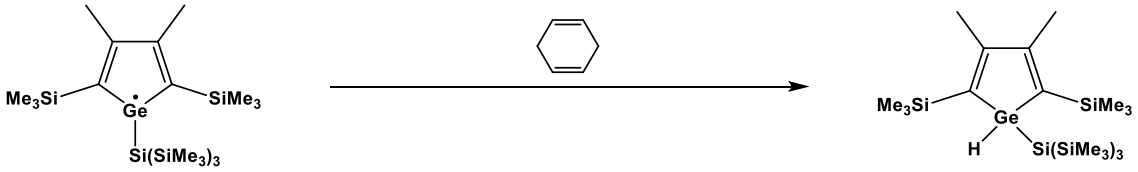

69 **75**

Scheme 34: Trapping reaction of the germolyl radical **69** with 1,4-cyclohexadiene to give the 1-hydrogen substituted germole **75**.

The NMR spectra of the products of the trapping reaction are shown in Figure 21. In the ^{1}H NMR spectrum a signal for a GeH with a shift of $\delta^{1}H = 5.40$ can be seen. The signals for the trimethylsilyl groups of the five-membered ring and the $Si(SiMe_3)_3$ group overlap. The $^{13}C\{^{1}H\}$ and the $^{29}Si\{^{1}H\}$ INEPT NMR show signals in the expected range for a 1-tris(trimethylsilyl)silylgermole. All detected signals are consistent with the 1-hydridogermole **75** which was also synthesised by the reaction of the 1-chlorogermole **46** with $LiAlH_4$.[81]

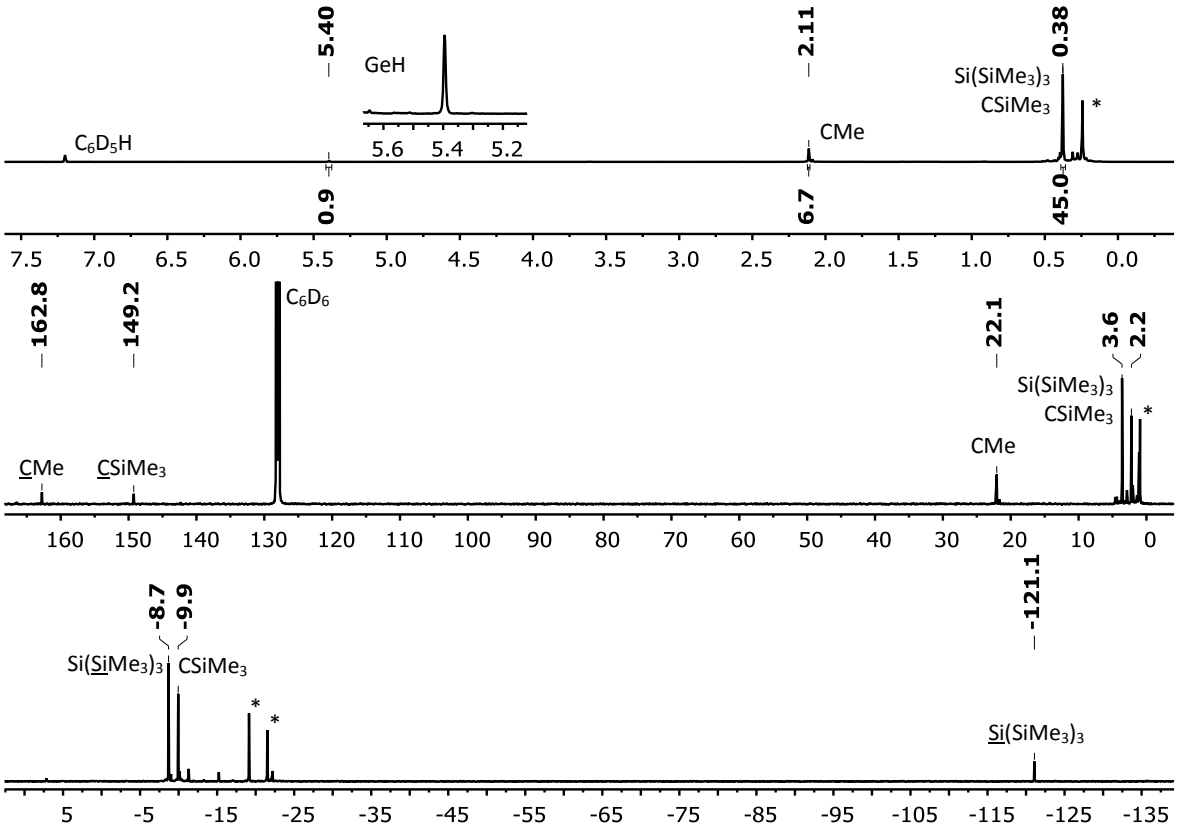

Figure 21: NMR spectra of the 1-hydridogermole **75** in C_6D_6; top: ^{1}H NMR (499.9 MHz, 305.0 K); middle: $^{13}C\{^{1}H\}$ NMR (125.7 MHz, 305.0 K); bottom: $^{29}Si\{^{1}H\}$ INEPT NMR (99.3 MHz, 305.1 K); * impurities.

A second 1-tris(trimethylsilyl)silyl substituted germolyl radical **76**, which was Si^{t}BuMe$_2$ substituted in 2,5-position, was synthesised by the reduction of germole **48** with potassium graphite (Scheme 27). However, the intensity of the EPR signal was very weak and the NMR spectra showed a complex reaction mixture. Therefore, no further trapping reactions were performed and only the obtained EPR spectrum will be discussed here (Figure 22).

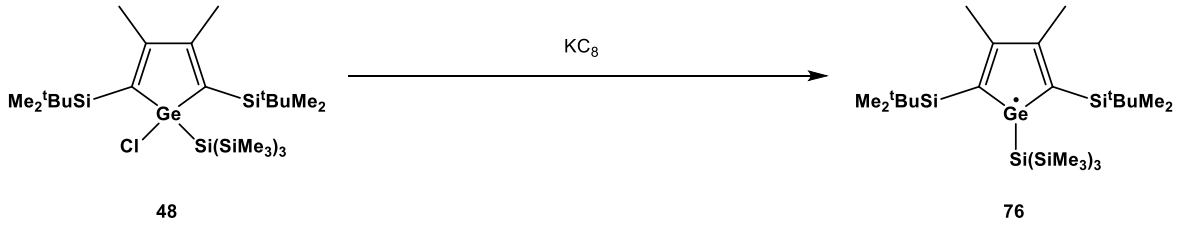

48 **76**

Scheme 35: Reduction of 1-chloro-1-tris(trimethylsilyl)silyl-2,5-bis(tert-butyldimethylsilyl)germole **48** to the respective germolyl radical **76**.

The EPR spectrum of **76** shows a similar germanium centred radical with the main singlet and the decet for the ^{73}Ge isotope. The hyperfine coupling constant is $a(^{73}Ge_{\alpha})$ = 2.0 mT and is therefore smaller than the one detected for the 2,5-bis(trimethylsilyl)germolyl radical **69**. This suggests the structure tends to be more planar. The observed hfcc for the tris(trimethylsilyl)silyl group is $a(^{29}Si_{\gamma})$ = 0.8 mT, and therefore, in the same range as in germolyl radical **69**.

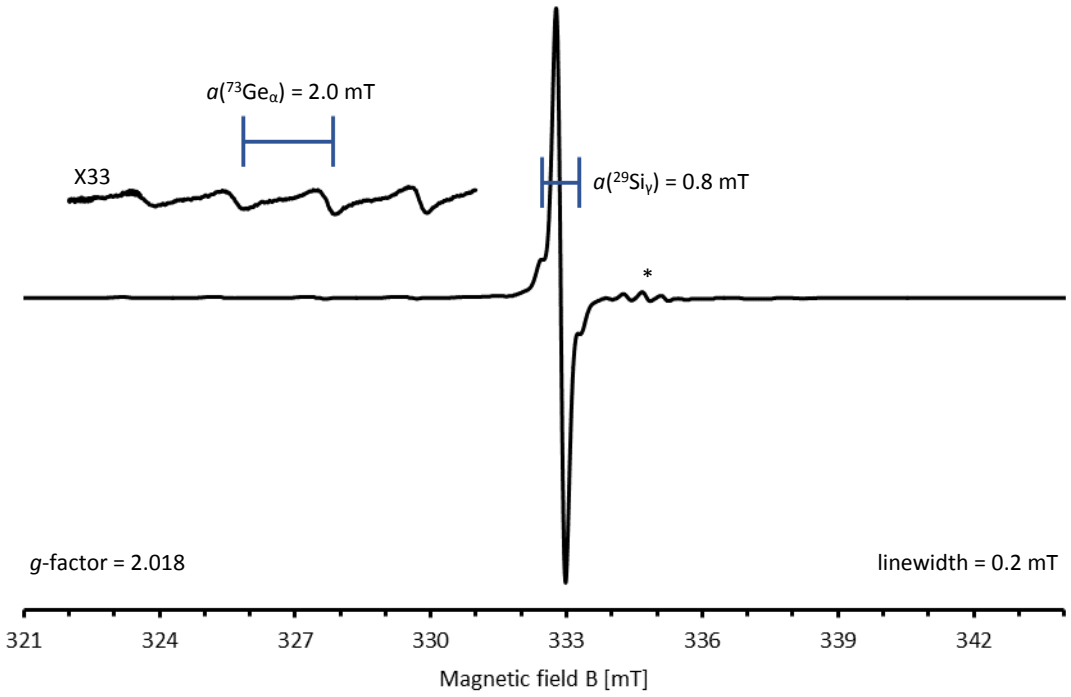

Figure 22: EPR spectrum of the 1-tris(trimethylsilyl)silyl-2,5-bis(tbutlymethylsilyl)germolyl radical **76** in heptane at room temperature; 9402.0 MHz; Mod.-Ampl. = 0.150 mT; MW-Att. = 3.0 dB; * impurity.

The last germole which was investigated in the radical synthesis was the 1-tris(trimethylsilyl)germyl-germole **47**. However, the reduction of the germolyl chloride **47** only resulted in a complex reaction mixture according to the NMR spectra and no radical species was detected by EPR spectroscopy.

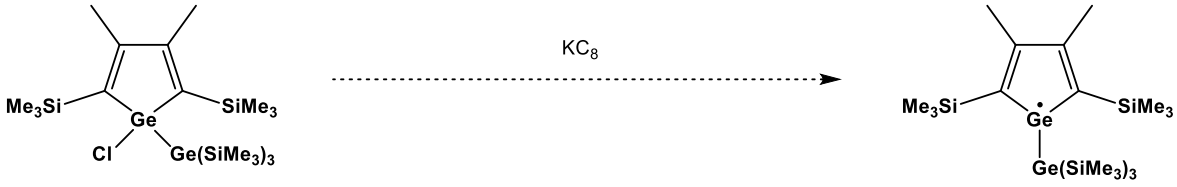

47 **77**

Scheme 36: Unsuccessful attempt on the reduction of 1-chloro-1-tris(trimethylsilyl)germylgermole **47** to the respective germolyl radical **77**.

3.2.5 Reduction of 1-Tris(trimethylsilyl)silylsilolyl chloride

After the synthesis of stable germolyl radicals by the reduction of their respective chlorides with potassium graphite, it was of great interest, to determine if the analogous siloles could also be transformed into radical species. Therefore, the 1-tris(trimethylsilyl)silylsilolyl chloride **56** was synthesised and its reduction investigated (Scheme 37). The only structural difference to germolyl chloride **46**, besides the heteroatom in the ring system, is the identity of the substituents at the 3,4-position. The methyl substituents are replaced by phenyl groups. This difference is related to the synthetic approach necessary to assemble the five-membered silole ring.

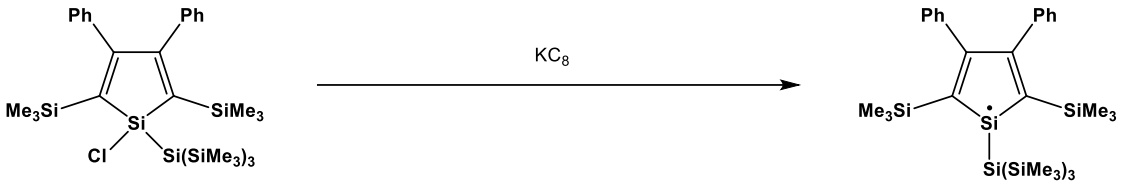

56 78

Scheme 37: Reduction of 1-chloro-1-tris(trimethylsilyl)silylsilole **56** to the respective silolyl radical **78**.

After performing the reduction of the chlorosilole **56** with potassium graphite under the same conditions as described for the germoles in Chapter 3.2.4, an EPR spectrum of a silicon-centred radical species was obtained (Figure 23).

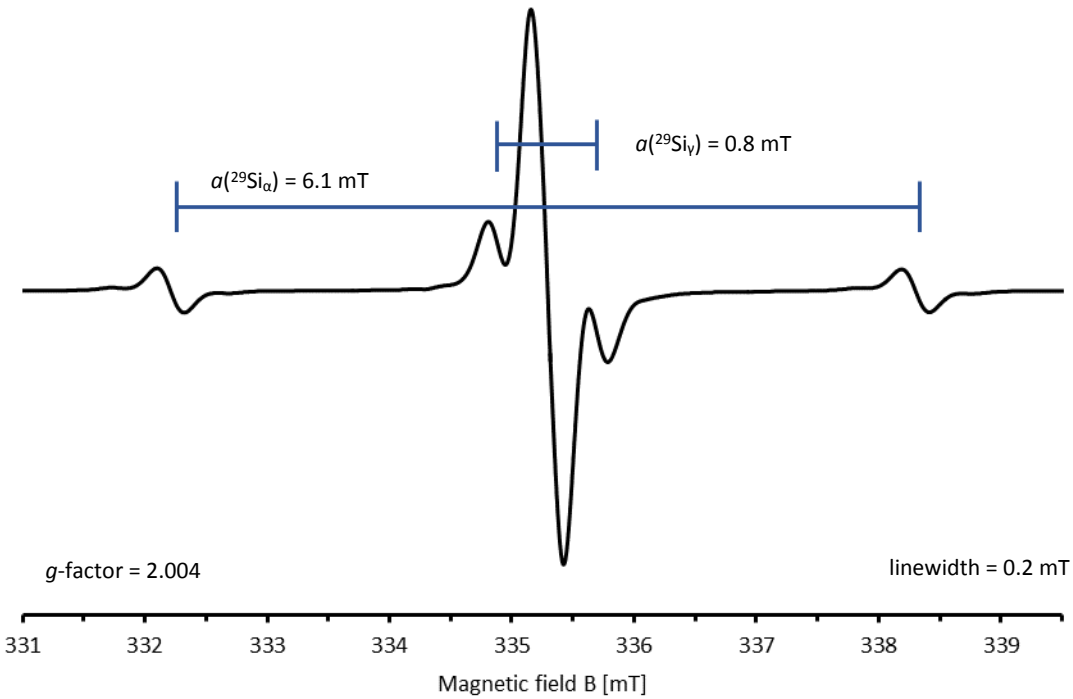

Figure 23: EPR spectrum of the 1-tris(trimethylsilyl)silylsilolyl radical **78** in hexane at room temperature; 9403.0 MHz; Mod.-Ampl. = 0.075 mT; MW-Att. = 3.0 dB.

In this spectrum, an intense singlet for an unpaired electron and a doublet with a lower intensity and a hyperfine coupling constant of $a(^{29}Si_{\alpha})$ = 6.1 mT, which is very characteristic for a silicon-centred radical[92,102,109], can be seen. This doublet is a result of coupling with the ^{29}Si isotope. A second doublet with higher intensity and a hfcc of $a(^{29}Si_{\gamma})$ = 0.8 mT is also detected. Due to the magnitude of the hfcc, which is the same as that observed in the EPR spectrum of germolyl radical **69**, and the increased intensity compared to $a(^{29}Si_{\alpha})$, this signal can be assigned to the three spectroscopically equivalent Si atoms of the tris(trimethylsilyl)silyl substituent. Upon expansion, further details of the EPR spectrum can be observed (Figure 24).

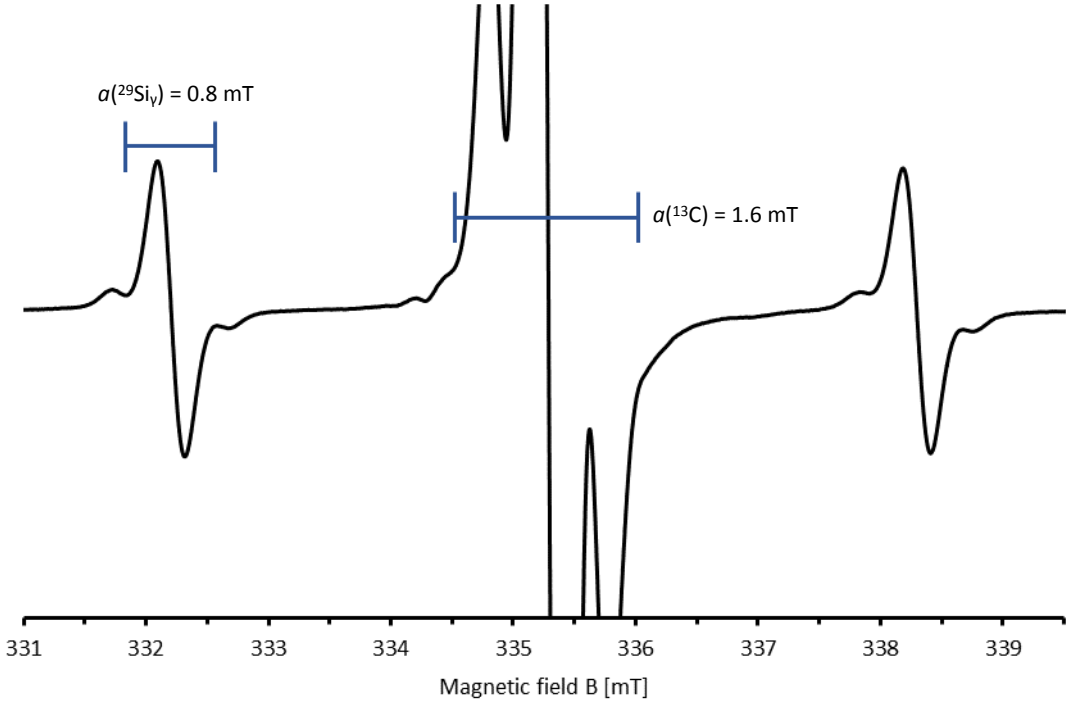

Figure 24: Excerpt of the EPR spectrum of the silolyl radical **78** and assumed assignment of hyperfine coupling constants.

In the expansion, the doublet assigned to $^{29}Si_{\gamma}$, resulted by the tris(trimethylsilyl)silyl group, is repeated in the doublet assigned to $^{29}Si_{\alpha}$. Additionally, another signal close to the centre of the signal with a hfcc of a = 1.6 mT can be seen. Due to its fairly low intensity, the doublet can be assigned to the carbon atoms of the ring system.

Similar to the investigations of the germolyl radical **69**, further information could be obtained if the central signal is recorded using low modulation frequency. In the spectrum, which is shown in Figure 25, another hyperfine coupling can be observed. The signal shows a very high multiplicity

which leads to the conclusion that it must be a hydrogen coupling of either the trimethylsilyl groups or the hydrogens on the phenyl groups. The hyperfine coupling constant is, at $a(^1H)$ = 0.02 mT, fairly small. In comparison, the hfcc of the phenyl hydrogens in the triphenylmethyl radical is $a(^1H)$ = 0.13 mT and for the tert-butyl and methyl hydrogens of the tris(tert-butyldimethylsilyl)silyl silyl radical synthesised by Kira et al.[109] is $a(^1H)$ = 0.03 mT and $a(^1H)$ = 0.01 mT, respectively.

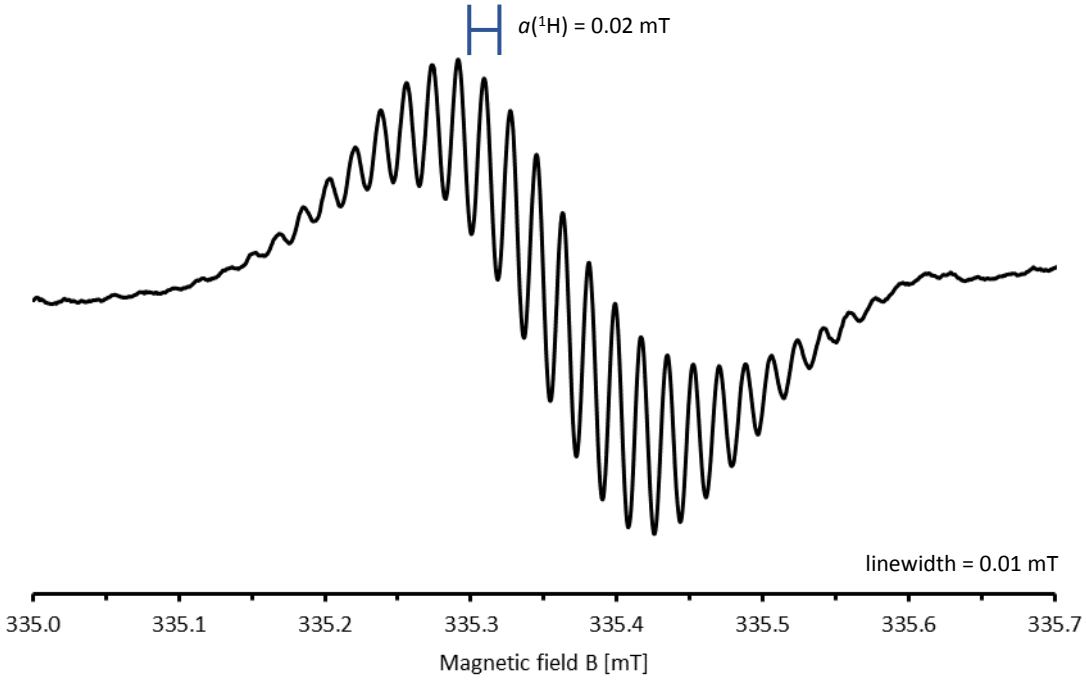

Figure 25: EPR spectrum of the main signal of the germolyl radical **78** in hexane at room temperature using low modulation frequency; 9407.0 MHz; Mod.-Ampl. = 0.005 mT; MW-Att. = 30.0 dB.

The analytical data obtained by EPR spectroscopy indicate that the synthesis of the tris(trimethylsilyl)silylsilolyl radical **78** was successful. The hyperfine couplings and the multiplicity of the signals are consistent with the assigned structure.

To further support the assignment of the signals, the obtained data were used to simulate the spectra. With the respective number of nuclei and the experimentally determined hyperfine coupling constants, the simulated spectrum was in good agreement with the experimental spectrum (Figure 26). Further details regarding the simulation and the input utilised for the EasySpin toolbox for MATLAB are presented in Chapter 7.1.3.

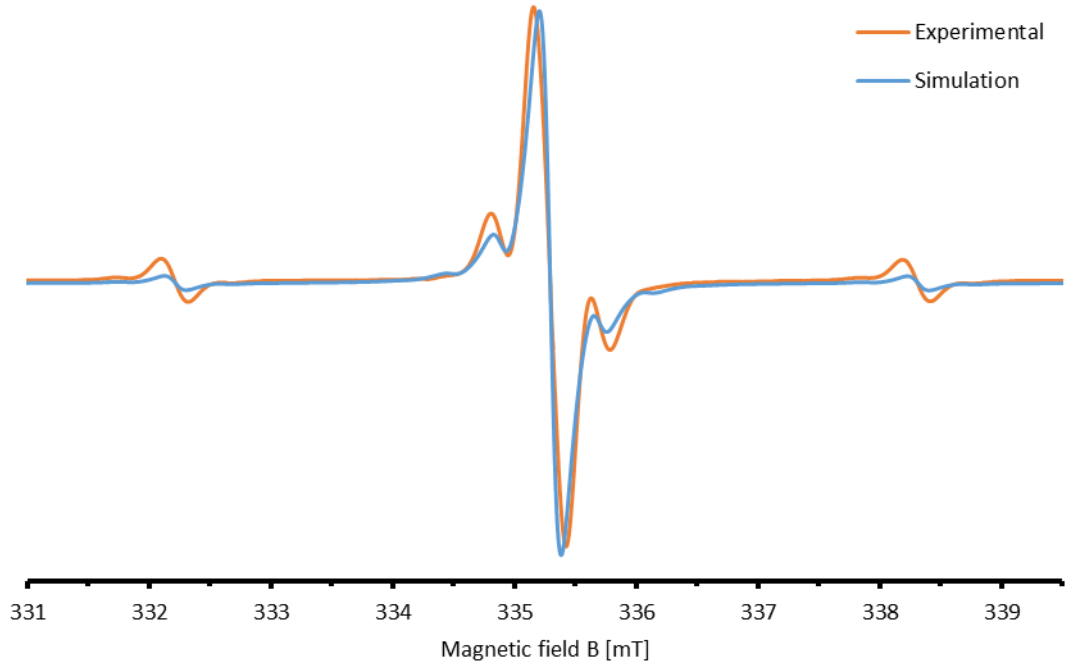

Figure 26: Simulated EPR spectrum of the tris(trimethylsilyl)silylsilolyl radical **78** with EasySpin.[104]

Notable differences in the stability of the silolyl radical **78** in comparison to the germolyl radical **69** were observed. In contrast to the persistency of the germolyl radical **69**, the signal of the silicon centred analogue **78** disappeared after several days and only a broad signal without any characteristic hyperfine couplings remained.

By comparison of the experimental data with known silicon-centred radicals, additional information was gleaned (Scheme 34). Similar to the comparison of germolyl radicals, the geometry at the silicon centre can be evaluated. As described in Chapter 3.2.4, the ^{29}Si hyperfine coupling constants are strongly dependent on the percentage of s-character of the orbital in which they are localised, and therefore, on the pyramidalisation at the radical centre. A similar trend, which has already been discussed for the germyl radicals, can also be seen for silicon-centred radicals, when the obtained hfcc is compared to two different silyl radicals synthesised by Sekiguchi et al.[92,102]

The silyl radical **79**,[92] shown in Figure 27, has a planar structure and a π-conjugated system, and thus, the unpaired electron is delocalised. This leads to low values for the hyperfine coupling constants. The silyl radical **80** is known to be planar at the silicon centre. However, the radical is not delocalised in a π-system. The radical is localised at silicon and shows a hfcc of $a(^{29}Si_{\alpha})$ = 5.8 mT. This value is lower compared to the one of the synthesised silolyl radical **78**, which has a hfcc of $a(^{29}Si_{\alpha})$ = 6.1 mT. Having a slightly larger hyperfine coupling constant suggests that the structure is also lacking π-conjugation into the ring system and that the silicon centre is pyramidalised.

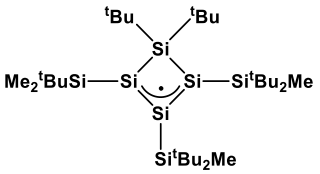

79 by Sekiguchi et al.[92]

g-factor = 2.006

$a(^{29}Si)$ = 4.1 mT
$a(^{29}Si)$ = 3.7 mT
$a(^{29}Si)$ = 1.6 mT

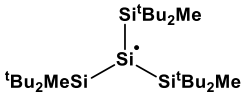

80 by Sekiguchi et al.[102]

g-factor = 2.006

$a(^{29}Si_{\alpha})$ = 5.8 mT
$a(^{29}Si_{\beta})$ = 0.8 mT

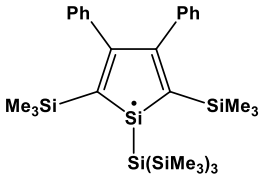

Silolyl radical **78**

g-factor = 2.004

$a(^{29}Si_{\alpha})$ = 6.1 mT
$a(^{29}Si_{\gamma})$ = 0.8 mT

Figure 27: Comparison of the tris(trimethylsilyl)silyl silolyl radical **78** with silicon centred radicals **79** and **80** synthesised by Sekiguchi et al.[92,102]

Similar quantum mechanical investigations for the structural dependence on the hyperfine coupling constants were carried out. The analogous model silolyl radical **81** was used to calculate the energy change, ΔE, and the change in the hfcc, $a(^{29}Si_{\alpha})$, while bending the SiH_3 group stepwise at the M06-2X/6-311+G(d,p) level of theory. The angle ε(X-Si-Si) was alternated in 5° steps. In Figure 28, the energy change is plotted against the angle of the substituent; the planar structure is set as a reference.

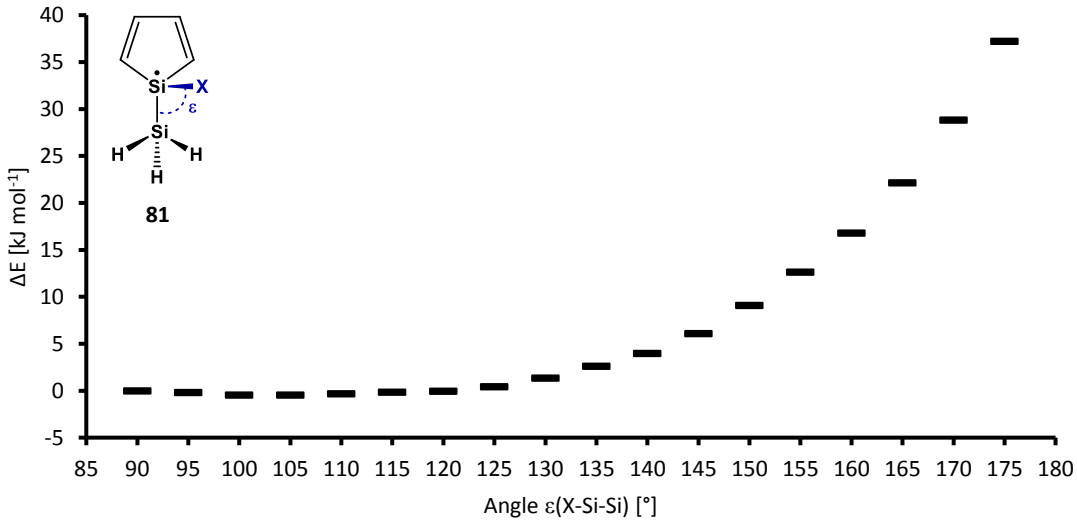

Figure 28: Bending potential of the SiH_3 group in the model silolyl radical **81** at the M06-2X/6-311+G(d,p) level of theory. The angle between the Si-Si vector and the orthogonal vector to the plane of the five-membered ring through the ring silicon atom ε(X-Si-Si), has been alternated in 5° steps to investigate the energy change ΔE between a planar and tetrahedral structure of these silolyl radicals.

There are no significant energy differences between the planar (ε(X-Si-Si) = 90°, ΔE = 0.0 kJ mol^{-1}) and a pyramidalised structure up to an angle of ε(X-Si-Si) = 130° (ΔE = 1.4 kJ mol^{-1}). Upon increasing the angle beyond 130°, the energy difference increases to ΔE = 37.2 kJ mol^{-1}

The influence of the pyramidalisation at the radical centre on the $a(^{29}Si_{\alpha})$ hyperfine coupling constant is plotted in Figure 29. In analogy to the results obtained for the model germolyl radical **73**, the differences between planar and pyramidalised structures are significant. The hfcc ranges from $a(^{29}Si_{\alpha})$ = 3.0 mT for a planar structure to $a(^{29}Si_{\alpha})$ = 22.6 mT for a pyramidalised structure with an angle of ε(X-Si-Si) = 170°. The range of $\Delta a(^{29}Si_{\alpha})$ = 19.6 mT illustrates the significant influence of the pyramidalisation at the silicon centre on the magnitude of the hyperfine coupling constant.

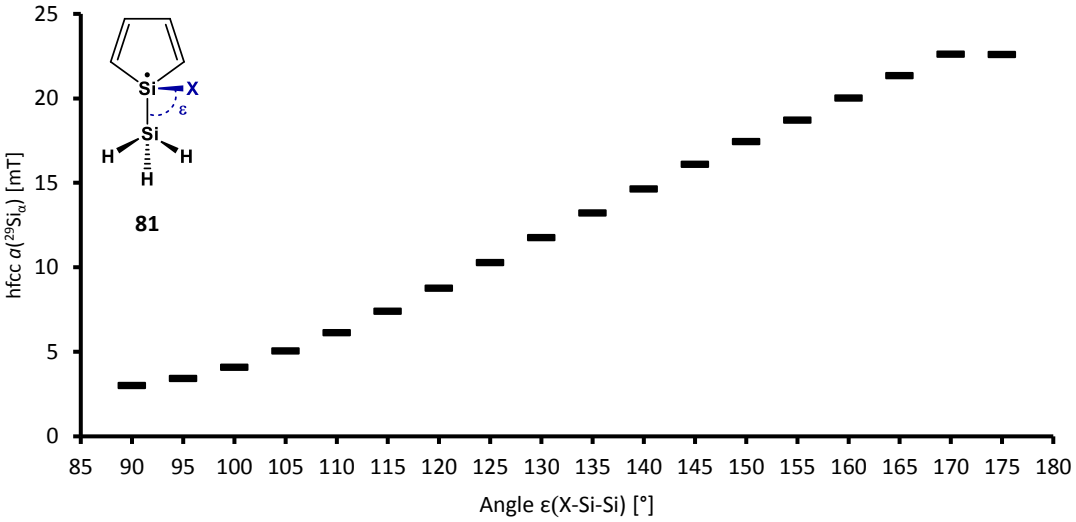

Figure 29: Dependence of the hfcc $a(^{29}Si_{\alpha})$ on the bending angle ε(X-Si-Si) of the SiH_3 group in the model silolyl radical **81** at the M06-2X/6-311+G(d,p) level of theory. The angle between the Si-Si vector and the orthogonal vector to the plane of the five-membered ring through the ring silicon atom ε(X-Si-Si), has been increased in 5° steps to investigate the change in $a(^{29}Si_{\alpha})$ between a planar and tetrahedral structure of the silolyl radical.

Additionally, quantum mechanical calculations of silolyl radical **78** were carried out. On the left in Figure 30 the optimised structure obtained using Gaussian at the M06-2X/Def2-TZVP level of theory is shown. Similar to the germanium centre in germolyl radical **69**, the silicon centre is pyramidalised with a sum of angles of ∑(Si) = 345°. The single and double bonds of the ring system are alternating similar as in the starting chlorosilole **56** (Table 6). No sign of π-conjugation with the radical centre is observed. On the right side of Figure 30 the spin density distribution, obtained by a single point calculation using ORCA at the PBE0/Def2-TZVPD level of theory, is shown. In the silolyl radical **78** the spin density is also mainly localised at the silicon centre with some contribution into the π-system.

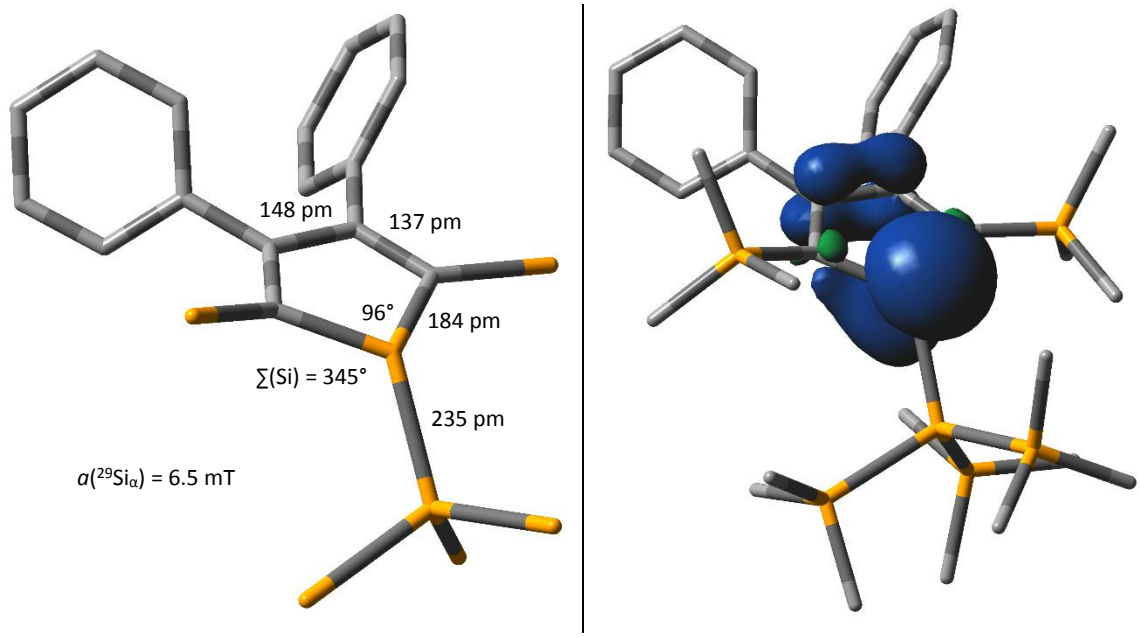

Figure 30: Calculated structure of silolyl radical **78**; ORCA single point calculation on the optimised structure obtained using Gaussian, PBE0/Def2-TZVPD//M06-2X/Def2-TZVP; carbon: grey; silicon: yellow; left: molecular structure, hydrogen atoms and methyl groups of trimethylsilyl groups are omitted for clarity; right: spin density at isovalue = 0.004, hydrogen atoms are omitted for clarity.

In contrast to the calculations performed on the germolyl radical **69**, the PEB0 method was used over the M06-2X method because the calculated hyperfine coupling constant of $a(^{29}Si_{\alpha})$ = 6.5 mT was in better agreement with the experimentally obtained of $a(^{29}Si_{\alpha})$ = 6.1 mT. Additional single point calculations using ORCA in combination with the M06-2X and PBE0 methods and the IGLOIII basis set, which is known to be suitable for the calculation of EPR parameters,[110] were carried out. The obtained hyperfine coupling constants were also in good agreement with the experimental values ($a(^{29}Si_{\alpha})$ = 6.0 mT at PBE0/IGLOIII; $a(^{29}Si_{\alpha})$ = 6.9 mT at M06-2X/IGLOIII). The IGLOIII basis set is not defined for germanium, and therefore, no calculations on germolyl radicals can be performed using this basis set.

As additional evidence for the synthesis of the tris(trimethylsilyl)silylsilolyl radical **78**, trapping reactions, which were already shown to be a successful approach for the germolyl radical **69**, were performed (Scheme 38).

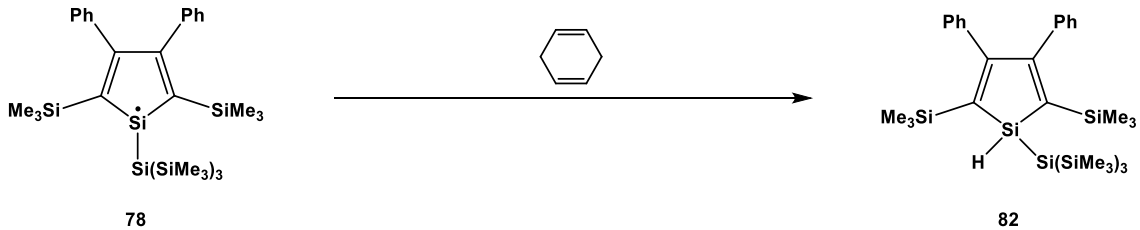

Scheme 38: Trapping reaction of the silolyl radical **78** with 1,4-cyclohexadiene to give the 1-hydrogen substituted silole **82**.

After reduction with one equivalent potassium graphite, the presence of the radical species was detected by EPR spectroscopy. The same sample was also analysed by NMR spectroscopy, where residual starting material was detected. Even though the reduction reaction was not complete, the trapping reaction was performed. In the following, the ^{1}H and ^{29}Si NMR spectra of the reaction mixture after the addition of 1,4-cyclohexadiene will be discussed (Figure 31 and Figure 32).

Figure 31 shows the ^{1}H NMR spectra before (top) and after (bottom) addition of the diene. In the top spectrum, only the signals related to the chlorosilole **56** with residual THF and some minor impurities can be seen. In the bottom NMR spectrum in Figure 31, which was recorded after the addition of 1,4-cyclohexadiene, the formation of the 1-hydrogen substituted silole **82** can be observed. A clear indication is the formation of the SiH with a signal at $\delta^{1}H$ = 5.28. In addition to the two singlets assigned to the $SiMe_3$ and $Si(SiMe_3)_3$ groups of the starting material, two singlets assigned to silole **82** were apparent. Integration of these signals gave the ratio of the 1-chlorosilole **56** and the 1-hydridosilole **82** as 57:43, which means only half of the starting material was reduced.

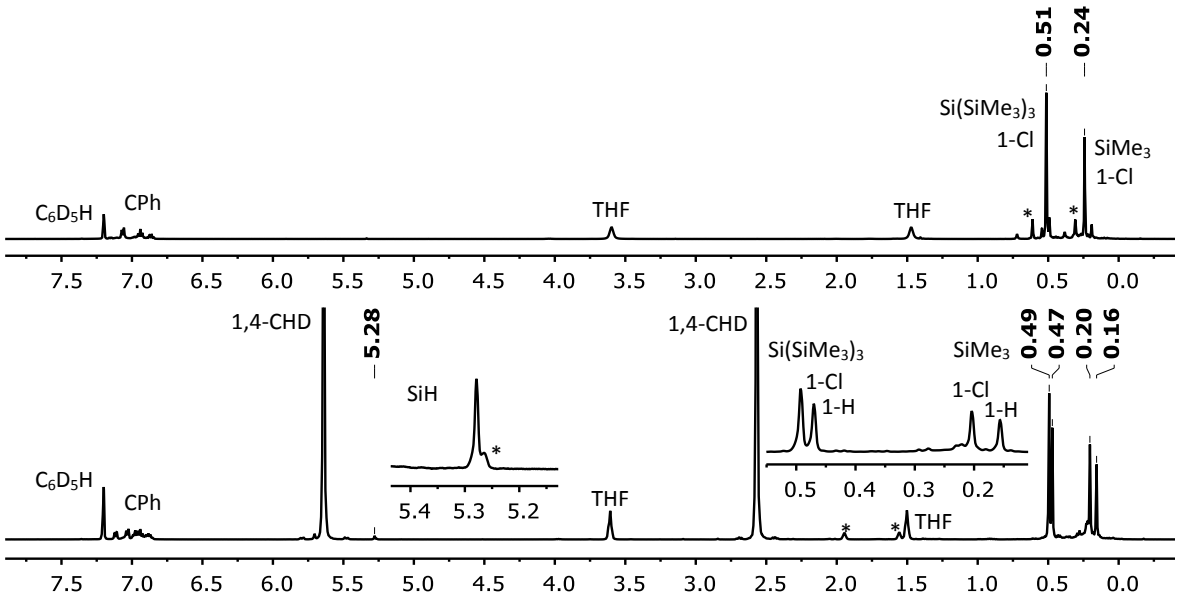

Figure 31: ^{1}H NMR spectra in C_6D_6; top: reaction mixture of silolyl radical **78** which still contained the chlorosilole **56** (499.9 MHz, 305.0 K); bottom: reaction mixture after the addition of 1,4-cyclohexadiene (1,4-CHD) to trap radical **78** as 1-hydrogen substituted silole **82** (499.9 MHz, 305.1 K); * impurities.

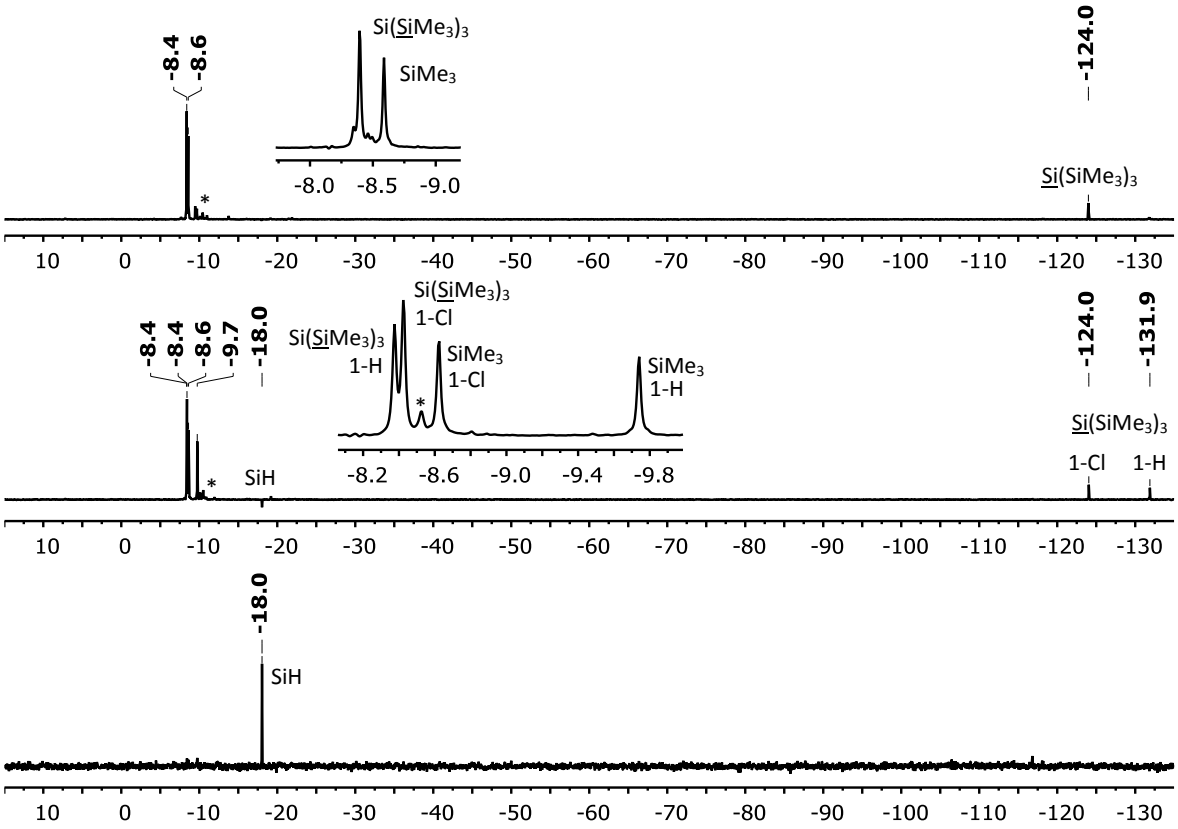

Figure 32: ^{29}Si INEPT NMR spectra in C_6D_6; top: reaction mixture of silolyl radical **78** which still contained the chlorosilole **56** (99.3 MHz, 305.0 K, D3 = 6.8 ms, D4 = 31.0 ms); middle and bottom: reaction mixture after the addition of 1,4-cyclohexadiene to trap radical **78** as 1-hydrogen substituted silole **82**; middle: (99.3 MHz, 305.0 K, D3 = 6.8 ms, D4 = 31.0 ms); bottom: (99.3 MHz, 305.0 K, D3 = 1.0 ms, D4 = 1.0 ms); * impurities.

In Figure 32, the ^{29}Si INEPT NMR spectra of the reaction with 1,4-cyclohexadiene are shown. The top spectrum was recorded before the addition of the diene and shows only the expected signals for the starting material. The middle spectrum was measured after the addition and another set of signals which can be assigned to the $SiMe_3$ and $Si(SiMe_3)_3$ groups were apparent. An additional signal, assigned to the SiH, was detected at a chemical shift of δ^{29}Si = -18.0. This signal was also the only observed signal if the ^{29}Si INEPT NMR spectrum was performed using parameters which are suitable for the observation of SiH groups (bottom spectrum, D3 = 1.0 ms, D4 = 1.0 ms). All detected signals are consistent with the formation of 1-hydridosilole **82** which was also synthesised independently by the reaction of 1-chlorosilole **56** with $LiAlH_4$.[89]

Unfortunately, it was, as with the germolyl radicals, not possible to obtain single crystals of the silolyl radical **78** suitable for X-ray analysis. Only crystals of the corresponding potassium salt of the silolyl anion **83** were isolated. The structure will be discussed in Chapter 3.3.2.

3.2.6 Formation of 1-Tris(trimethylsilyl)silyl Sila- and Germacyclopentadienyl Radicals

The reduction of the sila- and germacyclopentadienyl chlorides to their respective radicals was presented in Chapters 3.2.4 and 3.2.5. The mechanism of the reactions, however, does not appear to be a simple one electron reduction of the chloride by potassium graphite with the elimination of potassium chloride (Scheme 39).

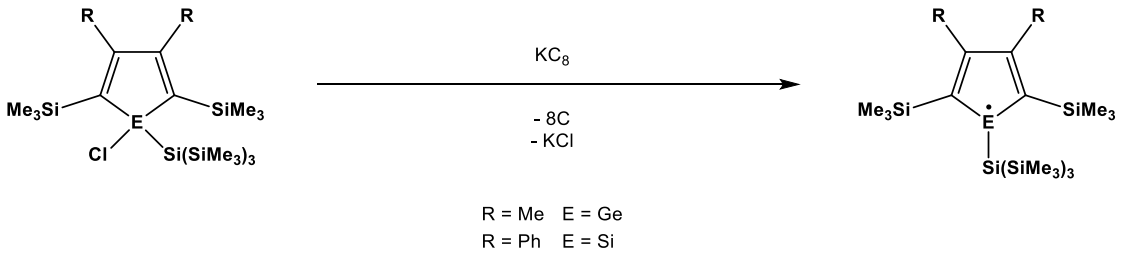

Scheme 39: Reduction of sila- or germacyclopentadienyl chloride with potassium graphite.

Several investigations suggested another reaction pathway to be operational for the synthesis of the radicals. First, the radicals were not observed in THF in which the reaction was performed. Only after changing the THF to a nonpolar solvent was the detection of the radicals by EPR spectroscopy observed. Second, the NMR spectra after the reduction often showed residual starting material. And third, most crystallisation attempts only gave single crystals of the potassium salt of the respective anion. These facts suggest that one equivalent of the potassium graphite overreduces half an equivalent of the heterolyl chloride to yield an equal mixture of the starting material and the respective anion. In the second step of the reaction, the anion and the residual starting material undergo a comproportionation reaction forming the respective radical (Scheme 40).

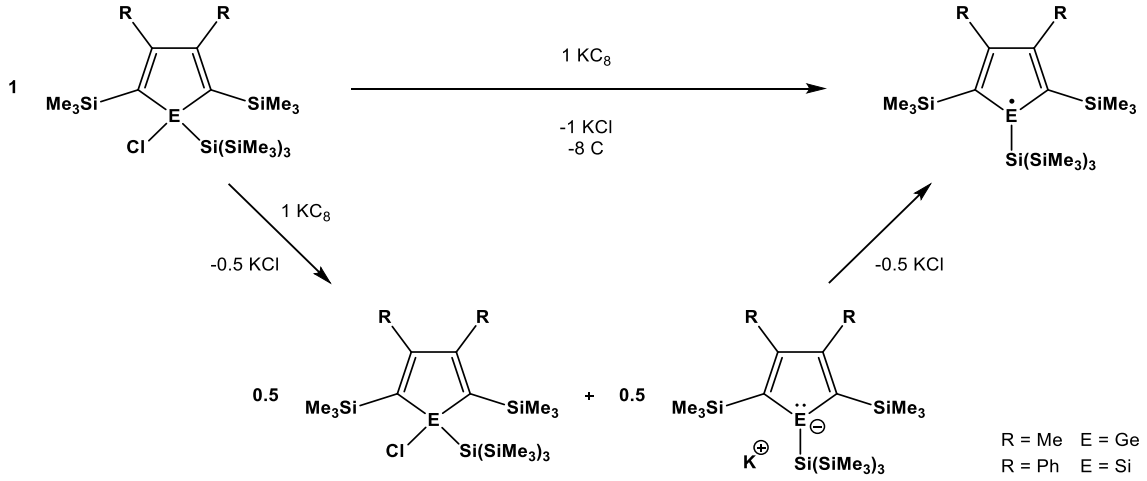

Scheme 40: Suggested reaction pathway for the formation of group 14 heterolyl radicals.

This would explain the presence of residual starting material in the NMR spectra and the crystallisation of the anions from the reaction mixture. Interestingly, the radical species was not detected in THF, the solvent in which the reaction was performed, even though THF should favour the reduction, because the anion is expected to be more reactive due coordination of to the solvent molecules to the potassium counter cation. However, the change to a nonpolar solvent may facilitate the elimination and precipitation of potassium chloride, leading to the radical species.

Experiments though in which chlorogermole **46** was treated with the respective anion **74** did not result in the formation of germolyl radical **69** (Scheme 41, top). Due to the poor solubility of the anions in nonpolar solvents, which were necessary for obtaining EPR spectra, THF was added to the reaction mixture. Only in the reaction of the chlorosilole **55** with the analogous anion **84**, was an EPR spectrum of a silicon centred radical detected. However, the weak intensity of the signal suggested that it was only formed in trace amounts. Even after several days and heating to 60 °C for several hours the intensity of the signal did not increase. Additionally, the NMR spectra of the reaction mixture only showed the presence of both compounds. The intensity of **55** and **84** did not decrease over the course of the reaction (Scheme 41, bottom).[87]

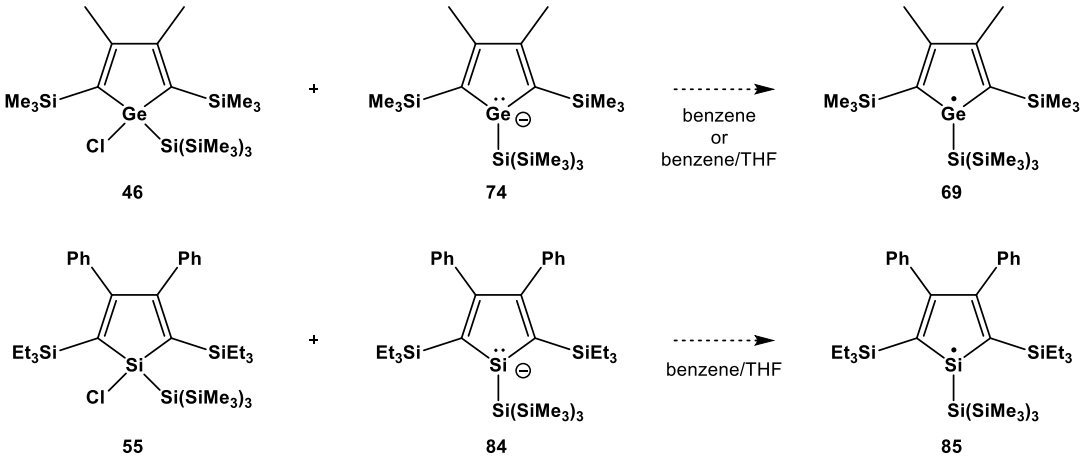

Scheme 41: Attempts on the comproportionation reaction of heterolyl chlorides **46** or **55** with their corresponding anions **74** or **84** to form germolyl or silolyl radical **69** or **85**.[87]

The comproportionation might be sensitive to the conditions of the reaction and it should be investigated further with different solvents. The formation of the radical species in the reduction reaction with potassium graphite might rely on the presence of residual graphite, which may catalyse the comproportionation. The absence of graphite in the reaction of the heterolyl chlorides with their anions might be the reason why the reaction does not take place to any significant extent.

Notable, an NMR spectrum of a mixture of germolyl anion **74** and 1,4-cyclohexadiene did not show the presence of the 1-hydridogermole **75**. This verified that the 1-hydridogermole **75** is not the reaction product of the anion **74** but of the respective radical species **69** (Scheme 42**).**

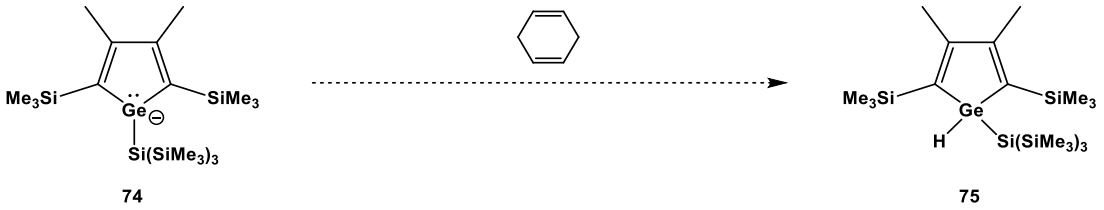

Scheme 42: Germolyl anion **75** does not react with the trapping reagent 1,4-cyclohexadiene to form the 1-hydridogermole **75**.

The overreduction of the germole radical **69** to the respective anion **74** can be understood by perusal of the calculated electron affinities ΔEA. As shown in Scheme 43, the calculated electron affinity from the germole cation **86** to the radical **69** is ΔEA = -557 kJ mol^{-1} and from radical **69** to anion **74** is ΔEA = -189 kJ mol^{-1}.

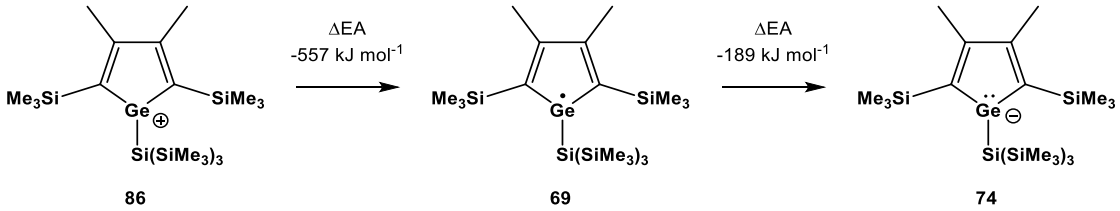

Scheme 43: Calculated electron affinity ΔEA of the 1-tris(trimethylsilyl)silylgermolyl cation **86**, radical **69** and anion **74** at the M06-2X/6-311+G(d,p) level of theory.

If these values are compared to the calculated electron affinities of the GeH_3 cation, radical and anion differences can be observed (Scheme 44). The electron affinity from the GeH_3 cation to the radical is 209 kJ mol^{-1} higher compared to the germole. However, upon going from the GeH_3 radical to the anion, the value is 62 kJ mol^{-1} lower. This indicated that the germole radical is favoured to be reduced to the respective anion in comparison to the GeH_3 radical and anion.

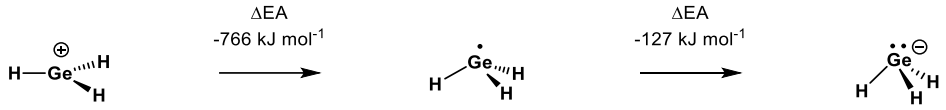

Scheme 44: Calculated electron affinity ΔEA of the GeH_3 cation, radical and anion at the M06-2X/6-311+G(d,p) level of theory.

3.3 Sila- and Germacyclopentadienyl Anions

In Chapters 3.2.4 and 3.2.5, the reduction of 1-tris(trimethylsilyl)silylsilolyl and -germolyl chlorides with potassium graphite to form their respective radicals was presented. During these reactions the formation of silolyl and germolyl anions were often observed. In the following, details of these anions will be discussed.

3.3.1 Germole Anions

In an attempt to synthesise the germolyl radical **69** in hexane, the potassium salt of the germolyl anion **74** crystallised. The crystals were suitable for X-ray analysis (a, Scheme 45). By performing the reduction reaction in THF with two equivalents of KC_8 the same potassium salt of the germolyl anion **74** was synthesised and isolated (b, Scheme 45).

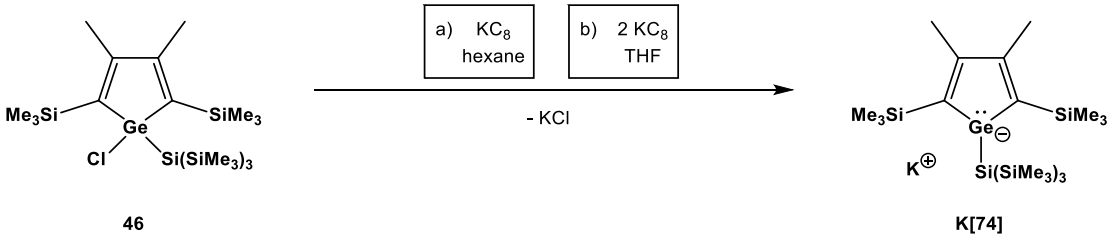

Scheme 45: Reduction of the chlorogermole **46** with potassium graphite at different conditions which led to the potassium salt of the germolyl anion **74**.

The anion was further identified by NMR spectroscopy of a C_6D_6 solution which contained some THF to increase the solubility. In addition to the X-ray diffraction analysis of the solvent free single crystals, a THF solvent complex of **K[74]** was also obtained as single crystals and analysed (Figure 35). The NMR spectra of the germolyl anion potassium salt **K[74]** are shown in Figure 33 and Figure 34. The signal pattern in the ^{1}H, ^{13}C and ^{29}Si NMR is identical to the one of the starting material **46** (Table 3) and of the 1-hydridogermole **75** (Figure 21). Interestingly, the $^{1}H^{29}Si$ HMBC NMR spectrum (Figure 34) shows a correlation of the hydrogen atoms of the ring methyl groups at the 3,4-position with the central silicon atom of the tris(trimethylsilyl)silyl group. This is a correlation across five bonds which is only rarely detected.

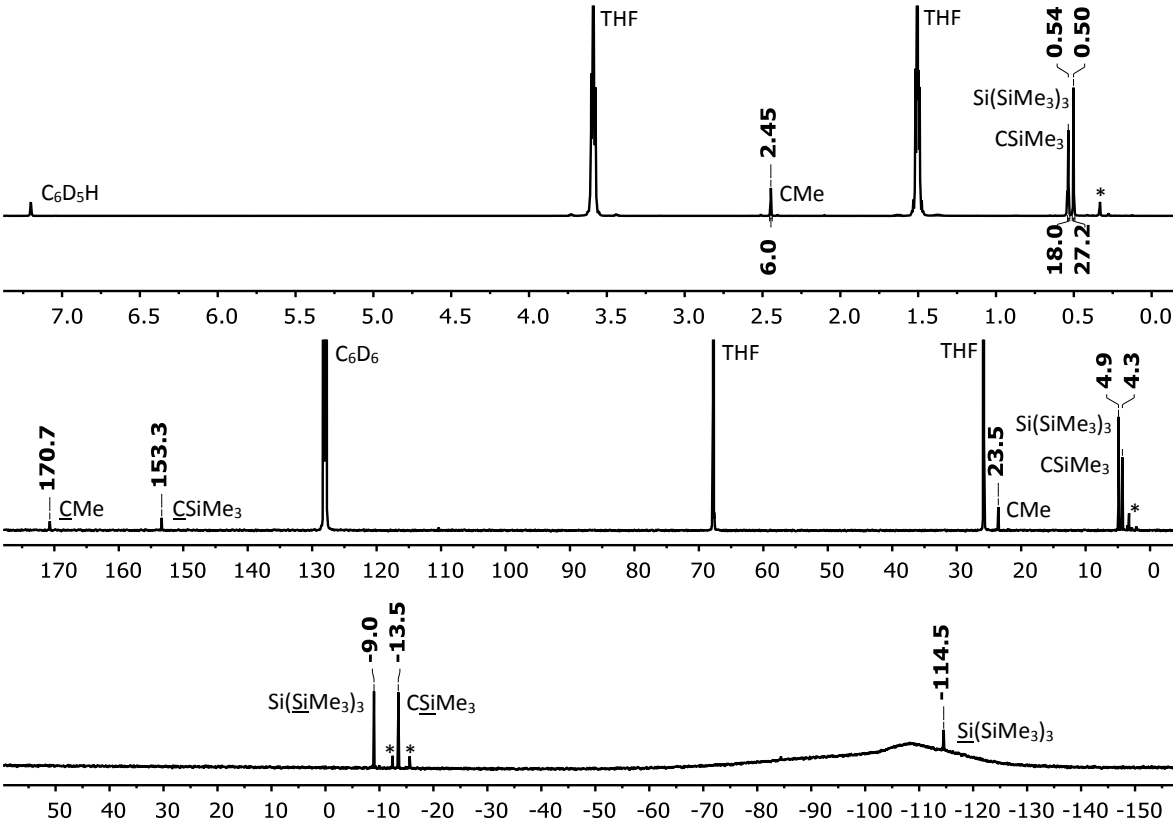

Figure 33: NMR spectra of germolyl anion salt **K[74]** in C_6D_6/THF; top: ^{1}H NMR (499.9 MHz, 304.9 K); middle: $^{13}C\{^{1}H\}$ NMR (125.7 MHz, 305.0 K); bottom: $^{29}Si\{^{1}H\}$ NMR (99.3 MHz, 305.0 K); * impurities.

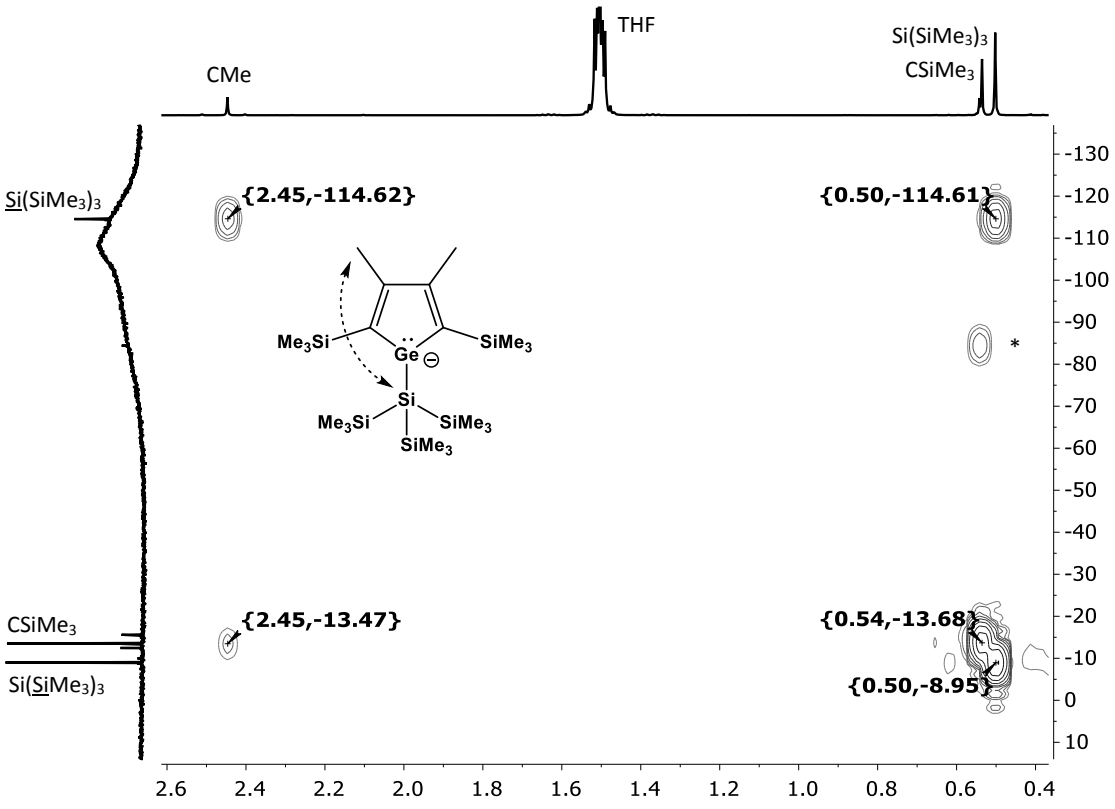

Figure 34: $^{1}H^{29}Si$ HMBC NMR spectrum (499.9 MHz/99.3 MHz) of germolyl anion salt **K[74]** in C_6D_6/THF at 305.0 K; * impurity.

The two obtained molecular structures of the solvent free and THF complexed contact ion pair of the potassium salt of the germolyl anion **74** are shown in Figure 35. Besides the coordination of a THF molecule to each of the potassium atoms, there are no significant structural differences (Table 10). Only the distances of the potassium atoms to the germanium atoms are slightly increased in the THF complexed structure ($\Delta d(Ge\text{-}K(\eta^1))$ = 7.6 pm; $\Delta d(Ge\text{-}K(\eta^5))$ = 3.8 pm).

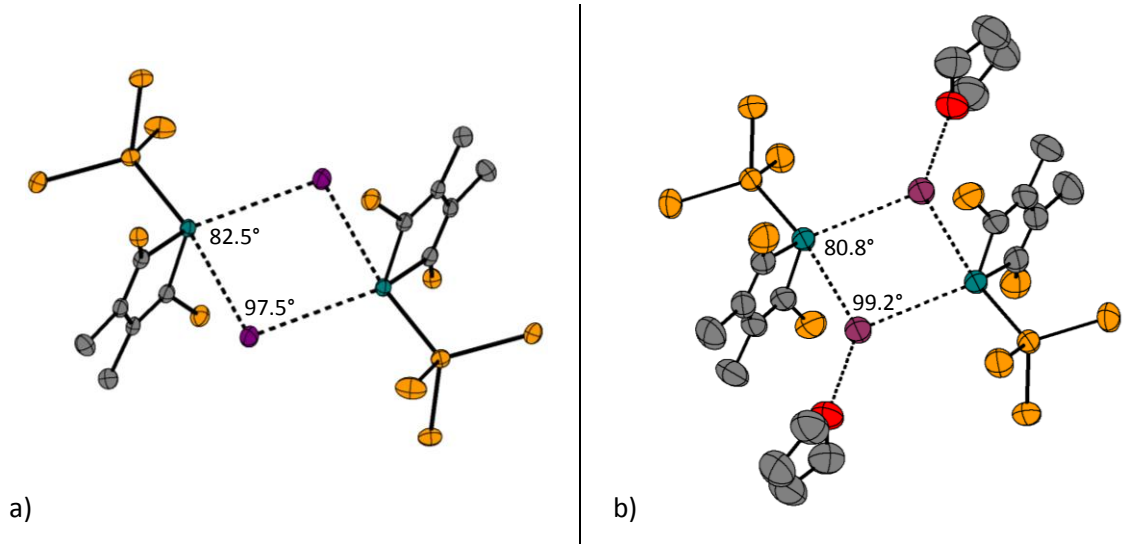

Figure 35: Molecular structures of potassium salt of the germolyl anion **74** a) solvent free, b) complexed by THF; carbon: grey; silicon: yellow; germanium: turquoise; potassium: purple; oxygen: red; hydrogen atoms and methyl groups of trimethylsilyl groups are omitted for clarity; thermal ellipsoids at 50% probability level.

However, the molecular structures show an interesting coordination in the solid state. Because of the tetrahedral structure at the germanium centre, which is indicated by the sum of angles of $\sum\alpha(Ge)$ = 292.6° and $\sum\alpha(Ge)_{THF}$ = 289.7° in Table 10, the lone pair is clearly localised at the germanium atom instead of being delocalised in the five-membered ring. The carbon single and double bonds of the ring system are also well defined and their alternation provides further evidence for the lack of conjugation of the lone pair. Such a structure type is typical for monoanions of heavier group 14 heteroles.[63,67] The dimer of the germolyl anion **74** was also optimised at the M06-2X/6-311+G(d,p)(Ge,Si,K),6-31G(d)(C,H) level of theory. Structural and experimental metrics are in good agreement (Table 10). The deviation of the calculated values is less than 0.5% for bond lengths and less than 2% for the distances of germanium and potassium atoms compared to the values of the molecular structure obtained from the solvent free crystals. This conformity supports that the results obtained by the used method and basis set are appropriate.

Table 10: Structural metrics of the potassium salt of the germolyl anion **74**, solvent free, THF complex and calculated (*italic*) at the M06-2X/6-311+G(d,p)(Ge,Si,K),6-31G(d)(C,H) level of theory; also comparison to the germolyl chloride **46** and germolyl anion salt **Li[87]** by Tilley et al.[67]

	C-C [pm]	C=C [pm]	C-Ge [pm]	Ge-Si [pm]	Ge-K (η^1) [pm]	Ge-K (η^5) [pm]	∑α(Ge)
germolyl anion salt **K[74]**							
solvent free	147.1	136.8	200.4	246.6	350.1	326.7	292.6°
THF complex	145.5	137.1	200.7	246.3	357.7	330.5	289.7°
calculated	*147.8*	*137.2*	*201.2*	*245.7*	*343.0*	*320.3*	*288.9°*
1-Cl-1-Si($SiMe_3$)-germole **46**	150.9	135.8	195.8	241.6	-	-	323.1°
germolyl anion salt **Li[87]** by Tilley et al.[67]	146.1	135.6	198.0	244.7	-	-	280.8°

The lithium salt of the 1-tris(trimethylsilyl)silyl substituted tetramethylgermolyl anion **87**, synthesised by Tilley et al.,[67] has similar metrics compared to the molecular structures of the potassium salt of the germolyl anion **74** (Table 10). The only difference is the counter cation. In the molecular structure of the salt **Li[87]** by Tilley et al., the lithium cation is complexed by 12-crown-4 and no coordination to the anion is observed. This indicates that the coordination of the potassium and the formation of a dimer in the molecular structures of germolyl anion salt **K[74]** has no significant influence on the structure of the anion.

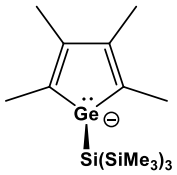

Li[87]

Tilley et al. [67]

To further elucidate that group 14 heterolyl monoanions prefer a tetrahedral structure at the central element atom the bending potentials of the SiH_3 group in model silolyl and germolyl anions **88** and **89** (E = Si, Ge) at the M06-2X/6-311+G(d,p) level of theory were calculated similar as in Chapter 3.2.4 and Chapter 3.2.5. The results are presented in Figure 36 and they indicate that the energy decreases in the model silolyl and germolyl anions if the SiH_3 substituent is bent from a planar to a pyramidalised structure. The increased stability gain of a localised lone pair at the germanium compared to the silicon analogue can be explained by the inert pair effect.[111]

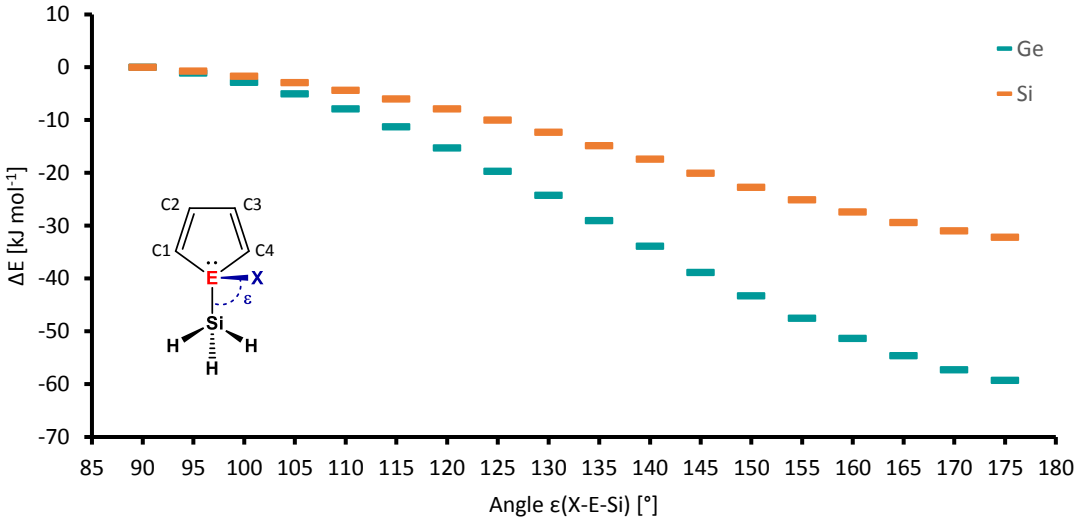

Figure 36: Bending potential of the SiH_3 group in model silolyl and germolyl anions **88** and **89** (E = Si, Ge) at the M06-2X/6-311+G(d,p) level of theory. The angle between the E-Si vector and the orthogonal vector to the plane of the five-membered ring through the atom E ε(X-E-Si), has been alternated in 5° steps to investigate the energy change ΔE between a planar and tetrahedral structure of these anions.

The structural metrics of the calculated model silolyl and germolyl anions **88** and **89** at four different bending angles of the SiH_3 group are summarised in Table 11. Especially the carbon-carbon bond lengths, which are increasing for the C2-C3 bond and decreasing for the C1-C2/C3-C4 bonds if the bending is increased, indicate the conjugation of a planar anion structure and the localisation of the lone pair at the element for a tetrahedral structure.

Table 11: Structural metrics of the model silolyl and germolyl anions **88** and **89** at four different bending angles of the SiH_3 group at the M06-2X/6-311+G(d,p) level of theory.

Model heterolyl anions **88** and **89**		C2-C3 [pm]	C1-C2/C3-C4 [pm]	C1/4-E [pm]	E-Si [pm]	∑α(E)
ε = 90°	E = Si	142	140	180	229	360°
	E = Ge	143	139	189	232	360°
ε = 115°	E = Si	143	139	182	229	350°
	E = Ge	144	138	191	234	350°
ε = 140°	E = Si	144	138	185	231	325°
	E = Ge	146	136	195	237	323°
ε = 165°	E = Si	145	136	189	233	290°
	E = Ge	146	136	199	241	287°

Another remarkable feature of the molecular structures of the germolyl anion salt **K[74]** is the fact that in both cases it is a dimeric structure of two anions connected by two potassium cations. Each potassium ion is η^1-coordinated to the localised lone pair at the germanium atom of one of the anion structures while coordinating η^5 to the ring of the other. The germanium and potassium

atoms are forming a rectangle (dashed line in Figure 35). To further investigate the structure, quantum mechanical calculations at the M06-2X/6-311+G(d,p)(Ge,Si,K),6-31G(d)(C,H) level of theory of the dimer and the η^1 and η^5 monomers were performed. Comparison of the energies of the optimised structures of each of the monomers shows the η^5-coordinated structure is favoured by ΔE = 20 kJ mol^{-1} (Figure 37). Additionally, the distances of the potassium and the germanium atoms are for both coordination types of the calculated monomers similar (d(Ge-K) = 313.2 pm for η^1; d(Ge-K) = 311.2 pm for η^5), but very different for the experimentally obtained dimeric structure (d(Ge-K) = 343.0 pm for η^1; d(Ge-K) = 320.3 pm for η^5; Figure 38). However, all distances are below the sum of the ionic radius[111] of potassium and the van der Waals radius[112] of germanium or carbon (Σr(Ge-K) = 363 pm, Σr(C-K) = 322 pm). The difference in the germanium and potassium distances, especially of the η^1-coordination, in addition to the energy difference suggests that the dimeric structure has to be considered as a dimer of two η^5-coordinated monomers.

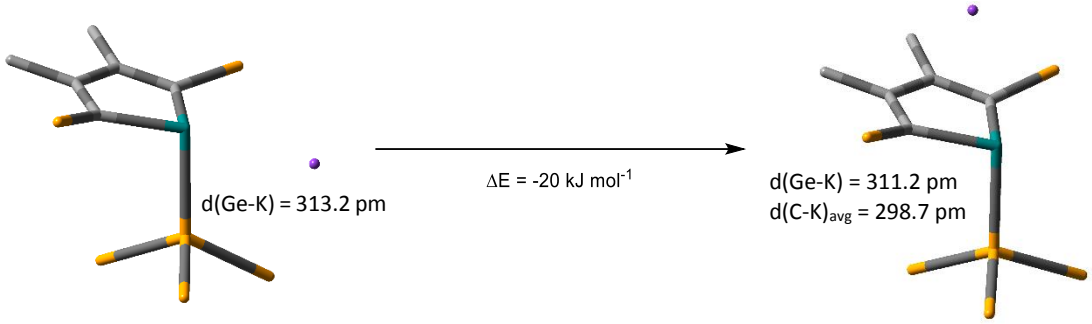

Figure 37: Optimised structures and calculated energy difference of the η^1- and η^5-coordinated monomer of the potassium salt **K[74]** of the germolyl anion at the M06-2X/6-311+G(d,p)(Ge, Si, K),6-31G(d)(C, H) level of theory; carbon: grey; silicon: yellow; germanium: turquoise; potassium: purple; hydrogen atoms and methyl groups of trimethylsilyl groups are omitted for clarity.

The dimer, observed in the solid state, is favoured by ΔE = 170 kJ mol^{-1} over the η^5-coordinated monomer when the calculated ground state energies at the same level of theory are compared (Figure 38, Table 12).

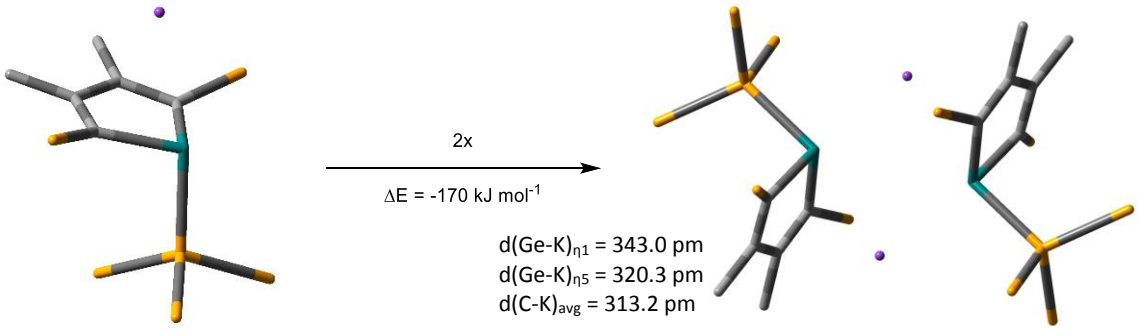

Figure 38: Modelling of the dimerisation of two η^5-coordinated monomers to the respective dimer of the potassium salt of the germolyl anion **74** at the M06-2X/6-311+G(d,p)(Ge,Si,K),6-31G(d)(C,H) level of theory; carbon: grey; silicon: yellow; germanium: turquoise; potassium: purple; hydrogen atoms and methyl groups of trimethylsilyl groups are omitted for clarity.

If the structures are optimised using the B3LYP method, the dimer of **K[74]** is favoured by ΔE = 103 kJ mol^{-1}. This value is decreased by ΔΔE = 67 kJ mol^{-1} compared to the value obtained by using the M06-2X method. The B3LYP method does not factor in dispersion interactions, which are known to play an important role in the stability of systems with polarisable substituents such as silyl groups.[113-115] By using the B3LYP-D3 functional, which is extended by the D3 version of Grimme's dispersion correction with the original D3 damping function[116], the dimeric structure of **K[74]** is even favoured by ΔE = 209 kJ mol^{-1}. The difference between the energies obtained by using the B3LYP and B3LYP-D3 methods represents the magnitude of the dispersion interactions. The resulting energy difference between the values obtained by these two methods of ΔΔE = 106 kJ mol^{-1} indicates that dispersion interactions play an important role in the formation of the dimeric structure of the potassium salt of the germolyl anion **74**. The energy difference between using M06-2X and B3LYP-D3 of ΔΔE = 33 kJ mol^{-1} is relatively high considering both methods take dispersion interactions into account. However, in the M06-2X method only short range dispersion interactions are implemented while in the B3LYP-D3 method long distance dispersion interactions are additionally considered.[115,117,118] This difference could explain that the energy value obtained by using M06-2X is between the values obtained by B3LYP and B3LYP-D3.

Table 12: Calculated energy differences of the η^5-coordinated monomer and the respective dimer of the potassium salt of the germolyl anion **74** with the M06-2X, B3LYP and B3LYP-D3 methods and the 6-311+G(d,p)(Ge,Si,K),6-31G(d)(C,H) basis set.

Method	ΔE [kJ mol^{-1}]
M06-2X	-170
B3LYP	-103
B3LYP-D3	-209

3.3.2 Silole Anions

During reduction reactions of silolyl chlorides with potassium graphite the formation of several potassium salts of silolyl anions and dianions were observed. The silolyl anion salt **K[83]** was formed during the synthesis of the respective silolyl radical **78** described in Chapter 3.2.5. The reduction reaction with potassium graphite was performed in THF, and after a solvent change to a mixture of benzene and hexane crystals of **K[83]** suitable for X-ray analysis were obtained (Scheme 46, Figure 40). However, the silolyl anion salt **K[83]** was not isolated, and therefore, no NMR data were recorded. Further attempts on the direct synthesis of **K[83]** yielded several other anionic siloles in which Si-Si bonds have been cleaved. These anions will be discussed in this chapter.

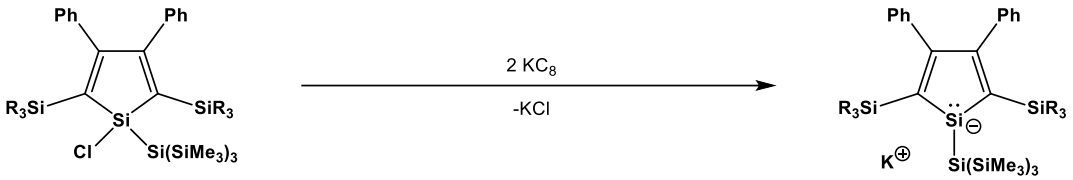

54 R = Me
55 R = Et

K[83] R = Me
K[84] R = Et

Scheme 46: Reduction of the silolyl chlorides **54** and **55**[87] with potassium graphite to the respective potassium salts of the silolyl anions **83** and **84**.[87]

The only silolyl anion which was synthesised, isolated, and further characterised by NMR spectroscopy (NMR data is given in Chapter 5.3) and X-ray analysis was the 1-tris(trimethylsilyl)-silylsilolyl anion as salt **K[84]** which has $SiEt_3$ substituents in 2,5-position (Scheme 46, Figure 39).[87]

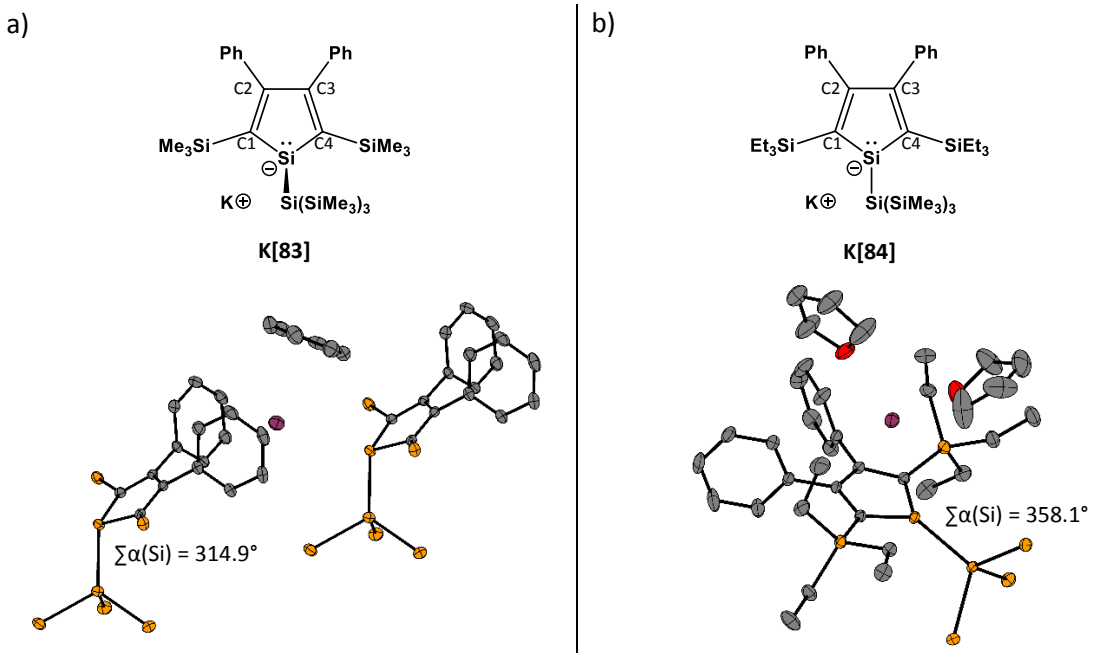

Figure 39: Potassium salts of 1-tris(trimethylsilyl)silyl substituted a) 2,5-$SiMe_3$-silolyl anion salt **K[83]**, b) 2,5-$SiEt_3$-silolyl anion salt **K[84]**; top: Lewis structure; bottom: molecular structure; carbon: grey; silicon: yellow; potassium: purple; oxygen: red; hydrogen atoms and methyl groups of trimethylsilyl groups are omitted for clarity; thermal ellipsoids at 50% probability level.

Even though the only difference between anions **83** and **84** is the $SiMe_3$ or $SiEt_3$ substitution in 2,5-position, the structures in the solid state are considerably different (Figure 39). The $SiMe_3$ substituted anion **83** has a pyramidalised silicon centre with a sum of angles of ∑α(Si) = 314.9°. The potassium counter cation is η^1-coordinated to the central silicon atom. The potassium atom is further coordinated to a benzene solvent molecule and two phenyl groups of the neighbouring silolyl anion aligning in a polymeric chain. The pyramidalised structure at the silicon centre indicates the localisation of the lone pair, and therefore, it is not conjugated with the π-system of the five-membered ring. The lack of conjugation is also indicated by the alternating carbon single and double

bond lengths of the ring, shown in Table 13. In contrast, the molecular structure of the $SiEt_3$ substituted anion **84** has a sum of angles at the silicon centre of ∑α(Si) = 358.1°, and is therefore, almost planar. The potassium counter cation is η^5-coordinated to the ring system in which the lone pair is delocalised, and to two THF solvent molecules (b, Figure 39). The conjugation of the ring system is further indicated by the equalising carbon-carbon bond lengths (Table 13).

Table 13: Structural metrics of the potassium salts of the silolyl anions **83** and **84** obtained by X-ray analysis and comparison to the calculated values (*italic*) of the η^1- and η^5-coordinated potassium salts and the free 2,5-$SiMe_3$-silolyl anion of **83** at the M06-2X/6-311+G(d,p) level of theory.

	C2-C3 [pm]	C1-C2/C3-C4 [pm]	C-Si [pm]	Si-$Si_{sub.}$ [pm]	Si-K (η^1) [pm]	Si-K (η^5) [pm]	∑α(Si)
2,5-$SiMe_3$ anion **83**:							
experimental	145.0	139.5	188.0	241.1	370.3	-	314.9°
η^1-coordinated	*146.9*	*137.5*	*188.6*	*240.7*	*317.8*	-	*307.9°*
η^5-coordinated	*141.7*	*143.0*	*181.6*	*234.5*	-	*317.7*	*357.7°*
free anion	*145.0*	*139.0*	*186.8*	*238.8*	-	-	*307.3°*
2,5-$SiEt_3$ anion **84**:							
experimental	141.5	143.6	182.0	236.6	-	330.6	358.1°

To further investigate the structure of the 2,5-$SiMe_3$-silolyl anion salt **K[83]**, quantum mechanical calculations at the M06-2X/6-311+G(d,p) level of theory of planar and tetrahedral structure were performed. The metrics of the optimised η^1-coordinated structure, which is shown in Table 13, are consistent with the experimentally obtained metrics (bond length deviation less than 1.5%) except for the Si-K distance, which suggests a weaker coordination of the potassium in the molecular structure. Surprisingly, if the energies of the optimised structures of the η^1- and η^5-coordinated potassium salt of the 2,5-$SiMe_3$-silolyl anion **83** are compared, the planar structure is favoured by ΔE = 38 kJ mol^{-1} even though the structure in the solid state is pyramidalised (Figure 40).

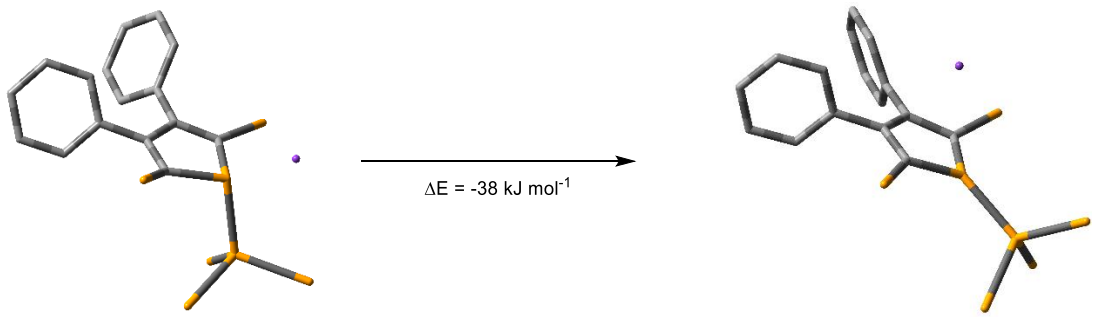

Figure 40: Optimised structures and calculated energy difference of the η^1- and η^5-coordinated potassium salt of the silolyl anion **83** at the M06-2X/6-311+G(d,p) level of theory; carbon: grey; silicon: yellow; potassium: purple; hydrogen atoms and methyl groups of trimethylsilyl groups are omitted for clarity.

A possible explanation for the inconsistent results could be the coordination of the benzene and the phenyl groups to the potassium cation in the molecular structure with the pyramidalised anion **83** which leads to the elongation of the Si-K distance of Δd(Si-K) = 53 pm. The potassium is therefore not available for the η^5-coordination which seems to be crucial to form a planar structure. The decreased coordination of the potassium suggests a more remote anion. Compared to the optimised structure of the potassium free anion, which is also pyramidalised, the metrics are in even better agreement to the molecular structure (bond length deviation less than 1.0%).

These results are consistent with the silolyl anions reported in the literature which are always pyramidalised at the silicon centre if the counter cation is complexed by e.g. crown ether. For example, the 2,3,4,5-tetramethyl-1-trimethylsilylsilolyl anion in the potassium salt **Ki[90]** by Tilley et al.[63] is pyramidalised at the silicon centre while the potassium cation is complexed by 18-crown-6. The distance between the central silicon and the η^1-coordinated potassium atom in **Ki[90]** is 360.4 pm. If the silolyl anion is η^5-coordinated to a transition metal complex such as in compound **91** and **92**, synthesised by Tilley et al.,[64,65] the silicon centre is nearly planar. Planar monosubstituted silolyl anions which are not coordinated to transition metal complexes such as **84** are not yet reported in the literature.

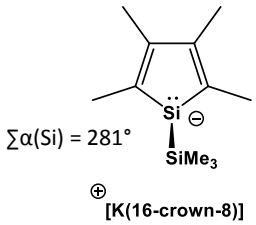

K[90]

Tilley et al.[63]

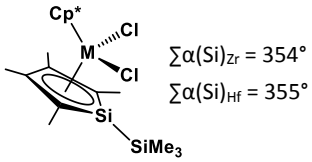

91 M = Zr
92 M = Hf

Tilley et al.[64,65]

Further, potassium salts of the silolyl anion **93**, the dianion **94**, and the bisanions **95** and **96** were obtained as single crystals suitable for X-ray analysis (Figure 41). The potassium salts of the anions **94**-**96** occurred as side products of the reduction of chlorosiloles with potassium graphite and the salt of the 1-$SiMe_3$-silolyl anion **93** was observed during a rearrangement reaction which is presented in Chapter 3.4.

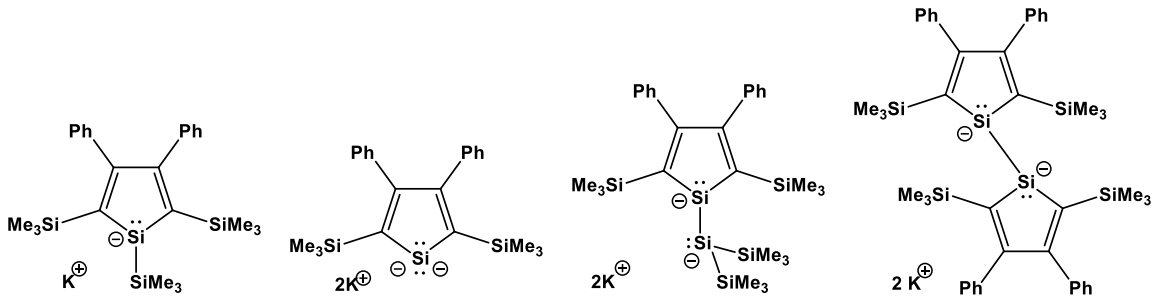

Figure 41: Potassium salts of silolyl anions **93**-**96** which were obtained as single crystals and analysed by X-ray analysis.

A possible mechanism for the formation of the dianions **94**-**96** is the overreduction of the silolyl anion **83** (Scheme 47). This could lead to a cleavage of the Si-Si bond of the substituent giving $KSi(SiMe_3)_3$ and the silolyl radical anion **97**. The radical anion **97** could be further reduced by KC_8 to the dianion **94** or dimerise to yield the dimeric bisanion **96**. Further reduction of the bisanion **96** with potassium graphite would also yield the silolyl dianion **94** which is already described for an analogue compound by Boudjouk et al.[119] Additionally, the formed $KSi(SiMe_3)_3$, which is well known to be able to abstract trimethylsilyl groups of persilylated silyl groups,[120] could react with residual silolyl anion **83** to give the bisanion **95**.

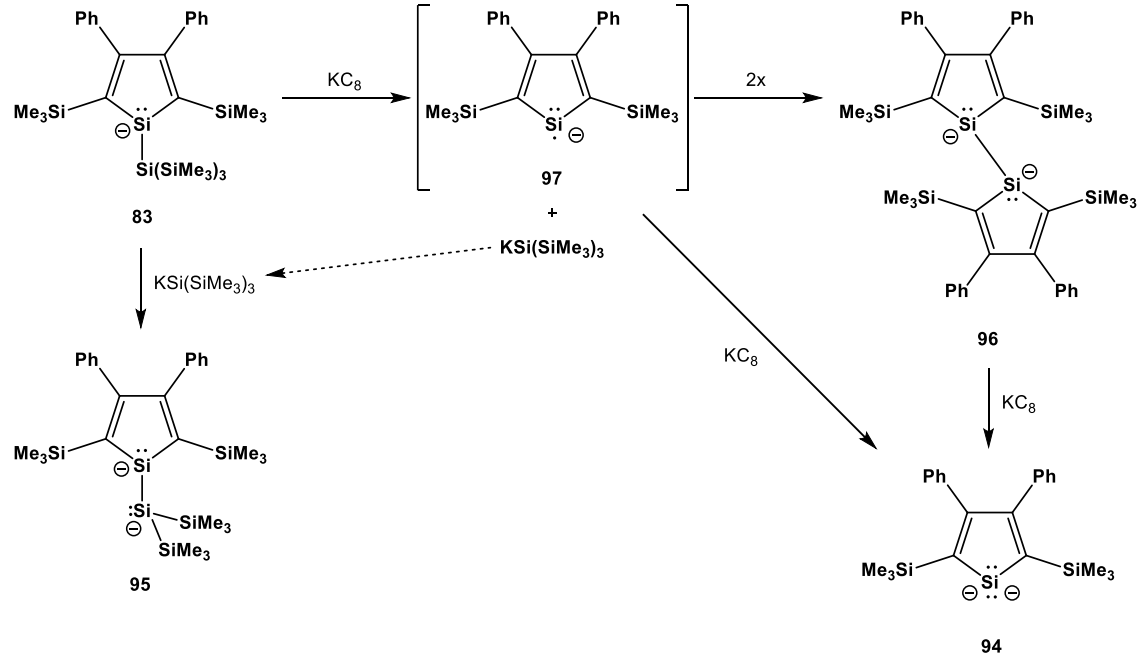

Scheme 47: Proposed mechanism of the formation of the dianion **94** and the bisanions **95** and **96**.

The variety of different anionic silolyl compounds which were observed during the reduction of the chlorosilole **54** with potassium graphite suggests that the reaction is very sensitive and that the conditions are too harsh to form the silolyl monoanion **83** quantitatively. The formation of the potassium salt of the trimethylsilylsilolyl anion **93**, which was obtained in the reaction of the chlorosiloles **54** and KO^{t}Bu, will be discussed in Chapter 3.4.2. The structural metrics of the potassium salts of the silolyl monoanions **83**, **84**, and **93**, the dianion **94**, the bisanion **95**, and the dimeric bisanion **96**, determined by X-ray analysis, are summarised in Table 14.

Table 14: Structural metrics of the potassium salts of the silolyl anions **83**-**84** and **93**-**96**.

Silole	C2-C3 [pm]	C1-C2/C3-C4 [pm]	C-Si [pm]	Si-Si$_{ring}$ [pm]	Si-K (η^1) [pm]	Si-K (η^5) [pm]	∑α(Si)
2,5-SiMe$_3$ dianion **94**	142.3	143.8	186.0	-	344.1	339.8	-
1-Si(SiMe$_3$)-2,5-SiMe$_3$ anion **83**	145.0	139.5	188.0	241.1	370.3	-	314.9°
1-Si(SiMe$_3$)-2,5-SiEt$_3$ anion **84**	141.5	143.6	182.0	236.6	-	330.6	358.1°
1-SiMe$_3$-2,5-SiMe$_3$ anion **93**	141.9	143.8	181.7	243.3	-	335.2 339.1	357.4°
1-Si(SiMe$_2$)-2,5-SiMe$_3$ bisanion **95**	142.2	144.1	183.1	232.6	340.2	341.7 330.0	357.1° ring[a] 324.4° subs.[b]
2,5-SiMe$_3$ dimeric bisanion **96**	140.3 - 145.2	141.5 - 144.3	180.0 - 184.0	229.4	-	326.3 - 342.8	326.8° - 360.0°

[a] Si atom in the ring system; [b] Si atom of the anionic silyl substituent

The molecular structure of the potassium salt of the 1-trimethylsilylsilolyl anion **93** is shown in Figure 42. The silicon centre of **93** has also a planar coordination with a sum of angles of ∑α(Si) = 357.4° and conjugated C-C bonds in the ring (Table 14). The potassium counter cations are η^5-coordinated to the anionic silole rings forming a polymeric chain (Figure 42, a). In the side view along the axis of two central silicon atoms in Figure 42 (b) it is shown that the neighbouring silolyl anions have a staggered conformation with a Si-Si-Si-Si torsion angle of 180.0°.

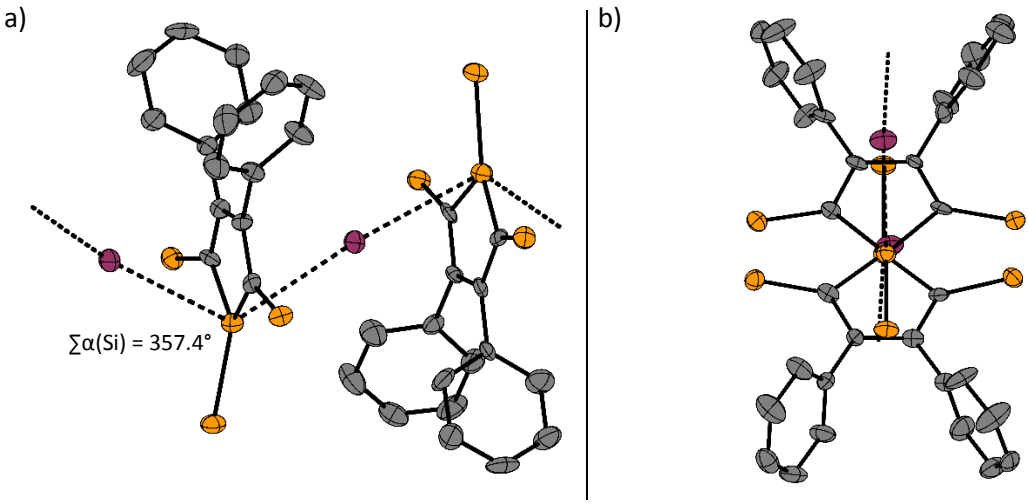

Figure 42: Molecular structure of the potassium salt of the 1-trimethylsilyl substiuted silolyl anion **93**; a) side view of the polymeric chain; b) view of a dimeric fragment of the chain along the axis of two central silicon atoms; carbon: grey; silicon: yellow; potassium: purple; hydrogen atoms and methyl groups of trimethylsilyl groups are omitted for clarity; thermal ellipsoids at 50% probability level.

The silolyl dianion **94** and the bisanion **95** were both obtained in the same reduction reaction of the chlorosilole **54** with potassium graphite (Figure 43). The silole rings and the potassium counter cations in the solid state structure of the dianion salt **K_2[94]** are forming a polymeric chain, similar as in the structure of the 1-$SiMe_3$ substituted silolyl anion salt **K_2[93]**. Each potassium atom is η^5-coordinated to one silole ring and η^1-coordinated to the central silicon atom of the neighbouring ring. Each silole ring is therefore coordinated to four potassium atoms, two η^5-coordinated and two η^1-coordinated. Neighbouring silolyl anionic rings have an inverse orientation which is indicated by the torsion angle of the central silicon atoms and the ring centres of 180.0°. The metrics, given in Table 14, show conjugation of the carbon bonds of the five-membered ring system which is consistent with known group 14 heterolyl dianions.[63,66]

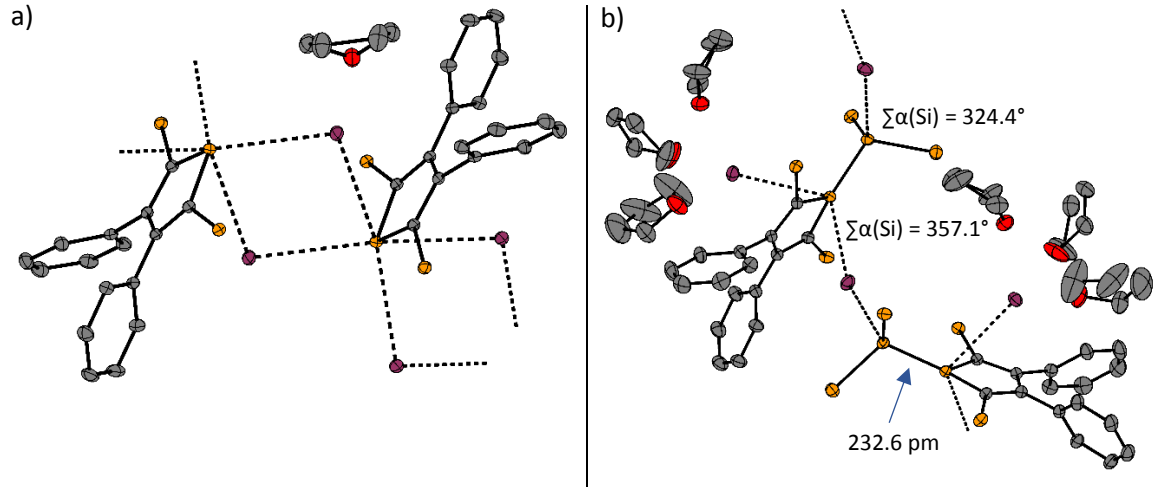

Figure 43: Molecular structure of the potassium salt of a) silolyl dianion salt **K_2[94]** b) 1-bis(trimethylsilyl)silylsilolyl bisanion salt **K_2[95]**; carbon: grey; silicon: yellow; potassium: purple; oxygen: red; hydrogen atoms and methyl groups of trimethylsilyl groups are omitted for clarity; thermal ellipsoids at 50% probability level.

The bisanion salt **K_2[95]** (Figure 43, b) has a unique molecular structure. Due to the fact that it is bisanionic two negative charges are distributed in the molecule. One lone pair is delocalised in the five-membered silole ring which is indicated by the η^5-coordination of one potassium counter cation on each side leading to a planar structure of the central silicon atom with a sum of angles of ∑α(Si) = 357.1°. The conjugation of the ring system is also indicated by equalising carbon-carbon bond lengths (Table 14). On one side of the ring, the potassium is further coordinated by three THF molecules. The potassium on the other side is η^1-coordinated to the central silicon of the $Si(SiMe_3)_2$ substituent of the neighbouring molecule at which the second lone pair is localised. The silicon of the $Si(SiMe_3)_2$ group has a sum of angles of ∑α(Si) = 324.4° which indicates its pyramidalisation. The bond length between the silicon of the five-membered ring and the anionic silyl substituent is d(Si-Si) = 232.6 pm, which is in the range of a silicon-silicon single bond.[95] A bisanionic silolyl compound such as **K_2[95]** has not yet been presented in the literature.

Crystals of another bisanionic silolyl compound (**96**) suitable for X-ray analysis were obtained during the reduction reaction of the chlorosilole **54** with two equivalents potassium graphite in THF (Figure 44). Surprisingly, the structure of compound **K_2[96]** shows the potassium salt of a dimeric bisanion in which two silolyl anionic rings formed a silicon-silicon bond after the $Si(SiMe_3)_3$ substituent has been cleaved off.

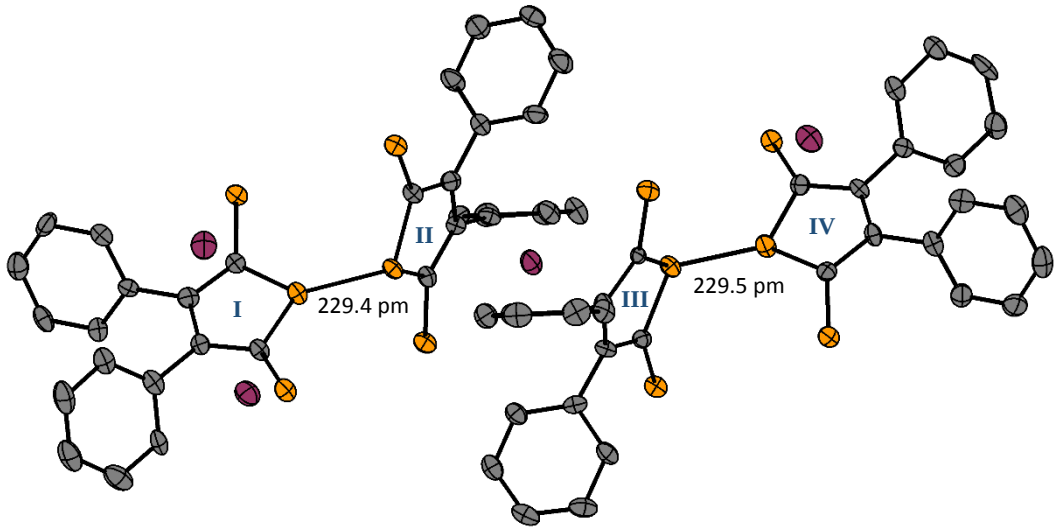

Figure 44: Molecular structure of the potassium salt of the dimeric bisanion **96**; carbon: grey; silicon: yellow; potassium: purple; hydrogen atoms and methyl groups of trimethylsilyl groups are omitted for clarity; thermal ellipsoids at 50% probability level.

The structure of the bisanion salt **K_2[96]** shows two dimers coordinated by four potassium counter cations. One silole ring (**I**) is η^5-coordinated by two potassium atoms and the silicon centre is planar (∑α(Si) = 360.0°). This first silole ring is bound to a second silole ring (**II**) in 1-position which has a

pyramidalised silicon centre (∑α(Si) = 326.8°). Silole ring **II** is forming a η^5-sandwich complex with another potassium atom and a silole ring (**III**) of the second dimer which also has a pyramidalised silicon centre (∑α(Si) = 336.2°). This silicon centre (**III**) is bound to the fourth silole ring (**IV**) which again has an almost planar coordinated silicon atom (∑α(Si) = 357.0°) but only one η^5-coordinated potassium cation. The potassium atoms which are not coordinated in a sandwich complex are further coordinated to phenyl rings of neighbouring anions or to benzene solvent molecules which have been omitted for clarity in Figure 44. Similar carbon-carbon bond lengths in the silole rings from 140.3 pm to 145.2 pm indicate conjugation (Table 14). Clear alternation of carbon single and double bonds is not observed, not even in the pyramidalised silole rings (**II**+**III**).

The Si-Si bond lengths between the silole rings in **96** are d(Si-Si) = 229.4 pm and d(Si-Si) = 229.5 pm. The calculated length of this bond at the M06-2X/6-311+G(d,p) level of theory of d(Si-Si) = 230.3 pm is in good agreement (deviation less than 0.4%). It is of interest that this bond is shorter than a Si-Si single bond if it is compared to the calculated Si-Si bond length of hexamethyldisilane at the same level of theory of d(Si-Si) = 234.3 pm or the single bond radii of d(Si-Si) = 232 pm, given by Pyykkö et al.[95] However, a comparison to the tetramethyldisilyl bisanion is more reasonable due to the fact that dimer **96** is bisanionic. The Si-Si bond length of the tetramethyldisilyl bisanion of d(Si-Si) = 240.1 pm is significantly longer which indicates repulsive interaction of neighbouring disilyl bisanions. This contradicts to the short Si-Si bond length observed in dimer **96** suggesting that the negative charges are delocalised in each of the ring systems. Additionally, the silicon-silicon bond length of the silolyl ring and the anionic silyl substituent in the previously discussed bisanion **95** of d(Si-Si) = 232.6 pm is also not elongated.

A possible reason for the formation of the bisanion **96** was the overreduction of the chlorosilole **54**. This resulted in the cleavage of the Si-Si bond of the $Si(SiMe_3)_3$ substituent and the central silicon atom, forming the silolyl radical anion **97** which dimerised to **96** (Scheme 47, Scheme 48).

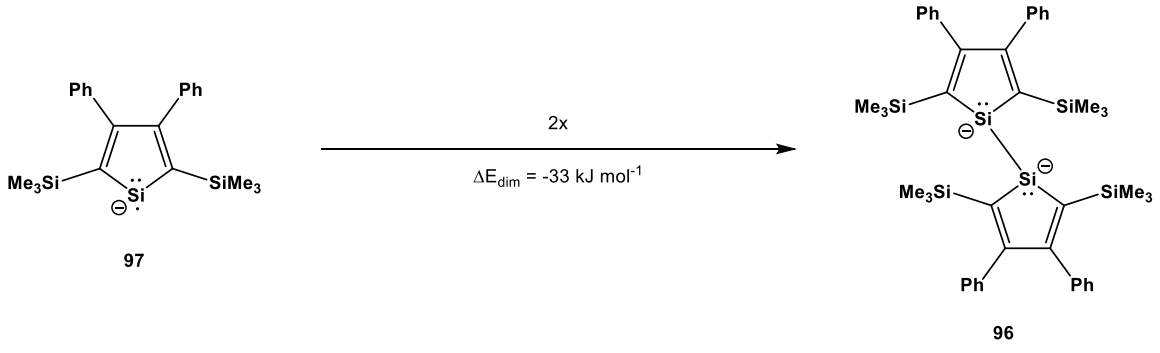

Scheme 48: Dimerisation reaction of silolyl radical anion **97** to the bisanion **96** and calculated dimerisation energy ΔE_{dim} at the M06-2X/6-311+G(d,p) level of theory.

The calculated bond dissociation energy ΔE_{diss} for the dimeric bisanion of **96** at the M06-2X/ 6-311+G(d,p) level of theory, which can be derived from the reaction energy of the dimerisation ΔE_{dim}, is only ΔE_{diss} = 33 kJ mol^{-1}. This value is fairly low compared to the bond dissociation energy of the trimethylsilyl radical and its dimer hexamethyldisilane of ΔE_{diss} = 318.1 kJ mol^{-1}. Such a low bond dissociation energy contradicts the short Si-Si bond length. However, if the endothermic dimerisation energy of the tetramethyldisilyl bisanion of ΔE_{dim} = 115.3 kJ mol^{-1} is considered, a monomeric dimethylsilyl radical anion is significantly favoured instead of a dimer.

Comparable bisanionic silolyl dimers are already reported in the literature by Boudjouk et al.[119] and Tilley et al.[63,66] but the compounds **98** and **99** were only detected by NMR spectroscopy and the analysis of the products after trapping reactions. No data from X-ray analysis were obtained.

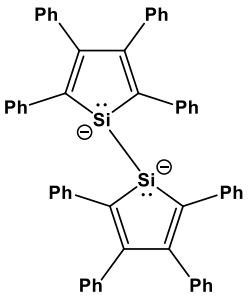

98
Boudjouk et al.[119]

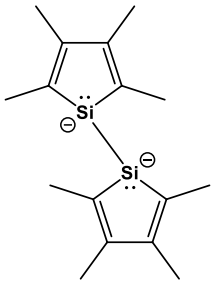

99
Tilley et al.[63,66]

3.4 Rearrangement Reactions of Sila- and Germacyclopentadienes

In addition to the reduction of chlorosiloles and -germoles with potassium graphite to their respective radicals, other organometallic reducing agents were investigated. While the use of methyl- or tert-butyllithium only resulted in substitution reactions in 1-position, the use of potassium tris(trimethylsilyl)silanide led to unexpected rearrangement reactions instead of reduction or substitution reactions.

3.4.1 Rearrangement Reactions of Germoles

The product in the reaction of the 1-tris(trimethylsilyl)silylchlorogermole **46** and $KSi(SiMe_3)_3$ was the 1,1-bis(trimethylsilyl)silole **100** (Scheme 49). In principal, a germole was transformed into a silole. Interestingly, an equal amount of tetrakis(trimethylsilyl)silane as a side product was also observed (Figure 45) which is an important fact for the formulation of a reaction mechanism later in this chapter.

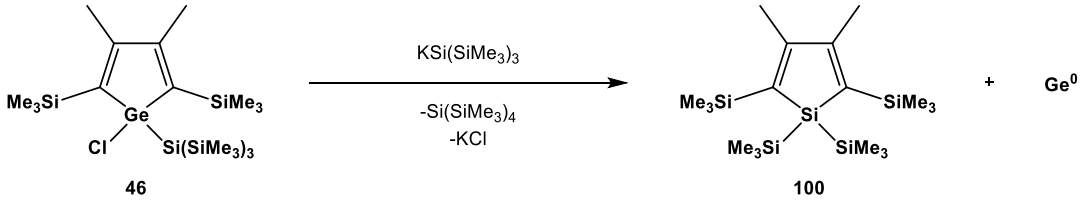

Scheme 49: Reaction of chlorogermole **46** with potassium tris(trimethylsilyl)silanide forming silole **100**, tetrakis(trimethylsilyl)silane, potassium chloride and elemental germanium.

The silole **100** and the side product $Si(SiMe_3)_4$ were not separable by crystallisation, sublimation or column chromatography but an alternative synthetic approach allowed the isolation, and therefore, full characterisation of silole **100**.[121] The analytical data were consistent with those obtained after the reaction of the chlorogermole **46** and $KSi(SiMe_3)_3$. The $^{29}Si\{^1H\}$ NMR spectra of silole **100** obtained by these independent routes are shown in Figure 45.

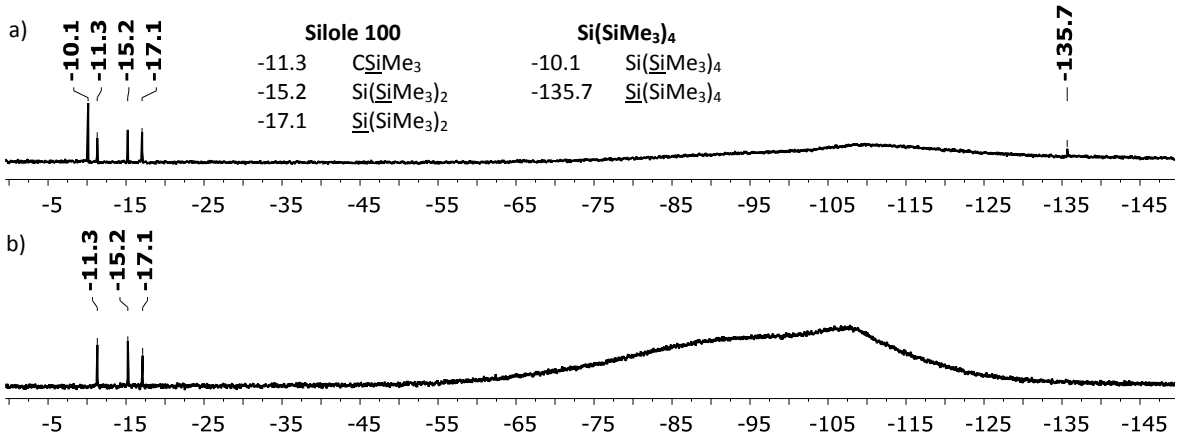

Figure 45: $^{29}Si\{^{1}H\}$ NMR spectra of silole **100** in C_6D_6; a) synthesised via the reaction of chlorogermole **46** and $KSi(SiMe_3)_3$ (99.3 MHz, 305.0 K); b) synthesised via alternative reaction pathway[121] (99.4 MHz, 289.2 K).

Additionally, a black solid precipitated during the course of the reaction, which was not soluble in organic solvents or water. X-ray fluorescence analysis (XRF, [wt%]) of the residue revealed that it contained 32% germanium, 31% potassium, and 29% chloride (calculated for the expected equimolar mixture: 49% Ge, 27% K, 24% Cl). The elimination of elemental germanium was another indicator for an unusual rearrangement reaction.

If the reaction was carried out by using the dichlorogermole **39** and two equivalents of $KSi(SiMe_3)_3$ identical products were observed (Scheme 50). Presumably, the first equivalent of $KSi(SiMe_3)_3$ reacts in a substitution reaction forming the chlorogermole **46** and the second equivalent leads to the rearrangement reaction.

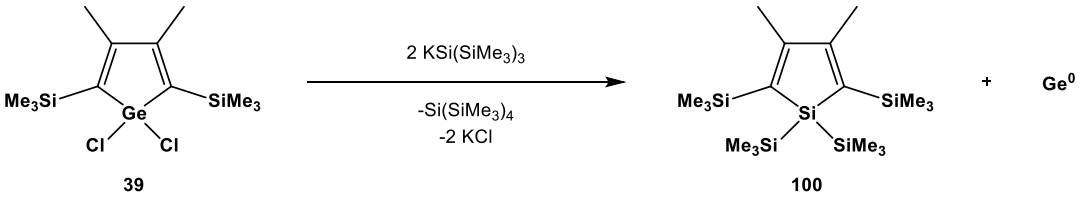

Scheme 50: Reaction of dichlorogermole **39** with two equivalents of potassium tris(trimethylsilyl)-silanide also forming silole **100**, tetrakis(trimethylsilyl)silane and elemental germanium.

It is well known that silyl anions are able to abstract terminal silyl substituents of persilylated silyl groups e.g. $Si(SiMe_3)_3$.[120] Therefore, the equimolar formation of $Si(SiMe_3)_4$ indicates that the $KSi(SiMe_3)_3$ abstracts a $SiMe_3$ group of the $Si(SiMe_3)_3$ substituent. In order to show that the first step of the rearrangement reaction is the abstraction of a trimethylsilyl group the reaction was performed using potassium tert-butoxide instead of $KSi(SiMe_3)_3$ (Scheme 51). KO^tBu is a common reagent to abstract terminal silyl groups of branched polysilanes.[88] Reacting KO^tBu with the chlorogermole **46** also led to the rearrangement reaction forming the silole **100** and elemental

germanium but the presence of several side products indicated that the reaction is not as selective as it is by using $KSi(SiMe_3)_3$. However, the formation of silole **100** and additional precipitation of germanium supports the proposed initial step of the reaction.

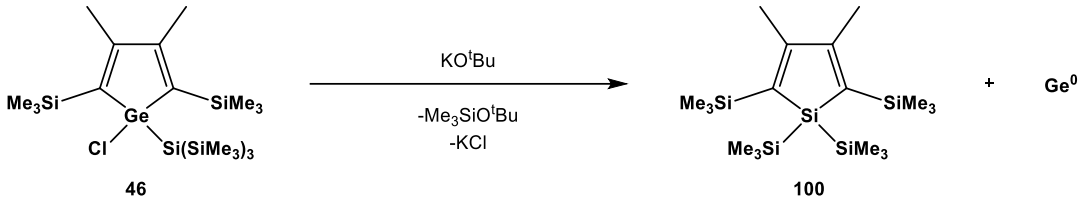

Scheme 51: Reaction of chlorogermole **46** with potassium tert-butoxide forming silole **100** and elemental germanium.

Based on these observations the following reaction pathway was proposed: By abstracting a trimethylsilyl group of germole **46** the germolylsilyl anion **101** is formed. Due to the chloride function at the germanium atom, which is in β-position to the silyl anion, potassium chloride is readily eliminated forming a germasilafulvene **102** (Scheme 52).

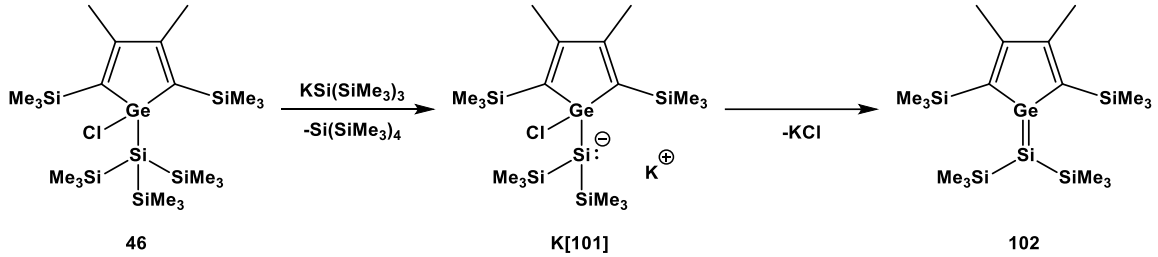

Scheme 52: Initial step of the proposed mechanism of the reaction of chlorogermole **46** with $KSi(SiMe_3)_3$ and additional elimination of potassium chloride to form the hypothetical germasilafulvene **102**.

Heavier analogues of fulvenes such as **102** have not been reported in the literature. Due to this fact and because no other evidence for **102** was observed during the reaction it can be assumed that fulvene **102** is not a stable intermediate. To be able to formulate the Ge-Si double bond in **102**, the germanium and the silicon must be planar coordinated. This is hindered by the trimethylsilyl groups in 2,5-position of the ring and on the silicon centre, which would be in the same plane if the structure was planar. Therefore, it can be assumed that the zwitterionic structure **103**, in which the substituted silyl group is orthogonal orientated to the plane of the ring forming a stable germolyl anion and a silyl cation, is a viable isomer (Scheme 53). As already discussed in Chapter 3.3.1, germolyl anions which are not coordinated to counter cations or transition metal complexes have their lone pair localised at the central germanium leading to a pyramidalisation.

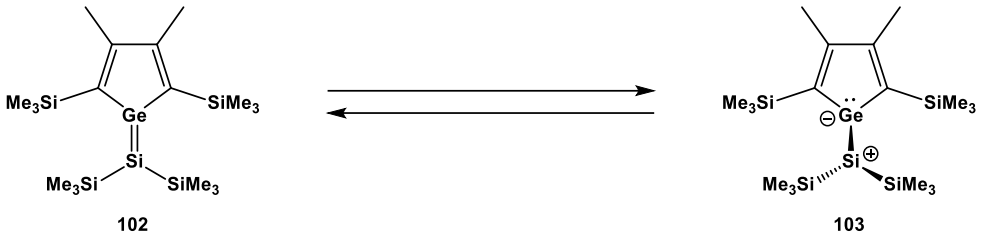

Scheme 53: Expected equilibrium of germasilafulvene **102** and the zwitterion **103**.

A pyramidalisation at the germanium centre would result in a decreased sum of angles ∑α(Ge), and therefore, in a bending of the silyl substituent towards the five-membered ring (Scheme 53). The decreased distance of the silyl group and the ring allows an intramolecular addition reaction in 2-position to form the bicyclic zwitterion **104** (Scheme 54).

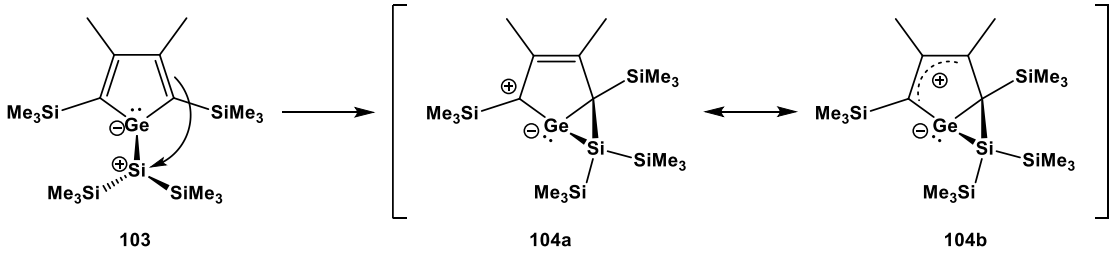

Scheme 54: Intramolecular substitution of the silyl substituent of zwitterion **103** at the 2-position of the five-membered ring forming the bicyclic zwitterion **104** which has the positive charge stabilised by an allylic function.

To support that bicyclic zwitterion **104** is a reasonable intermediate, quantum mechanical calculations at the M06-2X/6-311+G(d,p) level of theory were performed (Figure 46). While the fulvene **102** was optimised as an energy minimum, the structure of zwitterion **103** could not be optimised. Every optimisation attempt resulted in the bicyclic zwitterion **104** which was even energetically favoured over the fulvene structure **102** by ΔE = 28 kJ mol^{-1} (Figure 46). The cationic charge in **104** is conjugated into an allylic function which is a factor for its unexpected stability. Furthermore, the bicyclic zwitterion **104** could lose the charge separation and the highly strained three-membered ring by a silyl shift of the silyl group at the germyl anion to the positive charged carbon atom in 2-position of the five-membered ring forming a silicon-carbon bond and a less strained bicyclic system (Scheme 55). The product of this rearrangement would be the germylene **105** which is a germasilabicyclo[2.1.1]hexenylidene.

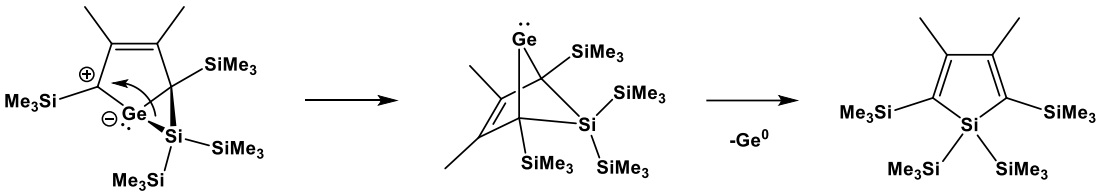

104 105 100

Scheme 55: Silyl group shift of bicyclic zwitterion **104** forming germylene **105** which can readily eliminate elemental germanium in a cycloreversion reaction leading to the experimentally observed silole **100**.

Comparison of the relative electronic energies of the proposed intermediates, shown in Figure 46, reveals that the germylene **105** is by far the most stable intermediate. It is favoured by $\Delta\Delta E$ = 108 kJ mol^{-1} over the bicyclic zwitterion **104** and by ΔE = 136 kJ mol^{-1} over the fulvene **102**. The triplet bisradical **106** is ΔE = 24 kJ mol^{-1} less favoured than the fulvene **102**, and therefore, not considered as a reasonable intermediate in the course of the rearrangement reaction. Further details on the proposed reaction mechanism will be discussed later in this chapter.

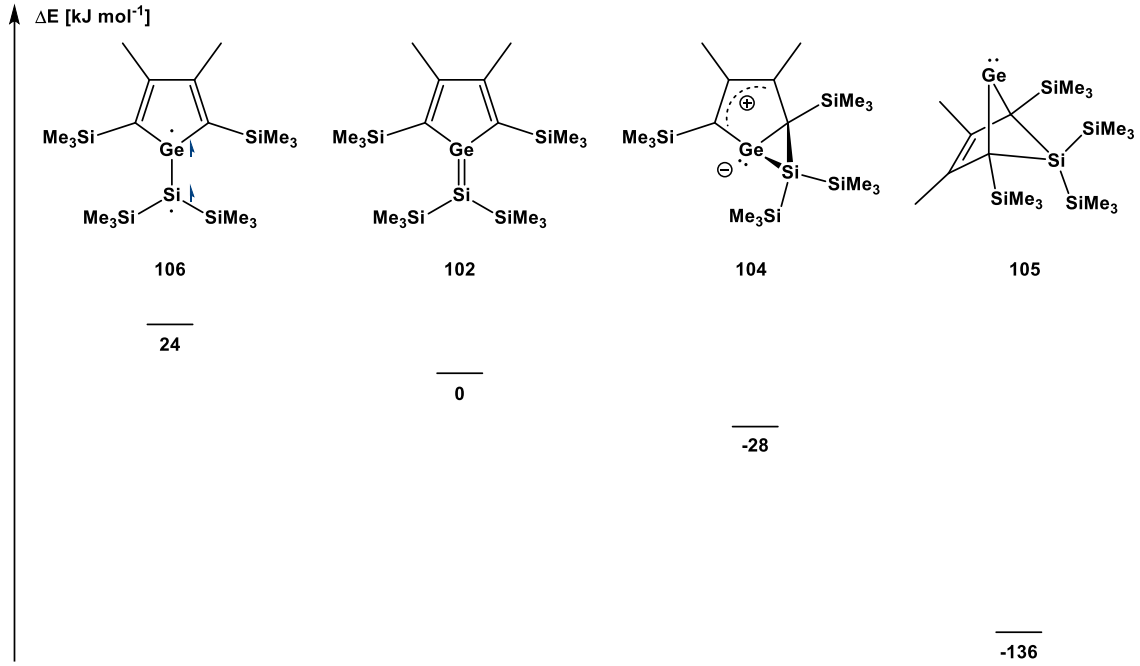

Figure 46: Comparison of the relative electronic energies ΔE of proposed intermediates of the rearrangement in the reaction of chlorogermole **46** and $KSi(SiMe_3)_3$ at the M06-2X/6-311+G(d,p) level of theory.

Additionally, germylene **105** is the most eligible intermediate to explain the formation of the silole **100**. Due to a cycloreversion reaction of **105** in which the two bonds of the germanium to the carbon atoms in 2,5-position of the ring system are cleaved, elemental germanium is eliminated and the

stable silole **100** is formed (Scheme 55). The relative electronic energy of the formation of silole **100** and atomic triplet germanium compared to the fulvene **102** is endothermic by ΔE_{rel} = 96 kJ mol^{-1} but the condensation of germanium atoms to form bulk germanium provides the required thermodynamic driving force yielding an exothermic reaction of ΔE = -272 kJ mol^{-1} calculated with a sublimation energy of bulk germanium of ΔE_{sub} = 368 kJ mol^{-1} (eq. 4).[122]

$$\Delta E = \Delta E_{rel} - \Delta E_{sub} = (96 - 368)\ kJ\ mol^{-1} = -272\ kJ\ mol^{-1} \qquad \text{eq. 4}$$

3.4.2 Rearrangement Reactions of Siloles

To further investigate the rearrangement observed in the reaction of the chlorogermole **46** with KSi(SiMe$_3$)$_3$, which is presented in Chapter 3.4.1, similar reactions were performed using analogous 1-tris(trimethylsilyl)silyl substituted siloles as starting materials. However, the obtained results were different than expected.

In contrast to the rearrangement reaction of the chlorogermole **46** in which elemental germanium precipitated, no elemental silicon was formed in the reaction of the chlorosilole **54** with KSi(SiMe$_3$)$_3$ (Scheme 56). However, Si(SiMe$_3$)$_4$ was found as a side product of the reaction indicating that the abstraction of a trimethylsilyl group is also the initial step of the reaction.

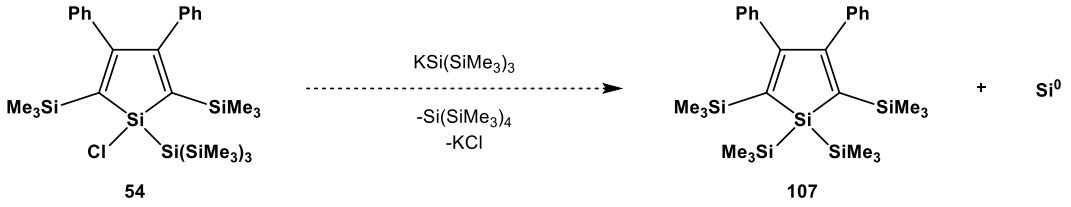

Scheme 56: Reaction of the chlorosilole **54** and KSi(SiMe$_3$)$_3$ does not result in the precipitation of elemental silicon and the formation of the expected silole **107**.

In the ^{29}Si NMR spectrum of the reaction mixture, four main signals and several signals in the range of δ^{29}Si = -6 to δ^{29}Si = -26 were detected. Two of the main signals were assigned to Si(SiMe$_3$)$_4$. The signal at δ^{29}Si = 32.2 is in the range of a central silicon of a silole ring (Table 5). The fourth signal showed an unexpected high field shift of δ^{29}Si = -210.6 (Figure 47). Typically, silyl anions and silicon compounds with a coordination number of six are detected at this field.[123-125] Additionally, the observed signal is at a higher field than the one of the central silicon of the used starting material potassium tris(trimethylsilyl)silanide (δ^{29}Si = -190.5, 305.0 K, C_6D_6/THF).

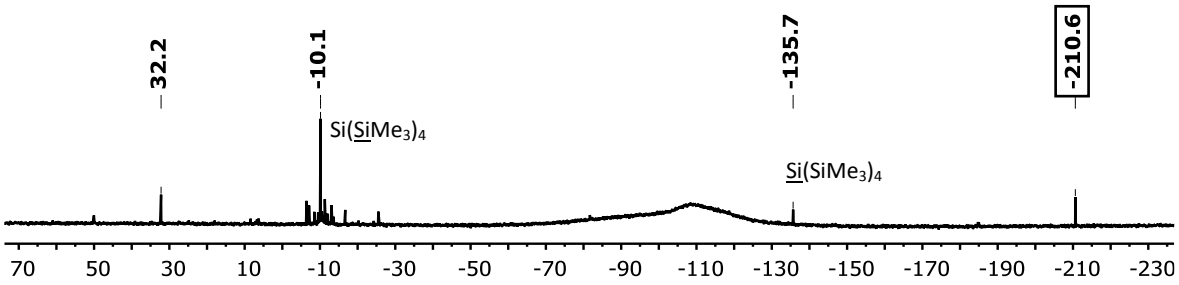

Figure 47: $^{29}Si\{^{1}H\}$ NMR spectrum (99.3 MHz, 305.0 K, C_6D_6) after the reaction of chlorosilole **54** and $KSi(SiMe_3)_3$ reveals the formation of $Si(SiMe_3)_4$ and an unexpected high field shifted signal at $\delta^{29}Si$ = 210.6.

The fact that $Si(SiMe_3)_4$ is formed but no elemental silicon precipitates suggests that the initial step of the reaction is the abstraction of a trimethylsilyl group but the rearrangement either gives a different product or it stops before the silicon is eliminated. The synthesised compound also showed high stability because heating of the NMR sample to 70 °C for several hours did not lead to a significant change of the NMR signals or to the precipitation of silicon.

Based on the recorded NMR spectra no distinct structure was assignable. Therefore, trapping reactions were performed. The addition of $HSiEt_3$ did not reveal reactivity with the product but the addition of MeOH yielded an unexpected 1,1-dimethoxysilacyclopentene **108** (Scheme 57).

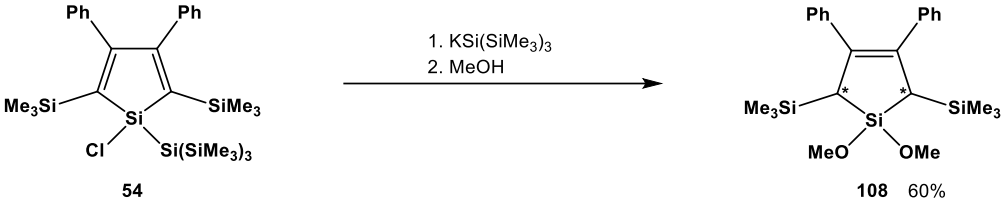

Scheme 57: Reaction of the chlorosilole **54** with $KSi(SiMe_3)_3$ and additional trapping with MeOH yielding an unexpected 1,1-dimethoxysilacyclopentene **108**.

The silacyclopentene **108** was isolated as a *cis/trans* mixture in a yield of 60%. Both isomers were fully characterised and their NMR signals assigned due to their intensity ratio of 2:1. However, it was not possible to assign a set of signals to an isomer because of the identical multiplicity of the signals. Even though the methoxy groups were expected to give one singlet for the *trans*-isomer and two singlets for the *cis*-isomer, the ^{1}H NMR spectrum only revealed two sets of two singlets and they were therefore not distinguishable.

Additionally, single crystals suitable for X-ray diffraction analysis of the *trans*-isomer were obtained. The molecular structure, shown in Figure 48, clearly indicates the differences to a silole structure. The carbon-carbon bond lengths of the five-membered ring reveal two single bonds and only one double bond. The loss of the double bonds is also indicated by the tetrahedral coordination of the carbon atoms in 2,5-position.

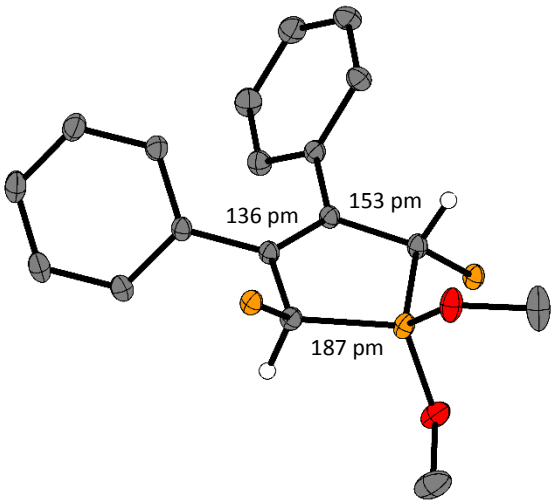

Figure 48: Molecular structure of silacyclopentene **108**; carbon: grey; silicon: yellow; oxygen: red; hydrogen: white; hydrogen atoms, except those in 2,5-position, and methyl groups of trimethylsilyl groups are omitted for clarity; thermal ellipsoids at 50% probability level.

The question arises how such a silacyclopentene **108** is formed (Scheme 58). It can be assumed that the first reaction steps are in analogy to the proposed mechanism presented in Chapter 3.4.1. The silylene **109** is formed by the addition of $KSi(SiMe_3)_3$ to the chlorosilole **54**. The silylene **109** has a degree of unsaturation of four. The observed silacyclopentene **108** has two methoxy groups and a degree of unsaturation of two. It can be assumed that two equivalents of methanol were added during the trapping reaction.

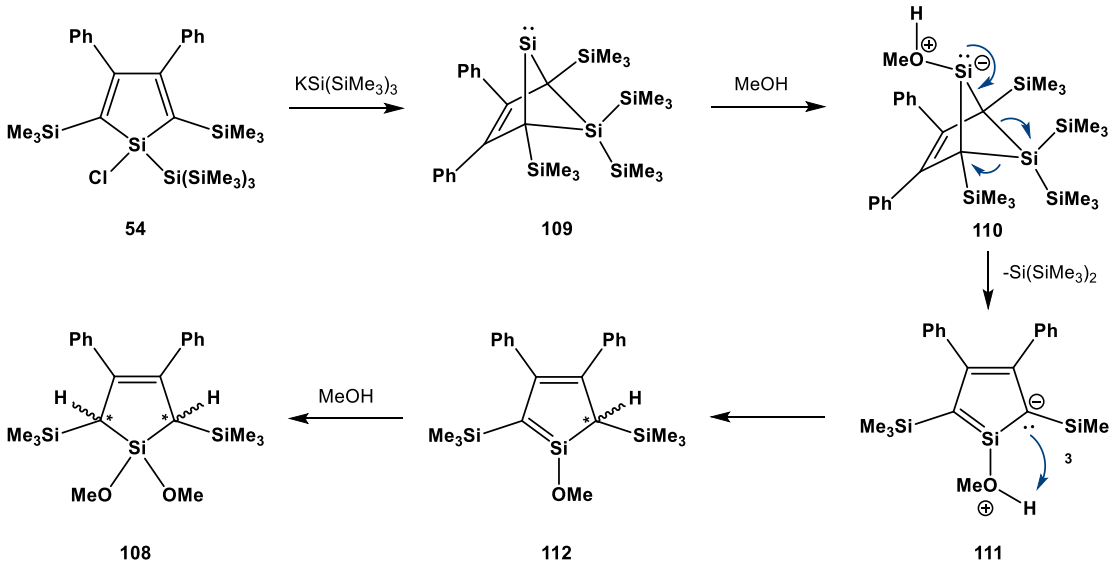

Scheme 58: Proposed mechanism of the reaction of the chlorosilole **54** with $KSi(SiMe_3)_3$ and additional trapping with MeOH yielding an unexpected 1,1-dimethoxysilacyclopentene **108**.

In a possible reaction mechanism methanol attacks the silylene **109** to give **110** and bis(trimethylsilyl)silylene is eliminated in a concerted reaction. The resulting zwitterion **111** would neutralise by a proton shift forming the 1-methoxysilacyclopentadiene **112**, which could add another equivalent of methanol to the silene function to give the dimethoxysilacyclopentene **108**. However, the formation of the dimethoxysilacyclopentene **108** by the addition of methanol is not a clear indication for the presence of the silylene **109**.

During the reaction of the chlorosilole **54** and KO^{t}Bu single crystals of the potassium salt of the trimethylsilylsilolyl anion **93**, suitable for X-ray analysis, were obtained. The silolyl anion **93**, whose structure is discussed in Chapter 3.3.2, was most likely formed due to an abstraction of a trimethylsilyl group of the silylene **109** by excess of potassium tert-butoxide[88] and a subsequent cycloreversion reaction in which elemental silicon is eliminated (Scheme 59).

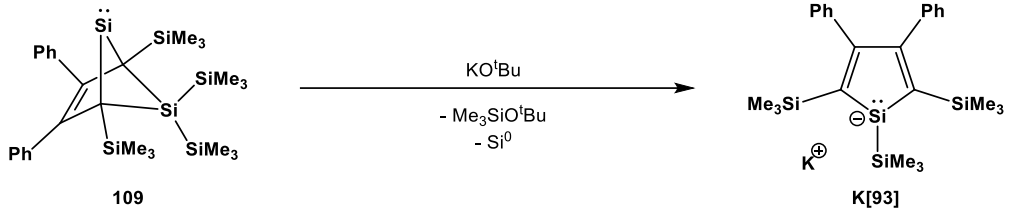

109 K[93]

Scheme 59: Proposed mechanism of the formation of trimethylsilylsilolyl anion salt **K[93]**.

Furthermore, another silole was used in this reaction to investigate if a similar rearrangement reaction occurs. The 1-tris(trimethylsilyl)silole **55** which bears triethylsilyl groups instead of trimethylsilyl groups in 2,5-position was reacted with KSi(SiMe$_3$)$_3$ (Scheme 60).

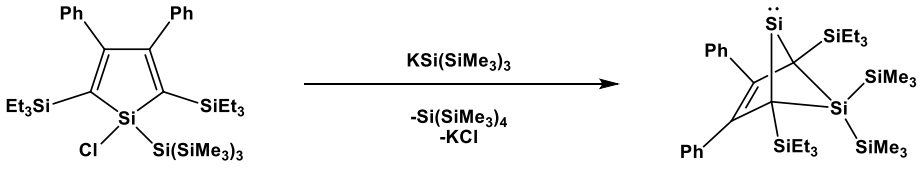

55 113

Scheme 60: Reaction of the 2,5-bis(triethylsilyl) substituted chlorosilole **55** and KSi(SiMe$_3$)$_3$ to give silylene **113**.

The results were similar to those obtained by using the 2,5-bis(trimethylsilyl) substituted chlorosilole **54**. The colour of the reaction mixture turned from pale yellow to red and no precipitation of elemental silicon was observed. However, it seemed to be a more selective reaction because the NMR spectra revealed less signals of impurities which allowed the assignment of the signals (Figure 49). The ^{29}Si NMR spectrum clearly indicates the formation of Si(SiMe$_3$)$_4$ and a similar high field shifted signal at δ^{29}Si = -211.8 is also detected. Additionally, the signal at δ^{29}Si = 33.3 is in

the range of ring silicon atoms and it correlates in the $^{1}H^{29}Si$ HMBC NMR to the methyl groups of the trimethylsilyl groups at $\delta^{29}Si$ = -25.8 and $\delta^{29}Si$ = -16.3. The signal at $\delta^{29}Si$ = -0.2 correlates to ethyl groups and it is therefore assigned to the triethylsilyl groups.

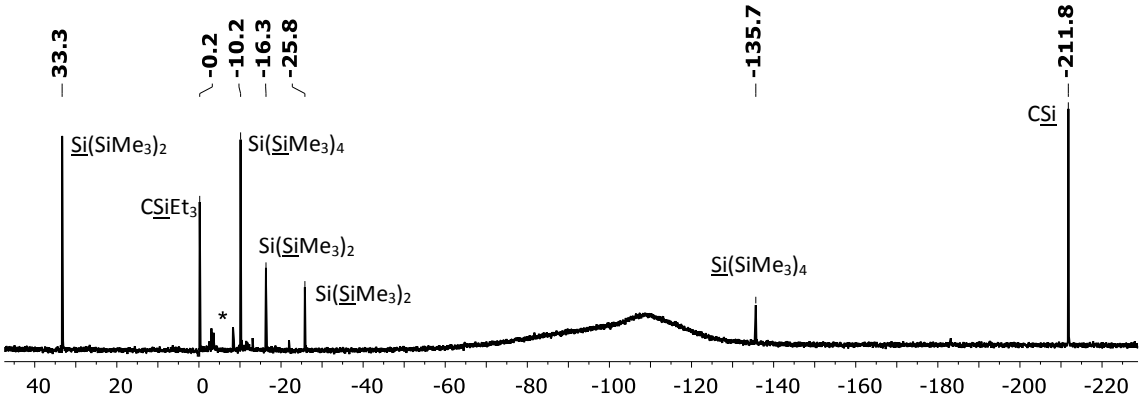

Figure 49: $^{29}Si\{^{1}H\}$ NMR spectrum (99.3 MHz, 305.0 K, C_6D_6) of silylene **113**; * impurities.

According to the expected number of signals for silylene **113**, one signal for a ring silicon atom, one signal for the $SiEt_3$ groups, one signal for each of the magnetically inequivalent $SiMe_3$ groups and one signal for the silylene silicon atom occurred. However, the chemical shift for the silylene at $\delta^{29}Si$ = -211.8 is not in the expected range. Usually silylenes are detected at a much lower field (Figure 50).[126] One of the most famous examples is the silylene **114** synthesised by Kira et al. which has a chemical shift of $\delta^{29}Si$ = 567.3.[127] The silicon centre in the Kira-silylene **114** is flanked by $SiMe_3$ groups and incorporated in a saturated five-membered alkyl ring, and therefore, only kinetically stabilised. The unique ^{29}Si NMR low field shift of the silylene clearly indicates an exceptionally deshielded dicoordinated silicon atom which is also supported by theoretical investigations.[126] The only known silylene that is based on a silole structure is the NHC stabilised silolylene **26** by Cui et al. which has a high field shifted signal at $\delta^{29}Si$ = -43.6.[73] However, NHC stabilised tricoordinated silylenes should be considered as neutral silyl anion equivalents[75] and are in the case of silolylene **26** comparable to silolyl monoanions.[63]

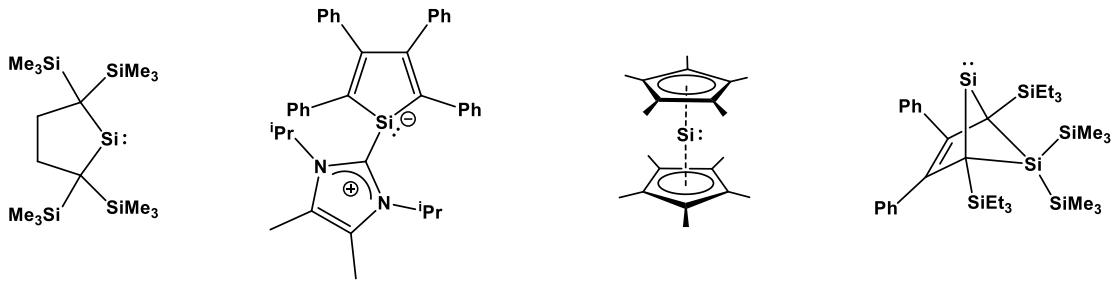

114 by Kira et al.[127] — $\delta^{29}Si$ = 567.3

26 by Cui et al.[73] — $\delta^{29}Si$ = -43.6

115 by Jutzi et al.[128-130] — $\delta^{29}Si$ = -398.0

Silylene **113** — $\delta^{29}Si$ = -211.8

Figure 50: Comparison of ^{29}Si NMR resonances of known silylenes with **113**.

In contrast, the decamethylsilicocene **115** reported by Jutzi et al., which was the first isolable silylene, shows an opposite extreme.[128-130] Due to the η^5-coordination of two cyclopentadienyl rings the silicon centre is highly shielded which is also reflected in a significant up field shift of the ^{29}Si NMR resonance of δ^{29}Si = -398.0. However, because of the high coordination of the silicon centre the silicocene **115** cannot be considered as a classical silylene.

To further investigate the silylenes **109** and **113** quantum mechanical calculations were performed. The structures were optimised at the M06-2X/6-311+G(d,p) level of theory and NMR chemical shifts were calculated at GIAO M06-L/6-311G(2d,p). The obtained results, which are summarised in Table 15, are in very good agreement with the experimental values. This strongly supports that the silylenes **109** and **113** were synthesised.

Table 15: Comparison of the experimental (99.3 MHz, 305.0 K, C_6D_6) and calculated (GIAO M06-L/ 6-311G(2d,p)//M06-2X/6-311+G(d,p)) ^{29}Si NMR chemical shifts of silylenes **109** and **113**.

	C<u>Si</u>	<u>Si</u>(SiMe$_3$)	C<u>Si</u>R$_3$	Si(<u>Si</u>Me$_3$)[b]	Si(<u>Si</u>Me$_3$)[c]
Silylene **109** (R = Me)					
Exp.	-210.6	32.2	-6.4[a]	-16.7[a]	-25.5[a]
Calcd.	*-231.7*	*31.2*	*-5.3/-6.2*	*-17.1*	*-23.8*
Silylene **113** (R = Et)					
Exp.	-211.8	33.3	0.2	-16.3	-25.8
Calcd.	*-219.9*	*30.4*	*-3.0/-5.2*	*-15.0*	*-25.5*

[a] Assignment by comparison to the calculated values; [b] equatorial; [c] axial.

The optimisation of the silylenes revealed an interesting type structure which will be further discussed at the structure of **113** (Figure 51). The carbon bond lengths between C1 and C2 or C3 and C4 are with d(C-C) = 149 pm in the range of single bonds.[95] The double bond between C2 and C3 with a length of d(C=C) = 141 pm is elongated compared to carbon double bonds of the silole starting material (Table 6). The silicon atom Si2 has a bond length of d(Si2-C) = 191 pm to the carbons C1 or C4 which is in a typical range for a silicon-carbon single bond.[95] The silylene silicon atom Si1 has an elongated single bond to the same carbon atoms with a length of d(Si1-C) = 205 pm. Such an elongation was also observed in the recently reported analogue germylene **116**.[131] In comparison, the silicon-carbon bond lengths in the Kira-silylene **114** are d(Si-C) = 191 pm.[127]

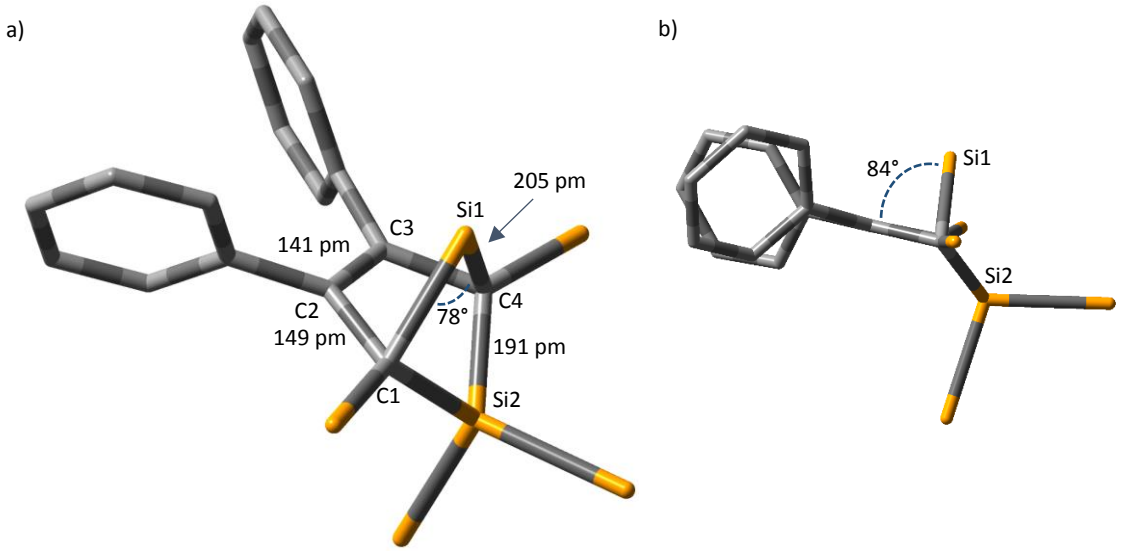

Figure 51: Calculated structure of silylene **113** at the M06-2X/6-311+G(d,p) level of theory; carbon: grey; silicon: yellow; hydrogen atoms, methyl and ethyl groups of silyl groups are omitted for clarity; a) top view; b) side view along the C1-C4 vector.

The angle at the silylene silicon atom in **113** is with ε(C1-Si1-C4) = 78° a more acute angle compared to the silylene **114** by Kira et al. (ε(C-Si-C) = 94°)[127] or silolylene **26** by Cui et al. (ε(C-Si-C) = 91°).[73] The most intriguing metric, however, is the angle between the C1-C2-C3-C4 and the C1-Si1-C4 planes which is ε = 84° (b, Figure 51). Such a small angle shows that the silylene silicon atom is bend towards the C2-C3 double bond, and therefore, indicates an interaction. This is also supported by the short distances of the silicon atom to the carbon atoms of the double bond of d(Si1-C2) = 210 pm and d(Si1-C3) = 212 pm which are only elongated by 5 pm and 7 pm compared to the bonds to C1 and C4. The most reasonable explanation for this is the π-orbital of the double bond donating electron density into the empty 3p-orbital of the silylene silicon atom (Figure 52, Figure 56). This interaction explains the elongation of the C2-C3 double bond length and also of the Si1-C1/C4 bond lengths. The molecular orbitals of silylene **113** were calculated at the M06-2X/6-311+G(d,p) level of theory to further elucidate this interaction. In Figure 52 the HOMO illustrates the delocalisation of π-electron density of the carbon-carbon double bond into the empty 3p orbital at the silicon. The LUMO shows the nodal plane of the alkenyl function and mostly distribution along one of the phenyl rings. The HOMO/LUMO energy gap of $\Delta E_{H/L}$ = 5.72 eV is significant and suggests a mostly nucleophilic reactivity similar as for a recently reported analogue germylene **116** ($\Delta E_{H/L}$ = 5.85 eV).[131]

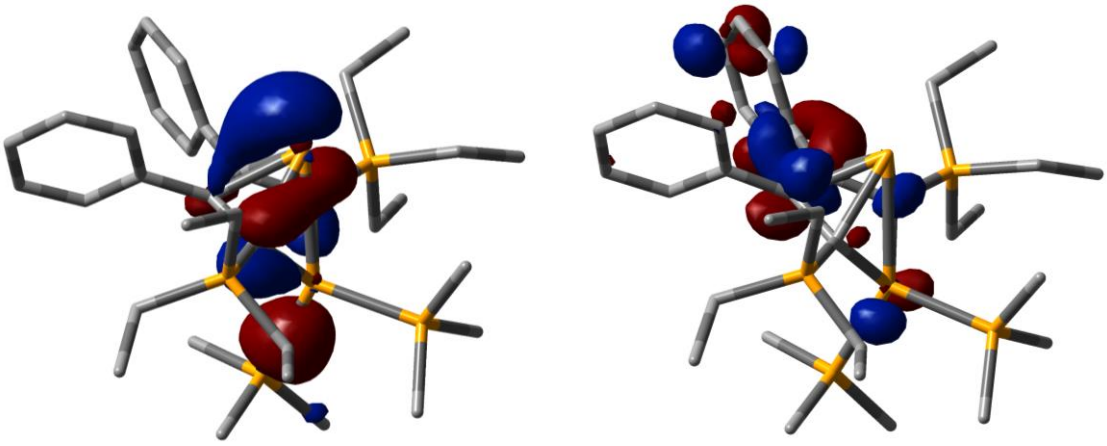

HOMO
E = -6.11 eV

LUMO
E = -0.39 eV

Figure 52: Calculated surface diagrams of selected molecular orbitals of silylene **113** at the M06-2X/ 6-311+G(d,p) level of theory; carbon: grey; silicon: yellow; hydrogen atoms are omitted for clarity; visualisation at an isovalue of 0.05.

Additionally, Atoms in Molecules (AIM) analysis[132] was performed on the parent silylene **117** at the M06-2X/Def2-QZVPD//M06-2X/6-311+G(d,p) level of theory (Figure 53). The interaction of the alkenyl function with the silylene is further supported by the presence of a bond path. The most important fact is that the bond path is not between the silicon and the C2 and C3 carbon atoms but between the silicon and the centre of the C2-C3 double bond. Such a T-shaped topology is typical for π-complexes as it is shown for the 2-norbornyl cation.[133,134] This T-shaped electron density distribution and its bond critical point (bcp), displayed in b) Figure 53, unequivocally indicate the interaction of the π-orbital of the double bond with the empty 3p-orbital of the silicon atom in the parent silylene **117**. In c) Figure 53 the contour plot of the Laplacian of the electron density through the plane of the silicon and the alkenyl function is displayed. The valence shell charge concentration (VSCC) at the silylene silicon atom clearly shows the presence of the lone pair.

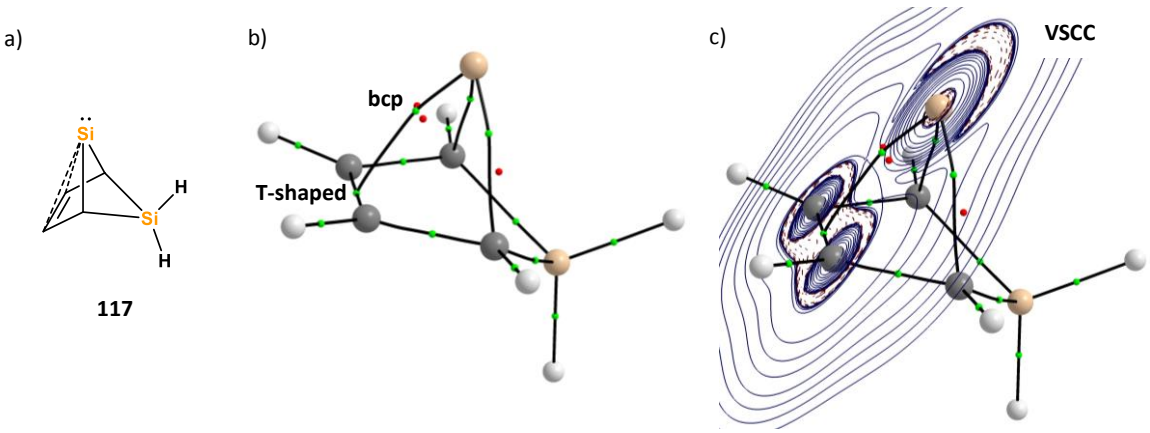

Figure 53: AIM analysis of the parent silylene **117** at the M06-2X/Def2-QZVPD//M06-2X/6-311+G(d,p) level of theory; hydrogen: white; carbon: grey; silicon: yellow; bond critical point (bcp): green; ring critical point (rcp): red; a) Lewis structure; b) AIM analysis; c) contour plot of the Laplacian of the electron density through the plane of the silicon atom and the alkenyl function.

To evaluate the strength of the interaction of the double bond and the silylene silicon atom an isodesmic reaction was investigated computationally at the M06-2X/6-311+G(d,p) level of theory (Scheme 61). The energy difference of the silylene **113** and its saturated analogue **119** in addition to the energy difference of the disilabicyclo[2.1.1]hexane **118** and the disilabicyclo[2.1.1]hexene **120** indicate the strength of the π-conjugation. The calculated isodesmic reaction energy of ΔE_{iso} = 137 kJ mol^{-1} underlines the significance of this interaction on the stabilisation of silylene **113**.

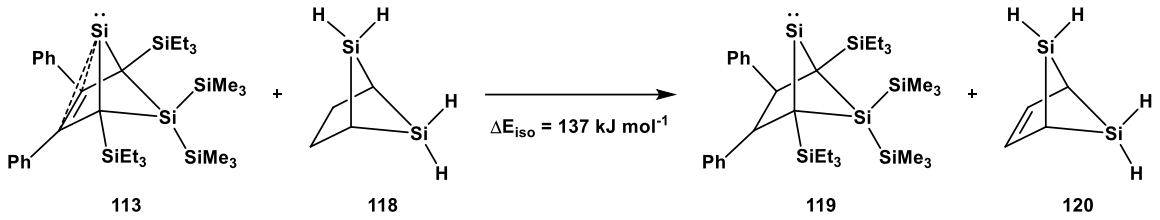

Scheme 61: Isodesmic reaction to determine the energy difference between silylene **113** and silylene **119** with a saturated double bond to indicate the stabilisation energy of the homoconjugation at the M06-2X/6-311+G(d,p) level of theory.

The collected data, which support the interaction of the alkenyl function and the silicon atom, show that **113** is not a typical silylene. The calculations strongly support that the structure of **113** has to be considered as a silylene stabilised by homoconjugation (Figure 54, Figure 56). Homoconjugation describes the orbital overlap of two π-systems which are separated by at least one non-conjugating group.[135] This intramolecular interaction is mostly observed in electron-deficient systems in which delocalisation of electron density of a remote alkenyl function into an empty p-orbital provides a stabilising effect. This type of stabilisation was extensively investigated in the past and it is therefore well-established in the context of carbocations and the potential aromatic character of this interaction, the so called homoaromaticity.[136,137]

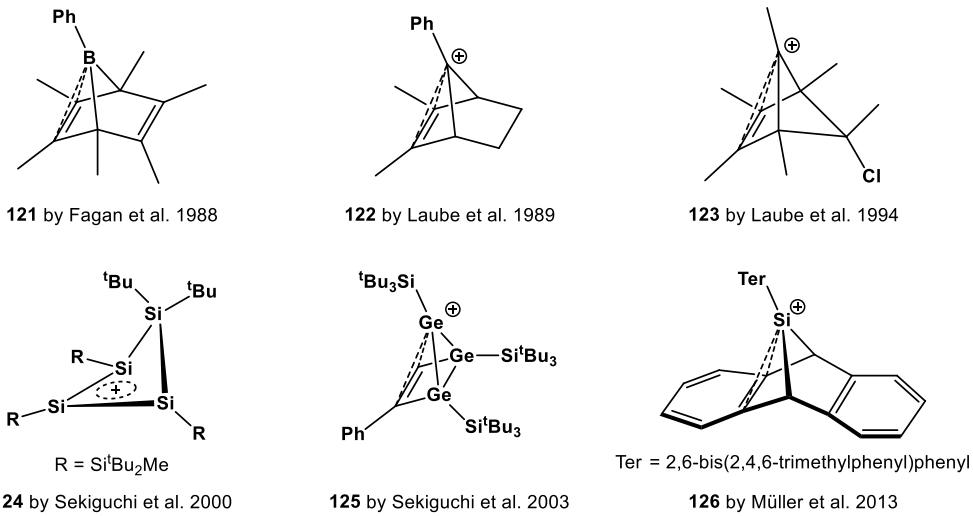

Figure 54: Electron-deficient main-group compounds stabilised by homoconjugation.[138-143]

While the pioneering work of these carbocations stabilised by homoconjugation, was performed by Winstein et al.[144,145] and Roberts et al.,[146] first structures, such as **122** or **123**, were reported by Laube et al. (Figure 54).[139,140] But also heavier group 14 homologues have been investigated by Sekiguchi et al., such as **124** and **125**,[138,141] or by our workgroup, such as **126**,[142] which revealed similar stabilising effects. Homoconjugation in neutral compounds was observed in several boranes such as **121** by Fagan et al.[143]

Neutral group 14 compounds which indicate this type of stabilisation, such as tetrylenes, however, have only been reported recently by our group in form of the germylene **116** or by low temperature matrix experiments and theoretical investigations of C_5H_6Si by Maier et al. which will be discussed later in this chapter.[131,147] Due to their high potential in bond activation and coordination chemistry,[148] tetrylenes have been investigated extensively in the past.[149] Besides the already mentioned unusual decamethylsilicocene **115**[128-130] and the Kira-silylene **114**[127], which is only kinetically stabilised, tetrylenes are usually stabilised by electron donation into their empty p-orbital. Therefore, the coordination of NHCs to tetrylenes, such as in the silolylene **26**[73], is a common stabilisation approach.[149-151] However, the resulting tricoordinated silicon atom is often comparable to silyl anions.[75,152] Most other tetrylenes are stabilised by electron donating substituents and can be categorised in types such as push-push (**I**), push-spectator (**II**), and push-pull (**III**). A few examples are shown in Figure 55. The silicon analogues (**I**) of the N-heterocyclic Arduengo carbenes[153] were reported by West et al.[154,155] Respective germanium compounds were already known at that point.[156-158] Examples of tetrylenes which are only stabilised by one electron donating group (**II**) are reported by Iwamoto et al.[159] and Kinjo et al.[160] A push-pull stabilisation (**III**), in which a silylene is incorporated between group 13 and 15 elements, was accomplished by Aldridge et al.[161]

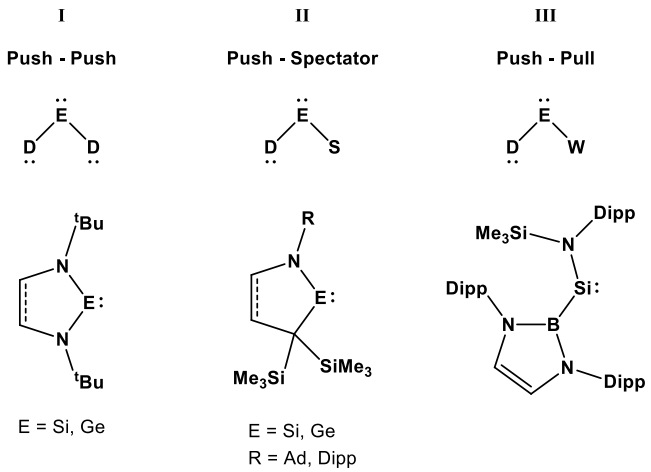

Figure 55: Different types of stabilisation for tetrylenes; E: heavier group 14 element; D: electron-donating group; W: electron-withdrawing group.[149,154-161]

The synthesis of a silylene stabilised by homoconjugation, such as **113**, has not been previously reported. This type of stabilisation also explains the observed particular features, such as the elongation of the C2-C3 double bond (Figure 51) and the unique high field shift in the ^{29}Si NMR spectrum (Figure 56). The donation of electron density of the π-orbital of the double bond into the empty 3p-orbital of the silylene is responsible for a high field shift of the silicon resonance.[126] Additionally, the coordination at the silicon is increased and, as mentioned before, silyl compounds with a higher coordination number show their resonance at a higher field in the ^{29}Si NMR spectra. Another fact which may contribute to the high field shift of the NMR resonance is the anisotropic effect of the double bond which has a shielding effect on the short-distanced silicon atom leading to a high field shift of the silicon NMR resonance.

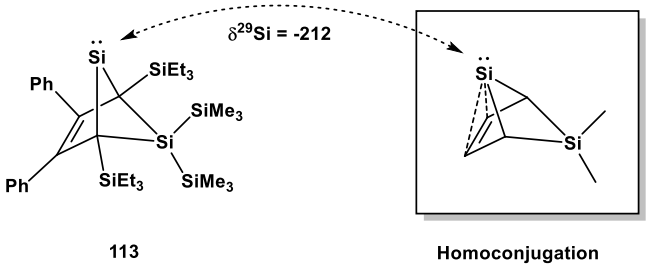

Figure 56: Stabilisation of silylene **113** by homoconjugation leading to a significant high field shift of the silylene silicon atom of δ^{29}Si = -212 in the ^{29}Si NMR spectrum.

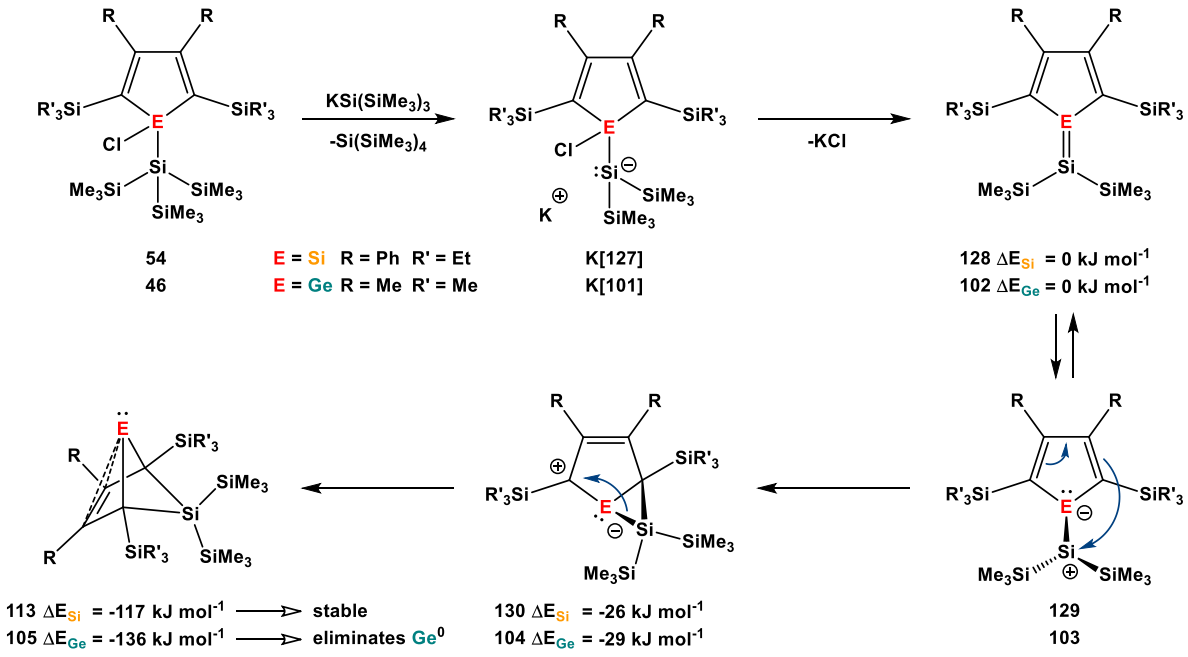

Scheme 62: Proposed mechanism and calculated relative energies ΔE at the M06-2X/6-311+G(d,p) level of theory of the rearrangement reaction of germole **46** or silole **54** to the respective germylene **105** or silylene **113**.

The proposed reaction mechanism of the formation of silylene **113** is analogous to the one of the germylene **105** reported in Chapter 3.4.1. Both rearrangement reactions, in addition to their relative energies, are summarised in Scheme 62. The only difference is that silylene **113** seems to be stable at room temperature, and therefore, no elimination of elemental silicon occurs. The relative reaction energies of the proposed intermediates are in the same range for both rearrangement reactions.

The germylene **105** shows a higher stability than silylene **113**, compared to the respective fulvenes **102** and **128** (Scheme 62). The relative reaction energy of the tetrylenes **105** or **113** to form the respective siloles **100** or **131** and the atomic triplet element is in both cases endothermic (Scheme 63). Considering the condensation of the element atoms to form bulk material calculated by the sublimation energy[111,122,162] provides the required thermodynamic driving force. The resulting relative energies reveal that the cycloreversion reaction of the tetrylenes **105** or **113** are both exothermic. However, the calculated value for germylene **105** is $\Delta\Delta E = 38$ kJ mol^{-1} more exothermic compared to the value of silylene **113**. This difference might explain why the silylene **113** is stable and the germylene **105** eliminates elemental germanium.

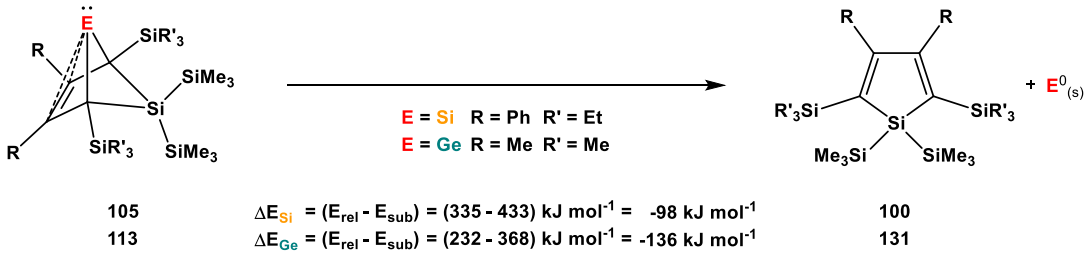

105 $\Delta E_{Si} = (E_{rel} - E_{sub}) = (335 - 433)$ kJ mol^{-1} = -98 kJ mol^{-1} 100

113 $\Delta E_{Ge} = (E_{rel} - E_{sub}) = (232 - 368)$ kJ mol^{-1} = -136 kJ mol^{-1} 131

Scheme 63: Calculated relative energies of the cycloreversion reaction of germylene **105** and silylene **113** forming the siloles **100** or **131** and the respective atomic triplet element at the M06-2X/ 6-311+G(d,p) level of theory; the condensation of the element atoms to form bulk material is considered by the sublimation energies.[111,122,162]

To further support the proposed mechanism calculations on the parent systems **117** and **132**, which only bear hydrogen substituents, were performed. In Figure 57 the calculated potential energy surfaces of the rearrangement reactions at the M06-2X/6-311+G(d,p) level of theory are shown. The relative energies of the proposed intermediates have a similar trend compared to the calculations of the experimentally investigated compounds (Scheme 62). In addition to the energy minima of the intermediates, the corresponding transition states between these intermediates were also found. Therefore, reaction barriers could be determined for each step and were found to be overall low which supports the proposed mechanism.

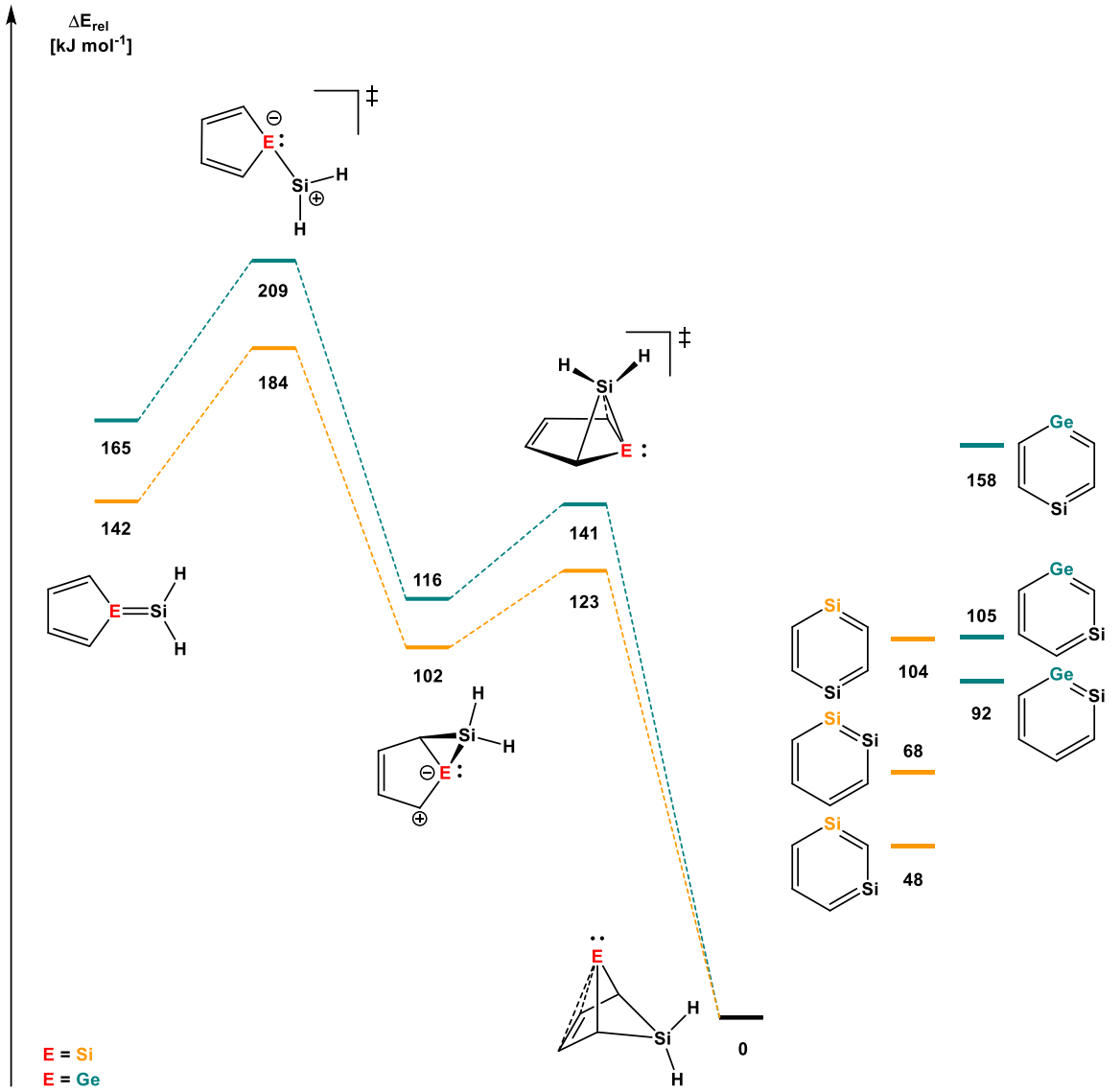

Figure 57: Calculated potential energy surface of the proposed mechanism of the formation of the parent system of the tetrylenes **117** and **132** and comparision to the relative energies of the valence isomeric disila- or germasilabenzenes at the M06-2X/6-311+G(d,p) level of theory.

Furthermore, the investigated silylenes and germylenes, which can also be considered as disila- and germasilabicyclo[2.1.1]hexenylidenes, are valence isomers of disila- and germasilabenzenes (Figure 57). It is of great interest that the relative energies of the benzene derivatives, compared to the respective tetrylenes, reveal that they are significantly less favoured suggesting the homoconjugative stabilisation to be more efficient than conventional electron delocalisation. Low temperature matrix investigations supported by DFT calculations of the C_5H_6Si analogue by Maier et al. revealed that a similar silylene structure, which is also stabilised by homoconjugation, shows high stability. However, in this case the analogue monosilabenzene was determined as the most stable structure.[147]

Recently two very similar compounds compared to the synthesised silylene **113** have been reported. The germylene **116**, synthesised by our group, has a highly comparable structure which shows a germylene stabilised by homoconjugation by a remote alkenyl function.[131] Only shortly before, tin compound **133** was reported by Saito et al. which seems to have a very similar structure as the germylene **116**. However, according to their analysis the electronic situation suggests that **133** has to be considered as a Sn^0 butadiene complex.[163]

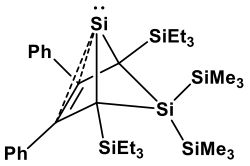

113

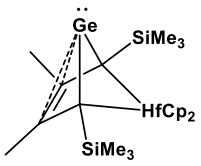

116

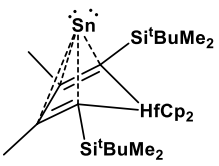

133

To determine the influence of the quaternary silyl substitution on the tetrylene, quantum mechanical calculations on the 3,4-dimethyl-2,5-bis(trimethylsilyl)heteroles with different central elements were performed at the M06-2X/6-311+G(d,p) level of theory. The relative energies ΔE of the proposed intermediates, summarised in Table 16, reveal that the germylene (ΔΔE = 60 kJ mol^{-1}) and the silylene (ΔΔE = 59 kJ mol^{-1}) with germyl substitution are significantly less stable compared to the respective silyl subsituted analouges. However, the exothermic relative energies for each of the tetrylenes suggest their formation is still favoured.

Table 16: Comparison of the calculated relative electronic energies ΔE [kJ mol^{-1}] of proposed intermediates with variation of the central elements of the rearrangement reaction presented in Chapter 3.4 at the M06-2X/6-311+G(d,p) level of theory.

R = $SiMe_3$	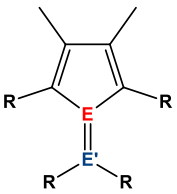	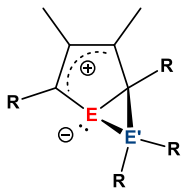	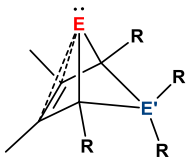
E = **Ge** **E'** = **Si**	0	-28	-136
E = **Si** **E'** = **Si**	0	-23	-116
E = **Ge** **E'** = **Ge**	0	-17	-76
E = **Si** **E'** = **Ge**	0	-10	-57

Another important factor for the synthesis of this type of tetrylenes is their potential to eliminate the central element in a cycloreversion reaction yielding the respective heterole, as already described for the proposed germylene **105** in Chapter 3.4.1. Therefore, the calculated relative energies of different tetrylenes and the respective heteroles are compared in Table 17. The formation of the element as bulk material was considered by the sublimation energy.[111,122,162] The calculated values indicate that the elimination of elemental germanium is favoured by $\Delta\Delta E$ = 40 kJ mol^{-1}, compared to the respective silicon analogues, which is consistent with the experimental observations. The difference of $\Delta\Delta E$ = 7 kJ mol^{-1} between silyl or germyl substitution in each case suggest only a minor influence on these values.

Table 17: Comparison of the calculated relative electronic energies ΔE [kJ mol^{-1}] of different tetrylenes and the respective heterole with its eliminated element considered by the sublimation energy[111,122,162] at the M06-2X/6-311+G(d,p) level of theory.

R = $SiMe_3$	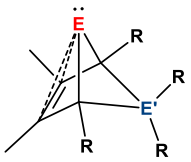	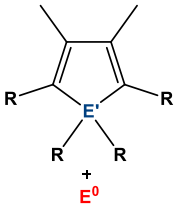
E = Ge **E'** = Si	0	-136
E = Si **E'** = Si	0	-96
E = Ge **E'** = Ge	0	-143
E = Si **E'** = Ge	0	-103

To investigate the reactivity of the tetrylenes the ability of silylene **113** to function as a σ-donor in organometallic transition metal complexes was tested by the reaction of the silylene **113** with $Fe(CO)_4$ forming the silylenyl $Fe(CO)_4$ complex **134** (Scheme 64). The $Fe(CO)_4$ fragment was formed *in situ* by the addition of $Fe_2(CO)_9$ to a THF solution of silylene **113** at room temperature. Residual $Fe_2(CO)_9$ was removed by filtration and the $Fe(CO)_5$ side product was removed in vacuum.

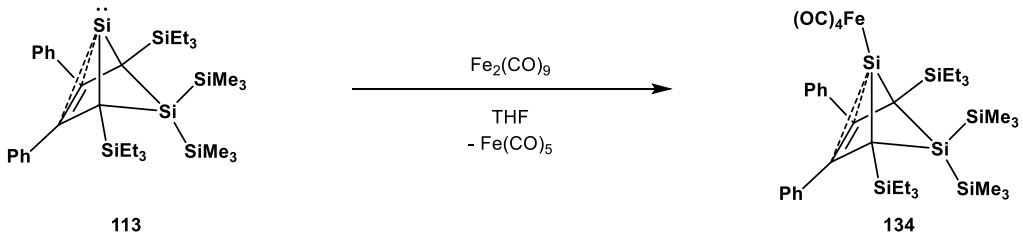

113 **134**

Scheme 64: Reaction of the silylene **113** with $Fe_2(CO)_9$ to form the silylenyl $Fe(CO)_4$ complex **134**.

The $Fe(CO)_4$ complex **134** was characterised by NMR spectroscopy and high resolution mass spectrometry (HR-MS (LIFDI) for $^{12}C_{38}{}^{1}H_{58}{}^{16}O^{56}Fe^{28}Si_6$: *m/z* [$M^+$] calculated: 802.2295; found: 802.2299). The number of NMR signals and their correlations were the same as for silylene **113** which suggests that the $Fe(CO)_4$ fragment was added but the general structure of the silylene remained the same. In the ^{29}Si NMR spectrum of **134**, five signals were detected in addition to the resonances of $Si(SiMe_3)_4$ (Figure 58, Table 18).

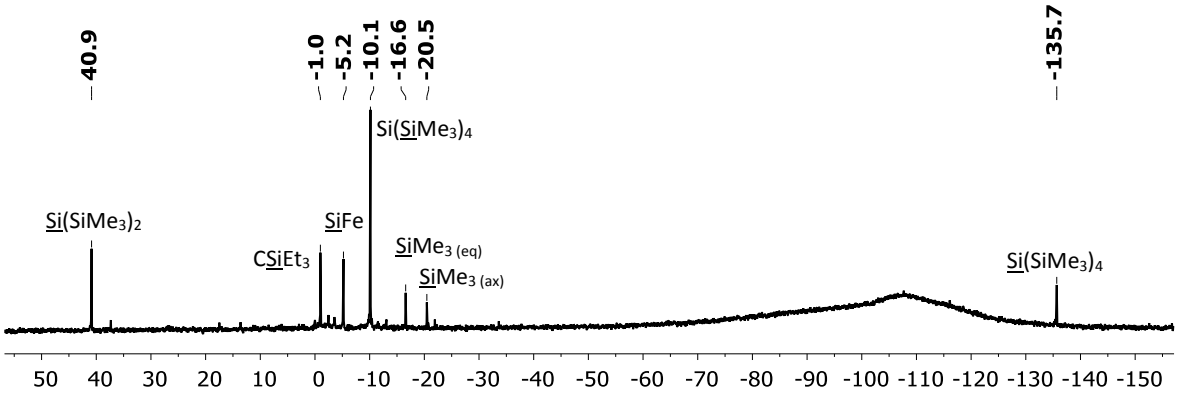

Figure 58: $^{29}Si\{^1H\}$ NMR spectrum (99.3 MHz, 305.0 K, C_6D_6) of the silylenyl $Fe(CO)_4$ complex **134**.

The signals for the $SiEt_3$ groups and for the equatorial $SiMe_3$ group were detected at the same range as for the silylene **113**. The resonance for the quaternary ring silicon atom and the axial $SiMe_3$ group have a slightly low field shift. The signal for the silylene silicon atom at $\delta^{29}Si$ = -211.8 disappeared and a new signal at a significant lower field of $\delta^{29}Si$ = -5.2 was detected. This signal was assigned to the $SiFe(CO)_4$ group. Additionally, in the ^{13}C NMR spectrum one signal for the carbonyl groups was detected at $\delta^{13}C$ = 215.6.

Table 18: Comparison of the ^{29}Si NMR chemical shifts of silylene **113** and the silylenyl $Fe(CO)_4$ complex **134** (99.3 MHz, 305.0 K, C_6D_6).

	C<u>Si</u>/C<u>Si</u>Fe	<u>Si</u>(SiMe$_3$)	C<u>Si</u>Et$_3$	Si(<u>Si</u>Me$_3$)[a]	Si(<u>Si</u>Me$_3$)[b]
Silylene **113**	-211.8	43.3	0.2	-16.3	-25.8
Silylenyl $Fe(CO)_4$ complex **134**	-5.2	40.9	-1.0	-16.6	-20.5

[a] equatorial $SiMe_3$; [b] axial $SiMe_3$.

The question arises if the $Fe(CO)_4$-fragment is equatorially or axially coordinated to the silylene (Figure 59). The calculated energy differences of both optimised structures at the M06-2X/ Def2-TZVP level of theory indicate that an equatorial coordination is favoured by ΔE = 11 kJ mol^{-1}. However, such a low energy difference is not a clear indicator for which coordination is present. In comparison, the analogue germylene **116** coordinates axially with the $Fe(CO)_4$-fragment.[131]

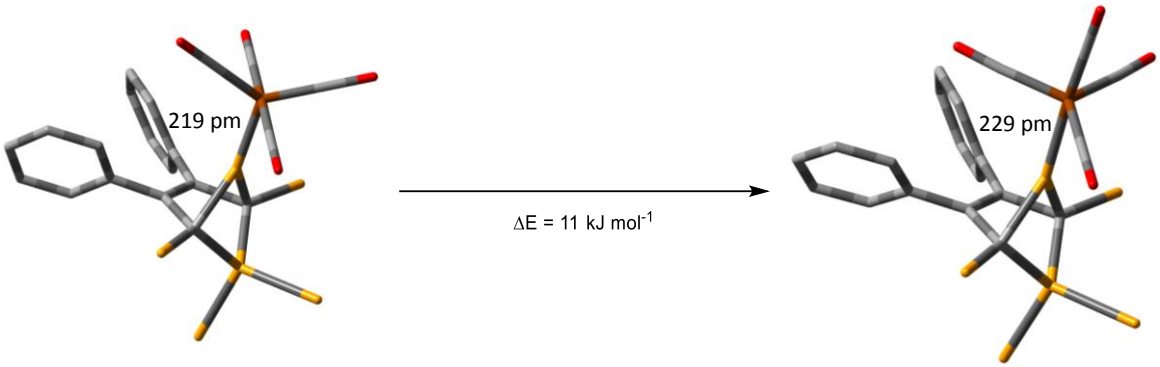

Figure 59: Optimised structures and the calculated energy difference of the equatorial and axial coordinated silylenyl $Fe(CO)_4$ complex **134** at the M06-2X/Def2-TZVP level of theory; carbon: grey; silicon: yellow; oxygen: red; iron: brown; hydrogen atoms, methyl and ethyl groups of silyl groups are omitted for clarity.

Regardless of the use of different solvents such as THF, Et_2O, pentane, hexane, benzene, toluene and $(Me_3Si)_2O$ at various temperatures no single crystals of silylene **113** or the silylenyl $Fe(CO)_4$ complex **134**, which were suitable for X-ray analysis, were obtained via crystallisation. The very good solubility of these compounds and the equimolar presence of the side product $Si(SiMe_3)_4$ often led to the formation of oily residues. Attempts to remove $Si(SiMe_3)_4$ via sublimation using an oil diffusion pump were not successful due to the stickiness of the residues.

4 Summary and Outlook

The focus of this thesis was the synthesis of halogen substituted sila- and germacyclopentadiene derivatives and the investigation of their behaviour under various reductive conditions with the aim to obtain stable silolyl and germolyl radicals. In this context, 1-halogermoles and siloles with various substitution patterns (**45**-**48** and **54**-**55**), as well as the respective precursor compounds, were synthesised, fully characterised and reduced with different reagents.

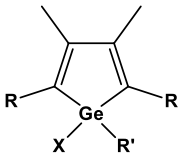

45 R' = Pemp R = $SiMe_3$
46 R' = $Si(SiMe_3)_3$ R = $SiMe_3$
47 R' = $Ge(SiMe_3)_3$ R = $SiMe_3$
48 R' = $Si(SiMe_3)_3$ R = Si^tBuMe_2

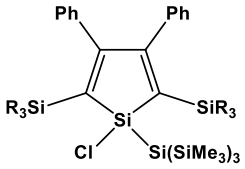

54 R = Me
55 R = Et

By the reduction of the respective 1-chlorogermole and silole with potassium graphite the 1-tris(trimethylsilyl) substituted germolyl and silolyl radicals **69** and **78** were successfully synthesised (Figure 60). These radicals were identified by EPR spectroscopy and trapping reactions with 1,4-cyclohexadiene resulting in the respective 1-hydrogen substituted derivative. Both radicals showed remarkable stability even in solution at room temperature. While the silolyl radical **78** was stable for several days, the germolyl radical **69** did not show any decomposition after several weeks.

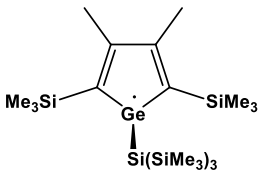

69

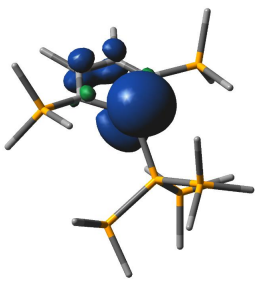

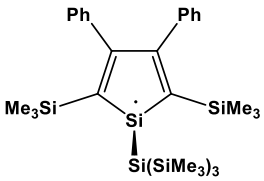

78

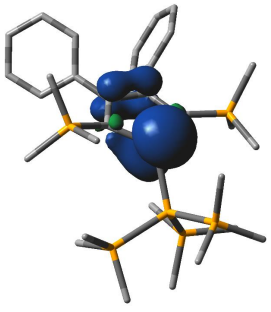

Figure 60: Germolyl and silolyl radicals **69** and **78** and their calculated spin density distributions; isovalue = 0.004; hydrogen atoms omitted for clarity; for details see Figure 20 and Figure 30.

The experimental results were supported by extensive quantum mechanical calculations. By comparison of several different substituents in 1-position the bulky $Si(SiMe)_3$ group was found to be most suitable to stabilise the radicals and to supress a dimerisation reaction. Furthermore, the calculations revealed that the pyramidalisation of the radical centre has a significant influence on

its hyperfine coupling constant. The agreement of the experimentally obtained hfcc with the computed suggested accurate structures, which revealed pyramidalised radical centres with a mainly localised spin density distribution (Figure 60). This high thermodynamic stability and the distinct localisation of the spin density are fundamental for the use of sila- and germacyclopenta-dienyl radicals as localised spin centres.

Despite the fact that both radicals showed high stability, no isolation of single crystals suitable for X-ray diffraction analysis was possible. Alternating the substitution pattern with bulkier and even unsymmetrical groups (**135**) could further increase the stability and might also allow the isolation as crystalline material.

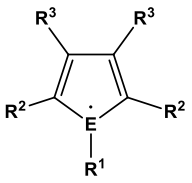

R^1 = $Si(^tBu)_3$,$Si(Si^tBu_2Me)_3$, Dipp
R^2 = $SiMe_3$, $Si(SiMe_3)_3$, Si^tBuMe_2
R^3 = alkyl, aryl
E = Si, Ge

135

These stable sila- and germacyclopentadienyl monoradicals are model compounds which set the base to design systems with multiple localised spin centres. Possible target structures are bisradicals which are bridged in 1-position by silyl (**136**) or phenylene groups or trimers based on the systems (**137**) reported by Tilley et al.[164,165] The combination of the here presented radicals with those reported by Sekiguchi et al. is also a possible approach (**138**).[59,102]

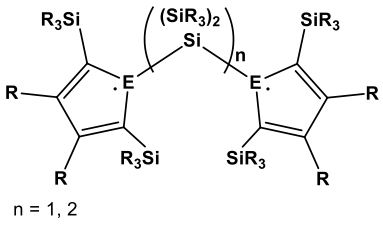

n = 1, 2

136

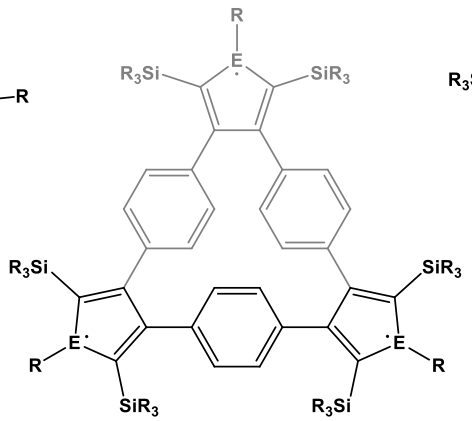

R = alkyl, aryl, silyl
E = Si, Ge

137

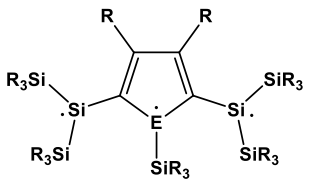

138

By creating localised spin centres in those heterocycles, interesting functionalities could be added. Especially the incorporation of those systems in macromolecules could lead to cooperative effects. The synthesis of persistent group 14 heterolyl radicals represents the first step in a promising approach for the design of magnetic molecular building blocks for highly functionalised polymers.

During the investigations on the radicals, several potassium salts of anionic heterolyl compounds were also synthesised and structurally characterised. Even though various group 14 heterolyl mono- and dianions have been reported in the literature, unprecedented compounds with unexpected structural motifs in the solid state were observed and discussed in this work.

While the germolyl anion **74** has a pyramidalised germanium centre, as expected for mono-substituted germolyl anions, it forms a dimeric structure in the solid state, in which, according to quantum mechanical calculations, dispersion interactions play a very important role (Figure 61).

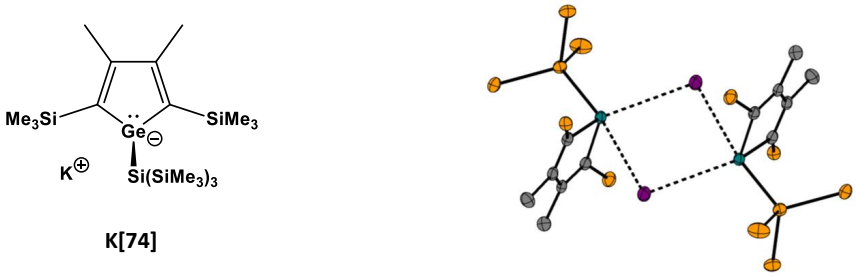

Figure 61: Germolyl anion **74** and the molecular structure of its potassium salt; hydrogen atoms and methyl groups of trimethylsilyl groups are omitted for clarity; for details see Figure 35.

In addition, the obtained silolyl anions **83** and **84**, which only differ in the substitution in 2,5-position, revealed different structures in the solid state (Figure 62). The trimethylsilyl substituted anion **83** has a pyramidalised silicon centre with a localised lone pair while the triethylsilyl substituted anion **84** has a planar structure with a conjugated ring system. In this work, it was shown that the formation of a pyramidalised or planar structure is very subtle and strongly depends on the η^5-coordination of the counter cation. A planar structure of monosubstituted silolyl anions which are not further coordinated to transition metal complexes such as in **84** has not been previously reported in the literature.

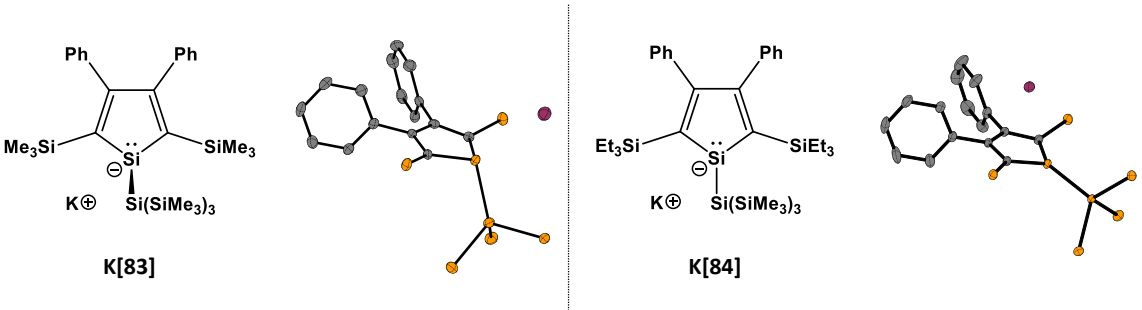

Figure 62: Silolyl anions **83** and **84** and the molecular structures of their potassium salts; hydrogen atoms, methyl and ethyl groups of silyl groups are omitted for clarity; for details see Figure 39.

Furthermore, solid state structures of additional silolyl anions were obtained and investigated. Analogues of the dimeric bisanion **96** have been reported in the literature but their molecular structure remained unknown. The solid state structure of **96**, obtained during this work, revealed high conjugation and an unexpectedly short Si-Si bond length. Additionally, the silolyl bisanion **95** which has an anionic substituent was also presented. This type of compound was also unprecedented so far.

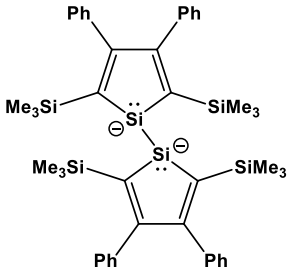

96

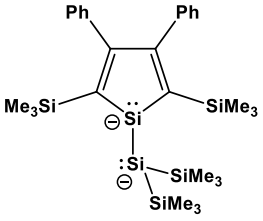

95

Due to the fact that group 14 heteroles are easily reduced to their anions, oxidation reactions of these anions to obtain the respective radicals and to investigate the reversibility of oxidation and reduction will be of great interest in future works (Scheme 65).

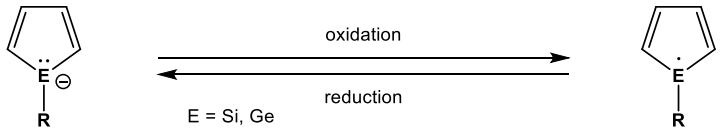

Scheme 65: Oxidation and reduction dependency of heterolyl anions and their respective radicals.

Apart from the described efforts to synthesise group 14 heterolyl radicals, an unexpected rearrangement reaction was observed in which a germole was transformed into a silole while elemental germanium precipitated. If the same reaction was carried out by using an analogue silole as starting material a new type of stable silylene was formed (Figure 63).

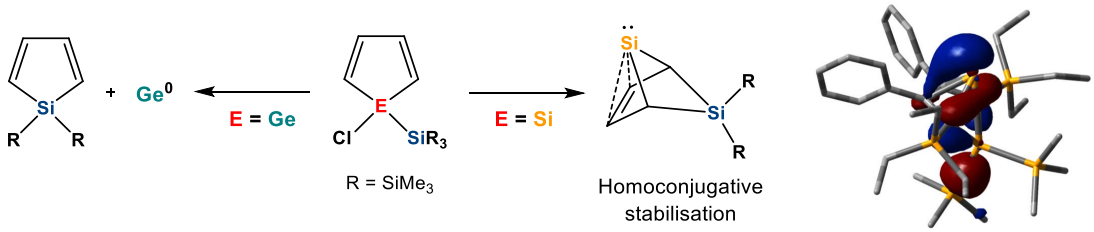

Figure 63: Rearrangement of germoles into siloles and elemental germanium and of siloles into a new type of silylenes which are stabilised by homoconjugation; calculated surface diagram of the HOMO of silylene **113**; hydrogen atoms are omitted for clarity; isovalue = 0.05; for details see Figure 52.

Extensive DFT calculations revealed that the most important factor for the astonishing stability of the silylene is a homoconjugative interaction of the dicoordinated silicon atom with a remote alkenyl function. The decisive experimental evidence for this interaction is the unique high field shift of the ^{29}Si NMR resonance. This homoconjugative stabilisation of tetrylenes was found to be more efficient than conventional electron delocalisation which is indicated by the fact that the tetrylenes are significantly favoured over the isomeric heavier homologues of benzene. The calculated HOMO/LUMO gap for the silylene is substantial and suggests a mostly nucleophilic reactivity pattern which was also investigated experimentally by the formation of a $Fe(CO)_4$ complex.

In future work, it will be of great interest to proof the proposed mechanism (**I**, Scheme 66) by an alternative approach (**II**, Scheme 66) in which a heterolyl dianion is treated with a dichlorosilane. Both reactions would most likely lead to a fulvene structure which rearranges to the tetrylene. The advantage of the alternative approach is that, besides potassium chloride, no further side products occur. Additionally, the introduction of different substituents would be possible which may facilitate the crystallisation of single crystals suitable for X-ray diffraction analysis.

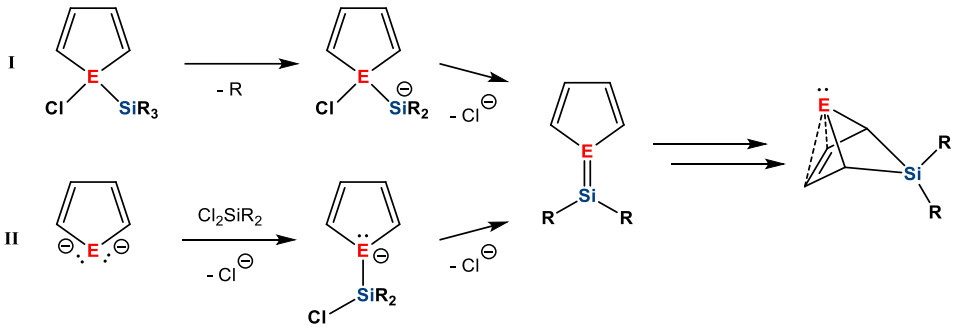

Scheme 66: Comparison of the proposed mechanism for the rearrangement reaction of the formation of the new type of tetrylenes (**I**) and an alternative approach (**II**).

The here presented type of tetrylene is unprecedented and it will therefore be of great interest to further investigate their reactivity in bond activation and their potential in coordination chemistry. Additionally, the delicate difference between the stable tetrylene and its cycloreversion reaction to the respective heterole and the group 14 element may open a new field of application.

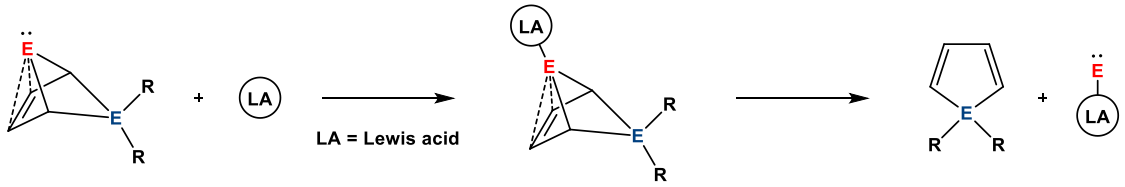

Scheme 67: Potential reactivity and application of this new type of tetrylene.

In combination with the already observed nucleophilicity of these tetrylenes, coordination to a substrate (**S**) with subsequent cycloreversion reaction may allow the selective deployment of or layering with group 14 elements which could be exploited for the synthesis of unprecedented functionalities and for material design (Scheme 67).

5 Experimental

5.1 General Preparative Procedures

Due to the sensitivity of the compounds all reactions were carried out under inert atmosphere using Schlenk techniques or a standard *mBraun Unilab* glove box. The glassware was stored in an oven at 120 °C and evacuated several times prior to use. Commercially available argon 5.0 or nitrogen 5.0 was used as the inert gas.

The solvents diethyl ether (Et_2O), tetrahydrofuran (THF), pentane, hexane, benzene and toluene were dried over alkali metals or alloys and freshly distilled before use or stored over molecular sieves (4 Å). Chloroform was also stored over molecular sieves (4 Å) after drying over $CaCl_2$. Methanol was dried over magnesium and stored over molecular sieves (3 Å) after distillation. All other chemicals were commercially available or prepared according to known literature procedures (see Chapter 5.2).

All NMR data were recorded on a *Bruker Avance 500* or a *Bruker Avance III 500*. ^{1}H NMR spectra were calibrated with the residual proton signal of the solvent as an internal reference. For ^{13}C NMR the central carbon signal of the respective solvent was used as reference (Table 19).

Table 19: References for ^{1}H und ^{13}C NMR spectra.

	Solvent	δ [ppm]
^{1}H NMR	C_6D_6	7.20 (C_6D_5H)
	$CDCl_3$	7.24 ($CHCl_3$)
^{13}C NMR	C_6D_6	128.0
	$CDCl_3$	77.0

^{29}Si NMR spectra were calibrated with Me_2SiHCl ($\delta^{29}Si$ = 11.1) as an external standard versus $SiMe_4$ ($\delta^{29}Si$ = 0.0). If not otherwise stated, the $^{29}Si\{^{1}H\}$ NMR inverse gated spectra were recorded with a relaxation delay D1 = 10 s. For $^{29}Si\{^{1}H\}$ NMR INEPT spectra the delays D3 = 0.0068 s and D4 = 0.0313 s, which perform well in detecting $SiMe_3$ groups, were used. Spectrometer frequencies and temperatures for each NMR experiment are indicated in the experimental part.

To interpret the spectra of known compounds, the respective literature was used. For unknown compounds DEPT135 NMR and 2D NMR spectra such as $^{1}H^{1}H$ COSY, $^{1}H^{13}C$ HMQC, $^{1}H^{13}C$ HMBC, $^{1}H^{29}Si$ HMQC or $^{1}H^{29}Si$ HMBC were measured to assign the signals.

EPR experiments were performed on a *Magnettech MiniScope MS 300 Bench-Top Spectrometer* with *H03 Temperature Controller* and a *Hamamatsu Lightningcure LC8 UV* radiation source (mercury-vapour lamp L10852, 240 nm to 400 nm, 250 nm band enhanced type). For the determination of *g*-factors an external *Hewlett Packard Frequency Counter 53181A* was used. IR measurements were recorded on a *Bruker Tensor 27 ATR* and X-ray fluorescence spectra (XRF) were measured on a *PANalytical Axios mAX* spectrometer.

GC/MS spectra were determined on a *Focus-GC* with a *DSQ mass spectrometer* (EI, 70 eV) by *Thermo.* As stationary phase, a column type DB-5 /25 m, 0.2 mm) was used. Mass spectra and high resolution mass spectra were recorded on a *Finnigan-Mat 95* or on a *DFS Thermo scientific* mass spectrometer.

Single crystal X-ray analyses were performed on a *Bruker Apex 2* with Mo Kα-radiation. For solving and refining the molecular structures, *SHELXL-97* was used and for the visualisation *Crystal Impact Diamond 4.2*.

Combustion analyses (C, H, N, S) were obtained on an *Euro EA Element Analyzer* with *EuroVector* equipment. The measured values are often inaccurate due to the formation and incomplete combustion of silicon or germanium carbide, even though vanadium peroxide was used to aid the combustion.

5.2 Starting Materials

Trimethylsilylpropyne and tert-butyldimethylsilylpropyne were synthesised according to the literature procedures.[76,77,166-168] Germanium tetrachloride,[169] germanium tetrabromide,[170] tetrakis(trimethylsilyl)silane,[171] and tetrakis(trimethylsilyl)germane[171] were prepared in the student laboratory. The potassium salts of tris(trimethylsilyl)silyl[88] and tris(trimethylsilyl)-germyl[172] anions were synthesised by the procedures of Marschner et al. Potassium graphite was prepared by heating eight equivalents of vacuum dried graphite with one equivalent of potassium to 120 °C until completion of the intercalation. 1,2,3,4,5-pentaphenylsilacyclopentadiene and 1-phenyl-2,5-bis(triisopropylsilyl)silacyclopentadiene were available in the laboratory from previous work.

5.2.1 Synthesis of Germoles

1,1-Dichloro-3,4-dimethyl-2,5-bis(trimethylsilyl)germacyclopentadiene **39**[81]

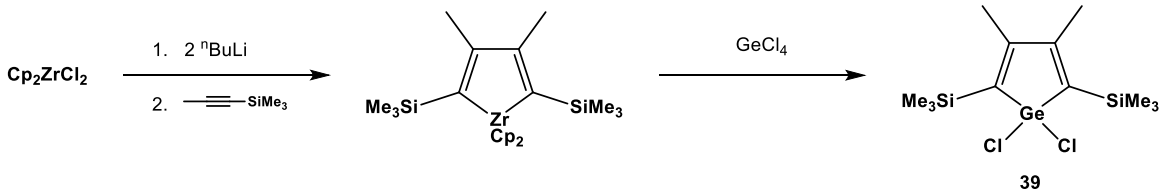

To 3.00 g (10.26 mmol) Cp_2ZrCl_2 suspended in 80 mL pentane at -90 °C, were slowly added 13.47 mL of ^{n}BuLi (21.55 mmol, 1.6 M in hexanes). After 1 h of stirring at that temperature, a solution of 2.42 g (21.55 mmol) trimethylsilylpropyne in 5 mL pentane was added dropwise and the reaction mixture was stirred for 16 h while warming to room temperature. The colour of the solution changed from pale yellow to red brown during this time. Subsequently, 10 mL of THF were added to the flask which was cooled to -10 °C before a solution of 2.20 g (10.26 mmol) of freshly condensed $GeCl_4$ in 5 mL pentane was added. The mixture was stirred and the solution was allowed to warm to room temperature. The colour of the solution changed from red brown to green, turquoise, blue and finally back to a pale yellow and a colourless solid precipitated (approx. 18 h). After filtration, 20 mL of water were added to the solution and stirred for 10 min. The phases were separated and the organic layer dried over $MgSO_4$, filtered and the solvent evaporated. The pale yellow residue was washed with ice cold EtOH. After evaporation of the residual solvent, 2.99 g (8.12 mmol, 79.2%) of the dichlorogermole **39** were obtained as colourless crystals. Even though an aqueous workup is possible, it is highly recommended to store the product under an inert atmosphere.

$C_{12}H_{24}Cl_2GeSi_2$ M = 368.04 g mol^{-1}

^{1}H NMR (499.9 MHz, 305.9 K, C_6D_6): δ = 0.35 (s, 18H, Si(C$\underline{H}_3$)$_3$), 1.68 (s, 6H, C$\underline{H}_3$).

^{13}C{^{1}H} NMR (125.7 MHz, 305.0 K, C_6D_6): δ = 0.1 (Si(C$\underline{H}_3$)$_3$), 19.4 (C(C$\underline{H}_3$)), 132.8 (C$\underline{C}$Si(CH$_3$)$_3$), 160.9 (C$\underline{C}$CH$_3$).

^{29}Si{^{1}H} NMR (99.3 MHz, 305.0 K, C_6D_6): δ = -7.7 ($\underline{Si}$(CH$_3$)$_3$).

MS (70 eV, EI): *m/z* (%) = 368 (<1) [M$^+$], 353 (2), 244 (6), 229 (10), 224 (19), 221 (8), 209 (21), 113 (12), 97 (100), 93 (11), 83 (9), 73 (58), 69 (14).

1,1-Dibromo-3,4-dimethyl-2,5-bis(trimethylsilyl)germacyclopentadiene **40**

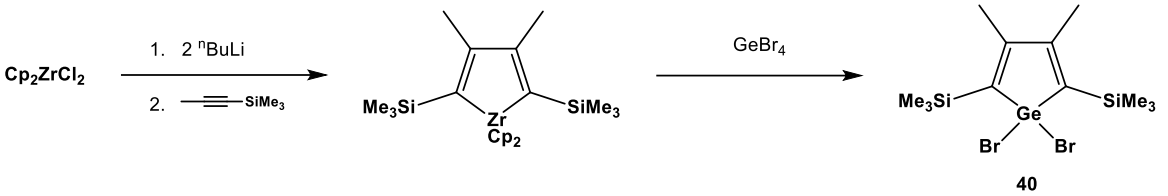

40

To 3.00 g (10.26 mmol) Cp_2ZrCl_2 suspended in 100 mL hexane at -90 °C, were slowly added 12.83 mL of ^{n}BuLi (20.53 mmol, 1.6 M in hexanes). After 1 h of stirring at that temperature, a solution of 3.04 mL (20.53 mmol) trimethylsilylpropyne in 10 mL hexane was added dropwise and the reaction mixture was stirred for 16 h while warming to room temperature. The colour of the solution changed from pale yellow to red brown during this time. Subsequently, the flask was cooled to -40 °C before a solution of 1.29 mL (10.26 mmol) of freshly condensed $GeBr_4$ in 10 mL hexane was added. The mixture was stirred and the solution was allowed to warm to room temperature. The colour of the solution changed from red brown to green, turquoise, blue and finally back to a pale yellow and a colourless solid precipitated (approx. 18 h). After filtration, the solvent was removed under vacuum and the residue recrystallised from hexane at -24 °C to yield 3.68 g (8.06 mmol, 78.6%) of dibromogermole **40** as pale yellow crystals.

$C_{12}H_{24}Br_2GeSi_2$ M = 456.93 g mol^{-1}

^{1}H NMR (499.9 MHz, 305.0 K, C_6D_6): δ = 0.39 (s, 18H, Si(C$\underline{H}_3$)$_3$), 1.70 (s, 6H, C$\underline{H}_3$).

^{13}C{^{1}H} NMR (125.7 MHz, 305.0 K, C_6D_6): δ = 0.4 (Si(C$\underline{H}_3$)$_3$), 19.4 (C(C$\underline{H}_3$)), 134.6 (C$\underline{C}$Si(CH$_3$)$_3$), 159.3 ($\underline{C}$CH$_3$).

^{29}Si{^{1}H} NMR (99.3 MHz, 305.0 K, C_6D_6): δ = -7.4 ($\underline{Si}$(CH$_3$)$_3$).

MS (70 eV, EI): *m/z* (%) = 456 (<1) [M$^+$], 441 (1), 244 (28), 209 (22), 151 (5), 139 (5), 113 (9), 97 (100), 83 (10), 73 (60), 68 (14).

HR-MS (70eV, EI): *m/z* = calcd.: 455.8990 ($^{12}C_{12}{}^{1}H_{24}{}^{79}Br_2{}^{74}Ge^{28}Si_2$)
found: 455.8978 [M$^+$]

EA calcd./found: C: 31.54/31.95 H: 5.29/5.31

Details of the X-ray diffraction analysis are presented in the appendix (7.2 Crystallographic Data).

1,1-Dichloro-3,4-dimethyl-2,5-bis(tert-butyldimethylsilyl)germacyclopentadiene **41**

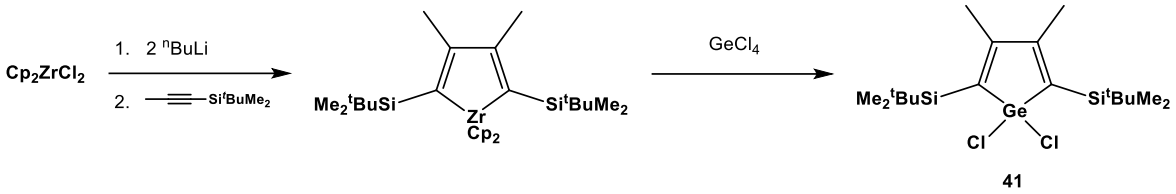

41

To 4.00 g (13.68 mmol) Cp_2ZrCl_2 suspended in 100 mL hexane at -90 °C, were slowly added 17.10 mL of ^{n}BuLi (27.37 mmol, 1.6 M in hexanes). After 1 h of stirring at that temperature, a solution of 5.49 mL (27.37 mmol) tert-butyldimethylsilylpropyne in 10 mL hexane was added dropwise and the reaction mixture was stirred for 16 h while warming to room temperature. The colour of the solution changed from pale yellow to red brown during this time. Subsequently the flask was cooled to -10 °C before a solution of 1.56 mL (13.68 mmol) of freshly condensed $GeCl_4$ in 10 mL hexane was added. The mixture was stirred and the solution allowed to warm to room temperature. The colour changed from red brown to green, turquoise, blue and finally back to a pale yellow and a colourless solid precipitated (approx. 18 h). After filtration, the solvent was removed under vacuum and the residue recrystallised from hexane at -24 °C to yield 1.13 g (2.50 mmol, 18.3%) of bis(tert-butyldimethylsilyl)dichlorogermole **41** as colourless crystals.

$C_{18}H_{36}Cl_2GeSi_2$ M = 452.19 g mol^{-1}

^{1}H NMR (499.9 MHz, 298.7 K, C_6D_6): δ = 0.40 (s, 12H, Si(C$\underline{H}_3$)$_2$), 1.00 (s, 18H, SiC(C$\underline{H}_3$)$_3$), 1.85 (s, 6H, C$\underline{H}_3$).

^{13}C{^{1}H} NMR (125.7 MHz, 299.1 K, C_6D_6): δ = -3.3 (Si(<u>C</u>H$_3$)$_2$), 19.0 (C(<u>C</u>H$_3$)), 21.3 (Si<u>C</u>(CH$_3$)$_3$), 27.5 (SiC(<u>C</u>H$_3$)$_3$), 132.0 (<u>C</u>Si^{t}BuMe$_2$), 161.7 (<u>C</u>Me).

^{29}Si{^{1}H} NMR (99.3 MHz, 299.0 K, C_6D_6): δ = 0.4 (<u>Si</u>^{t}BuMe$_2$).

MS (70 eV, EI): *m/z* (%) = 452 (<1) [M$^+$], 395 (2), 271 (19), 235 (3), 97 (100), 73 (54), 57 (41).

HR-MS (70eV, EI): *m/z* = calcd.: 452.0939 ($^{12}C_{18}{}^{1}H_{36}{}^{35}Cl_2{}^{74}Ge{}^{28}Si_2$)
found: 452.0921 [M$^+$]

EA calcd./found: C: 47.81/44.61 H: 8.03/7.66

1,1-Dibromo-3,4-dimethyl-2,5-bis(tert-butyldimethylsilyl)germacyclopentadiene **42**

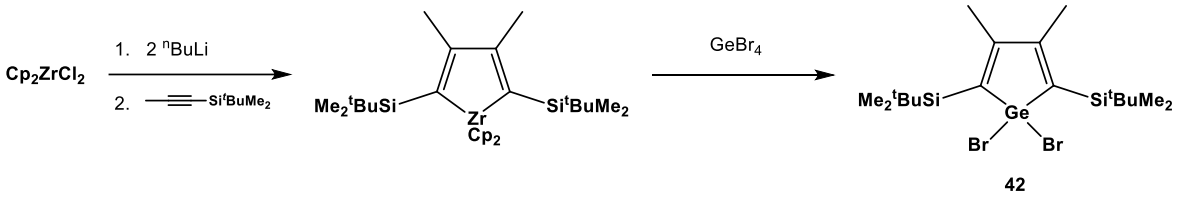

42

To 1.37 g (4.68 mmol) Cp_2ZrCl_2 suspended in 20 mL hexane at -80 °C, were slowly added 5.85 mL of ^{n}BuLi (9.36 mmol, 1.6 M in hexanes). After 1 h of stirring at that temperature, a solution of 1.45 g (9.36 mmol) tert-butyldimethylsilylpropyne in 5 mL hexane was added dropwise and the reaction mixture was stirred for 16 h while warming to room temperature. The colour of the solution changed from pale yellow to red brown. Subsequently, the flask was cooled to -10 °C before a solution of 1.84 g (4.68 mmol) freshly condensed $GeBr_4$ in 5 mL hexane was added. The mixture was stirred and the solution allowed to warm to room temperature. The colour of the solution changed from red brown to green, turquoise, blue and finally back to a pale yellow and a colourless solid precipitated (approx. 18 h). After filtration, the solvent was removed under vacuum and the residue recrystallised from hexane at -24 °C to yield 0.88 g (1.63 mmol, 34.7%) of bis(tert-butyldimethyl-silyl)dibromogermole **42** as pale yellow crystals.

$C_{18}H_{36}Br_2GeSi_2$ M = 541.09 g mol^{-1}

^{1}H NMR (499.9 MHz, 305.1 K, C_6D_6): δ = 0.46 (s, 12H, Si(C$\underline{H}_3$)$_2$), 1.01 (s, 18H, SiC(C$\underline{H}_3$)$_3$), 1.85 (s, 6H, C$\underline{H}_3$).

^{13}C{^{1}H} NMR (125.7 MHz, 305.0 K, C_6D_6): δ = -2.9 (Si(C$\underline{H}_3$)$_2$), 19.1 (C(C$\underline{H}_3$)), 21.2 (SiC(CH$_3$)$_3$), 27.8 (SiC(C$\underline{H}_3$)$_3$), 134.0 (C$\underline{C}$Si^{t}BuMe$_2$), 159.9 (C$\underline{C}$Me).

^{29}Si{^{1}H} NMR (99.3 MHz, 305.0 K, C_6D_6): δ = 0.7 ($\underline{Si}^{t}$BuMe$_2$).

MS (70 eV, EI): *m/z* (%) = 541 (<1) [M^{+}], 483 (2), 315 (24), 335 (6), 139 (11), 97 (100), 73 (42), 57 (19).

Details of the X-ray diffraction analysis are presented in the appendix (7.2 Crystallographic Data).

5.2.2 Functionalisation of Germoles

1-Bromo-1-tert-butyl-3,4-dimethyl-2,5-bis(trimethylsilyl)germacyclopentadiene **43**

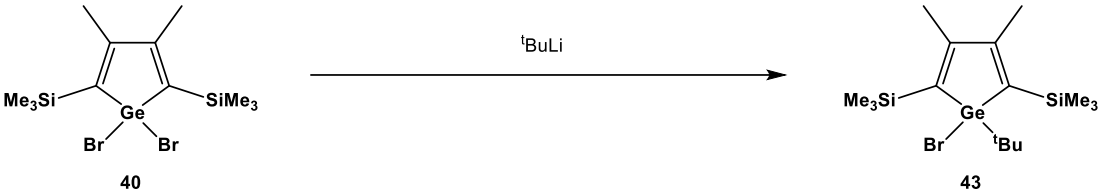

To 0.45 g (0.99 mmol) dibromogermole **40** dissolved in 4 mL of hexane at -90 °C, were added 0.62 mL of ^{t}BuLi (0.99 mmol, 1.6 M in pentane). The reaction mixture was stirred for 17 h while warming to room temperature. The solvent was then removed under vacuum and hexane was added. The salts were removed by filtration and the solvent removed again. The residue was vacuum transferred ($2 \cdot 10^{-2}$ mbar, 180 °C) to yield 0.13 g (0.30 mmol, 30.5%) of tert-butylbromo-germole **43** as a colourless solid.

$C_{16}H_{33}BrGeSi_2$ M = 434.14 g mol^{-1}

^{1}H NMR (499.9 MHz, 305.0 K, C_6D_6): δ = 0.37 (s, 18H, Si(C$\underline{H}_3$)$_3$), 1.24 (s, 9H, GeC(C$\underline{H}_3$)$_3$), 1.91 (s, 6H, C$\underline{H}_3$).

^{13}C{^{1}H} NMR (125.7 MHz, 305.0 K, C_6D_6): δ = 1.3 (Si(C$\underline{H}_3$)$_3$), 20.7 (C$\underline{H}_3$), 28.9 (C(C$\underline{H}_3$)$_3$), 30.1 (C(CH$_3$)$_3$) 137.2 (C$\underline{C}$SiMe$_3$), 163.2 (C$\underline{C}$Me).

^{29}Si{^{1}H} NMR (99.3 MHz, 305.0 K, C_6D_6): δ = -8.8 ($\underline{Si}$Me$_3$).

MS (70 eV, EI): *m/z* (%) = 434 (4) [M^{+}], 377 (24), 265 (11), 195 (12), 155 (10), 113 (18), 97 (100), 73 (98), 57 (91).

HR-MS (70eV, EI): *m/z* = calcd.: 434.0516 ($^{12}C_{16}{}^{1}H_{33}{}^{79}Br^{74}Ge^{28}Si_2$)
found: 434.0501 [M^{+}]

1-Chloro-1-pentamethylphenyl-3,4-dimethyl-2,5-bis(trimethylsilyl)germacyclopenta-diene **45**

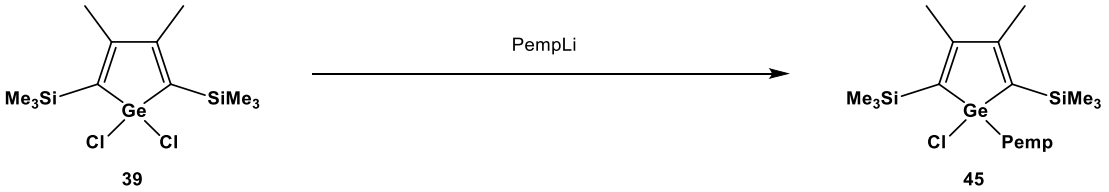

To of 0.34 g (1.49 mmol) of PempBr in 10 mL of Et_2O at -80 °C, were added 1.57 mL of ^{t}BuLi (2.99 mmol, 1.9 M in pentane). The reaction mixture was stirred for 1 h while warming to -30 °C. To 0.50 g (1.36 mmol) of dichlorogermole **39** were added 10 mL Et_2O. Both flasks were cooled to -80 °C and the PempLi solution was transferred to the germole solution. The reaction mixture was stirred for 17 h while warming to room temperature. The solvent was then removed under vacuum and hexane was added. The salts were removed by filtration and the filtrate was concentrated under vacuum. The 1-pentamethylphenyl germole **45** crystallised from hexane at -24 °C as a colourless solid (0.31 g, 0.65 mmol, 47.9%).

$C_{23}H_{39}ClGeSi_2$ M = 479.82 g mol^{-1}

^{1}H NMR (499.9 MHz, 305.1 K, C_6D_6): δ = 0.30 (s, 18H, Si(C$\underline{H}_3$)$_3$), 1.97 (s, 6H, C$\underline{H}_3$), 2.01 (s, 3H, *p*-C$\underline{H}_3$), 2.01 (s, 6H, *m*-C$\underline{H}_3$), 2.59 (s br, 6H, *o*-C$\underline{H}_3$).

^{13}C{^{1}H} NMR (125.7 MHz, 305.0 K, C_6D_6): δ = 0.6 (Si($\underline{C}H_3$)$_3$), 16.6 (*m*-$\underline{C}H_3$), 16.9 (*p*-$\underline{C}H_3$), 20.3 (C$\underline{C}H_3$), 21.1 (br, *o*-$\underline{C}H_3$), 133.3 (Ar), 133.7 (Ar), 137.2 (Ar), 138.8 (br, Ar) 142.7 ($\underline{C}SiMe_3$), 159.9 ($\underline{C}$Me).

^{29}Si{^{1}H} NMR (99.3 MHz, 305.0 K, C_6D_6): δ = -8.6 ($\underline{Si}Me_3$).

MS (70 eV, EI): *m/z* (%) = 480 (<1) [M$^+$], 372 (2), 357 (3), 283 (11), 268 (8), 219 (5), 189 (5), 147 (8), 133 (15), 105 (6), 97 (30), 92 (11), 73 (100), 59 (8).

HR-MS (70eV, EI): *m/z* = calcd.: 480.1485 ($^{12}C_{23}{}^{1}H_{39}{}^{35}Cl^{74}Ge^{28}Si_2$)
found: 480.1477 [M$^+$]

EA calcd./found: C: 57.57/57.98 H: 8.19/8.26

1-Chloro-1-tris(trimethylsilyl)silyl-3,4-dimethyl-2,5-bis(trimethylsilyl)germacyclopenta-diene **46**

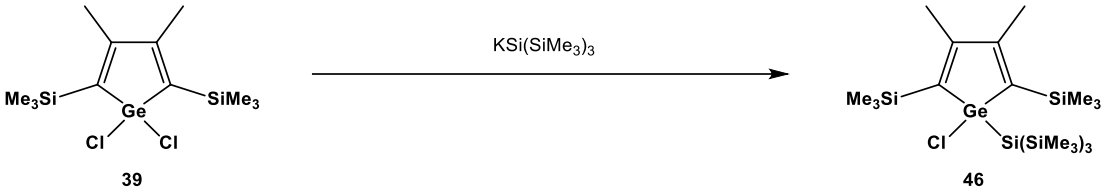

39 **46**

To 1.34 g (3.65 mmol) of dichlorogermole **39** in 3 mL THF at -80 °C, was slowly added a solution of 1.27 g (3.65 mmol) of freshly prepared $KSi(SiMe_3)_3$ dissolved in 7 mL THF. The reaction mixture was stirred for 18 h while warming to room temperature. After removal of the solvents under vacuum, hexane was added and the resulting suspension was filtered. The filtrate was reduced under vacuum and the residue stored at -24 °C. After removal of the solvent, 1.33 g (2.29 mmol, 63.9%) of the silyl substituted germole **46** were isolated as colourless crystals.

$C_{21}H_{51}ClGeSi_6$ M = 580.23 g mol^{-1}

^{1}H NMR (499.9 MHz, 305.0 K, C_6D_6): δ = 0.40 (s, 27H, $Si(Si(C\underline{H}_3)_3)_3$), 0.45 (s, 18H, $Si(C\underline{H}_3)$), 2.01 (s, 6H, $C\underline{H}_3$).

$^{13}C\{^1H\}$ NMR (125.7 MHz, 305.0 K, C_6D_6): δ = 2.1 ($Si(\underline{C}H_3)_3$), 3.6 ($SiSi(\underline{C}H_3)_3$), 21.2 ($\underline{C}H_3$), 150.5 ($\underline{C}SiMe_3$), 160.6 ($\underline{C}Me$).

$^{29}Si\{^1H\}$ NMR (99.3 MHz, 305.0 K, C_6D_6): δ = -109.0 ($\underline{Si}SiMe_3$), -9.0 ($C\underline{Si}Me_3$), -8.3 ($Si\underline{Si}Me_3$).

MS (70 eV, EI): *m/z* (%) = 580 (<1) [M$^+$], 399 (4), 341 (3), 325 (4), 298 (4), 281 (7), 186 (11), 173 (18), 131 (13), 97 (13), 73 (100) C_3H_9Si.

HR-MS (70eV, EI): *m/z* = calcd.: 580.1501 ($^{12}C_{21}{}^1H_{51}{}^{35}Cl^{74}Ge^{28}Si_6$)
found: 580.1499 [M$^+$]

EA calcd./found: C: 43.47/43.46 H: 8.86/9.06

Details of the X-ray diffraction analysis are presented in the appendix (7.2 Crystallographic Data).

1-Chloro-1-tris(trimethylsilyl)silyl-3,4-dimethyl-2,5-bis(tert-butyldimethylsilyl)germacyclo-pentadiene **48**

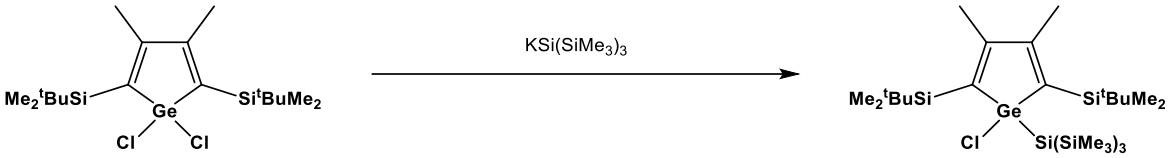

41 48

To 1.00 g (2.21 mmol) of bis(tert-butyldimethylsilyl)dichlorogermole **41** in 6 mL THF at -80 °C, were slowly added 6.37 mL of freshly prepared $KSi(SiMe_3)_3$ (2.21 mmol, 0.35 M in THF). The reaction mixture was stirred for 18 h while warming to room temperature. After removal of the solvents under vacuum, hexane was added and the resulting suspension was filtered. The filtrate was reduced under vacuum and the residue stored at -24 °C. Two fractions crystallised. The first (0.76 g) contained 63% starting material **41** and 37% germole **48** as determined by ^{1}H NMR spectroscopy. The second fraction contained 0.12 g (0.18 mmol, 8.2%) of the silyl substituted bis(tert-butyldi-methylsilyl)germole **48** as colourless crystals.

$C_{27}H_{63}ClGeSi_6$ M = 664.39 g mol^{-1}

^{1}H NMR (500.1 MHz, 298. K, C_6D_6): δ = 0.39 (s, 27H, $Si(Si(C\underline{H}_3)_3)_3$), 0.43 (s, 6H, $Si(C\underline{H}_3)_2$), 0.62 (s, 6H, $Si(C\underline{H}_3)_2$), 1.04 (s, 18H, $C(C\underline{H}_3)_3$), 2.07 (s, 6H, $C\underline{H}_3$).

^{13}C{^{1}H} NMR (125.8 MHz, 298.7 K, C_6D_6): δ = -1.9 ($Si^tBu(\underline{C}H_3)_2$), -0.6 ($Si^tBu(\underline{C}H_3)_2$), 3.7 ($SiSi(\underline{C}H_3)_3$), 20.6 ($C(\underline{C}H_3)_3$), 22.7 ($\underline{C}CH_3$), 27.9 ($C(\underline{C}H_3)_3$), 154.3 ($\underline{C}Si^tBuMe_2$), 158.9 ($\underline{C}Me$).

^{29}Si{^{1}H} NMR (99.7 MHz, 298.4 K, C_6D_6): δ = -106.4 ($\underline{Si}SiMe_3$), -8.1 ($Si\underline{Si}Me_3$), -2.8 ($\underline{Si}^tBuMe_2$).

MS (70 eV, EI): *m/z* (%) = 664 (<1) [M^+], 608 (<1), 383 (2), 207 (5), 189 (4), 173 (14), 157 (6), 131 (12), 115 (7), 97 (11), 73 (100) C_3H_9Si, 57 (7).

HR-MS (70eV, EI): *m/z* = calcd.: 664.2440 ($^{12}C_{27}{}^1H_{63}{}^{35}Cl^{74}Ge^{28}Si_6$)
found: 664.2445 [M^+]

EA calcd./found: C: 48.81/47.21 H: 9.56/9.15

Details of the X-ray diffraction analysis are presented in the appendix (7.2 Crystallographic Data).

1-Chloro-1-tris(trimethylsilyl)germyl-3,4-dimethyl-2,5-bis(trimethylsilyl)germacyclopenta-diene **47**

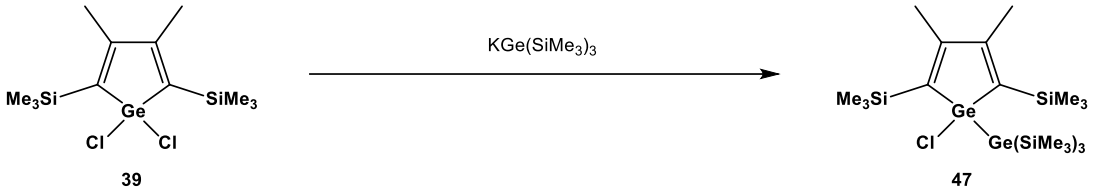

39 **47**

To 0.63 g (1.72 mmol) of dichlorogermole **39** in 5 mL THF at -80 °C, was slowly added a solution of 0.63 g (1.89 mmol) of freshly prepared $KGe(SiMe_3)_3$ dissolved in 4 mL THF. The reaction mixture was stirred for 18 h while warming to room temperature and changing colour from pale yellow to dark red. After removal of the solvents under vacuum, pentane was added and the resulting suspension was filtered. The solvent was removed and the residue recrystallised from pentane at -24 °C to yield 0.15 g (0.24 mmol, 14.2%) of the silyl substituted germole **47** as colourless crystals.

$C_{21}H_{51}ClGe_2Si_5$ M = 624.77 g mol^{-1}

^{1}H NMR (499.9 MHz, 305.0 K, C_6D_6): δ = 0.43 (s, 27H, Ge(Si(C$\underline{H}_3$)$_3$)$_3$), 0.45 (s, 18H, CSi(C$\underline{H}_3$)), 2.02 (s, 6H, CC$\underline{H}_3$).

^{13}C{^{1}H} NMR (125.8 MHz, 298.4 K, C_6D_6): δ = 2.1 (Si($\underline{C}$H$_3$)$_3$), 4.2 (GeSi($\underline{C}$H$_3$)$_3$), 21.3 (C$\underline{C}$H$_3$), 132.0 ($\underline{C}$SiMe$_3$), 161.7 ($\underline{C}$Me).

^{29}Si{^{1}H} NMR (99.3 MHz, 305.0 K, C_6D_6): δ = -2.4 (Ge$\underline{Si}$Me$_3$), -9.1 (C$\underline{Si}$Me$_3$).

MS (70 eV, EI): *m/z* (%) = 624 (<1) [M$^+$], 293 (7), 219 (7), 186 (5), 169 (4), 145 (10), 131 (14), 129 (8), 115 (4), 97 (10), 73 (100) C_3H_9Si, 59 (5).

HR-MS (70eV, EI): *m/z* = calcd.: 626.0944 ($^{12}C_{21}{}^1H_{51}{}^{35}Cl^{74}Ge_2{}^{28}Si_5$)
found: 626.0950 [M$^+$]

EA calcd./found: C: 40.37/40.43 H: 8.23/8.18

Details of the X-ray diffraction analysis are presented in the appendix (7.2 Crystallographic Data).

5.2.3 Synthesis of Siloles

1,1-Dichloro-3,4-diphenyl-2,5-bis(trimethylsilyl)silacyclopentadiene **54**[78,82,83,85]

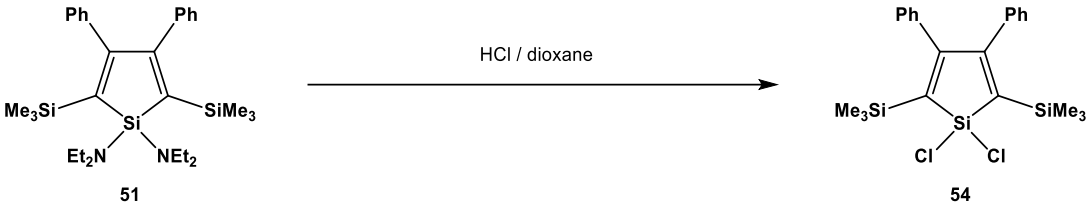

51 54

To 6.85 g (13.14 mmol) of diamino silole **51** dissolved in 100 mL diethyl ether at -80 °C, was slowly added a solution of 13.80 mL of HCl (55.21 mmol, 4 M in dioxane) dissolved in 30 mL diethyl ether. The reaction mixture was stirred for 18 h while warming to room temperature and a colourless solid precipitated. After removal of the solvents under vacuum, hexane was added and the resulting suspension filtered. The solvents were removed and the residue purified by vacuum transfer ($1 \cdot 10^{-3}$ mbar, 150 °C) to yield 3.91 g (8.73 mmol, 66.4%) of dichlorosilole **54** as a colourless solid.

$C_{22}H_{28}Cl_2Si_3$ M = 447.62 g mol^{-1}

^{1}H NMR (499.9 MHz, T = 305.1 K, C_6D_6): δ = 0.16 (s, 18H, Si(C$\underline{H}_3$)$_3$), 6.74 – 6.77 (m, 4H, $C_6\underline{H}_5$), 6.81 – 6.85 (m, 6H, $C_6\underline{H}_5$).

^{13}C{^{1}H} NMR (125.7 MHz, T = 305.0 K, C_6D_6): δ = 0.4 (Si$\underline{C}H_3$), 127.3 ($\underline{C}_6H_5$), 127.5 ($\underline{C}_6H_5$), 128.4 ($\underline{C}_6H_5$), 136.5 ($\underline{C}SiMe_3$), 140.5 (*i*-$\underline{C}_6H_5$), 170.2 ($\underline{C}C_6H_5$).

^{29}Si{^{1}H} NMR (99.3 MHz, T = 305.0 K, C_6D_6): δ = -8.0 ($\underline{Si}Me_3$), 19.2 ($\underline{Si}Cl_2$).

MS (70 eV, EI): *m/z* (%) = 446 (2) [M^+], 431 (5), 410 (33), 395 (27), 353 (6), 323 (4), 301 (2), 265 (6), 245 (10), 217 (5), 183 (7), 159 (87), 135 (10), 129 (29), 105 (10), 93 (10), 73 (100) C_3H_9Si, 63 (7).

NMR shifts and multiplicity are consistent to those presented in the literature.[82]

1,1-Dichloro-3,4-diphenyl-2,5-bis(triethylsilyl)silacyclopentadiene **55**[83,86,87]

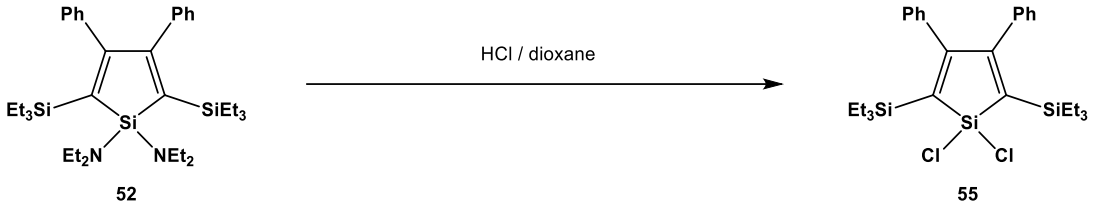

52 55

To 5.13 g (8.48 mmol) of diamino silole **52** dissolved in 250 mL diethyl ether at -80 °C, was slowly added a solution of 8.48 mL of HCl (33.91 mmol, 4 M in dioxane). The reaction mixture was stirred for 20 min before the cooling was removed. After stirring for 10 min at room temperature the solvents were removed under vacuum. Subsequently, hexane was added and the resulting suspension filtered. The filtrate was concentrated under vacuum and 2.04 g (3.84 mmol, 45.3%) of dichlorosilole **55** crystallised at -24 °C as a colourless solid.

$C_{28}H_{40}Cl_2Si_3$ M = 531.78 g mol^{-1}

^{1}H NMR (499.9 MHz, T = 305.1 K, C_6D_6): δ = 0.68 (q, $^{3}J_{H,H}$ = 7.9 Hz, 12H, SiC$\underline{H}_2$CH$_3$), 1.02 (t, $^{3}J_{H,H}$ = 7.9 Hz, 18H, SiCH$_2$C$\underline{H}_3$), 6.79 – 6.88 (m, 10H, C$_6\underline{H}_5$).

^{13}C{^{1}H} NMR (125.7 MHz, T = 305.0 K, C_6D_6): δ = 4.5 (Si$\underline{C}$H$_2$CH$_3$), 7.8 (SiCH$_2\underline{C}$H$_3$), 127.3 ($\underline{C}_6$H$_5$), 127.4 ($\underline{C}_6$H$_5$), 128.3 ($\underline{C}_6$H$_5$), 134.9 ($\underline{C}$SiEt$_3$), 140.7 (*i*-$\underline{C}_6$H$_5$), 170.7 ($\underline{C}C_6$H$_5$).

^{29}Si{^{1}H} NMR (99.3 MHz, T = 305.0 K, C_6D_6): δ = 0.3 ($\underline{Si}$Et$_3$), 19.0 ($\underline{Si}$Cl$_2$).

HR-MS (70eV, EI): *m/z* = calcd.: 530.1809 ($^{12}C_{28}{}^{1}H_{40}{}^{35}Cl_2{}^{28}Si_3$)
found: 530.1815 [M$^+$]

EA calcd./found: C: 63.24/61.40 H: 7.58/7.90

5.2.4 Functionalisation of Siloles

1-Chloro-1-tris(trimethylsilyl)silyl-3,4-diphenyl-2,5-bis(trimethylsilyl)silacyclopenta-diene **56**

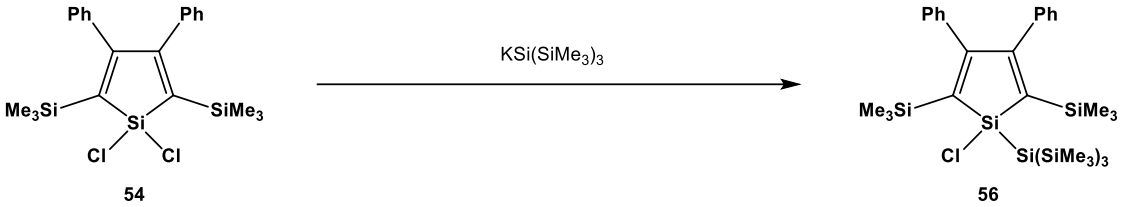

54 56

To 2.01 g (4.49 mmol) of dichlorosilole **54** in 20 mL THF at -80 °C, were slowly added 7.40 mL (4.93 mmol, 0.67 M in THF) of freshly prepared $KSi(SiMe_3)_3$. The reaction mixture was stirred for 18 h while warming to room temperature. After removal of the solvents under vacuum, hexane was added and the resulting suspension filtered. The filtrate was concentrated under vacuum and 2.02 g (3.06 mmol, 68.1%) of the silyl substituted silole **56** crystallised at -24 °C as a yellow solid.

$C_{31}H_{55}ClSi_7$ M = 659.83 g mol^{-1}

^{1}H NMR (499.9 MHz, 305.0 K, C_6D_6): δ = 0.25 (s, 18H, Si($C\underline{H}_3$)$_3$), 0.52 (s, 27H, SiSi($C\underline{H}_3$)$_3$), 6.84 – 6.89 (m, 2H, *p*-$C_6\underline{H}_5$), 6.91 – 6.97 (m, 4H, *m*-$C_6\underline{H}_5$), 7.04 – 7.09 (m, 4H, *o*-$C_6\underline{H}_5$).

^{13}C{^{1}H} NMR (125.7 MHz, T = 305.0 K, C_6D_6): δ = 2.8 (Si($\underline{C}H_3$)$_3$), 4.3 (SiSi($\underline{C}H_3$)$_3$), 127.0 (*p*-C_6H_5), 127.4 (*m*-C_6H_5), 129.3 (br, *o*-C_6H_5), 141.8 (*i*-$\underline{C}_6H_5$), 151.2 ($\underline{C}SiMe_3$), 168.8 ($\underline{C}C_6H_5$).

^{29}Si{^{1}H} NMR (99.3 MHz, T = 305.0 K, C_6D_6): δ = -124.0 ($\underline{Si}(SiMe_3)_3$), -8.6 ($C\underline{Si}Me_3$), -8.4 (Si($\underline{Si}Me_3$)$_3$), 29.7 ($Cl\underline{Si}Si(SiMe_3)_3$).

HR-MS (70eV, EI): *m/z* = calcd.: 658.2372 ($^{12}C_{31}{}^1H_{55}{}^{35}Cl^{28}Si_7$)
found: 658.2364 [M$^+$]

EA calcd./found: C: 56.43/56.73 H: 8.40/8.85

Details of the X-ray diffraction analysis are presented in the appendix (7.2 Crystallographic Data).

1-Chloro-1-tris(triethylsilyl)silyl-3,4-diphenyl-2,5-bis(trimethylsilyl)silacyclopenta-diene **57**[86,87]

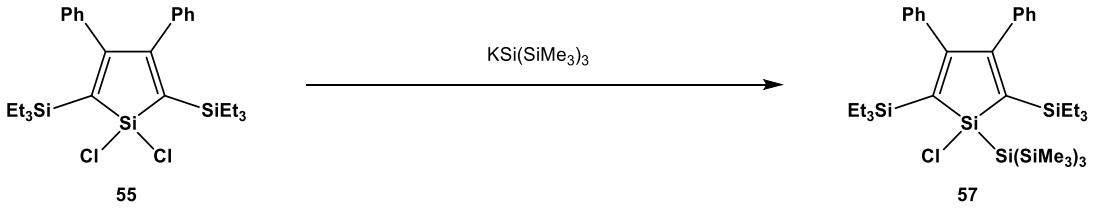

To 0.99 g (1.86 mmol) of dichlorosilole **55** in 10 mL THF at -80 °C, was slowly added a solution of 0.53 g (1.86 mmol) of freshly prepared $KSi(SiMe_3)_3$ dissolved in 10 mL THF. The reaction mixture was stirred for 3 d while warming to room temperature. After removal of the solvents under vacuum, hexane was added and the resulting suspension filtered. The filtrate was concentrated under vacuum and the residue purified by Kugelrohr distillation (T = 250 °C, p = $1 \cdot 10^{-2}$ mbar) to yield 0.71 g (0.95 mmol, 51.3%) of the silyl substituted silole **57** as a yellow solid.

$C_{37}H_{67}ClSi_7$ M = 743.99 g mol^{-1}

^{1}H NMR (499.9 MHz, 305.1 K, C_6D_6): δ = 0.52 (s, 27H, Si($C\underline{H}_3$)$_3$), 0.67 – 0.74 (m, 6H, Si$C\underline{H}_2CH_3$), 0.96 – 1.02 (m, 6H, Si$C\underline{H}_2CH_3$), 1.02 – 1.06 (m, 18H, Si$CH_2C\underline{H}_3$), 6.84 – 6.88 (m, 2H, *p*-$C_6\underline{H}_5$), 6.91 – 6.96 (m, 4 H, *m*- $C_6\underline{H}_5$), 7.06 – 7.10 (m, 4 H, *o*-$C_6\underline{H}_5$).

^{13}C{^{1}H} NMR (125.7 MHz, T = 305.0 K, C_6D_6): δ = 4.3 (Si($\underline{C}H_3$)$_3$), 6.9 (Si$\underline{C}H_2CH_3$), 8.4 (Si$CH_2\underline{C}H_3$), 127.0 (*p*-C_6H_5), 127.3 (*m*-C_6H_5), 128.3 (*o*-C_6H_5), 142.0 (*i*-$\underline{C}_6H_5$), 150.6 ($\underline{C}$SiEt$_3$), 168.5 ($\underline{C}C_6H_5$).

^{29}Si{^{1}H} NMR (99.3 MHz, T = 305.0 K, C_6D_6): δ = -122.7 ($\underline{Si}$(SiMe$_3$)$_3$), -8.2 (Si($\underline{Si}$Me$_3$)$_3$), -2.0 ($\underline{Si}$Et$_3$), 28.9 (Cl$\underline{Si}$Si(SiMe$_3$)$_3$).

HR-MS (LIFDI): *m/z* = calcd.: 742.3311 ($^{12}C_{37}{}^1H_{67}{}^{35}Cl^{28}Si_7$)
found: 742.3327 [M^+]

EA calcd./found: C: 59.73/60.28 H: 9.08/9.14

5.3 Reduction Reactions of Germoles and Siloles

3,3',4,4'-Tetramethyl-1,1'-di-tert-butyl-2,2',5,5'-tetrakis(trimethylsilyl)-1,1'-bisgermole **63**

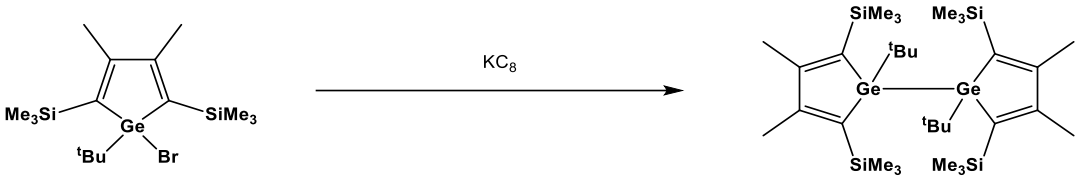

43 63

A solution of 0.13 g (0.30 mmol) of tert-butyl germole **43** dissolved in 4 mL THF was cooled to -90 °C and then 0.04 g (0.30 mmol) of KC_8 were added. The reaction mixture was stirred for 3.5 h while warming to 0 °C. After stirring for another 45 min after warming to room temperature, the solvents were removed. The residue was dissolved in hexane and filtered over silica gel. Subsequently, the solvents were removed under vacuum and 0.09 g (0.12 mmol, 82.3%) of the bisgermole **63** were obtained. Recrystallisation of **63** from hexane at room temperature yielded single crystals suitable for X-ray analysis.

$C_{32}H_{66}Ge_2Si_4$ M = 708.48 g mol^{-1}

^{1}H NMR (499.9 MHz, 305.1 K, THF capillary in C_6D_6): δ = 0.52 (s br, 36H, Si(C$\underline{H}_3$)$_3$), 1.50 (s, 18H, C(C$\underline{H}_3$)$_3$), 2.49 (s, 12H, CC$\underline{H}_3$).

^{13}C{^{1}H} NMR (125.7 MHz, 305.0 K, THF capillary in C_6D_6): δ = 2.8 (Si($\underline{C}$H$_3$)$_3$), 21.9 (C$\underline{C}$H$_3$), 28.9 ($\underline{C}$(CH$_3$)$_3$), 31.7 (C($\underline{C}$H$_3$)$_3$), 143.8 ($\underline{C}$SiMe$_3$), 163.5 ($\underline{C}$Me).

^{29}Si{^{1}H} NMR (99.3 MHz, 305.0 K, THF capillary in C_6D_6): δ = -10.0 (C$\underline{Si}$Me$_3$).

Details of the X-ray diffraction analysis are presented in the appendix (7.2 Crystallographic Data).

1-Tris(trimethylsilyl)silyl-3,4-dimethyl-2,5-bis(trimethylsilyl)germacyclopentadienyl radical **69**

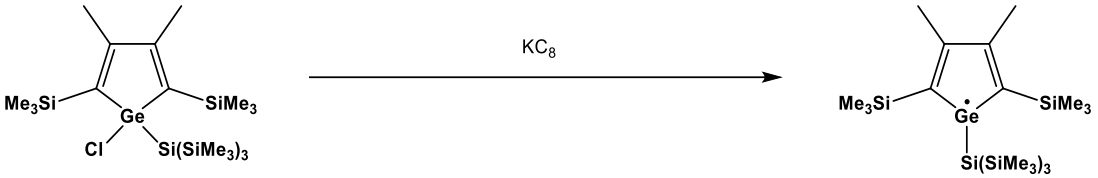

46 69

A solution of 0.15 g (0.26 mmol) of tris(trimethylsilyl)silyl germolyl chloride **46** in 2 mL THF was cooled to -30 °C and then 0.05 g (0.34 mmol) of KC_8 were added. The reaction mixture was stirred for 16 h while warming to room temperature. After removal of the solvents under vacuum the residue was suspended in hexane and filtered using a PTFE syringe filter. The resulting solution was used to record the EPR spectra of the 1-tris(trimethylsilyl)silyl germolyl radical **69**. Trapping reactions were also performed using a hexane or a benzene solution. 1,4-cyclohexadiene was added at room temperature and the reaction mixture was stirred for 30 min to give the 1-hydrogen substituted germole **75**.

$C_{21}H_{51}GeSi_6$ M = 544.78 g mol^{-1}

1-Tris(trimethylsilyl)silyl-3,4-dimethyl-2,5-bis(tert-butyldimethylsilyl)germacyclopenta-dienyl radical **76**

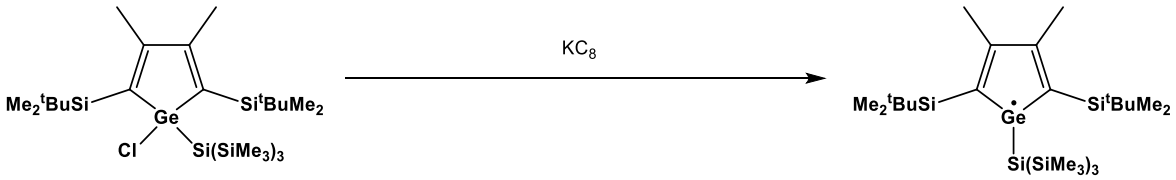

48 76

2 mL THF were condensed on a mixture of 0.08 g (0.12 mmol) chlorogermole **48** and 0.02 g (0.16 mmol) of KC_8 which were cooled by liquid nitrogen. An EtOH cooling bath was used to allow the reaction mixture to slowly warm from -100 °C to room temperature. Subsequently the solvent was removed under vacuum and 1 mL of heptane was added to the residue. After the settling of the graphite and precipitated potassium chloride the solution was used to record the EPR spectra of the 1-tris(trimethylsilyl)silylgermolyl radical **76**.

$C_{27}H_{63}GeSi_6$ M = 628.94 g mol^{-1}

1-Tris(trimethylsilyl)silyl-3,4-diphenyl-2,5-bis(trimethylsilyl)silacyclopentadienyl radical **78**

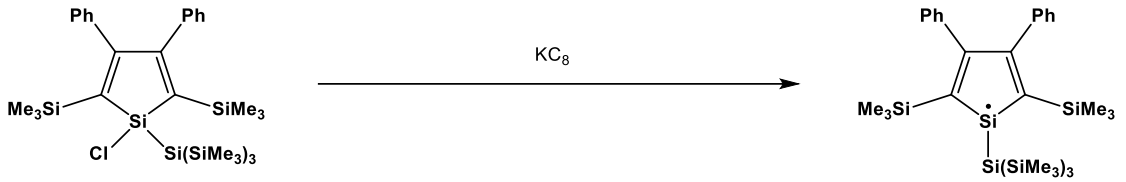

56 78

A solution of 0.15 g (0.23 mmol) of tris(trimethylsilyl)silyl silolyl chloride **56** dissolved in 2 mL THF was cooled to -30 °C and then 0.04 g (0.30 mmol) of KC_8 were added. The reaction mixture was stirred for 16 h while warming to room temperature. After removal of the solvents under vacuum the residue was suspended in hexane and filtered using a PTFE syringe filter. The resulting solution was used to record the EPR spectra of the 1-tris(trimethylsilyl)silyl silolyl radical **78**. Trapping reactions were also performed using a hexane or a benzene solution. 1,4-cyclohexadiene was added at room temperature and the reaction mixture was stirred for 30 min to give the 1-hydrogen substituted silole **82**.

$C_{31}H_{55}Si_7$ M = 624.38 g mol^{-1}

Potassium-1-tris(trimethylsilyl)silyl-3,4-dimethyl-2,5-bis(trimethylsilyl)germacyclopenta-dienyl anion **K[74]**

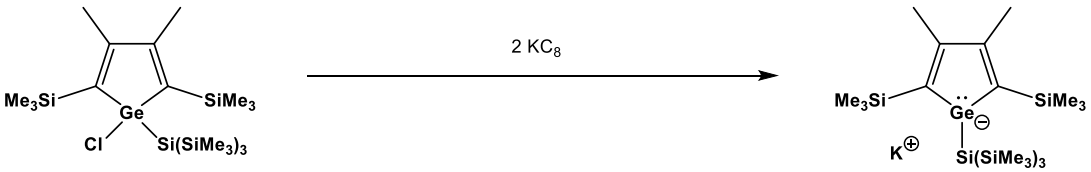

46 K[74]

A: In THF

To 0.15 g (0.26 mmol) of chlorogermole **46** dissolved in 3 mL THF at -30 °C, were added 0.07 g (0.53 mmol) of potassium graphite. The reaction mixture was stirred for 4 h while warming to room temperature. After concentrating the solution to 0.5 mL, 1.5 mL hexane were added and the resulting suspension was filtered using a PTFE syringe filter. Slow evaporation of the solvent at -30 °C yielded red crystals. After removal of the solvent, 0.07 g (0.13 mmol, 48.7%) of the silyl substituted germolyl anion salt **K[74]** were isolated.

B: In hexane

To 0.06 g (0.11 mmol) of chlorogermole **46** in 3 mL hexane at -24 °C, were added 0.01 g (0.11 mmol) of potassium graphite. The reaction mixture turned red after stirring for 3 d. Slow evaporation of the solvent at room temperature led to the formation of red crystals of the silyl substituted germolyl anion salt **K[74]** which were suitable for X-ray analysis.

$C_{21}H_{51}GeKSi_6$ M = 583.88 g mol^{-1}

^{1}H NMR (499.9 MHz, 304.9 K, C_6D_6/THF): δ = 0.50 (s, 27H, Si(Si(C$\underline{H}_3$)$_3$)$_3$), 0.54 (s, 18H, Si(C$\underline{H}_3$), 2.45 (s, 6H, C$\underline{H}_3$).

^{13}C{^{1}H} NMR (125.7 MHz, 305.0 K, C_6D_6/THF): δ = 4.3 (Si(C$\underline{H}_3$)$_3$), 4.9 (SiSi(C$\underline{H}_3$)$_3$), 23.6 (C$\underline{C}$H$_3$), 153.3 (C$\underline{C}$SiMe$_3$), 170.7 (C$\underline{C}$Me).

^{29}Si{^{1}H} NMR (99.3 MHz, 305.0 K, C_6D_6/THF): δ = -114.6 (Si(Si$\underline{Si}$Me$_3$)$_3$), -13.5 (C$\underline{Si}$Me$_3$), -9.0 (Si(Si$\underline{Si}$Me$_3$)$_3$).

Details of the X-ray diffraction analysis are presented in the appendix (7.2 Crystallographic Data).

Potassium-1-tris(trimethylsilyl)silyl-3,4-diphenyl-2,5-bis(triethylsilyl)silacyclopentadienyl anion **K[84]**

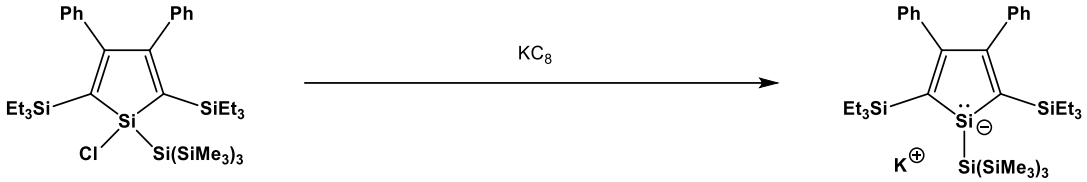

55 **K[84]**

3 mL THF were condensed on a mixture of 0.20 g (0.27 mmol) of chlorosilole **55** and 0.04 g (0.32 mmol) of KC_8 which were cooled by liquid nitrogen. An EtOH cooling bath was used to allow the reaction mixture to slowly warm from -90 °C to room temperature. The colour of the reaction mixture turned from pale yellow to dark red during this time. After removal of the solvents under vacuum the residue was suspended in hexane and filtered using a PTFE syringe filter. Slow evaporation of the solvent at room temperature yielded red crystals. After removal of the solvent, 0.03 g (0.04 mmol, 16.3%) of the silyl substituted silolyl anion salt **K[84]** were isolated.

$C_{37}H_{67}KSi_7$ M = 747.64 g mol^{-1}

^{1}H NMR (499.9 MHz, 305.1 K, C_6D_6): δ = 0.55 (s, 27H, Si(C$\underline{H}_3$)$_3$), 0.75 (q, $^3J_{H,H}$ = 7.8 Hz, 12H, SiC$\underline{H}_2$CH$_3$), 1.08 (t, $^3J_{H,H}$ = 7.8 Hz, 18H, SiCH$_2$C$\underline{H}_3$), 6.97 (d, $^3J_{H,H}$ = 7.3 Hz, 4H, o-C$_6$H$_5$), 7.00 – 7.05 (m, 2H, p-C$_6$H$_5$), 7.08 (t, $^3J_{H,H}$ = 7.3 Hz, 4H, m-C$_6$H$_5$).

$^{13}C\{^1H\}$ NMR (125.7 MHz, 305.0 K, C_6D_6): δ = 5.0 ($Si(\underline{C}H_3)_3$), 8.8 ($Si\underline{C}H_2CH_3$), 9.1 ($SiCH_2\underline{C}H_3$), 124.9 (*p*-$\underline{C}_6H_5$), 126.6 (*m*-C_6H_5), 130.5 ($\underline{C}SiEt_3$), 131.6 (*o*-$\underline{C}_6H_5$), 144.7 ($\underline{C}C_6H_5$), 147.2(*i*-C_6H_5).

$^{29}Si\{^1H\}$ NMR (99.3 MHz, 305.0 K, C_6D_6): δ = -119.1 ($\underline{Si}(Si(Me_3)_3)$, -9.8 ($Si(\underline{Si}(Me_3)_3)$, -3.1 ($\underline{Si}Et_3$), 31.8 ($\underline{Si}Si(SiMe_3)_3$).

Details of the X-ray diffraction analysis are presented in the appendix (7.2 Crystallographic Data).

5.4 Rearrangement Reactions

1,1,2,5-Tetrakis(trimethylsilyl)-3,4-dimethyl-silacyclopentadiene **100**

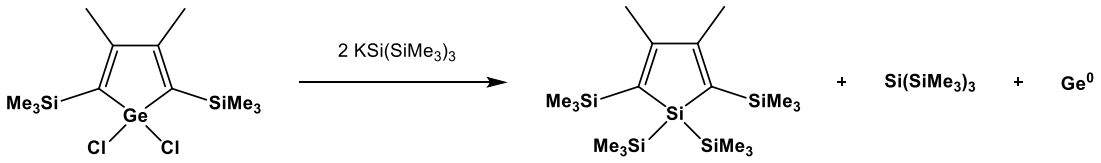

39 **100**

To 0.11 g (0.30 mmol) of dichlorogermole **39** in 8 mL THF at -90 °C, were added 2.65 mL (0.63 mmol, 0.24 M in THF) of freshly prepared $KSi(SiMe_3)_3$. The colour of the reaction mixture changed from pale yellow to dark red. After stirring for 18 h while warming to room temperature, the colour changed back to pale yellow and a black solid precipitated. The solvents were removed under vacuum and the residue dissolved in hexane. After filtration over silica gel, the solvents were removed, yielding 0.14 g of a colourless solid. NMR analysis showed that it contained 55% $Si(SiMe_3)_4$ and 45% silole **100** which were not separable. The calculated yields were 0.07 g (0.18 mmol, 59.1%) of silole **100** and 0.07 g (0.22 mmol, 72.2%) of $Si(SiMe_3)_4$.

Treatment of 1-tris(trimethylsilyl)silyl substituted germolyl chloride **46** with on equivalent of potassium tris(trimethylsilyl)silanide or potassium tert-butoxide under the same reaction conditions also gives silole **100** and elemental germanium.

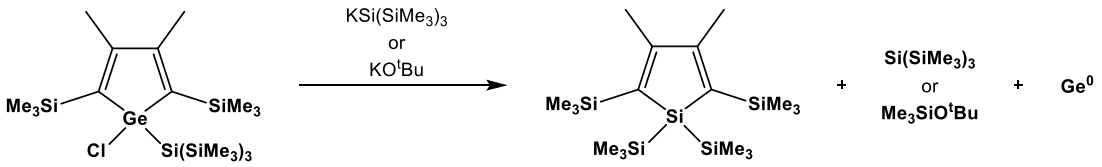

46 **100**

$C_{18}H_{24}Si_5$ M = 398.96 g mol^{-1}

^{1}H NMR (499.9 MHz, 305.1 K, C_6D_6): δ = 0.27 (s, 18H, Si(C$\underline{H}_3$)$_3$), 0.39 (s, 18H, Si(C$\underline{H}_3$)$_3$), 2.09 (s, 6H, C$\underline{H}_3$).

^{13}C{^{1}H} NMR (125.7 MHz, 305.0 K, C_6D_6): δ = 2.0 (SiSi(C$\underline{H}_3$)$_3$), 2.2 (CSi(C$\underline{H}_3$)$_3$), 21.7 (CC$\underline{H}_3$), 142.4 (C$\underline{C}$SiMe$_3$), 166.4 (C$\underline{C}$CH$_3$).

^{29}Si{^{1}H} NMR (99.3 MHz, 305.0 K, C_6D_6): δ = -17.1 ($\underline{Si}$SiMe$_3$), -15.2 (Si$\underline{Si}$Me$_3$), -11.3 (C$\underline{Si}$Me$_3$).

MS (70 eV, EI): *m/z* (%) = 398 (1) [M$^+$], 383 (1), 325 (14), 267 (3), 213 (4), 155 (10), 125 (9), 97 (12), 74 (9), 73 (100) C_3H_9Si, 72 (11), 59 (4).

HR-MS (70eV, EI): *m/z* = calcd.: 398.3125 ($^{12}C_{18}{}^{1}H_{42}{}^{28}Si_5$)
found: 398.2127 [M$^+$]

XRF of residue [wt%]: calcd.: 47% Ge, 27% K, 24% Cl
found: 32% Ge, 31% K, 29% Cl

NMR shifts and multiplicity are coherent to those of previous work where the silole **100** was synthesised by a different method.[121]

1,1-Dimethoxy-3,4-diphenyl-2,5-bis(trimethylsilyl)silacyclopent-3-ene **108**

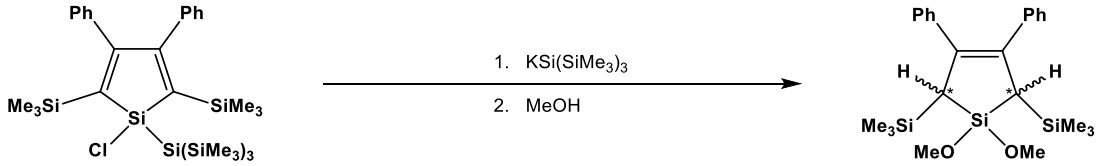

54 **108**

To 0.07 g (0.10 mmol) of the silyl substituted silole **54** dissolved in 3 mL THF at -90 °C, were added 0.65 mL (0.10 mmol, 0.16 M in hexane) of freshly prepared KSi(SiMe$_3$)$_3$. The reaction mixture was stirred for 1.5 h while warming to -20 °C. The colour of the solution changed from pale yellow to black-blue. After cooling the solution to -90 °C, 0.4 mL of MeOH were added and the colour changed to pale yellow. The solvents were removed at room temperature and the residue dissolved in hexane and filtered over silica gel. After removal of the solvents, 0.03 g (0.06 mmol, 59.4%) of dimethoxy silacyclopentene **108** were isolated as a *cis/trans* mixture. Slow evaporation of a hexane solution at -24 °C led to the formation of single crystals of the *trans* isomer suitable of X-ray analysis.

$C_{24}H_{36}O_2Si_3$ M = 440.81 g mol^{-1}

Confomer A:

^{1}H NMR (499.9 MHz, 304.9 K, C_6D_6): δ = 0.08 (s, 18H, Si(C<u>H</u>$_3$)$_3$), 1.74 (s, 1H, C<u>H</u>), 3.56 (s, 3H, SiOMe), 3.60 (s, 3H, SiOMe), 6.85 – 7.13 (m, C_6<u>H</u>$_5$, superposition of *cis* and *trans* isomer).

^{13}C{^{1}H} NMR (125.7 MHz, 305.0 K, C_6D_6): δ = 0.1 (Si(<u>C</u>H$_3$)$_3$), 27.2 (<u>C</u>HSiMe$_3$), 50.5 (SiO<u>C</u>H$_3$), 50.6 (SiO<u>C</u>H$_3$), 126.2 (<u>C</u>$_6$H$_5$), 127.6 (<u>C</u>$_6$H$_5$), 129.5 (<u>C</u>$_6$H$_5$), 143.0 (q-C), 143.3 (q-C).

^{29}Si{^{1}H} NMR (99.3 MHz, 305.0 K, C_6D_6): δ = 0.5 (<u>Si</u>Me$_3$), 7.8 (SiOMe).

MS (70 eV, EI): *m/z* (%) = 440 (<1) [M$^+$], 336 (4), 321 (8), 263 (3), 219 (13), 105 (7), 89 (12), 73 (100) C_3H_9Si, 59 (28).

Confomer B:

^{1}H NMR (499.9 MHz, 304.9 K, C_6D_6): δ = 0.05 (s, 18H, Si(C<u>H</u>$_3$)$_3$), 1.82 (s, 1H, C<u>H</u>), 3.51 (s, 3H, SiOMe), 3.56 (s, 3H, SiOMe), 6.85 – 7.13 (m, C_6<u>H</u>$_5$, superposition of *cis* and *trans* isomer).

^{13}C{^{1}H} NMR (125.7 MHz, 305.0 K, C_6D_6): δ = 0.0 (Si(<u>C</u>H$_3$)$_3$), 25.3 (<u>C</u>HSiMe$_3$), 50.8 (SiO<u>C</u>H$_3$), 126.1 (<u>C</u>$_6$H$_5$), 127.8 (<u>C</u>$_6$H$_5$), 129.9 (<u>C</u>$_6$H$_5$), 138.0 (q-C), 139.7 (q-C).

^{29}Si{^{1}H} NMR (99.3 MHz, 305.0 K, C_6D_6): δ = 1.1 (<u>Si</u>Me$_3$), 6.8 (SiOMe).

MS (70 eV, EI): *m/z* (%) = 440 (<1) [M$^+$], 336 (4), 321 (9), 219 (15), 105 (6), 89 (12), 73 (100) C_3H_9Si, 59 (30).

HR-MS (70eV, EI): *m/z* =	calcd.:	440.2018	($^{12}C_{24}{}^{1}H_{36}{}^{16}O_2{}^{28}Si_3$)
	found:	440.2024	[M$^+$]
EA calcd./found:	C: 65.39/62.60		H: 8.23/8.27

Details of the X-ray diffraction analysis are presented in the appendix (7.2 Crystallographic Data).

2,3-Diphenyl-1,4-bis(triethylsilyl)-5,5-bis(trimethylsilyl)-5,6-disilabicyclo[2.1.1]hex-2-en-6-ylidene **113**

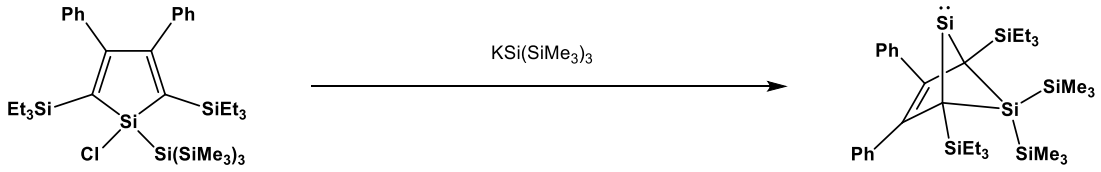

55 113

To 0.31 g (0.41 mmol) of the silyl substituted silole **55** dissolved in 3 mL THF at -80 °C, was slowly added a solution of 0.12 g (0.41 mmol) of freshly prepared $KSi(SiMe_3)_3$ dissolved in 3 mL THF. The reaction mixture was stirred for 16 h while warming to room temperature. During the reaction, the colour changed from pale yellow to dark red and then to red brown. After removal of the solvents under vacuum, 3 mL of C_6D_6 were added and the resulting suspension was filtered using a PTFE syringe filter. Numerous crystallisation attempts did not succeed. Attempts to remove $Si(SiMe_3)_4$ via sublimation using an oil diffusion pump was not possible due to the stickiness of the residue. The red brown solution of **113** in C_6D_6 was used for NMR and mass spectrometric analysis and also for further reactions.

$C_{34}H_{58}Si_6$ M = 635.35 g mol^{-1}

^{1}H NMR (499.9 MHz, 305.1 K, C_6D_6): δ = 0.42 (s, 9H, Si(C$\underline{H}_3$)$_3$), 0.43 – 0.49 (m, 12H, SiC$\underline{H}_2$CH$_3$), 0.47 (s, 9H, Si(C$\underline{H}_3$)$_3$), 0.96 (t, $^3J_{H,H}$ = 7.9 Hz, 12H, SiCH$_2$C$\underline{H}_3$), 6.86 – 6.97 (m, 6H, C$_6\underline{H}_5$), 7.49 (s br, 4 H, C$_6\underline{H}_5$).

^{13}C{^{1}H} NMR (125.7 MHz, 305.0 K, C_6D_6): δ = 0.8 (Si(C$\underline{H}_3$)$_3$), 3.1 (Si(C$\underline{H}_3$)$_3$), 6.4 (SiC$\underline{H}_2$CH$_3$), 8.6 (SiCH$_2$C$\underline{H}_3$), 40.3 (C$\underline{C}$SiEt$_3$), 127.6 (C$_6\underline{H}_5$), 127.7 (C$_6\underline{H}_5$), 131.2 (br, C$_6\underline{H}_5$), 138.3 (q-C), 139.5 (q-C).

^{29}Si{^{1}H} NMR (99.3 MHz, 305.0 K, C_6D_6): δ = -211.8 ($\underline{Si}$), -25.8 (Si($\underline{Si}$Me$_3$)$_2$), -16.3 (Si($\underline{Si}$Me$_3$)$_2$), -0.2 ($\underline{Si}$Et$_3$), 33.3 ($\underline{Si}$(SiMe$_3$)$_2$).

HR-MS (LIFDI): *m/z* = calcd.: 634.3149 ($^{12}C_{34}{}^1H_{58}{}^{28}Si_6$)
found: 634.3138 [M$^+$]

2,3-Diphenyl-1,4-bis(triethylsilyl)-5,5-bis(trimethylsilyl)-5,6-disilabicyclo[2.1.1]hex-2-en-6-ylidene $Fe(CO)_4$ complex **134**

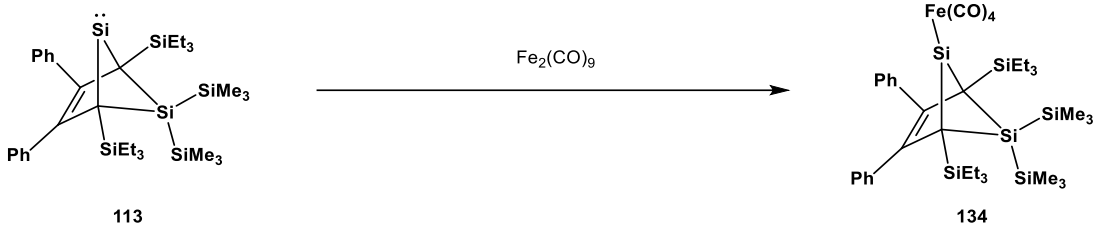

113 134

To 1.5 mL of a C_6D_6 solution which contained 0.12 g (0.21 mmol) of the silylene **113** at room temperature, were added 0.09 g (0.26 mmol) of $Fe_2(CO)_9$ and 3 mL THF. The pale red reaction mixture was stirred for 16 h and then the solvents were removed under vacuum. The residue was extracted with hexane and filtered using a PTFE syringe filter. The solvents were removed under vacuum and the residue dissolved in C_6D_6. The resulting solution of **113** was used for NMR and mass spectrometric analysis. Numerous crystallisation attempts did not succeed.

$C_{38}H_{58}FeO_4Si_6$ M = 803.23 g mol^{-1}

^{1}H NMR (499.9 MHz, 305.0 K, C_6D_6): δ = 0.40 (s, 9H, Si(C$\underline{H}_3$)$_3$), 0.68 (s, 9H, Si(C$\underline{H}_3$)$_3$), 0.66 – 0.74 (m, 12H, SiC$\underline{H}_2$CH$_3$), 0.97 (t, $^3J_{H,H}$ = 7.9 Hz, 12H, SiCH$_2$C$\underline{H}_3$), 6.89 – 7.01 (m, 6H, C$_6\underline{H}_5$), 7.53 (d, $^3J_{H,H}$ = 7.6 Hz, 4H, C$_6\underline{H}_5$).

^{13}C{^{1}H} NMR (125.7 MHz, 305.0 K, C_6D_6): δ = 2.1 (Si($\underline{C}$H$_3$)$_3$), 2.7 (Si($\underline{C}$H$_3$)$_3$), 7.5 (Si$\underline{C}$H$_2$CH$_3$), 8.9 (SiCH$_2\underline{C}$H$_3$), 52.0 ($\underline{C}$SiEt$_3$), 127.9 ($\underline{C}_6$H$_5$), 128.3 ($\underline{C}_6$H$_5$), 130.7 ($\underline{C}_6$H$_5$), 136.6 (q-C), 141.6 (q-C), 215.6 (Fe($\underline{C}$O)$_4$).

^{29}Si{^{1}H} NMR (99.3 MHz, 305.0 K, C_6D_6): δ = -20.5 (Si($\underline{Si}$Me$_3$)$_2$), -16.6 (Si($\underline{Si}$Me$_3$)$_2$), -5.2 ($\underline{Si}$Fe), -1.0 ($\underline{Si}$Et$_3$), 40.9 ($\underline{Si}$(SiMe$_3$)$_2$).

HR-MS (LIFDI): *m/z* = calcd.: 802.2295 ($^{12}C_{38}{}^1H_{58}{}^{16}O^{56}Fe^{28}Si_6$)
found: 802.2299 [M$^+$]

IR (ATR, Si(SiMe$_3$)$_4$ mixture) [cm^{-1}]: $\tilde{\nu}_{CO}$ = 2059, 2029, 1994, 1973

6 Literature

[1] J. Dubac, A. Laporterie, G. Manuel, *Chem. Rev.* **1990**, *90*, 215.
[2] S. Yamaguchi, T. Endo, M. Uchida, T. Izumizawa, K. Furukawa, K. Tamao, *Chem. Eur. J.* **2000**, *6*, 1683.
[3] S. Yamaguchi, K. Tamao, *J. Chem. Soc., Dalton Trans.* **1998**, 3693.
[4] K. Tamao, M. Uchida, T. Izumizawa, K. Furukawa, S. Yamaguchi, *J. Am. Chem. Soc.* **1996**, *118*, 11974.
[5] S. Yamaguchi, K. Tamao, *Bull. Chem. Soc. Jpn.* **1996**, *69*, 2327.
[6] E. G. Janzen, J. B. Pickett, W. H. Atwell, *J. Organomet. Chem.* **1967**, *10*, 6.
[7] D. H. O'Brien, D. L. Breeden, *J. Am. Chem. Soc.* **1981**, *103*, 3237.
[8] R. Kondo, T. Yasuda, Y. S. Yang, J. Y. Kim, C. Adachi, *J. Mater. Chem.* **2012**, *22*, 16810.
[9] H. Nie, B. Chen, C. Quan, J. Zhou, H. Qiu, R. Hu, S. J. Su, A. Qin, Z. Zhao, B. Z. Tang, *Chem. Eur. J.* **2015**, *21*, 8137.
[10] K. Tamao, S. Yamaguchi, Y. Ito, Y. Matsuzaki, T. Yamabe, M. Fukushima, S. Mori, *Macromolecules* **1995**, *28*, 8668.
[11] S. Yamaguchi, T. Goto, K. Tamao, *Angew. Chem. Int. Ed.* **2000**, *39*, 1695.
[12] S. Horst, N. R. Evans, H. A. Bronstein, C. K. Williams, *J. Polym. Sci., Part A: Polym. Chem.* **2009**, *47*, 5116.
[13] B. L. Lucht, M. A. Buretea, T. D. Tilley, *Organometallics* **2000**, *19*, 3469.
[14] K. Tamao, S. Yamaguchi, M. Shiro, *J. Am. Chem. Soc.* **1994**, *116*, 11715.
[15] A. J. Boydston, Y. Yin, B. L. Pagenkopf, *J. Am. Chem. Soc.* **2004**, *126*, 3724.
[16] N. A. Morra, B. L. Pagenkopf, *Org. Synth.* **2008**, *85*, 53.
[17] J. Lee, Q.-D. Liu, D.-R. Bai, Y. Kang, Y. Tao, S. Wang, *Organometallics* **2004**, *23*, 6205.
[18] E. H. Braye, W. Hübel, I. Caplier, *J. Am. Chem. Soc.* **1961**, *83*, 4406.
[19] Z. Li, Y. Dong, B. Mi, Y. Tang, M. Häussler, H. Tong, Y. Dong, J. W. Y. Lam, Y. Ren, H. H. Y. Sung, K. S. Wong, P. Gao, I. D. Williams, H. S. Kwok, B. Z. Tang, *J. Phys. Chem. B* **2005**, *109*, 10061.
[20] M. Saito, M. Nakamura, T. Tajima, M. Yoshioka, *Angew. Chem. Int. Ed.* **2007**, *46*, 1504.
[21] M. Katkevics, S. Yamaguchi, A. Toshimitsu, K. Tamao, *Organometallics* **1998**, *17*, 5796.
[22] P. J. Fagan, W. A. Nugent, *J. Am. Chem. Soc.* **1988**, *110*, 2310.
[23] P. J. Fagan, W. A. Nugent, J. C. Calabrese, *J. Am. Chem. Soc.* **1994**, *116*, 1880.
[24] S. Yamaguchi, R.-Z. Jin, K. Tamao, *J. Organomet. Chem.* **1998**, *559*, 73.
[25] U. Bankwitz, H. Sohn, D. R. Powell, R. West, *J. Organomet. Chem.* **1995**, *499*, 7.
[26] X. Yan, C. Xi, *Acc. Chem. Res.* **2015**, *48*, 935.
[27] E. Negishi, S. J. Holmes, J. M. Tour, J. A. Miller, F. E. Cederbaum, D. R. Swanson, T. Takahashi, *J. Am. Chem. Soc.* **1989**, *111*, 3336.
[28] J. E. Hill, G. Balaich, P. E. Fanwick, I. P. Rothwell, *Organometallics* **1993**, *12*, 2911.
[29] S. Yamaguchi, R.-Z. Jin, K. Tamao, F. Sato, *J. Org. Chem.* **1998**, *63*, 10060.
[30] F. Carre, E. Colomer, J. Y. Corey, R. J. P. Corriu, C. Guerin, B. J. L. Henner, B. Kolani, W. W. C. Wong Chi Man, *Organometallics* **1986**, *5*, 910.
[31] S. Yamaguchi, R.-Z. Jin, S. Ohno, K. Tamao, *Organometallics* **1998**, *17*, 5133.
[32] M. D. Curtis, *J. Am. Chem. Soc.* **1969**, *91*, 6011.
[33] P. Dufour, M. Dartiguenave, Y. Dartiguenave, J. Dubac, *J. Organomet. Chem.* **1990**, *384*, 61.
[34] F. Meier-Brocks, E. Weiss, *J. Organomet. Chem.* **1993**, *453*, 33.
[35] K.-i. Kanno, M. Kira, *Chem. Lett.* **1999**, *28*, 1127.
[36] Y. Liu, T. C. Stringfellow, D. Ballweg, I. A. Guzei, R. West, *J. Am. Chem. Soc.* **2001**, *124*, 49.
[37] I. S. Toulokhonova, T. C. Stringfellow, S. A. Ivanov, A. Masunov, R. West, *J. Am. Chem. Soc.* **2003**, *125*, 5767.

[38] A. A. Ovchinnikov, *Theor. Chim. Acta* **1978**, *47*, 297.
[39] A. Rajca, *Chem. Rev.* **1994**, *94*, 871.
[40] J. Kanamori, *J. Phys. Chem. Solids* **1959**, *10*, 87.
[41] J. B. Goodenough, *Phys. Rev.* **1955**, *100*, 564.
[42] J. B. Goodenough, *J. Phys. Chem. Solids* **1958**, *6*, 287.
[43] L. Salem, C. Rowland, *Angew. Chem.* **1972**, *84*, 86.
[44] F. Breher, *Coord. Chem. Rev.* **2007**, *251*, 1007.
[45] M. Abe, *Chem. Rev.* **2013**, *113*, 7011.
[46] E. Niecke, A. Fuchs, F. Baumeister, M. Nieger, W. W. Schoeller, *Angew. Chem.* **1995**, *107*, 640.
[47] O. Schmidt, A. Fuchs, D. Gudat, M. Nieger, W. Hoffbauer, E. Niecke, W. W. Schoeller, *Angew. Chem.* **1998**, *110*, 995.
[48] E. Niecke, A. Fuchs, M. Nieger, *Angew. Chem.* **1999**, *111*, 3213.
[49] E. Niecke, A. Fuchs, M. Nieger, O. Schmidt, W. W. Schoeller, *Angew. Chem.* **1999**, *111*, 3216.
[50] W. W. Schoeller, C. Begemann, E. Niecke, D. Gudat, *J. Phys. Chem. A* **2001**, *105*, 10731.
[51] M. Sebastian, M. Nieger, D. Szieberth, L. Nyulászi, E. Niecke, *Angew. Chem.* **2004**, *116*, 647.
[52] M. Sebastian, A. Hoskin, M. Nieger, L. Nyulászi, E. Niecke, *Angew. Chem.* **2005**, *117*, 1429.
[53] H. Amii, L. Vranicar, H. Gornitzka, D. Bourissou, G. Bertrand, *J. Am. Chem. Soc.* **2004**, *126*, 1344.
[54] D. Scheschkewitz, H. Amii, H. Gornitzka, W. W. Schoeller, D. Bourissou, G. Bertrand, *Science* **2002**, *295*, 1880.
[55] C. Cui, M. Brynda, M. M. Olmstead, P. P. Power, *J. Am. Chem. Soc.* **2004**, *126*, 6510.
[56] K. Takeuchi, M. Ichinohe, A. Sekiguchi, *J. Am. Chem. Soc.* **2011**, *133*, 12478.
[57] T. Beweries, R. Kuzora, U. Rosenthal, A. Schulz, A. Villinger, *Angew. Chem. Int. Ed.* **2011**, *50*, 8974.
[58] A. Hinz, R. Kuzora, U. Rosenthal, A. Schulz, A. Villinger, *Chem. Eur. J.* **2014**, *20*, 14659.
[59] T. Nozawa, M. Nagata, M. Ichinohe, A. Sekiguchi, *J. Am. Chem. Soc.* **2011**, *133*, 5773.
[60] Y. Liu, D. Ballweg, T. Müller, I. A. Guzei, R. W. Clark, R. West, *J. Am. Chem. Soc.* **2002**, *124*, 12174.
[61] J. H. Hong, P. Boudjouk, *J. Am. Chem. Soc.* **1993**, *115*, 5883.
[62] W. P. Freeman, T. D. Tilley, A. L. Rheingold, *J. Am. Chem. Soc.* **1994**, *116*, 8428.
[63] W. P. Freeman, T. D. Tilley, L. M. Liable-Sands, A. L. Rheingold, *J. Am. Chem. Soc.* **1996**, *118*, 10457.
[64] J. M. Dysard, T. D. Tilley, *J. Am. Chem. Soc.* **2000**, *122*, 3097.
[65] J. M. Dysard, T. D. Tilley, *J. Am. Chem. Soc.* **1998**, *120*, 8245.
[66] W. P. Freeman, T. D. Tilley, G. P. A. Yap, A. L. Rheingold, *Angew. Chem. Int. Ed.* **1996**, *35*, 882.
[67] W. P. Freeman, T. D. Tilley, F. P. Arnold, A. L. Rheingold, P. K. Gantzel, *Angew. Chem. Int. Ed.* **1995**, *34*, 1887.
[68] M. Saito, M. Yoshioka, *Coord. Chem. Rev.* **2005**, *249*, 765.
[69] B. Goldfuss, P. v. R. Schleyer, *Organometallics* **1997**, *16*, 1543.
[70] R. West, H. Sohn, D. R. Powell, T. Müller, Y. Apeloig, *Angew. Chem. Int. Ed.* **1996**, *35*, 1002.
[71] B. Goldfuss, P. v. R. Schleyer, F. Hampel, *Organometallics* **1996**, *15*, 1755.
[72] R. West, H. Sohn, U. Bankwitz, J. Calabrese, Y. Apeloig, T. Mueller, *J. Am. Chem. Soc.* **1995**, *117*, 11608.
[73] Y. Gao, J. Zhang, H. Hu, C. Cui, *Organometallics* **2010**, *29*, 3063.
[74] M. Kako, S. Oba, R. Uesugi, S. Sumiishi, Y. Nakadaira, K. Tanaka, T. Takada, *J. Chem. Soc., Perkin Trans. 2* **1997**, 1251.
[75] D. Lutters, C. Severin, M. Schmidtmann, T. Müller, *J. Am. Chem. Soc.* **2016**, *138*, 6061.
[76] C. R. W. Reinhold, *Masterarbeit* **2012**, Carl von Ossietzky Universität Oldenburg.
[77] B. Urschel, *Dissertation* **2008**, Goethe Universität Frankfurt/Main.

[78] B. Urschel, *Diplomarbeit* **2005**, Goethe Universität Frankfurt/Main.
[79] M. Westerhausen, B. Stein, M. W. Ossberger, H. Görls, J. C. G. Ruiz, H. Nöth, P. Mayer, *ARKIVOC* **2007**, *iii*, 46.
[80] Z. Dong, *unpublished results* **2015**, Carl von Ossietzky Universität Oldenburg.
[81] D. Wachtendorf, *Forschungspraktikum* **2016**, Carl von Ossietzky Universität Oldenburg.
[82] S. Yamaguchi, R.-Z. Jin, K. Tamao, M. Shiro, *Organometallics* **1997**, *16*, 2230.
[83] S. Künzler, *Bachelorarbeit* **2013**, Carl von Ossietzky Universität Oldenburg.
[84] J. Küppers, *Forschungspraktikum* **2015**, Carl von Ossietzky Universität Oldenburg.
[85] J. Nimoth, *Forschungspraktikum* **2015**, Carl von Ossietzky Universität Oldenburg.
[86] T. Lenk, *Bachelorarbeit* **2016**, Carl von Ossietzky Universität Oldenburg.
[87] J. M. Winkler, *Forschungspraktikum* **2016**, Carl von Ossietzky Universität Oldenburg.
[88] C. Marschner, *Eur. J. Inorg. Chem.* **1998**, *1998*, 221.
[89] D. Lutters, *unpublished results* **2016**, Carl von Ossietzky Universität Oldenburg.
[90] J. Zhou, A. Rieker, *J. Chem. Soc., Perkin Trans. 2* **1997**, 931.
[91] M. M. Olmstead, L. Pu, R. S. Simons, P. P. Power, *Chem. Commun.* **1997**, 1595.
[92] A. Sekiguchi, T. Matsuno, M. Ichinohe, *J. Am. Chem. Soc.* **2001**, *123*, 12436.
[93] C. A. Tolman, *J. Am. Chem. Soc.* **1970**, *92*, 2956.
[94] M. Reißmann, *Dissertation* **2014**, Carl von Ossietzky Universität Oldenburg.
[95] P. Pyykkö, M. Atsumi, *Chem. Eur. J.* **2009**, *15*, 12770.
[96] D. Förster, H. Dilger, F. Ehret, M. Nieger, D. Gudat, *Eur. J. Inorg. Chem.* **2012**, *2012*, 3989.
[97] O. Puntigam, D. Förster, N. A. Giffin, S. Burck, J. Bender, F. Ehret, A. D. Hendsbee, M. Nieger, J. D. Masuda, D. Gudat, *Eur. J. Inorg. Chem.* **2013**, *2013*, 2041.
[98] K. Mochida, H. Kikkawa, Y. Nakadaira, *Chem. Lett.* **1988**, *17*, 1089.
[99] G. W. Sluggett, W. J. Leigh, *Organometallics* **1992**, *11*, 3731.
[100] W. P. Neumann, K.-D. Schultz, *J. Chem. Soc., Chem. Commun.* **1982**, 43.
[101] C. H. Schiesser, S. Zahirovic, *J. Chem. Soc., Perkin Trans. 2* **1999**, 933.
[102] A. Sekiguchi, T. Fukawa, M. Nakamoto, V. Y. Lee, M. Ichinohe, *J. Am. Chem. Soc.* **2002**, *124*, 9865.
[103] V. Y. Lee, A. Sekiguchi, *Eur. J. Inorg. Chem.* **2005**, *2005*, 1209.
[104] S. Stoll, A. Schweiger, *J. Magn. Reson.* **2006**, *178*, 42.
[105] M. J. Frisch, G. W. Trucks, H. B. Schlegel, G. E. Scuseria, M. A. Robb, J. R. Cheeseman, G. Scalmani, V. Barone, B. Mennucci, G. A. Petersson, H. Nakatsuji, M. Caricato, X. Li, H. P. Hratchian, A. F. Izmaylov, J. Bloino, G. Zheng, J. L. Sonnenberg, M. Hada, M. Ehara, K. Toyota, R. Fukuda, J. Hasegawa, M. Ishida, T. Nakajima, Y. Honda, O. Kitao, H. Nakai, T. Vreven, J. A. Montgomery Jr., J. E. Peralta, F. Ogliaro, M. J. Bearpark, J. Heyd, E. N. Brothers, K. N. Kudin, V. N. Staroverov, R. Kobayashi, J. Normand, K. Raghavachari, A. P. Rendell, J. C. Burant, S. S. Iyengar, J. Tomasi, M. Cossi, N. Rega, N. J. Millam, M. Klene, J. E. Knox, J. B. Cross, V. Bakken, C. Adamo, J. Jaramillo, R. Gomperts, R. E. Stratmann, O. Yazyev, A. J. Austin, R. Cammi, C. Pomelli, J. W. Ochterski, R. L. Martin, K. Morokuma, V. G. Zakrzewski, G. A. Voth, P. Salvador, J. J. Dannenberg, S. Dapprich, A. D. Daniels, Ö. Farkas, J. B. Foresman, J. V. Ortiz, J. Cioslowski, D. J. Fox, *Gaussian 09*, Gaussian, Inc., Wallingford, CT, USA **2009.**
[106] F. Neese, *WIREs Comput. Mol. Sci.* **2012**, *2*, 73.
[107] D. Rappoport, F. Furche, *J. Chem. Phys.* **2010**, *133*, 134105.
[108] F. Weigend, R. Ahlrichs, *Phys. Chem. Chem. Phys.* **2005**, *7*, 3297.
[109] M. Kira, T. Obata, I. Kon, H. Hashimoto, M. Ichinohe, H. Sakurai, S. Kyushin, H. Matsumoto, *Chem. Lett.* **1998**, *27*, 1097.
[110] W. Kutzelnigg, U. Fleischer, M. Schindler, *The IGLO-Method: Ab Initio Calculation and Interpretation of NMR Chemical Shifts and Magnetic Susceptibilities, Vol. 23*, Springer-Verlag, Heidelberg **1990**

[111] A. F. Holleman, E. Wiberg, N. Wiberg, *Lehrbuch der Anorganischen Chemie*, 102. Auflage, Walter de Gruyter **2007.**
[112] M. Mantina, A. C. Chamberlin, R. Valero, C. J. Cramer, D. G. Truhlar, *J. Phys. Chem. A* **2009**, *113*, 5806.
[113] L. Albers, *Dissertation* **2015**, Carl von Ossietzky Universität Oldenburg.
[114] J. P. Wagner, P. R. Schreiner, *Angew. Chem. Int. Ed.* **2015**, *54*, 12274.
[115] S. Grimme, *WIREs Comput. Mol. Sci.* **2011**, *1*, 211.
[116] S. Grimme, J. Antony, S. Ehrlich, H. Krieg, *J. Chem. Phys.* **2010**, *132*, 154104.
[117] L. Goerigk, H. Kruse, S. Grimme, *ChemPhysChem* **2011**, *12*, 3421.
[118] E. G. Hohenstein, S. T. Chill, C. D. Sherrill, *J. Chem. Theory Comput.* **2008**, *4*, 1996.
[119] J.-H. Hong, P. Boudjouk, S. Castellino, *Organometallics* **1994**, *13*, 3387.
[120] H. Gilman, R. L. Harrell, *J. Organomet. Chem.* **1967**, *9*, 67.
[121] H. Steinert, *Bachelorarbeit* **2015**, Carl von Ossietzky Universität Oldenburg.
[122] V. I. Severin, A. V. Tseplyaeva, N. E. Khandamirova, Y. A. Priselkov, N. A. Chernova, I. V. Golubtsov, *Mendeleev Commun.* **1991**, *1*, 43.
[123] H. Marsmann, in *Oxygen-17 and Silicon-29*, Springer Berlin Heidelberg, Berlin, Heidelberg **1981**, 65-235.
[124] H. C. Marsmann, in *Silicon-29 NMR - eMagRes*, John Wiley & Sons, Ltd **2011**.
[125] J. Wagler, U. Böhme, E. Kroke, in *Functional Molecular Silicon Compounds I: Regular Oxidation States* (Ed.: D. Scheschkewitz), Springer International Publishing, Cham **2014**, 29-105.
[126] T. Müller, *J. Organomet. Chem.* **2003**, *686*, 251.
[127] M. Kira, S. Ishida, T. Iwamoto, C. Kabuto, *J. Am. Chem. Soc.* **1999**, *121*, 9722.
[128] P. Jutzi, U. Holtmann, D. Kanne, C. Krüger, R. Blom, R. Gleiter, I. Hyla-Kryspin, *Chem. Ber.* **1989**, *122*, 1629.
[129] T. Kühler, P. Jutzi, in *Adv. Organomet. Chem., Vol. 49*, Academic Press **2003**, 1-34.
[130] P. Jutzi, D. Kanne, C. Krüger, *Angew. Chem. Int. Ed.* **1986**, *25*, 164.
[131] Z. Dong, C. R. W. Reinhold, M. Schmidtmann, T. Müller, *Angew. Chem. Int. Ed.* **2016**, *55*, 15899.
[132] *AIMAll (Version 16.10.31),* T. A. Keith, TK Gristmill Software, Overland Park KS, USA, **2016**, (aim.tkgristmill.com).
[133] N. H. Werstiuk, H. M. Muchall, *J. Mol. Struct. THEOCHEM* **1999**, *463*, 225.
[134] N. H. Werstiuk, H. M. Muchall, *J. Phys. Chem. A* **2000**, *104*, 2054.
[135] P. Muller, in *Pure Appl. Chem., Vol. 66* **1994**, p. 1077.
[136] R. V. Williams, *Chem. Rev.* **2001**, *101*, 1185.
[137] R. V. Williams, H. A. Kurtz, in *Adv. Phys. Org. Chem., Vol. 29* (Ed.: D. Bethell), Academic Press **1994**, 273-331.
[138] A. Sekiguchi, T. Matsuno, M. Ichinohe, *J. Am. Chem. Soc.* **2000**, *122*, 11250.
[139] T. Laube, C. Lohse, *J. Am. Chem. Soc.* **1994**, *116*, 9001.
[140] T. Laube, *J. Am. Chem. Soc.* **1989**, *111*, 9224.
[141] Y. Ishida, A. Sekiguchi, Y. Kabe, *J. Am. Chem. Soc.* **2003**, *125*, 11468.
[142] C. Gerdes, W. Saak, D. Haase, T. Müller, *J. Am. Chem. Soc.* **2013**, *135*, 10353.
[143] P. J. Fagan, E. G. Burns, J. C. Calabrese, *J. Am. Chem. Soc.* **1988**, *110*, 2979.
[144] S. Winstein, M. Shatavsky, C. Norton, R. B. Woodward, *J. Am. Chem. Soc.* **1955**, *77*, 4183.
[145] S. Winstein, E. T. Stafford, *J. Am. Chem. Soc.* **1957**, *79*, 505.
[146] W. G. Woods, R. A. Carboni, J. D. Roberts, *J. Am. Chem. Soc.* **1956**, *78*, 5653.
[147] G. Maier, H. P. Reisenauer, *Eur. J. Org. Chem.* **2003**, *2003*, 479.
[148] M. Driess, *Nat. Chem.* **2012**, *4*, 525.
[149] Y. Mizuhata, T. Sasamori, N. Tokitoh, *Chem. Rev.* **2009**, *109*, 3479.
[150] A. C. Filippou, O. Chernov, G. Schnakenburg, *Angew. Chem. Int. Ed.* **2009**, *48*, 5687.

[151] R. S. Ghadwal, H. W. Roesky, S. Merkel, J. Henn, D. Stalke, *Angew. Chem. Int. Ed.* **2009**, *48*, 5683.
[152] D. Lutters, *Dissertation* **2016**, Carl von Ossietzky Universität Oldenburg.
[153] A. J. Arduengo, R. L. Harlow, M. Kline, *J. Am. Chem. Soc.* **1991**, *113*, 361.
[154] M. Denk, R. Lennon, R. Hayashi, R. West, A. V. Belyakov, H. P. Verne, A. Haaland, M. Wagner, N. Metzler, *J. Am. Chem. Soc.* **1994**, *116*, 2691.
[155] R. West, M. Denk, in *Pure Appl. Chem., Vol. 68* **1996**, p. 785.
[156] A. Meller, C.-P. Gräbe, *Chem. Ber.* **1985**, *118*, 2020.
[157] J. Pfeiffer, W. Maringgele, M. Noltemeyer, A. Meller, *Chem. Ber.* **1989**, *122*, 245.
[158] W. A. Herrmann, M. Denk, J. Behm, W. Scherer, F.-R. Klingan, H. Bock, B. Solouki, M. Wagner, *Angew. Chem. Int. Ed.* **1992**, *31*, 1485.
[159] T. Kosai, S. Ishida, T. Iwamoto, *Angew. Chem. Int. Ed.* **2016**, *55*, 15554.
[160] L. Wang, Y. S. Lim, Y. Li, R. Ganguly, R. Kinjo, *Molecules* **2016**, *21*, 990.
[161] A. V. Protchenko, K. H. Birjkumar, D. Dange, A. D. Schwarz, D. Vidovic, C. Jones, N. Kaltsoyannis, P. Mountford, S. Aldridge, *J. Am. Chem. Soc.* **2012**, *134*, 6500.
[162] Y. Zhang, J. R. G. Evans, S. Yang, *J. Chem. Eng. Data* **2011**, *56*, 328.
[163] T. Kuwabara, M. Nakada, J. Hamada, J. D. Guo, S. Nagase, M. Saito, *J. Am. Chem. Soc.* **2016**, *138*, 11378.
[164] J. R. Nitschke, T. Don Tilley, *J. Organomet. Chem.* **2003**, *666*, 15.
[165] V. H. Gessner, J. F. Tannaci, A. D. Miller, T. D. Tilley, *Acc. Chem. Res.* **2011**, *44*, 435.
[166] E. Corey, H. Kirst, J. Katzenellenbogen, *J. Am. Chem. Soc.* **1970**, *92*, 6314.
[167] J. Suffert, D. Toussaint, *J. Org. Chem.* **1995**, *60*, 3550.
[168] N. J. Fitzmaurice, W. R. Jackson, P. Perlmutter, *J. Organomet. Chem.* **1985**, *285*, 375.
[169] G. Brauer, *Handbuch der präparativen anorganischen Chemie*, Ferdinand Enke Verlag Stuttgart **1975**
[170] J. Hlina, J. Baumgartner, C. Marschner, *Organometallics* **2010**, *29*, 5289.
[171] H. Gilman, C. L. Smith, *J. Organomet. Chem.* **1967**, *8*, 245.
[172] J. Fischer, J. Baumgartner, C. Marschner, *Organometallics* **2005**, *24*, 1263.

7 Appendix

7.1 Computational Details

Quantum mechanical calculations and their analysis were performed using Gaussian09[105], ORCA[106], and AIMALL.[132] The level of theory is stated at each calculation. Energy minima of each stationary point were identified by subsequent frequency calculations in which the number of imaginary frequencies was ensured to be zero (NImag = 0).

An example Z-matrix input for the calculations with altering specific angles of the model sila- and germacyclopentadienyl radicals and anions using Gaussian and an example input for the determination of EPR *g*-factors and hyperfine coupling constants using ORCA are given below.

All calculations are summarised in an Excel sheet which can be found in addition to all output files on the attached DVD.

EPR spectra were simulated using the EasySpin Toolbox for MATLAB developed by Stoll et al.[104] The inputs which were used for the sila- and germacyclopentadienyl radicals are given below.

7.1.1 Gaussian Example Input

Example Z-matrix input for the calculations with altering specific angles of the model sila- and germacyclopentadienyl radicals and anions using Gaussian:

```
%chk=germol_SiH3_zmatrix_6_rad.chk
%mem=1000MB
%nproc=4
# M062X/6-311+G(d,p) fopt=Z-matrix pop=always

Optimierung der Struktur von germol SiH3 Anion mit M062X Variation Winkel

0 2
Ge
X       1       1.0
Si      1       B1      2       Wvari
H       3       B2      1       W1      2       D4
H       3       B3      1       W2      4       D1
H       3       B3      1       W2      4       -D1
C       1       B4      2       90.     3       -D2
C       1       B4      2       90.     3       D2
H       7       B5      1       W4      2       D3
H       8       B5      1       W4      2       -D3
C       7       B6      1       W5      2       -90.
C       8       B6      1       W5      2       90.
H       11      B7      7       W6      1       D5
H       12      B7      8       W6      1       -D5

 B1=2.39
 B2=1.47
 B3=1.47
 B4=1.93
 B5=1.08
 B6=1.35
 B7=1.09
 W1=109.47
 W2=109.47
 W4=130.16
 W5=106.42
 W6=122.8
 D1=120.0
 D2=133.
 D3=90.
 D5=180.0
 D4=180.0

 Wvari=90.0     S       17      5.0
```

7.1.2 ORCA Example Input

```
!ZORA UKS M062X def2-tzvpd TightSCF Grid5
%pal nprocs 12
end
%method
   SpecialGridAtoms 32;
   SpecialGridIntAcc 9.0;
end
%rel
   SOCType 3
   SOCFlags 1,3,3,1
   PictureChange true
end

* xyz 0 2
  C          2.02392500    1.49247900   -0.01698000
  C          3.11920400    0.86483800   -0.51810400
  C          3.15789200   -0.62810100   -0.50120900
  C          2.09958500   -1.29878900    0.02292300
  Ge         0.80791800    0.07263000    0.53650800
  Si         1.82569400    3.28123100    0.44627900
  Si         1.96179600   -3.10804500    0.42430500
  Si        -1.54497900   -0.06013800    0.00104600
  Si        -2.70791100   -0.55400300    1.99358300
  Si        -1.72488600   -1.66843200   -1.73388500
  Si        -2.37763100    1.90782300   -1.00565100
  C          4.32900200    1.59500400   -1.04230600
  H          4.11938900    2.65125600   -1.19147500
  H          5.17391300    1.50957300   -0.35239400
  H          4.65617100    1.18271500   -1.99821300
  C          4.38972200   -1.30025300   -1.04864200
  H          5.29193700   -0.97073100   -0.52667400
  H          4.32504700   -2.38239600   -0.96970000
  H          4.52681500   -1.05409800   -2.10449900
  C          0.51351000   -3.29071600    1.61306800
  H         -0.35433300   -2.70391900    1.30450900
  H          0.19668100   -4.33122600    1.71629500
  H          0.81766600   -2.93283500    2.60020800
  C          3.46798900   -3.74153700    1.35503100
  H          3.25263200   -4.73068700    1.76728800
  H          4.35608900   -3.83118000    0.72923200
  H          3.70764600   -3.07730900    2.18769700
  C          1.74024600   -4.16953100   -1.11085800
  H          0.90415700   -3.84555900   -1.73043900
  H          2.64219100   -4.13003700   -1.72625300
  H          1.57165900   -5.21311100   -0.83360500
  C          1.28018300    4.33995000   -1.00766400
  H          2.09367400    4.41160200   -1.73378200
  H          0.41444900    3.92856000   -1.52667700
  H          1.03343900    5.35354300   -0.68251100
  C          0.58871800    3.31437000    1.86413600
  H          1.07127900    2.90732000    2.75680700
  H          0.25518300    4.32902100    2.09342300
  H         -0.29594400    2.70627500    1.66421300
  C          3.41041000    4.02690700    1.13598000
  H          3.88834800    3.33645500    1.83409800
  H          4.13626600    4.28651700    0.36527000
  H          3.16876400    4.94077400    1.68452500
  C         -1.51341400    2.12256200   -2.66625700
  H         -1.73157800    3.11039700   -3.08079400
  H         -0.42967000    2.02553700   -2.56782400
  H         -1.84997400    1.37619300   -3.38841000
  C         -4.23252900    1.67702200   -1.27839600
  H         -4.77985400    2.04315800   -0.40823000
  H         -4.54742600    2.27026300   -2.14139100
  H         -4.52812800    0.64400400   -1.45545100
  C         -2.24067300    3.52003100   -0.04644000
  H         -2.87580000    4.25108600   -0.55574500
  H         -2.60488400    3.42202300    0.97779000
  H         -1.23155000    3.92356700   -0.00950400
  C         -1.54392400   -0.31857100    3.44788500
  H         -2.06910000   -0.48863800    4.39089300
  H         -0.70500800   -1.01512300    3.39120200
  H         -1.13240900    0.69348800    3.46148300
  C         -3.37829500   -2.31031700    2.00024700
  H         -2.58932300   -3.05380800    1.87727600
  H         -3.88298200   -2.50712500    2.94973800
  H         -4.10777400   -2.45208400    1.19985400
  C         -4.17024700    0.61300100    2.18497800
  H         -3.86042000    1.65908100    2.14624400
  H         -4.91120200    0.44986300    1.40072300
  H         -4.65769000    0.44323900    3.14841600
  C         -0.25289500   -1.45177300   -2.88158800
  H         -0.25371000   -0.45075500   -3.31760300
  H          0.69618700   -1.58162400   -2.35887100
  H         -0.30223800   -2.17764500   -3.69791600
  C         -1.83312900   -3.44955100   -1.13344300
  H         -1.01732400   -3.75447100   -0.48143000
  H         -2.77247900   -3.61750100   -0.60373300
  H         -1.82334700   -4.10618700   -2.00866500
  C         -3.29408900   -1.40981800   -2.74498500
  H         -3.36668900   -0.41302200   -3.18005900
  H         -3.29938900   -2.13531300   -3.56325700
  H         -4.18903600   -1.58460400   -2.14406700
*

%eprnmr          gtensor true printlevel 3
                 Nuclei = all Ge { aiso, adip, fgrad}
                 Nuclei = all Si { aiso, adip, fgrad }
                 Nuclei = all C { aiso, adip, fgrad }
                 Nuclei = all H { aiso, adip, fgrad }
end
```

7.1.3 EasySpin Toolbox for MATLAB Inputs

1-Tris(trimethylsilyl)silylgermolyl radical **69**:

```
% Ge SuSilyl Rad
%==========================================================================

clear
Sys.A = [mt2mhz(2.2,2.017802) mt2mhz(3.0,2.017802) mt2mhz(1.60,2.017802)
mt2mhz(0.70,2.017802) mt2mhz(2.7,2.017802)];
Sys.n = [1 1 1 1 1];
Sys.g = [2.017802]
Sys.lwpp = [0.01 0.22];
Exp.mwFreq = 9.4043;
Exp.Range = [317 347];
Exp.nPoints = 1e4;

Sys.Nucs = '(12,13)C,(12,13)C,(28,29)Si,(28,29)Si,Ge';
Sys.Abund = {[0.98 0.02],[0.98 0.02],[0.95,0.05],[0.85,0.15],1};

garlic(Sys,Exp);
```

1-Tris(trimethylsilyl)silylsilolyl radical **78**:

```
% Si SuSilyl Rad
%==========================================================================

clear
Sys.A = [mt2mhz(1.6, 2.003644) mt2mhz(6.1, 2.003644) mt2mhz(0.8,
2.003644)];
Sys.n = [1 1 1];
Sys.g = [2.003644]
Sys.lwpp = [0.01 0.18];
Exp.mwFreq = 9.402785;
Exp.Range = [331 340];
Exp.nPoints = 1e4;

Sys.Nucs = '(12,13)C,(28,29)Si,(28,29)Si';
Sys.Abund = {[0.98 0.02],[0.95,0.05],[0.85,0.15]};


garlic(Sys,Exp);
```

7.2 Crystallographic Data

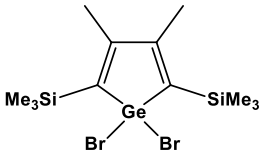

40

Empirical formula	C12 H24 Br1.85 Cl0.15 Ge Si2	
Formula weight	450.23	
Temperature	120(2) K	
Wavelength	0.71073 Å	
Crystal system	Monoclinic	
Space group	P 21/n	
Unit cell dimensions	a = 12.3229(3) Å	α= 90°.
	b = 10.1607(2) Å	β= 108.7930(10)°.
	c = 16.0917(4) Å	γ = 90°.
Volume	1907.42(8) Å^3	
Z	4	
Density (calculated)	1.568 Mg/m^3	
Absorption coefficient	5.611 mm^{-1}	
F(000)	893	
Crystal size	0.250 x 0.200 x 0.080 mm^3	
Theta range for data collection	1.825 to 34.972°	
Index ranges	-19<=h<=19, -16<=k<=16, -25<=l<=25	
Reflections collected	56168	
Independent reflections	8384 (R(int) = 0.0304)	
Observed reflections (I > 2(I))	7247	
Completeness to theta = 25.242°	100.0 %	
Absorption correction	Semi-empirical from equivalents	
Max. and min. transmission	0.6983 and 0.3135	
Refinement method	Full-matrix least-squares on F^2	
Data / restraints / parameters	8384 / 0 / 164	
Goodness-of-fit on F^2	1.064	
Final R indices (I>2sigma(I))	R1 = 0.0197, wR2 = 0.0414	
R indices (all data)	R1 = 0.0270, wR2 = 0.0436	
Extinction coefficient	0.00046(8)	
Largest diff. peak and hole	0.765 and -0.492 e.Å^{-3}	

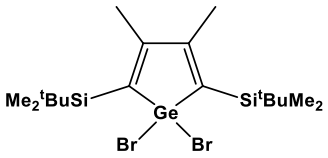

42

Empirical formula	C18 H36 Br2 Ge Si2	
Formula weight	541.06	
Temperature	100(2) K	
Wavelength	0.71073 Å	
Crystal system	Orthorhombic	
Space group	Pnma	
Unit cell dimensions	a = 13.2415(5) Å	α = 90°.
	b = 25.2601(10) Å	β = 90°.
	c = 7.1949(3) Å	γ = 90°.
Volume	2406.56(17) Å^3	
Z	4	
Density (calculated)	1.493 Mg/m^3	
Absorption coefficient	4.692 mm^{-1}	
F(000)	1096	
Crystal size	0.240 x 0.160 x 0.040 mm^3	
Theta range for data collection	1.612 to 34.971°	
Index ranges	-21<=h<=20, -40<=k<=40, -11<=l<=11	
Reflections collected	82726	
Independent reflections	5393 (R(int) = 0.0320)	
Observed reflections (I > 2(I))	4717	
Completeness to theta = 34.971°	100.0 %	
Absorption correction	Numerical	
Max. and min. transmission	0.8178 and 0.3907	
Refinement method	Full-matrix least-squares on F^2	
Data / restraints / parameters	5393 / 0 / 115	
Goodness-of-fit on F^2	1.082	
Final R indices (I>2sigma(I))	R1 = 0.0214, wR2 = 0.0500	
R indices (all data)	R1 = 0.0275, wR2 = 0.0517	
Extinction coefficient	n/a	
Largest diff. peak and hole	2.096 and -0.619 e.Å^{-3}	

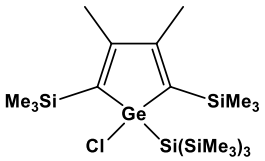

46

Empirical formula	C21 H51 Cl Ge Si6	
Formula weight	580.19	
Temperature	120(2) K	
Wavelength	0.71073 Å	
Crystal system	Monoclinic	
Space group	P 21/c	
Unit cell dimensions	a = 21.4429(6) Å	α= 90°.
	b = 9.3756(3) Å	β= 114.1310(10)°.
	c = 18.3533(5) Å	γ = 90°.
Volume	3367.31(17) $Å^3$	
Z	4	
Density (calculated)	1.144 Mg/m^3	
Absorption coefficient	1.211 mm^{-1}	
F(000)	1240	
Crystal size	0.400 x 0.200 x 0.150 mm^3	
Theta range for data collection	2.081 to 36.318°	
Index ranges	-35<=h<=35, -15<=k<=15, -30<=l<=30	
Reflections collected	161992	
Independent reflections	16336 (R(int) = 0.0300)	
Observed reflections (I > 2(I))	14392	
Completeness to theta = 36.318°	100.0 %	
Absorption correction	Numerical	
Max. and min. transmission	0.8898 and 0.6427	
Refinement method	Full-matrix least-squares on F^2	
Data / restraints / parameters	16336 / 0 / 279	
Goodness-of-fit on F^2	1.041	
Final R indices (I>2sigma(I))	R1 = 0.0217, wR2 = 0.0557	
R indices (all data)	R1 = 0.0279, wR2 = 0.0581	
Extinction coefficient	n/a	
Largest diff. peak and hole	0.528 and -0.356 $e.Å^{-3}$	

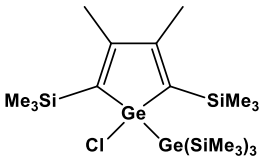

47

Empirical formula	C21 H51 Cl Ge2 Si5	
Formula weight	624.69	
Temperature	100(2) K	
Wavelength	0.71073 Å	
Crystal system	Monoclinic	
Space group	$P2_1/c$	
Unit cell dimensions	a = 21.4687(13) Å	α = 90°.
	b = 9.3837(6) Å	β = 114.088(3)°.
	c = 18.3555(11) Å	γ = 90°.
Volume	3375.8(4) $Å^3$	
Z	4	
Density (calculated)	1.229 Mg/m^3	
Absorption coefficient	2.045 mm^{-1}	
F(000)	1312	
Crystal size	0.350 x 0.300 x 0.250 mm^3	
Theta range for data collection	2.078 to 36.318°	
Index ranges	-35<=h<=35, -15<=k<=15, -30<=l<=30	
Reflections collected	177107	
Independent reflections	16363 (R(int) = 0.0243)	
Observed reflections (I > 2(I))	14645	
Completeness to theta = 36.318°	100.0 %	
Absorption correction	Numerical	
Max. and min. transmission	0.6715 and 0.4973	
Refinement method	Full-matrix least-squares on F^2	
Data / restraints / parameters	16363 / 0 / 279	
Goodness-of-fit on F^2	1.083	
Final R indices (I>2sigma(I))	R1 = 0.0188, wR2 = 0.0458	
R indices (all data)	R1 = 0.0234, wR2 = 0.0470	
Extinction coefficient	n/a	
Largest diff. peak and hole	0.528 and -0.513 $e.Å^{-3}$	

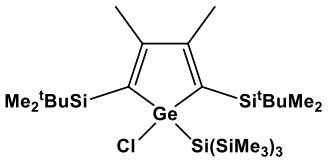

48

Empirical formula	C27 H63 Cl Ge Si6	
Formula weight	664.35	
Temperature	170(2) K	
Wavelength	0.71073 Å	
Crystal system	Monoclinic	
Space group	$P2_1/n$	
Unit cell dimensions	a = 12.0431(4) Å	α = 90°.
	b = 19.7673(6) Å	β = 94.4670(18)°.
	c = 33.3647(11) Å	γ = 90°.
Volume	7918.7(4) $Å^3$	
Z	8	
Density (calculated)	1.115 Mg/m^3	
Absorption coefficient	1.037 mm^{-1}	
F(000)	2864	
Crystal size	0.400 x 0.300 x 0.200 mm^3	
Theta range for data collection	1.198 to 30.034°	
Index ranges	-16<=h<=16, -27<=k<=27, -46<=l<=46	
Reflections collected	259215	
Independent reflections	23152 (R(int) = 0.0353)	
Observed reflections (I > 2(I))	18542	
Completeness to theta = 30.034°	100.0 %	
Absorption correction	Numerical	
Max. and min. transmission	0.8593 and 0.6824	
Refinement method	Full-matrix least-squares on F^2	
Data / restraints / parameters	23152 / 0 / 735	
Goodness-of-fit on F^2	1.015	
Final R indices (I>2sigma(I))	R1 = 0.0350, wR2 = 0.0817	
R indices (all data)	R1 = 0.0514, wR2 = 0.0899	
Extinction coefficient	n/a	
Largest diff. peak and hole	0.988 and -0.651 $e.Å^{-3}$	

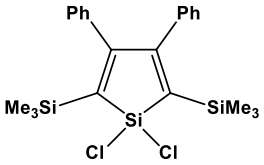

54

Empirical formula	C22 H28 Cl2 Si3	
Formula weight	447.61	
Temperature	120(2) K	
Wavelength	0.71073 Å	
Crystal system	Monoclinic	
Space group	C 2/c	
Unit cell dimensions	a = 20.3223(8) Å	α = 90°.
	b = 10.3918(4) Å	β = 100.0463(14)°.
	c = 11.4370(5) Å	γ = 90°.
Volume	2378.29(17) $Å^3$	
Z	4	
Density (calculated)	1.250 Mg/m^3	
Absorption coefficient	0.430 mm^{-1}	
F(000)	944	
Crystal size	0.240 x 0.240 x 0.120 mm^3	
Theta range for data collection	2.035 to 36.315°	
Index ranges	-33<=h<=33, -17<=k<=17, -19<=l<=19	
Reflections collected	90173	
Independent reflections	5746 (R(int) = 0.0269)	
Observed reflections (I > 2(I))	5189	
Completeness to theta = 36.315°	100.0 %	
Absorption correction	Semi-empirical from equivalents	
Max. and min. transmission	1.0000 and 0.9691	
Refinement method	Full-matrix least-squares on F^2	
Data / restraints / parameters	5746 / 0 / 126	
Goodness-of-fit on F^2	1.057	
Final R indices (I>2sigma(I))	R1 = 0.0231, wR2 = 0.0691	
R indices (all data)	R1 = 0.0266, wR2 = 0.0721	
Extinction coefficient	n/a	
Largest diff. peak and hole	0.522 and -0.242 $e.Å^{-3}$	

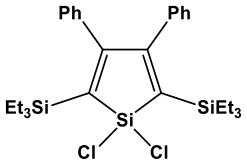

55

Empirical formula	C28 H40 Cl2 Si3	
Formula weight	531.77	
Temperature	100(2) K	
Wavelength	0.71073 Å	
Crystal system	Monoclinic	
Space group	$P2_1/c$	
Unit cell dimensions	a = 17.0016(8) Å	α = 90°.
	b = 17.3553(8) Å	β = 93.406(2)°.
	c = 30.4559(14) Å	γ = 90°.
Volume	8970.7(7) $Å^3$	
Z	12	
Density (calculated)	1.181 Mg/m^3	
Absorption coefficient	0.352 mm^{-1}	
F(000)	3408	
Crystal size	0.320 x 0.280 x 0.140 mm^3	
Theta range for data collection	1.340 to 33.728°	
Index ranges	-26<=h<=26, -27<=k<=27, -47<=l<=47	
Reflections collected	406540	
Independent reflections	35825 (R(int) = 0.0359)	
Observed reflections (I > 2(I))	28233	
Completeness to theta = 33.728°	100.0 %	
Absorption correction	Semi-empirical from equivalents	
Max. and min. transmission	1.0000 and 0.9718	
Refinement method	Full-matrix least-squares on F^2	
Data / restraints / parameters	35825 / 0 / 920	
Goodness-of-fit on F^2	1.054	
Final R indices (I>2sigma(I))	R1 = 0.0315, wR2 = 0.0798	
R indices (all data)	R1 = 0.0480, wR2 = 0.0883	
Extinction coefficient	n/a	
Largest diff. peak and hole	0.545 and -0.308 $e.Å^{-3}$	

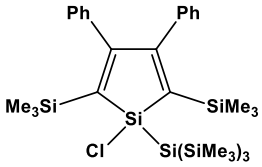

56

Empirical formula	C31 H55 Cl Si7	
Formula weight	659.83	
Temperature	120(2) K	
Wavelength	0.71073 Å	
Crystal system	Monoclinic	
Space group	P 21/c	
Unit cell dimensions	a = 20.2817(11) Å	α = 90°.
	b = 16.1278(9) Å	β = 90.5238(16)°.
	c = 12.0475(7) Å	γ = 90°.
Volume	3940.6(4) Å^3	
Z	4	
Density (calculated)	1.112 Mg/m^3	
Absorption coefficient	0.329 mm^{-1}	
F(000)	1424	
Crystal size	0.240 x 0.200 x 0.030 mm^3	
Theta range for data collection	1.263 to 30.033°	
Index ranges	-28<=h<=28, -22<=k<=22, -16<=l<=16	
Reflections collected	143024	
Independent reflections	11533 (R(int) = 0.0521)	
Observed reflections (I > 2(I))	9756	
Completeness to theta = 30.033°	98.2 %	
Absorption correction	Semi-empirical from equivalents	
Max. and min. transmission	1.0000 and 0.9705	
Refinement method	Full-matrix least-squares on F^2	
Data / restraints / parameters	11533 / 0 / 368	
Goodness-of-fit on F^2	1.115	
Final R indices (I>2sigma(I))	R1 = 0.0362, wR2 = 0.0931	
R indices (all data)	R1 = 0.0482, wR2 = 0.1008	
Extinction coefficient	n/a	
Largest diff. peak and hole	0.434 and -0.235 e.Å^{-3}	

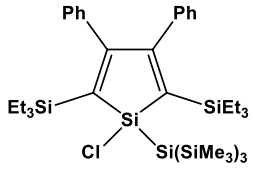

57

Empirical formula	C37 H67 Cl Si7	
Formula weight	743.98	
Temperature	100(2) K	
Wavelength	0.71073 Å	
Crystal system	Monoclinic	
Space group	$P2_1/n$	
Unit cell dimensions	a = 9.0905(15) Å	$\alpha = 90°$.
	b = 42.812(7) Å	$\beta = 107.773(2)°$.
	c = 12.1043(19) Å	$\gamma = 90°$.
Volume	4485.9(13) $Å^3$	
Z	4	
Density (calculated)	1.102 Mg/m^3	
Absorption coefficient	0.296 mm^{-1}	
F(000)	1616	
Crystal size	0.260 x 0.120 x 0.030 mm^3	
Theta range for data collection	1.830 to 25.025°	
Index ranges	-10<=h<=10, -50<=k<=50, -14<=l<=14	
Reflections collected	99138	
Independent reflections	7924 (R(int) = 0.1025)	
Observed reflections (I > 2(I))	5975	
Completeness to theta = 25.025°	100.0 %	
Absorption correction	Semi-empirical from equivalents	
Max. and min. transmission	1.0000 and 0.8945	
Refinement method	Full-matrix least-squares on F^2	
Data / restraints / parameters	7924 / 0 / 432	
Goodness-of-fit on F^2	1.058	
Final R indices (I>2sigma(I))	R1 = 0.0442, wR2 = 0.0914	
R indices (all data)	R1 = 0.0696, wR2 = 0.1012	
Extinction coefficient	n/a	
Largest diff. peak and hole	0.352 and -0.342 $e.Å^{-3}$	

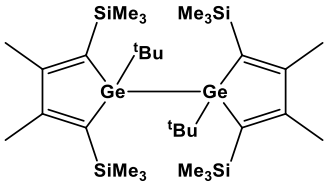

63

Empirical formula	C32 H66 Ge2 Si4	
Formula weight	708.38	
Temperature	120(2) K	
Wavelength	0.71073 Å	
Crystal system	Monoclinic	
Space group	P 21/n	
Unit cell dimensions	a = 23.7577(7) Å	α= 90°.
	b = 12.5176(3) Å	β= 97.334(2)°.
	c = 27.0215(7) Å	γ = 90°.
Volume	7970.2(4) $Å^3$	
Z	8	
Density (calculated)	1.181 Mg/m^3	
Absorption coefficient	1.647 mm^{-1}	
F(000)	3024	
Crystal size	0.300 x 0.200 x 0.150 mm^3	
Theta range for data collection	1.520 to 32.032°	
Index ranges	-35<=h<=35, -18<=k<=18, -40<=l<=40	
Reflections collected	302018	
Independent reflections	27735 (R(int) = 0.0472)	
Observed reflections (I > 2(I))	21909	
Completeness to theta = 32.032°	100.0 %	
Absorption correction	Semi-empirical from equivalents	
Max. and min. transmission	0.8273 and 0.6735	
Refinement method	Full-matrix least-squares on F^2	
Data / restraints / parameters	27735 / 0 / 729	
Goodness-of-fit on F^2	1.023	
Final R indices (I>2sigma(I))	R1 = 0.0297, wR2 = 0.0681	
R indices (all data)	R1 = 0.0466, wR2 = 0.0745	
Extinction coefficient	n/a	
Largest diff. peak and hole	0.715 and -0.666 $e.Å^{-3}$	

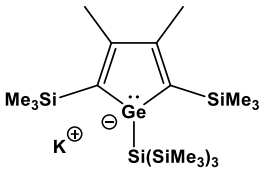

K[74] (solvent free)

Empirical formula	C21 H51 Ge K Si6	
Formula weight	583.84	
Temperature	120(2) K	
Wavelength	0.71073 Å	
Crystal system	Monoclinic	
Space group	P 21/c	
Unit cell dimensions	a = 11.7796(7) Å	α = 90°.
	b = 19.0710(10) Å	β = 110.2735(16)°.
	c = 15.9294(9) Å	γ = 90°.
Volume	3356.8(3) $Å^3$	
Z	4	
Density (calculated)	1.155 Mg/m^3	
Absorption coefficient	1.259 mm^{-1}	
F(000)	1248	
Crystal size	0.240 x 0.160 x 0.040 mm^3	
Theta range for data collection	1.731 to 28.698°	
Index ranges	-15<=h<=15, -25<=k<=25, -21<=l<=21	
Reflections collected	86131	
Independent reflections	8663 (R(int) = 0.0740)	
Observed reflections (I > 2(I))	6450	
Completeness to theta = 28.698°	100.0 %	
Absorption correction	Semi-empirical from equivalents	
Max. and min. transmission	1.0000 and 0.8949	
Refinement method	Full-matrix least-squares on F^2	
Data / restraints / parameters	8663 / 0 / 279	
Goodness-of-fit on F^2	1.000	
Final R indices (I>2sigma(I))	R1 = 0.0364, wR2 = 0.0790	
R indices (all data)	R1 = 0.0631, wR2 = 0.0884	
Extinction coefficient	n/a	
Largest diff. peak and hole	0.539 and -0.446 $e.Å^{-3}$	

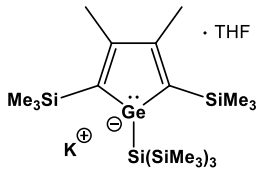

K[74] (THF coordinated)

Empirical formula	C25 H59 Ge K O Si6	
Formula weight	655.95	
Temperature	250(2) K	
Wavelength	0.71073 Å	
Crystal system	Tetragonal	
Space group	$P4_2/m$	
Unit cell dimensions	a = 15.062(2) Å	α = 90°.
	b = 15.062(2) Å	β = 90°.
	c = 17.316(4) Å	γ = 90°.
Volume	3928.2(15) $Å^3$	
Z	4	
Density (calculated)	1.109 Mg/m^3	
Absorption coefficient	1.084 mm^{-1}	
F(000)	1408	
Crystal size	0.300 x 0.250 x 0.200 mm^3	
Theta range for data collection	1.352 to 27.103°	
Index ranges	-19<=h<=19, -19<=k<=19, -22<=l<=22	
Reflections collected	138759	
Independent reflections	4482 (R(int) = 0.0319)	
Observed reflections (I > 2(I))	3557	
Completeness to theta = 27.103°	100.0 %	
Absorption correction	Semi-empirical from equivalents	
Max. and min. transmission	1.0000 and 0.9275	
Refinement method	Full-matrix least-squares on F^2	
Data / restraints / parameters	4482 / 0 / 171	
Goodness-of-fit on F^2	1.081	
Final R indices (I>2sigma(I))	R1 = 0.0359, wR2 = 0.0917	
R indices (all data)	R1 = 0.0506, wR2 = 0.1062	
Extinction coefficient	n/a	
Largest diff. peak and hole	0.422 and -0.163 $e.Å^{-3}$	

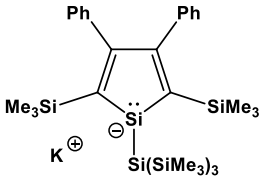

K[83]

Empirical formula	C37 H61 K Si7	
Formula weight	741.58	
Temperature	100(2) K	
Wavelength	0.71073 Å	
Crystal system	Monoclinic	
Space group	$P2_1/n$	
Unit cell dimensions	a = 9.9262(9) Å	$\alpha = 90°$.
	b = 18.0089(16) Å	$\beta = 98.799(3)°$.
	c = 24.452(2) Å	$\gamma = 90°$.
Volume	4319.7(7) $Å^3$	
Z	4	
Density (calculated)	1.140 Mg/m^3	
Absorption coefficient	0.341 mm^{-1}	
F(000)	1600	
Crystal size	0.160 x 0.100 x 0.040 mm^3	
Theta range for data collection	1.410 to 25.027°	
Index ranges	-11<=h<=11, 0<=k<=21, 0<=l<=29	
Reflections collected	16583	
Independent reflections	16583 (R(int) = ?)	
Observed reflections (I > 2(I))	11379	
Completeness to theta = 25.027°	100.0 %	
Absorption correction	Semi-empirical from equivalents	
Max. and min. transmission	1.000000 and 0.931710	
Refinement method	Full-matrix least-squares on F^2	
Data / restraints / parameters	16583 / 0 / 463	
Goodness-of-fit on F^2	1.005	
Final R indices (I>2sigma(I))	R1 = 0.0484, wR2 = 0.0925	
R indices (all data)	R1 = 0.0901, wR2 = 0.1079	
Extinction coefficient	n/a	
Largest diff. peak and hole	0.290 and -0.302 $e.Å^{-3}$	

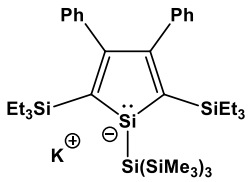

K[84]

Empirical formula	C45 H83 K O2 Si7	
Formula weight	891.84	
Temperature	100(2) K	
Wavelength	0.71073 Å	
Crystal system	Monoclinic	
Space group	$P2_1/n$	
Unit cell dimensions	a = 17.0247(8) Å	α = 90°.
	b = 18.1113(9) Å	β = 110.0431(13)°.
	c = 18.2892(9) Å	γ = 90°.
Volume	5297.7(4) $Å^3$	
Z	4	
Density (calculated)	1.118 Mg/m^3	
Absorption coefficient	0.291 mm^{-1}	
F(000)	1944	
Crystal size	0.400 x 0.150 x 0.100 mm^3	
Theta range for data collection	1.411 to 30.034°	
Index ranges	-23<=h<=23, -25<=k<=25, -25<=l<=22	
Reflections collected	152939	
Independent reflections	15505 (R(int) = 0.0498)	
Observed reflections (I > 2(I))	12157	
Completeness to theta = 30.034°	100.0 %	
Absorption correction	Semi-empirical from equivalents	
Max. and min. transmission	1.0000 and 0.9332	
Refinement method	Full-matrix least-squares on F^2	
Data / restraints / parameters	15505 / 0 / 511	
Goodness-of-fit on F^2	1.069	
Final R indices (I>2sigma(I))	R1 = 0.0381, wR2 = 0.0898	
R indices (all data)	R1 = 0.0563, wR2 = 0.0989	
Extinction coefficient	n/a	
Largest diff. peak and hole	0.755 and -0.736 $e.Å^{-3}$	

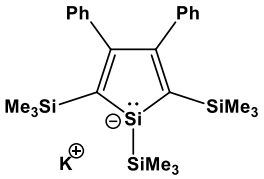

K[93]

Empirical formula	C25 H37 K Si4	
Formula weight	489.00	
Temperature	100(2) K	
Wavelength	0.71073 Å	
Crystal system	Monoclinic	
Space group	$P2_1/n$	
Unit cell dimensions	a = 12.2022(13) Å	$\alpha = 90°$.
	b = 11.7019(13) Å	$\beta = 90.145(7)°$.
	c = 19.344(2) Å	$\gamma = 90°$.
Volume	2762.1(5) $Å^3$	
Z	4	
Density (calculated)	1.176 Mg/m^3	
Absorption coefficient	0.377 mm^{-1}	
F(000)	1048	
Crystal size	0.200 x 0.120 x 0.040 mm^3	
Theta range for data collection	1.053 to 21.966°	
Index ranges	-12<=h<=12, -12<=k<=12, -20<=l<=20	
Reflections collected	37100	
Independent reflections	3372 (R(int) = 0.1439)	
Observed reflections (I > 2(I))	2324	
Completeness to theta = 21.966°	99.8 %	
Absorption correction	Semi-empirical from equivalents	
Max. and min. transmission	1.0000 and 0.9260	
Refinement method	Full-matrix least-squares on F^2	
Data / restraints / parameters	3372 / 0 / 281	
Goodness-of-fit on F^2	1.049	
Final R indices (I>2sigma(I))	R1 = 0.0528, wR2 = 0.1071	
R indices (all data)	R1 = 0.0964, wR2 = 0.1244	
Extinction coefficient	n/a	
Largest diff. peak and hole	0.362 and -0.333 $e.Å^{-3}$	

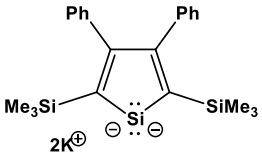

K_2[94]

Empirical formula	C30 H44 K2 O2 Si3	
Formula weight	599.12	
Temperature	100(2) K	
Wavelength	0.71073 Å	
Crystal system	Triclinic	
Space group	P-1	
Unit cell dimensions	a = 10.3874(4) Å	α = 68.719(2)°.
	b = 11.8915(5) Å	β = 70.7867(19)°.
	c = 15.1500(6) Å	γ = 79.654(2)°.
Volume	1642.77(12) $Å^3$	
Z	2	
Density (calculated)	1.211 Mg/m^3	
Absorption coefficient	0.422 mm^{-1}	
F(000)	640	
Crystal size	0.440 x 0.160 x 0.120 mm^3	
Theta range for data collection	1.506 to 34.971°	
Index ranges	-16<=h<=16, -19<=k<=19, -24<=l<=24	
Reflections collected	49374	
Independent reflections	49374 (R(int) = ?)	
Observed reflections (I > 2(I))	36670	
Completeness to theta = 34.971°	100.0 %	
Absorption correction	Semi-empirical from equivalents	
Max. and min. transmission	1.000000 and 0.913569	
Refinement method	Full-matrix least-squares on F^2	
Data / restraints / parameters	49374 / 0 / 341	
Goodness-of-fit on F^2	1.068	
Final R indices (I>2sigma(I))	R1 = 0.0414, wR2 = 0.0899	
R indices (all data)	R1 = 0.0675, wR2 = 0.1003	
Extinction coefficient	n/a	
Largest diff. peak and hole	0.598 and -0.496 $e.Å^{-3}$	

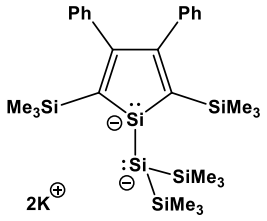

K_2[95]

Empirical formula	C40 H70 K2 O3 Si6	
Formula weight	845.70	
Temperature	100(2) K	
Wavelength	0.71073 Å	
Crystal system	Orthorhombic	
Space group	$P2_12_12_1$	
Unit cell dimensions	a = 13.4616(6) Å	α = 90°.
	b = 16.3060(7) Å	β = 90°.
	c = 22.1621(9) Å	γ = 90°.
Volume	4864.7(4) $Å^3$	
Z	4	
Density (calculated)	1.155 Mg/m^3	
Absorption coefficient	0.375 mm^{-1}	
F(000)	1824	
Crystal size	0.440 x 0.420 x 0.180 mm^3	
Theta range for data collection	1.550 to 34.971°	
Index ranges	-21<=h<=21, -26<=k<=26, -35<=l<=35	
Reflections collected	222907	
Independent reflections	21374 (R(int) = 0.0374)	
Observed reflections (I > 2(I))	19110	
Completeness to theta = 34.971°	100.0 %	
Absorption correction	Semi-empirical from equivalents	
Max. and min. transmission	1.0000 and 0.9499	
Refinement method	Full-matrix least-squares on F^2	
Data / restraints / parameters	21374 / 0 / 472	
Goodness-of-fit on F^2	1.080	
Final R indices (I>2sigma(I))	R1 = 0.0366, wR2 = 0.0896	
R indices (all data)	R1 = 0.0451, wR2 = 0.0950	
Absolute structure parameter	-0.006(6)	
Extinction coefficient	n/a	
Largest diff. peak and hole	0.709 and -0.419 $e.Å^{-3}$	

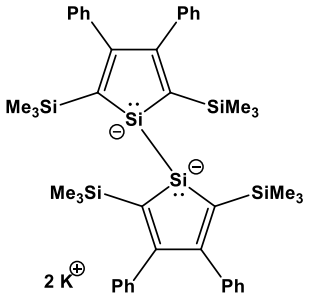

K_2[96]

Empirical formula	C68 H80 K2 Si6	
Formula weight	1144.06	
Temperature	100(2) K	
Wavelength	0.71073 Å	
Crystal system	Monoclinic	
Space group	$P2_1$	
Unit cell dimensions	a = 19.0377(8) Å	α = 90°.
	b = 18.0780(8) Å	β = 105.5486(18)°.
	c = 19.9778(9) Å	γ = 90°.
Volume	6624.0(5) $Å^3$	
Z	4	
Density (calculated)	1.147 Mg/m^3	
Absorption coefficient	0.289 mm^{-1}	
F(000)	2440	
Crystal size	0.150 x 0.150 x 0.050 mm^3	
Theta range for data collection	1.312 to 23.255°	
Index ranges	-21<=h<=21, -20<=k<=20, -22<=l<=19	
Reflections collected	124622	
Independent reflections	19002 (R(int) = 0.1199)	
Observed reflections (I > 2(I))	13269	
Completeness to theta = 23.255°	100.0 %	
Absorption correction	Semi-empirical from equivalents	
Max. and min. transmission	1.0000 and 0.8815	
Refinement method	Full-matrix least-squares on F^2	
Data / restraints / parameters	19002 / 1 / 1393	
Goodness-of-fit on F^2	1.017	
Final R indices (I>2sigma(I))	R1 = 0.0522, wR2 = 0.0943	
R indices (all data)	R1 = 0.0995, wR2 = 0.1109	
Absolute structure parameter	0.27(4)	
Extinction coefficient	n/a	
Largest diff. peak and hole	0.338 and -0.328 e.$Å^{-3}$	

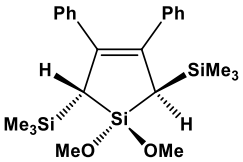

108 (trans)

Empirical formula	C24 H36 O2 Si3	
Formula weight	440.80	
Temperature	100(2) K	
Wavelength	0.71073 Å	
Crystal system	Monoclinic	
Space group	I2/a	
Unit cell dimensions	a = 12.2723(6) Å	α = 90°.
	b = 10.4514(5) Å	β = 101.2987(14)°.
	c = 19.8730(13) Å	γ = 90°.
Volume	2499.6(2) Å^3	
Z	4	
Density (calculated)	1.171 Mg/m^3	
Absorption coefficient	0.207 mm^{-1}	
F(000)	952	
Crystal size	0.400 x 0.300 x 0.200 mm^3	
Theta range for data collection	2.090 to 34.971°	
Index ranges	-19<=h<=19, -16<=k<=16, -31<=l<=32	
Reflections collected	65648	
Independent reflections	5481 (R(int) = 0.0206)	
Observed reflections (I > 2(I))	4991	
Completeness to theta = 34.971°	100.0 %	
Absorption correction	Semi-empirical from equivalents	
Max. and min. transmission	1.0000 and 0.9633	
Refinement method	Full-matrix least-squares on F^2	
Data / restraints / parameters	5481 / 0 / 136	
Goodness-of-fit on F^2	1.071	
Final R indices (I>2sigma(I))	R1 = 0.0278, wR2 = 0.0848	
R indices (all data)	R1 = 0.0309, wR2 = 0.0883	
Extinction coefficient	n/a	
Largest diff. peak and hole	0.540 and -0.245 e.Å^{-3}	

7.3 Abbreviations

a	hyperfine coupling constant (EPR)
AIM	atoms in molecules
Ampl	amplitude
Ar	aryl
Ar*	3,5-dimethylphenyl
ATR	attenuated total reflectance
Att	attenuation
avg	average
bcp	bond critical point
br	broad
^{n}Bu	n-butyl
^{t}Bu	tert-butyl
calcd	calculated
CHD	cyclohexadiene
COSY	correlation spectroscopy
Cp	cyclopentadienyl
Cp*	pentamethylcyclopentadienyl
d	day or doublet
DEPT	distortionless enhancement by polarization transfer
DFT	density functional theory
dim	dimerisation
Dipp	2,6-diisopropylphenyl
diss	dissociation
DME	dimethoxyethane
Dsi	bis(trimethylsilyl)methyl
E	energy
EA	electron affinity or elemental analysis
EI	electron ionisation
em	emission
EPR	electron paramagnetic resonance
eq	equation
Et	ethyl
et al	et alii; and others
GC	gas chromatography
h	hour
H/L	HOMO/LUMO
hfcc	hyperfine coupling constant
HMBC	heteronuclear multiple bond coherence
HMQC	heteronuclear multiple quantum coherence
HOMO	highest occupied molecular orbital

HR	high-resolution
INEPT	insensitive nuclei enhanced by polarisation transfer
IR	infrared
J	coupling constant (NMR)
LIFDI	liquid injection field desorption ionisation
LUMO	lowest occupied molecular orbital
m	*meta*
m	multiplet
max	maximum
Me	methyl
Mes	mesityl; 2,4,6-trimethylphenyl
Mes*	2,4,6-tri-tert-butylphenyl
min	minimum
min	minute
M_n	number average molar mass
Mod	modulation
MS	mass spectrometry
MW	microwave
Naph	naphthyl
NHC	N-heterocyclic carbene
NImag	number of imaginary frequencies
NMR	nuclear magnetic resonance
o	*ortho*
OLED	organic light-emitting diode
p	*para*
Pemp	pentamethylphenyl
Ph	phenyl
^{i}Pr	isopropyl
PTFE	polytetrafluoroethylene
q	quartet
rcp	ring critical point
rel	relative
s	singlet
sub	sublimation or substituent
t	triplet
TEMPO	2,2,6,6-tetramethylpiperidinyloxyl
Ter	terphenyl; 2,6-diarylphenyl
TfO	triflate; trifluoromethanesulfonyl
THF	tetrahydrofuran
UV-Vis	ultraviolet-visible
VSCC	valence shell charge concentration
XRF	X-ray fluorescence

8 Curriculum Vitae

Crispin Rudolf Willy Reinhold

Kleine Str. 6 • 26121 Oldenburg • +49 176 / 218 454 49

crispin.reinhold@uni-oldenburg.de

30.06.1985 in Ratzeburg

Education

12/2012 - present	**PhD in chemistry** Carl von Ossietzky University of Oldenburg Institute of Chemistry, work group of Prof. Thomas Müller, *„Sila- and Germacyclopentadienes: Radicals, Anions, and a New Type of Tetrylene“*
WS 2009/2010 – SS 2012	**Master of Science (M.Sc.) in chemistry** Carl von Ossietzky University of Oldenburg Institute of Chemistry, work group of Prof. Thomas Müller, *„Synthesis of Phenylene Bridged Metallolyl Halogene Compounds“*
WS 2006/2007 – SS 2009	**Bachelor of Science (B.Sc.) in chemistry** Carl von Ossietzky University of Oldenburg Institute of Chemistry, work group of Prof. Thomas Müller, *„Synthesis of Steric Hindered Silyl Phosphanes“*
06/2005	**Diploma** Lauenburgische Gelehrtenschule Ratzeburg Kreis Herzogtum Lauenburg

Professional Experience

08/2015	**7th Summer School of the European Federation of EPR groups on Advanced EPR, Berlin**
05/2014	**Technion – Israel Institute of Technology, Haifa, Israel** Faculty of Chemistry, work group of Prof. Yitzhak Apeloig; four-week research stay to improve EPR spectroscopic measuring skills
11/2012 - present	**Carl von Ossietzky University of Oldenburg** research assistant; supervision of bachelor and master theses, research students and the annual course in preparative inorganic chemistry

09/2010 – 01/2011	**University of Western Ontario, London, Ontario, Canada** Department of Chemistry, work group of Prof. Kim M. Baines; scientific internship, Results published in *Organometallics*
WS 2009/2010 – SS 2012	**Carl von Ossietzky University of Oldenburg** research assistant; three times TA for students in the first semester, two times TA for students training for the Chemistry Olympics; tutoring groups of 12-20 students in the chemistry lab
06 – 09/2006	**Korn's PC Corner**, Ratzeburg, temporary job, IT-systems
06 – 12/2005	**Markt – Apotheke**, Ratzeburg, temporay job, Drug Delivery

Conferences and Contributions

08-09/2016	**Poster: Transformation of Germoles into Siloles via Unusual Tetrylenes** Crispin R. W. Reinhold, Zhaowen Dong, Jan M. Winkler, Thomas Müller 19. Norddeutsches Doktorandenkolloquium 2016, Universität Hamburg, Hamburg International Conference on the Coordination and Organometallic Chemistry of Germanium, Tin and Lead 2016, Pardubice, Czech Republic
09/2015	**Talk: Sila- and Germacyclopentadienyl Radicals vs. Anions** Crispin R. W. Reinhold, Thomas Müller 18. Norddeutsches Doktorandenkolloquium 2016, Goslar
07-08/2015	**Poster: Sila- and Germacyclopentadienyl Radicals vs. Anions** Crispin R. W. Reinhold, Thomas Müller 7th Summer School of the European Federation of EPR groups on Advanced EPR, Berlin 14. International Symposium on Inorganic Ring Systems, Universität Regensburg, Regensburg
08-09/2014	**Poster: Persistent Sila- and Germacyclopentadienyl Radicals** C. R. W. Reinhold, T. Müller 17. Vortragstagung für Anorganische Chemie der Wöhler-Vereinigung 2014, Saarland University, Saarbrücken 17. Norddeutsches Doktorandenkolloquium 2014, Leibniz Institute for Catalysis, Rostock XVII International Symposium on Organosilicon Chemistry 2014, Technische Universität Berlin, Berlin
09/2013	**Poster: Synthesis and Reactivity Studies of Metallolyl Compounds** C. R. W. Reinhold, T. Müller 16. Norddeutsches Doktorandenkolloquium 2013, University of Bremen, Bremen GDCh Wissenschaftsforum Chemie 2013, Darmstadtium, Darmstadt

08/2011	**Poster: Addition of Aldehydes to Germenes: The Influence of Solvent** C. J. Allan, C. R. W. Reinhold, L. C. Pavelka, K. M. Baines Inorganic Discussion Weekend 2011, Crown Plaza Niagara Falls, Niagara Falls, Canada
08/2011	**Poster and flash presentation: Silyl Cationic Frustrated Lewis Paris – A Progress Report** M. Reißmann, J. Intemann, R. Panisch, C. R. W. Reinhold, A. Schäfer, T. Müller XVI International Symposium on Organosilicon Chemistry 2011, McMaster University, Hamilton, Canada
11/2010	**Poster: Addition of Aldehydes to Germenes: The Influence of Solvent** C. J. Allan, C. R. W. Reinhold, L. C. Pavelka, K. M. Baines Inorganic Discussion Weekend 2010, University of Windsor, Windsor, Canada

Awards and Achievements

12/2016	**Publication: „A Germylene Stabilized by Homoconjugation"** Z. Dong, C. R. W. Reinhold, M. Schmidtmann, T. Müller Z. Dong, C. R. Reinhold, M. Schmidtmann, T. Müller, *Angew. Chem. Int. Ed.* **2016**, *55*, 15899.
04/2015	**Publication: „Oligosilanylated Antimony Compounds"** R. Zitz, K. Gatterer, C. R. W. Reinhold, T. Müller, J. Baumgartner, C. Marschner, *Organometallics* **2015**, *34*, 1419.
01/2015	**Heinz – Neumüller Foundation Scholarship**
03/2012	**OLB / EWE – Award for outstanding student performance**
08/2011	**„Poster of Distinction" at the Inorganic Discussion Weekend 2011**
08/2011	**Selected for a flash presentation at the XVI International Symposium on Organosilicon Chemistry 2011**
05/2011	**Publication: „Addition of Aldehydes to Germenes: The Influence of Solvent"** C. J. Allan, C. R. W. Reinhold, L. C. Pavelka, K. M. Baines, *Organometallics* **2011**, *30*, 3010.

Additional Information

Languages	**German (mother tongue), English (fluent), qualification in Latin**
01-06/2006	**Travelling in Australia and South East Asia**
Further interests	**sport climbing, bouldering, cycling**